Universidad Autónoma de Madrid

Departamento de Bioquímica

PSGL-1/P-selectin interaction: regulation of immune and vascular homeostasis

Tesis doctoral

Rafael González Tajuelo

Madrid, 2017

Departamento de Bioquímica

Facultad de Medicina

Universidad Autónoma de Madrid

PSGL-1/P-selectin interaction: regulation of immune and vascular homeostasis

Memoria presentada por el licenciado en Biología:

Rafael González Tajuelo

para optar al título de Doctor por la Universidad Autónoma de Madrid

Director de la Tesis: Ana C. Urzainqui Mayayo, Doctora en Ciencias Biológicas.

Este trabajo se realizó en el Servicio de Inmunología del Hospital Universitario de la Princesa.

Madrid, 2017

Ana Carmen Urzainqui Mayayo, Doctora en Ciencias Biológicas,

CERTIFICA:

Que Rafael González Tajuelo, licenciado en Biología por la Universidad Complutense de Madrid, ha realizado bajo mi dirección el trabajo de investigación correspondiente a su Tesis Doctoral con el título:

PSGL-1/P-selectin interaction: regulation of immune and vascular homeostasis

Revisado este trabajo, el que suscribe considera el trabajo realizado satisfactorio y autoriza su presentación para ser evaluado por el tribunal correspondiente.

Y para que así conste y a los efectos oportunos, firma el presente certificado en Madrid a 22 de Febrero de 2017.

Fdo. Dra. Ana C. Urzainqui Mayayo

Summary

Summary

The correct function of the immune system is based on its ability to distinguish self-antigens from those that are part of pathogens. For this reason, redundant mechanisms have evolved to avoid an inflammatory response against antigens of the own organism. When these mechanisms fail, autoimmunity occurs.

In recent years, the interaction of the leukocyte receptor PSGL-1 with its ligand in endothelial cells, P-selectin, has been shown to be necessary for the maintenance of peripheral tolerance and immune system homeostasis.

In the present thesis, it is detailed how female PSGL-1 deficient mice are prone to develop pulmonary arterial hypertension as a part of an autoimmune syndrome similar to scleroderma. Using the reduction of blood flow acceleration time in the pulmonary artery as a marker of pulmonary hypertension, we described that PSGL-1-deficient females progressively increase their pulmonary pressure, reaching significant differences at 15 months of age. With aging, and associated with an increase in Th1 response, there is an increase in the pulmonary concentration of angiotensin II together with a decrease in the vasodilator receptor AT2R, observed from the young age. In this context, isolated arteries of PSGL-1-deficient female mice exhibited a higher KCL-dependent vasoconstriction, and a lower nitric oxide-dependent vasodilator response. Accordingly, lung endothelial cells from PSGL-1 deficient females exhibited reduced amounts of nitric oxide. Importantly, we have found that P-selectin deficient female mice also develop PAH with ageing.

This thesis also describes that P-selectin deficiency leads to the appearance of an autoimmune syndrome similar to human systemic lupus erythematosus in mice. This syndrome is characterized by the presence of circulating autoantibodies, including anti-double-stranded DNA antibodies, and the deposition of immune complexes in skin and glomeruli. P-selectin deficient mice present a reduced naïve T cell population and elevated effector subsets with reduced IL-10 producing leukocytes. Mice deficient in P-selectin exhibit dermatitis and lupus nephritis, which become more severe with aging, coinciding with the increase in the circulating and dermal Th17 populations. Lupus dermatitis developed by P-selectin deficient mice is characterized by an increase in plasmacytoid dendritic cells, T lymphocytes, and by an alteration in the balance between effector and regulatory T lymphocytes. Finally, the study of skin biopsies of patients with cutaneous lupus erythematosus and healthy controls revealed that P-selectin expression was reduced in the skin vessels of cutaneous lupus patients.

Resumen

Resumen

El correcto funcionamiento del sistema inmune se basa en su capacidad para distinguir los antígenos propios de aquellos que forman parte de patógenos. Para ello, ha desarrollado mecanismos redundantes que evitan una respuesta inflamatoria frente a antígenos propios. Cuando estos mecanismos fallan se produce autoinmunidad. En los últimos años, en nuestro laboratorio se ha puesto de manifiesto que la interacción del receptor leucocitario PSGL-1 con su ligando en células endoteliales, P-selectina, es necesaria para el mantenimiento de la tolerancia periférica y la homeostasis del sistema inmune.

En esta tesis, se detalla cómo los ratones hembra deficientes en PSGL-1 son proclives a desarrollar hipertensión arterial pulmonar como una parte del síndrome autoinmune similar a la esclerodermia. Utilizando como marcador de hipertensión pulmonar la reducción del tiempo de aceleración del flujo sanguíneo en la arteria pulmonar, describimos que las hembras deficientes en PSGL-1 aumentan progresivamente su presión pulmonar, alcanzando diferencias significativas a los 15 meses de edad. Asociado a un incremento de la respuesta Th1, se produce un aumento en la concentración pulmonar de angiotensina II y una disminución del receptor vasodilatador AT2R. En este contexto, las arterias aisladas de ratones hembra deficientes en PSGL-1 presentan una mayor vasoconstricción dependiente de KCL, y una menor respuesta vasodilatadora dependiente de óxido nítrico. En concordancia, las células endoteliales de pulmón de hembras deficientes en PSGL-1 presentan una cantidad reducida de óxido nítrico. De la misma manera, los ratones hembra deficientes en P-selectina desarrollan hipertensión arterial pulmonar con el envejecimiento.

La deficiencia en P-selectina provoca la aparición en ratones de un síndrome autoinmune similar al lupus eritematoso humano, caracterizado por la presencia de autoanticuerpos circulantes, incluidos los anticuerpos anti-ADN de doble cadena, y por los depósitos de inmunocomplejos en la piel y los glomérulos. Los ratones deficientes en P-selectina presentan menos linfocitos T naïve, más T efectores y una reducción en las poblaciones de leucocitos productores de IL-10. Los ratones deficientes en P-selectina presentan dermatitis y nefritis lúpica, que se vuelven más severas con el envejecimiento. La dermatitis lúpica de los ratones deficientes en P-selectina se caracteriza por un aumento de las células dendríticas plasmacitoides, los linfocitos T, y por una alteración del balance entre linfocitos T efectores y reguladores. Por último, el estudio de biopsias de piel de pacientes con lupus eritematoso cutáneo y controles sanos reveló que la expresión de P-selectina estaba reducida en los vasos de la piel de los pacientes de lupus cutáneo.

Index

Index

List of abbreviations

List of abbreviations

aa: Aminoacid

ACE: Angiotensin Converting Enzyme

Ach: Acetylcholine

ACR: American College of Rheumatology

ADAM: α-Disintegrin-And-Metalloprotease

AEP: Active Effective Pressure

AID: Activation Induced Deaminase

ANAs: Anti-Nuclear Antiboies

AngI: Angiotensin I

AngII: Angiotenin II

APC: Alophycocyanin

APC-Cy7: APC-Cyanin 7

AT1R: Angiotensin II Receptor 1

AT2R: Angiotensin II Receptor 2

BSA: Bovine Serum Albumin

BTK: Bruton Tyrosine Kinase

BV421: Brilliant Violet 421

cAMP: Cyclic Adenosin monophosphate

cDC: Conventional Dendritic Cells

cLE: Cutaneous Lupus Erythematosus

CMV: Cytomegalovirus

CR: Consensus Repeats

CTD: Connective Tissue Disease

DAB: 3,3'-Diaminobenzidine

DAR-4M AM: diaminorhodamine-4M acetoxymethyl ester

DSS: Dextran Sodium Sulphate

EBV: Epstein-Barr Virus

ECG: Electrocardiogram

EDTA: Ethylenediaminetetraacetic acid

ENAs: Extractable Nuclear Antibodies

eNOS: Endothelial Nitric Oxide Synthase

ERAs: Endothelin Receptor Antagonists

ERK: Extracellular signa-Regulated Kinases

ERM: Ezrin Radixin Moesin

E-sel: E-selectin

ET: Ejection Time

ET-1: Endothelin 1

ETA: Endothelin 1 Receptor A

ETB: Endothelin 1 Receptor B

FDA: Food and Drug Administration

FITC: Fluorescein Isothiocyanate

GC: Germinal Center

G-CSF: Granulocyte-Colony Stimulating Factor

GM-CSF: Granulocyte Monocyte-Colony Stimulating Factor

GWAS: Genome Wide Association Study

H&E: Hematoxylin and Eosin

HHV: Human Herpes Virus

HIV: Human Immunodeficiency Virus

HPV: Human Papiloma Virus

HRP: Horseradish Peroxidase

5-HT: Serotonin

HUVEC: Human Umbilical Vein Endothelial Cells

ICAM-1: Intercellular Adhesion Molecule 1

IDO: Indoleamine 2 3-Dioxygenase

IFN: Interferon

IL: Interleukin

iNOS: Inducible Nitric Oxide Synthase

ITAM: Immunoreceptor Tyrosine-based

kb: Kilobase

kDa: KiloDalton

LPS: Lipopolysaccharide

L-sel: L-selectin

LV: Left Ventricle

MCT: Monocrotaline

MHC-II: Major Histocompatibility Complex Class II

MFI: Mean Fluorescence Intensity

moDCs: monocyte-derived Dendritic Cells

mPAP: mean Pulmonary Artery Pressure

NK: Natural Killer cells

nNOS: Neuronal Nitric Oxide Synthase
NO: Nitric Oxide
NSAID: Non Steroid Anti-inflammatory Drug
NSIP: Non Specific Interstitial Pneumoniae
PAT: Pulmonary Acceleration Time
PAH: Pulmonary Arterial Hypertension
PASMC: Pulmonary Artery Smooth Muscle Cells
PBS: Phosphate Buffered Saline
pDC: plasmacytoid Dendritic Cells
PE: Phycoerythrin
PE-Cy7: Phycoerythrin-Cyanin 7
PerCP: Peridinin Chlorophyll
PH: Pulmonary Hypertension
PGI2: Prostacyclin
PI3K: Phosphatidylinositol-4,5-bisphosphate 3-Kinase
PLC: Phospholipase C
P-sel: P-selectin
PSGL-1: P-Selectin Glycoprotein Ligand 1
RAAS: Renin Angiotensin Aldosterone System
RV: Right Ventricle
S: Interventricular Septum
SLAN: 6-Sulfo N-Acetyl Lactosamine
sLe^X: sialyl Lewis X
SLE: Systemic Lupus Erythematosus
SLEDAI: SLE disease activity index
SLICC: Systemic Lupus International Collaborating Clinics
αSMA: alpha Smooth Muscle Actin
SNP: Sodium Nitroprusside
snRNP: small nucleolar Ribonucleoprotein
SSc: Systemic Sclerosis
Syk: Spleen Tyrosine Kinase
Tc: Cytotoxic T cells
TGF-β: Transforming Growth Factor beta
Th: Helper T cells
TLR: Toll-Like Receptor
TNF-α: Tumor Necrosis Factor α
Treg: regulatory T cells
VCAM-1: Vascular Cell Adhesion Molecule 1
VSMC: Vascular Smooth Muscle Cells
WT: Wild Type

Introduction

Introduction

1. PSGL-1 and P-selectin

1.1 Chromosomic location, structure and expression of PSGL-1

Selplg is the gene coding for P-Selectin Glycoprotein ligand-1 (PSGL-1). It is located at chromosome 12 in humans, and at chromosome 5 in mice. The human and mice genes have the same structure, with two exons and the coding region corresponding to the second one (1, 2). Mice and human PSGL-1 proteins also have high degree of homology both in structure and aminoacid sequence (2).

PSGL-1 is a type I transmembrane protein of 120 kDa that dimerizes through a disulfide bridge. The core protein is formed by an extended mucin ectodomain composed of serine, threonine, and proline-rich decameric repeats (3, 4) bearing sites for potential O-glycan modification (14-16 repeats in humans and 15 in mice) (2, 5) (Figure I1). Several post-translational modifications are needed for the correct recognition by P-selectin (P-sel), E-selectin (E-sel) and L-selectin (L-sel), such as O- and N-glycosylations, sialylation, fucosylation or tyrosyl sulfation. (6, 7). The region participating in selectin recognition is disialylated and monofucosylated with a terminal sialyl Lewis X (sLe^X; NeuAcα2,3Galβ1,4[Fucα1,3]GlcNAcβ1-R) (8, 9) (Figure I1). Sulfation of tyrosine residues near the N-terminus is necessary to produce high-affinity P-sel/PSGL-1 interaction (10). However, PSGL-1 recognition by E-sel is tyrosine sulfation-independent but requires O-glycan modifications in decameric repeats proximal to membrane (11). The aminoacid sequences of human and mouse PSGL-1 cytoplasmic domains are highly conserved, and have been implicated in PSGL-1 intracellular signaling (12) and re-distribution to the uropod in activated cells (13).

PSGL-1 is expressed in all leukocyte lineages and also in platelets (4). PSGL-1 is also expressed on certain endothelial cells, such as mesenteric lymph node venules in the context of an ileitis murine model (14), human umbilical vein endothelial cells (HUVEC), foreskin microvascular cells and in atherosclerotic coronary arteries (15).

The expression of PSGL-1 can be modulated by different stimuli. Activation of monocyte-derived dendritic cells (moDCs) and langerhans cells raises the expression levels of PSGL-1 (16) and activation of platelets with thrombin also leads to an increase in surface PSGL-1 (17). One mechanism for altering PSGL-1 expression and function includes proteolytic processing of PSGL-1 extracellular domains. Several proteases have been reported to act as PSGL-1 sheddases (4), such as the snake venom metalloproteases Mocarhagin and Triflamp, or endogenous enzymes such as cathepsin G, neutrophil elastase, β secretase BACE1, and members of the α-disintegrin-and-metalloprotease (ADAM) family of metalloproteases. Indeed, ADAM8 can cleave PSGL-1 in vitro with the subsequent impairment of THP1 cell rolling over HUVEC monolayers (18). In fact, apoptosis, in vitro activation with phorbol myristate acetate or in vivo treatment with lipopolisaccharide (LPS), granulocyte-colony stimulating

factor (G-CSF) or granulocyte monocyte-colony stimulating factor (GM-CSF) leads to reduced PSGL-1 expression in neutrophils and increased levels of extracellular soluble PSGL-1 (19-21). In addition to protease cleavage, the expression of glycosyltransferases that regulate the addition of carbohydrate groups rises as the dominant way of regulating PSGL-1 function. Glycosyltransferases relevant for modification of P-sel binding are constitutively expressed in neutrophils and monocytes (22). Megakaryocytes also appear to express a full contingent of glycosyltransferases, and as a result platelets express functional PSGL-1 (17, 23). However, naïve T cells are not able to bind to P- and E-sel even though PSGL-1 is expressed on their surface because α1,3fucosyltransferases IV and VII (FucT-IV and FucT-VII) are upregulated upon activation (24, 25). Likewise, Th1 but not Th2 cells are able to bind P- and E-sel (25, 26).

1.2 Chromosomic location, structure and expression of P-selectin

The gene coding for P-selectin (*Selp*) is located at chromosome 1 in both humans and mice (27). In humans, the gene spans over >50 kb, including 17 exons (16 coding exons), and is translated into a 140 kDa protein (830aa) (27-29). In mice, 15 out 16 exons code for the P-sel protein, resulting in a transcript of 3,438 bp that can be translated into a 768 aa polypeptide (30, 31).

Selectins (P-, E- and L-selectin) are type I transmembrane proteins that mediate adhesion of leukocytes and platelets to endothelial cells and to each other. The extracellular rod of selectins contains a N-terminal C-type lectin domain, an epidermal growth factor-like domain and a series of consensus repeats (CR) that is different among the three selectins, with 9, 2 and 6 repeats for P-, E- and L-sel, respectively (3, 32) (Figure I1). The lectin domain contains a Ca^{2+}-binding site, which is critical for the interaction with the fucose moiety of sLe^X (33, 34). The lectin domains of the three selectins share about 60% homology, with subtle differences in carbohydrate binding and that conferr selectin specificity (24).

L-sel (CD62L) is constitutively expressed on all leukocyte populations, mediating homing to secondary lymphoid organs and leukocyte-leukocyte interactions. PSGL-1 modifications needed for the interaction with L- and P-sel are the same (3, 4). E-sel (CD62E) is expressed on endothelial cells. Its expression is regulated at transcriptional level by inflammatory mediators, and is constitutively expressed in adult skin and bone marrow (35).

P-sel (CD62P) is stored in α-granules of platelets and in Weibel–Palade bodies of endothelial cells, and is translocated to the cell surface of endothelial cells and platelets upon activation (3, 32) by different mediators such as thrombin, histamine, or complement (36). Tumor necrosis factor alpha (TNF-α), interleukin 1 beta (IL-1β), or LPS increase transcription of P-sel mRNA in most mammals, including mice, but not in primates, including humans (37, 38). In addition, constitutive expression of P-sel has been reported on lung and choroids plexus microvessel endothelium, and on peritoneal macrophages (32, 39).

1.3. PSGL-1/P-selectin signaling and adhesion

The interaction of PSGL-1 with its ligands is relevant for multiple physiologic and physiopathologic processes. Binding under flow of PSGL-1 on circulating leukocytes to P- and E-sel on the vessel wall mediates inflammatory and surveillance functions of the immune system. During immune surveillance, lymphoid cells continuously recirculate between blood and lymphoid organs to search for their cognate antigens. Although the role of L-sel mediating homing to secondary lymphoid organs is well established (40, 41), PSGL-1 participates in the homing of leukocytes to both lymphoid and non-lymphoid tissues such lymph nodes (42), colonic lamina propria (43), lung (44) or bone marrow (35). The homing of early T lymphocyte progenitors to thymus is also mediated by PSGL-1/P-sel interaction (45).

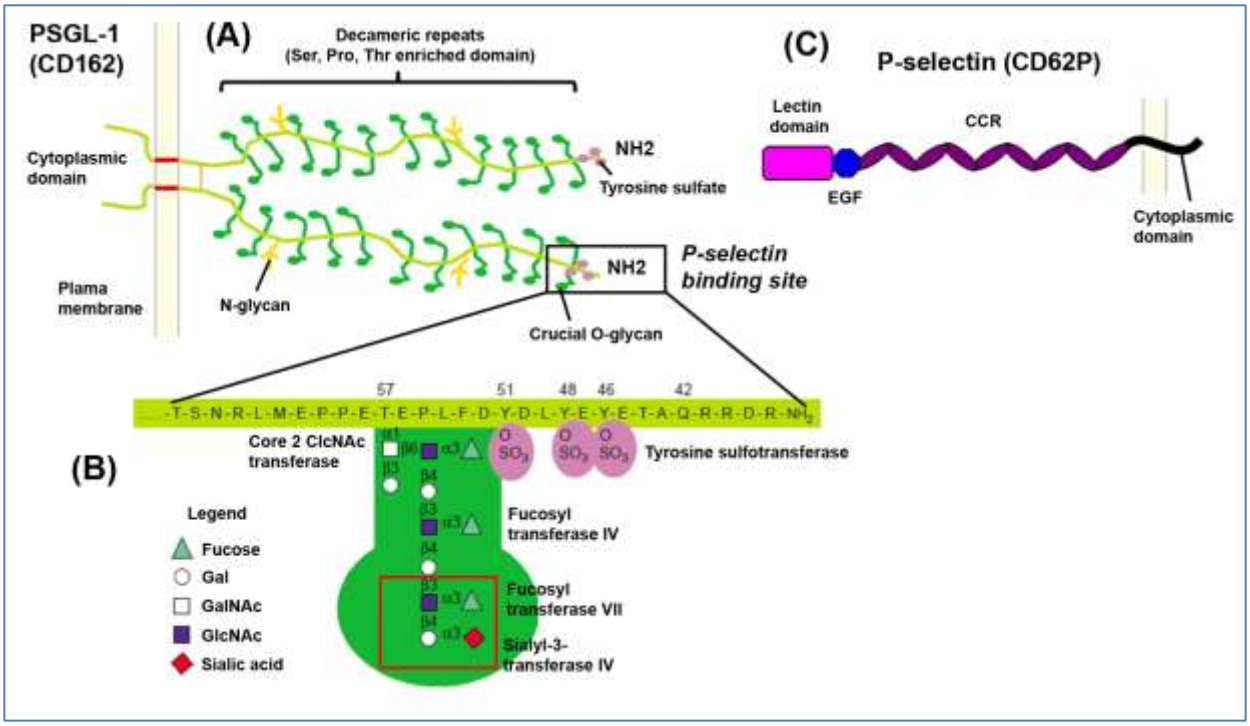

Figure I1. Structure of the human PSGL-1 homodimer and P-selectin. (A) PSGL-1: N-terminal tyrosine sulfates (purple) are followed by a long, extended glycoprotein backbone (light green) with many O-linked carbohydrates (dark green) and some N-linked carbohydrates (yellow). A stabilizing disulfide bond (S–S) (orange line) is located near the plasma membrane, and the transmembrane domain (red) and the short cytoplasmic tail are also shown. **(B)** P-selectin binding site. Tyrosine sulfates (purple) and the crucial O-glycan at T57 (dark green) are represented. Typical carbohydrate side-chains are shown, with the responsible enzymes indicated next to the respective linkage. The sLe^x (minimal selectin recognition) motif is highlighted by a red box. **(C)** P-selectin: the cytoplasmic and transmembrane domain is represented in black. The 9 consensus repeats (CR) ar represented as purple ovals. The EGF-like domain is represented in blue. The lectin domain, which binds PSGL-1, is highlighted in pink. Adapted from *Trends Mol Med.* 2003; 9 (6): 263-8.

Leukocyte extravasation starts with the tethering and rolling of leukocytes on activated endothelium. As the longest protein of the selectin family, P-sel transiently binds to PSGL-1 on the

surface of leukocytes, establishing the initial contacts with endothelial cells. This transient interaction slows down leukocytes, resulting in a rolling movement on the vessel wall (40), that is essential for the subsequent firm adhesion (Figure I2). PSGL-1/P-sel interaction mediates the capture and fast rolling (20– 40 μm/s) of leukocytes on the endothelium whereas E-sel mediates leukocyte slow rolling (3–7 μm/s) (46). During the rolling process, engagement of PSGL-1 by selectins activates β1 (47, 48) and β2 (49-51) leukocyte integrins whose affinity for their vascular ligands aids in inducing leukocyte adhesion under flow (52). Integrin activation by E-sel is mediated by the adaptor protein ADAP12 and Fcγ receptors, Src kinases and Spleen tyrosine kinase (Syk) that phosphorylate the Bruton tyrosine kinase (BTK) followed by an activation of Phospholipase Cγ2 (PLCγ2)- or Phosphatidylinositol-4,5-bisphosphate 3-Kinase (PI3K)-dependent pathways (36, 40, 53).

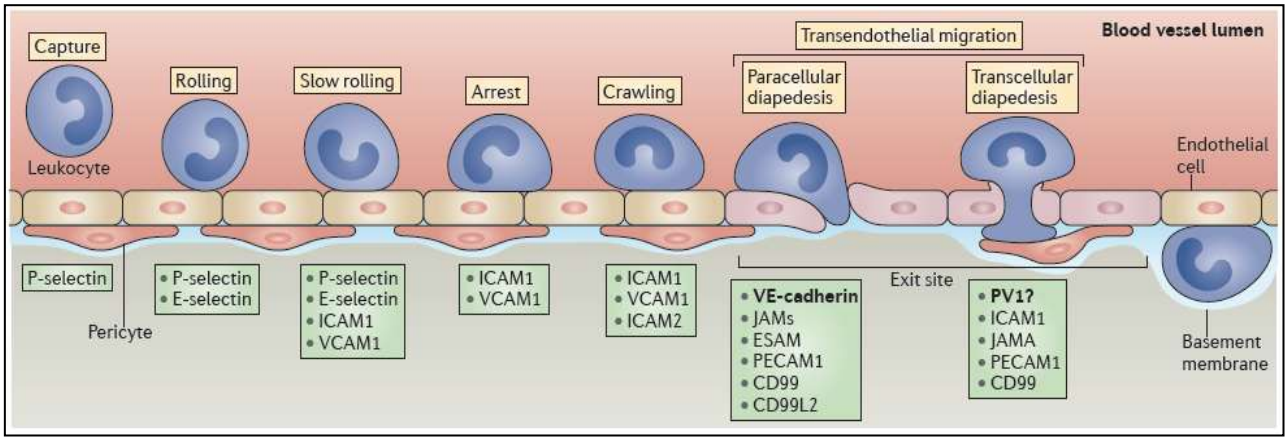

Figure I2. The multistep cascade of leukocyte extravasation. A range of cell adhesion receptors on endothelial cells (green squares) mediates the capture, rolling, arrest and crawling of leukocytes on the luminal endothelial cell surface, prior to the transmigration through the endothelial barrier. Adapted from *Nat Rev Immunol.* 2015; 15: 692-704.

In addition, Syk phosphorylation induced by PSGL-1 interaction with P-sel is required for optimal rolling on P-sel (54) as well as for E-sel-dependent slow rolling of neutrophils and for integrin activation and leukocyte adhesion (55).

1.4 PSGL-1/P-selectin interaction in immune system homeostasis and tolerance

As described above, PSGL-1 engagement activates Syk, triggering an intracellular signaling cascade that permits leukocyte rolling and activation of integrins. In addition, the interaction of PSGL-1 with the three selectins induces its association with Syk through the actin-linking proteins of the ezrin-radixin-moesin (ERM) family, in an ITAM-dependent manner that leads to the activation of the transcription factor cFos, implicated in the gene expression of different interleukins and cytokines, including IL-10 or transforming growth factor beta (TGF-β) (12, 16). In this sense, the intracellular signals elicited by PSGL-1/P-sel interaction trigger a tolerogenic program in human moDCs characterized by the upregulation of IL-10, IDO and TGF-β, and the downregulation of MHC-II and costimulatory molecules such as CD86 and CD40 (16). These tolerogenic DCs promote naïve T cell

differentiation to regulatory T cells (Tregs) in human allogeneic moDC/T cell recognition assays (16). Accordingly, it was demonstrated that mice lacking PSGL-1 have a 33% reduction of the natural Treg population in the thymus (16). A consequence of Treg reduction in PSGL-1 deficient mice would be the disease exacerbation found in these mice under different experimental mouse models of inflammatory disease such as dextrane sodium sulfate (DSS)-induced colitis, scleroderma or lupus-prone Mrl/lpr mouse model (43, 56, 57). More importantly, an autoimmune syndrome which shares multiple characteristics with human systemic sclerosis (SSc) progressively develops in the total absence of PSGL-1(58). Likewise, P-sel absence has also been related to increased inflammation in mice (56, 59), resulting in more severe gromerulonephritis, what could be explained by the lack of tolerance signals elicited by PSGL-1 in leukocytes. PSGL-1 controls proliferation of human hematopoietic progenitors (60, 61) as well as T cell proliferation and exhaustion (39). As a consequence, T cells isolated from PSGL-1 deficient mice show enhanced adhesion and increased proliferation rates and are more effective in clearing viral infections, due to reduced exhaustion of $CD8^+$ T lymphocytes in a $CD4^+$ T lymphocyte-dependent manner (62, 63).

1.5 Other ligands of PSGL-1 and P-selectin

PSGL-1 binds to several chemokines such as CCL19, CCL21 and CCL27, suggesting that PSGL-1 could also regulate chemokine-mediated responses (4, 42, 64). CCL27, a selective chemoattractant for memory T cells to cutaneous sites requires PSGL-1 aminoterminal tyrosine sulfation but not O-glycosilation or N-Glycosilation. (64). CCL19 and CCL21 are constitutively expressed in lymph nodes and their interaction with PSGL-1 contributes to naïve and memory T cells homing to these organs. As in the case of CCL27, O-glycosylation is not necessary for CCL21 binding, but it is not clear whether tyrosine sulfation is required, although the existence of a common binding site for CCL19 shared by PSGL-1 and CCR7 was identified (65). The capability of PSGL-1 to interact with these chemokines has been proposed to synergize with CCR7 signaling in the homing of naïve T lymphocytes to secondary lymphoid organs , provided that activated T cells are less efficient in binding CCL21 and CCL27 (42).

PSGL-1 can also bind to pathogens. PSGL-1 can bind to human enterovirus 71 (66) and it has been described that aminoterminal tyrosine sulfation is necessary for viral infection (67). Moreover, PSGL-1 binds to pneumococcal capsular polysaccharide and amidase LytA, playing a critical role in the recognition, uptake and killing of *Streptococcus pneumoniae* by neutrophils (68). *Staphylococcus aureus* has been proposed to bind PSGL-1, since recombinant SSL5 and SSL11 bind sLe^X moieties of PSGL-1 on leukocytes and, when assayed in vitro, interfere with the binding of neutrophils to P-sel and neutrophil adhesion and rolling (69, 70).

Finally, it has been recently described that soluble Siglec-5, a member of the sialic acid-binding immunoglobulin-like lectin family, is able to bind to PSGL-1 in a Ca^{2+} dependent manner, and can interfere with the rolling of leukocytes on P-sel in vitro and preventing the recruitment of leukocytes to sites of inflammation in vivo (71).

Regarding P-sel, in addition to PSGL-1, CD24 and Pentraxin-3 (PTX-3) have been found to bind P-sel (72, 73).

2. Pulmonary Arterial Hypertension

2.1 Defintion, epidemiology and symptoms

Pulmonary arterial hypertension (PAH) is a rare, progressive and severe disease affecting pulmonary vasculature and heart. The prevalence in the population is around 1.1-2.4 cases per 1 million inhabitants per year (74-76), being women more frequently affected by PAH (2:1) (75, 76). PAH is internationally defined by right-heart catheterization showing precapillary pulmonary hypertension with a mean pulmonary artery pressure (mPAP) of >25 mmHg (77).

Persistent dyspnea on exertion is present in almost all patients even in the presence of mild hemodynamic abnormalities (77, 78), constituting the most frequent symptom of PAH. Fatigue, weakness and worsening dyspnea are associated with disease progression. In the most severe form of PAH, chest pain, syncope, jugular vein extension, and edema are considered signs of right heart failure (77, 78).

2.2 Classification of Pulmonary Hypertension (PH)

In the 2nd World Symposium on PH, held in 1998, a clinical classification was established with the objective of individualizing different categories of PH sharing similar pathological findings, similar hemodynamic characteristics and, similar management (79). This classification is currently used by the United States FDA (Food and Drug Administration) and the European Agency for Drug Evaluation for the labeling of new drugs approved for PH (Table I1).

Group 1 (PAH) agglutinates different forms of precapillary PH with diverse etiologies. First, idiopathic PAH (iPAH) is defined as sporadic disease with neither a family history of PAH nor an identified risk factor (77). Heritable PAH includes all the cases with an identified genetic origin that are associated with a familial history. In Group 1 are also classified PAH variants induced by drug and toxins, as well as PAH cases associated with other syndromes and diseases, such as infectious agents, congenital heart disease and connective tissue diseases.

Groups 2 and 3 comprise postcapillary PH caused by left heart or lung diseases, respectively. Group 4 includes chronic thromboembolic pulmonary hypertension, whereas Group 5 agglutinates other forms of PH with multifactorial mechanisms that are not yet completely understood.

2.3 Pathophysiology

PAH is characterized by distal pulmonary vascular remodeling resulting from endothelial dysfunction, uncontrolled vascular smooth muscle and endothelial cell proliferation, and inflammation

that promotes hypertrophy of pulmonary arteries and luminal obliteration (80) (Figure I3). To reestablish functional blood flow, plexiform structures consisting of microvessels are formed in the lumen of obliterated lung vessels. These pathologic events increase pulmonary vascular resistance and augment pulmonary artery pressure leading to an increment in the hemodynamic load on the right ventricle (RV). To compensate, the RV adapts with an increment in its wall thickness and contractility (81). When the RV is no longer able to adapt its function to the increasing load, death ensues from right heart failure.

1. Pulmonary arterial hypertension (PAH)	1.1 Idiopathic PAH
	1.2 Heritable PAH
	1.2.1 BMPR2
	1.2.2 ALK-1, ENG, SMAD9, CAV1, KCNK3
	1.2.3 Unknown
	1.3 Drug and toxin induced
	1.4 Associated with:
	1.4.1 Connective tissue disease
	1.4.2 HIV infection
	1.4.3 Portal hypertension
	1.4.4 Congenital heart diseases
	1.4.5 Schistosomiasis
1'. Pulmonary veno-occlusive disease and/or pulmonary capillary hemangiomatosis 1''. Persistent pulmonary hypertension of the newborn (PPHN)	
2. Pulmonary hypertension due to left heart disease	
3. Pulmonary hypertension due to lung diseases and/or hypoxia	
4. Chronic thromboembolic pulmonary hypertension (CTEPH)	
5. Pulmonary hypertension with unclear multifactorial mechanisms	5.1 Hematologic disorders
	5.2 Systemic disorders: sarcoidosis, pulmonary histiocytosis
	5.3 Metabolic disorders
	5.4 Others: tumoral obstruction, fibrosing mediastinitis, chronic renal failure, segmental PH

Table I1. Pulmonary hypertension classification. Summarised PH classification according to the 2nd World Symposium on pulmonary hypertension (1998).

2.4 Etiopathogenesis of PAH

a. Genetic factors

Germline mutations in the bone morphogenetic protein receptor 2 (*BMPR2*) gene, a member of the TGF-β signaling family, can be detected in up to 70% of patients with heritable PAH (82-85). Moreover, mutations in *BMPR2* have also been found in 5-40% of patients previously diagnosed of

iPAH (82, 86, 87). However, only 20% of family members carrying *BMPR2* mutations develop PAH, indicating low levels of penetrance of heritable PAH (75, 88).

Apart from *BMPR2*, mutations in other members of the TGF-β signaling pathway have been associated with the development of PAH. Thus, several studies have demonstrated allele variants of *ACVRL1* (89), *ENG* (90), *Smad1*, *Smad4*, *Smad5*, *Smad8*, *Smad9* (91, 92) and *CAV-1*(93) in patients with idiopathic or heritable PAH.

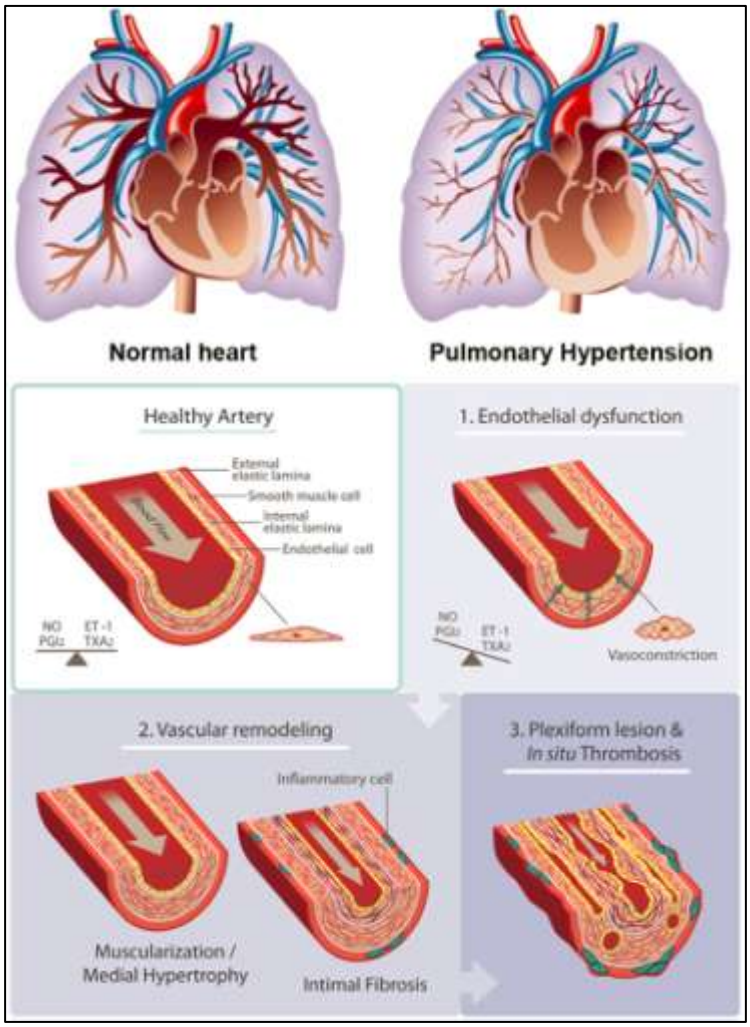

Figure I.3. The pathophysiology of PAH. Cellular changes in PAH. Healthy endothelium regulates the vascular tone to maintain a low-resistance pulmonary vasculature. 1) In PAH, dysfunctional endothelium alters vasodilator/vasoconstrictor balance to increase contractility of pulmonary arteries. 2) Abnormal proliferation of smooth muscle cells leads to muscularization of peripheral pulmonary arteries and medial hypertrophy. Increased proliferation and progressive migration of smooth muscle cells further results in intimal fibrosis. 3) Formation of plexiform lesions and in situ thrombus occlude the vessel lumen. These dysregulated events lead to progressive reduction of the blood flow, thus causing PAH. ET-1 indicates endothelin-1; NO, nitric oxide; PGI2, prostacyclin; and TXA_2, thromboxane A2. Adapted from *Circulation Research.* 2014; 115: 115-130 and the National Center for Chronic Disease Prevention and Health Promotion.

b. Drugs and toxins

Exposure to certain drugs or substances has explained several cases of primary PAH. Aminorex and fenfluramine are anorexigen drugs that promote the release of catecholamines, and both drugs were withdrawn from markets by FDA because of their association with PAH in 1968 (94) and 1997 (95), respectively. Ingestion of toxic rapeseed oil, as the colza oil commercialized in 1981 in Spain, also triggered the development of an aggressive PAH (96). To a lesser extent, benfluorex (95), amphetamines, metamphetamine (97) and the tyrosine kinase inhibitor dasatinib used for the treatment of chronic myelogenous leukaemia (98) have been associated with PAH.

c. Cellular and molecular factors

A number of molecular mechanisms have been shown to play a role in the control of pulmonary pressure and to be deregulated in PAH patients.

Nitric oxide (NO)

NO is a lipophilic gas generated by three different isoforms of nitric oxide synthases (NOS): neuronal (nNOS), inducible (iNOS) and endothelial NOS (eNOS). NOS catalyzes the reaction of L-arginine, NADPH and oxygen which requires iron protoporphyrin IX (haem), tetrahydrobiopterin, FAD, and FMN as cofactors (99) (100):

$$\text{L-arginine} + 2O_2 + 3/2(\text{NADPH} + H^+) \rightarrow \text{NO} + \text{L-citrulline} + 3/2\text{NADP}^+ + 2H_2O$$

NO released by endothelial cells binds its G-protein coupled receptors on the surface of vascular smooth muscle cells (VSMC), activating the cyclic guanosin monophosphate (cGMP) signaling pathway which leads to the increase in intracellular Ca^{2+} levels, Akt phosphorylation and calcineurin activation. In this context, NO is probably the most important endothelium-derived vasodilator, and a key regulator of vascular tone (101). NO also inhibits leukocyte adhesion (102, 103) and platelet aggregation (104), as well as VSMC proliferation and migration (105-108).

In fact, decreased pulmonary vascular eNOS expression/activity has been described in numerous animal models of PH in vivo and in humans with this disease (109). Pulmonary artery endothelial cells from patients with iPAH produce decreased amounts of NO (110) and lungs from patients with PAH have been reported to express reduced levels of eNOS (111). In addition, eNOS knockout mice showed enhanced leukocyte adhesion to vascular endothelium associated with increased expression of P-sel (112), and showed increased RV systolic pressure when exposed to hypoxia (113). Moreover, reduced NO bioavailability has been linked to impaired endothelium-dependent vasodilation and VSMC proliferation (114). In PAH, the reduced NO bioavailability may be explained by eNOS uncoupling, low L-arginine intracellular concentration, increased reactive oxygen species levels or endogenous competitive inhibitors of eNOS (such as asymmetric dimethylarginine) (115).

Phosphodiesterase-5 (PDE-5) inhibitors enhance the antiproliferative and vasodilating effects of endogenous NO by preventing cGMP inactivation by PDE-5 (115, 116).

Prostacyclin (PGI_2)

PGI_2 is an araquidonic acid metabolite vasodilator that is produced by endothelial cells and acts via the cyclic adenosine monophosphate (cAMP) pathway (117).

The expression of the key enzyme for PGI_2 synthesis, PGI_2 synthase, is reduced in pulmonary arteries of patients with PAH, hepato-pulmonary PH, and human immunodeficiency virus (HIV)-associated PH (118). Moreover, production of prostacyclin is reduced in endothelial cells of patients with PAH (119). Furthermore, administration of prostacylcin or its analogs in experimental PH models leads to decreased PAP and RV pressure (120, 121).

Serotonin (5-HT)

Serotonin has been described as an important mediator of PAH, inducing vasoconstriction and VSMC proliferation (122, 123). Indeed, treatment of rats or *BMPR2*$^{-/-}$ mice with serotonin potentiates the effects of hypoxia on mPAP, RV hypertrophy and pulmonary vascular remodeling (122, 124). On the other hand, mice lacking the 5-HT transporter, where platelets (the main reservoir of systemic 5-HT) are depleted of 5-HT, the development pulmonary vascular remodeling in response to chronic hypoxia is reduced (125).

Endothelin-1 (ET-1)

ET-1 is a 21 aa peptide that is produced by cleavage of a larger precursor in endothelial cells, and in smaller amounts in pulmonary artery smooth muscle cells (PASMC) (126) and lung fibroblasts (127). ET-1 biosynthesis is induced by different stimuli, including hypoxia, growth factors, cytokines, shear stress, and thrombin in endothelial cells (128-131). ET-1 binds to two different seven-transmembrane G protein-coupled receptors: endothelin receptor type A (ETA) and type B (ETB) (132, 133). Activation of ETA and/or ETB on vascular smooth muscle cells (134) and fibroblasts (127) mediates vasoconstriction and proliferation (135, 136). On the other hand, activation of ETB receptors on endothelial cells enhances the clearance of circulating ET-1 (up to 80% of circulating ET-1 in lung circulation) (137) and increases their production of PGI_2 and NO (132, 138).

Elevated concentrations of ET-1 in the lung and plasma of human patients and experimental animal models of PAH have been described (135, 139, 140). Both selective and non selective ET receptor antagonists (ERAs) can prevent or attenuate experimental PAH by increasing vasodilation and preventing vascular and right heart hypertrophy (141, 142). In fact, bosentan (a non selective ERA that antagonizes ET-1 binding to both ETA and ETB, blocking irreversibly their activity (143)) was approved by the FDA in 2001 for the treatment of PAH. Selective ETA receptors antagonists, like ambrisentan (144), have been developed because of their potential benefits based on the preservation of the vasodilator and clearance functions specific to ETB receptors, and the prevention of vasoconstriction and cellular proliferation mediated by ETA receptors (144, 145).

Immune system and autoimmunity

There is increasing evidence for the important role of the immune system in the pathogenesis of PAH. For example, circulating levels of several cytokines and chemokines (such as IL-6, IL-1β, TNF-α and MCP-1) are elevated in patients with iPAH and may be associated with a worse clinical outcome (146-148).

In addition, pathogen infections such as schistosomiasis (149), Human Herpes Virus 8 (HHV-8) (150), and HIV (151) have also been associated with higher prevalence of PAH.

Systemic sclerosis (SSc) represents the major cause of connective tissue disease (CTD)-associated PAH (77). The prevalence of PAH among SSc patients has been estimated in several studies, ranging from 2% (152) to more than 25% (153), although the majority of reports established a prevalence of 5-

15% (78, 154-156). With the improvement of renal care, PAH has emerged as the major cause of mortality of SSc patients (77, 157, 158). Interestingly, autoantibodies against the angiotensin II receptor 1 (AT1R) and ETA have been found in patients with SSc-PAH and CTD-associated PAH (159), that could account for the increased activation of these pathways in PAH.

The renin-angiotensin-aldosterone system (RAAS) and PAH

The RAAS plays a pivotal role in maintaining an adequate blood pressure, by regulating sodium and water balance in the kidney, and by increasing systemic vascular resistance on peripheral blood vessels (160).

In the canonic pathway, when blood pressure falls, due to blood loss, dehydration or ventricular pump failure, the juxtaglomerular cells, located next to the afferent arterioles of the renal glomeruli, release renin into the bloodstream. Renin cleaves angiotensinogen, which is secreted by the liver, to angiotensin I (AngI). Once in the circulation, AngI is hydrolyzed to angiotensin II (AngII) by angiotensin converting enzyme (ACE), which is located primarily in the pulmonary and renal endothelium (160) (Figure I4). AngII activates AT1R on endothelial and VSMC to initiate a vasoconstrictor response and stimulate aldosterone synthesis by the adrenal gland (160). In contrast, angiotensin type 2 receptor (AT2R) mediates vasodilation, reduced proliferation, apoptosis and decreased inflammation (161). Aldosterone then binds to its receptors on the renal tubules to initiate sodium and water retention to increase circulating blood volume and, then recovering blood pressure (162).

In addition to the canonical pathway, other vasoactive peptides, receptors and enzymes have been identified to play a role in the physiological functions of the RAAS. Angiotensinogen and angiotensin(1-12) can be cleaved into AngII by some peptidases such as chymase, that is expressed in mast cells, skeletal muscle and endothelial cells (163-166). ACE2, a homologue of ACE, catalyzes the conversion of AngI and AngII to Ang(1-7), an heptapeptide that binds to the Mas receptor and counteracts the vasoconstrictor effects of AngII, without stimulating aldosterone secretion (167).

There is clear evidence that the renin-angiotensin signaling system contributes to the disease pathology. In patients with iPAH, increased levels of renin, AngI, and AngII were observed in association with disease progression and mortality (168). Moreover, ACE expression and activity and increased AT1R signaling have been reported to be elevated in the lung arteries of rats exposed to hypoxia (169, 170) and patients lung tissue (168, 171).

Treatment with ACE inhibitors (enalapril or captopril) or an AT1R antagonist (losartan) delayed disease progression, reduced pulmonary artery pressure, RV hypertrophy and pulmonary vascular remodeling in rats with monocrotaline-induced PAH (168, 169, 172, 173). On the other hand, overexpression or external activation of ACE2 in a monocrotaline (MCT) mouse model was able to prevent the increase in RV pressure and remodeling, as well as pulmonary vessel muscularization (174,

175) and MCT-induced inflammation (176), in an ang(1-7)-Mas receptor interaction-dependent manner (175).

Angiotensin II and inflammation

AngII has also been described as a pro-inflammatory molecule by regulating the expression of cytokines such as IL-12 or TNF-α in monocytes and macrophages as well as the production of NO through the activation of AT1R (177). AngII also promotes the expression of endothelial adhesion molecules such as E-sel, P-sel, Vascular cell adhesion molecule 1 (VCAM-1) and Intercellular adhesion molecule 1 (ICAM-1), facilitating leukocyte rolling and extravasation, increasing inflammation (178). In addition, in inflammatory conditions, local macrophage chemoattractant protein-1 (MCP-1) augments AngII synthesis (179).

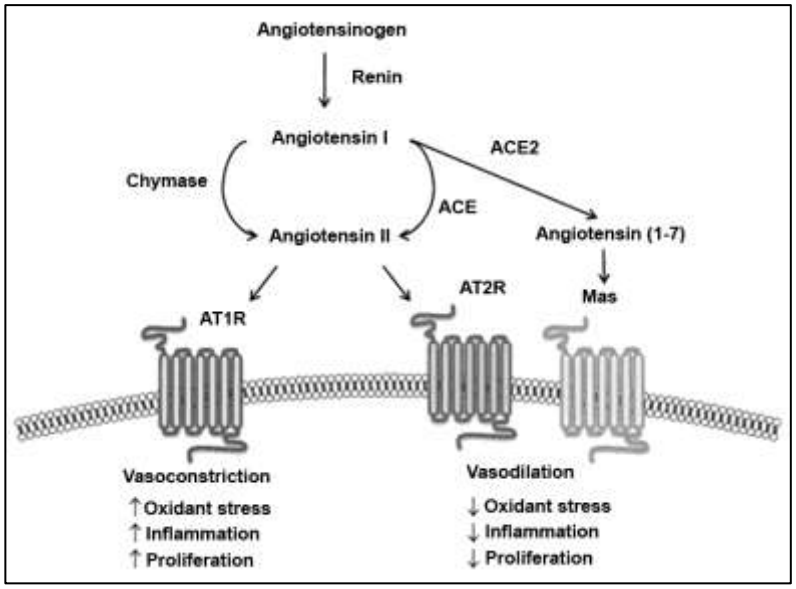

Figure I4. The renin angiotensin system. Angiotensin II may be generated from angiotensin I by the actions of angiotensin-converting enzyme (ACE) or chymase. Angiotensin I may also be cleaved by angiotensin-converting enzyme 2 (ACE2) to yield angiotensin-(1–7). Angiotensin II binds to the angiotensin type 1 receptor (AT1R) and the angiotensin type 2 receptor (AT2R), which have opposing effects on vascular structure and function. Angiotensin-(1–7), which binds to the Mas receptor, is considered vasculoprotective. Adapted from *Pulm Circ*. 2014; 4 (2): 200-10.

3. Systemic lupus erythematosus (SLE)

3.1 Definition, epidemiology, symptoms and treatment

Systemic lupus erythematosus (SLE) is a chronic, inflammatory autoimmune disease characterized by the production of autoantibodies against double stranded DNA (dsDNA) and nuclear antigens, immune complex deposition, complement activation and polyclonal expansion of auto-reactive lymphocytes (180-183).

Interestingly, the incidence of lupus has nearly tripled in the last 40 years, mainly due to improved diagnosis of mild disease (183). The prevalence of lupus ranges from approximately 40 cases per 100,000 persons among Northern Europeans (181) to 73 cases per 100,000 persons in the USA (184). Higher prevalence has been found among black and Asian (185, 186) population in both USA (2.3-fold higher in black persons than in white persons) (184) and Europe (206 per 100,000 persons) (186, 187). Apart from race, SLE is a strongly gender-biased disease. SLE predominantly affects women (6-10:1 ratio of women to men) in the childbearing years (181, 182, 184, 188, 189).

In the last 50-60 years, the life expectancy of SLE patients has improved from an approximate 4-year survival rate of 50% in the 1950s to a 15-year survival rate of 80% today (181), even though since 1959, only one agent (belimumab) has been approved by the FDA for use in SLE (189).

Criteria for SLE classification were developed in 1971 (190), and revised in 1982 (191) and 1997 (192). Further revision was accomplished by the Systemic Lupus International Collaborating Clinics (SLICC) in 2012 (193) (Table I.2). These criteria distinguish patients with the disease in question from those without the disease. The American College of Rheumatology (ACR) classification criteria were developed for clinical studies of lupus to ensure that cases reported in the literature do in fact have the disease. In addition to the wide variety of manifestations, SLE runs an unpredictable course. Clinical manifestations of SLE include inflammation of the skin and internal organs, which are translated into non-specific symptoms like fever, arthralgia, skin rashes and anemia (183, 188). The ACR Criteria are summarized in Table I2. To describe disease activity of SLE patients, a SLE disease activity index (SLEDAI) score has been stablished (194).

Mild lupus treatment includes non steroid anti-inflammatory drugs (NSAIDs), anti-malarial drugs (hydroxychloroquine) and low-dose corticosteroids, whereas more severe forms of SLE are managed with higher doses of corticosteroids and other immunosuppressive agents, such as tacrolimus, azathioprine, methotrexate, cyclophosphamide and mycophenolate mofetil (189, 195). Clinical trials of anti-CD20 antibody (rituximab) have failed to show significant effects, although this therapy has been used off-label to treat refractory cases with success (195). Promising results of a couple of studies targeting the IFN-α pathway have been published. Both sifalimumab (196), a monoclonal antibody that neutralizes IFN-α (Phase IIb) and anifrolumab (197), a type I IFN receptor antagonist (Phase II) were effective in reducing disease activity in association with a reduction in the expression of IFN-regulated genes (195-197). Nevertheless, to date there is not curative treatment for SLE.

3.2 Etiopathogenesis of SLE

SLE etiology is complex and not fully understood nowadays, with intertwined genetic, hormonal and environmental factors contributing to the pathology of this syndrome. These factors lead to an irreversible break in immunological tolerance manifested by immune responses against endogenous nuclear antigens.

Criteria	Definition
Malar rash	Fixed erythema, flat or raised, over the malar eminences, tending to spare the nasolabial folds
Discoid rash	Erythematous raised patches with adherent keratotic scaling and follicular plugging; atrophic scarring occurs in older lesions
Photosensitivity	Skin rash as a result of unusual reaction to sunlight, by patient history or physician observation
Oral ulcers	Oral or nasopharyngeal ulceration, usually painless, observed by a physician
Arthritis	Non-erosive arthritis involving two or more peripheral joints, characterized by tenderness, swelling or effusion
Serositis	a. Pleuritis: convincing history of pleuritic pain or rub heard by a physician or evidence of pleural effusion or b. Pericarditis: documented by ECG or rub or evidence of pericardial effusion
Renal disorder	a. Persistent proteinuria >0.5 g per day or >3+ if quantification is not performed b. Cellular casts: may be red cell, hemoglobin, granular tubular, or mixed
Neurological disorder	a. Seizures*, or b. Psychosis* *in the absence of off ending drugs or known metabolic derangements
Haematologic disorder	a. Hemolytic anaemia with reticulocytosis, or b. Leucopenia: <4000/mm3, or c. Lymphopenia: <1500/mm3, or d. Thrombocytopenia: <100 000/mm3 in the absence of off ending drugs
Immunologic disorder	a. Anti-DNA: antibody to native DNA in abnormal titre, or b. Anti-Sm: presence of antibody to Sm nuclear antigen, or c. Positive finding of antiphospholipid antibodies
Antinuclear antibody	An abnormal titre of antinuclear antibody by immunofluorescence or an equivalent assay at any point in time and in the absence of drugs known to be associated with ‘drug-induced lupus’ syndrome

Table I2. The American College of Rheumatology revised classification criteria for systemic lupus erythematosus

a. Gender and sexual hormones

Since the majority of SLE patients are female, a strong influence of sexual hormones has been postulated as a pivotal component in SLE development. Regarding epidemiologic data, the incidence rates decline to 3:1 in the pre-adolescent population and to 5:1 after menopause, compared with women in the childbearing age (10:1) (198, 199). The X chromosome encodes several immune-related genes, such as CD40L, CXCR3, *O*-linked N-acetylglucosamine transferase, FOXP3, Toll like receptor (TLR) 7, TLR8, IL-2R-γ, tyrosine-protein kinase BTK, and IL-9R (199, 200). Chromosome abnormalities have also highlighted an important role for X chromosome, which is randomly inactivated in early stages of embryogenesis. For example, the prevalence of SLE among Turner syndrome patients (women who bear only one copy of X chromosome) is lower (201). However, among Klinefelter syndrome patients (XXY), the prevalence is 14-fold higher than for age-matched men (202). At the molecular level, 17-β

estradiol acts mainly as an enhancer of humoral immunity, promoting IL-4 and IL-10 secretion (203). Prolactin increases antibody production as well as B cell survival, and triggers IFN-γ and IL-6 secretion (204). On the other hand, testosterone inhibits Th1 and B cell differentiation, antibody production, and NK cytotoxicity (205).

b. Genetic factors

The concordance rate for lupus is 25-70% between monozygotic twins and approximately 1-2% between dizygotic twins (181, 183, 206, 207), indicating that genetic factors are relevant, but not sufficient for the development of SLE.

Genome-wide association studies (GWAS) have confirmed the importance for SLE susceptibility of different genes associated with the immune response and inflammation (*HLA-DR*, *PTPN22*, *STAT4*, *IRF5*, *BLK*, *OX40L*, *FCGR2A*, *BANK1*, *SPP1*, *IRAK1*, *TNFAIP3*, *C2*, *C4*, *CIq*, *PXK*), DNA repair (*TREX1*), adherence of leukocyte to the endothelium (*ITGAM*), and tissue response to injury (*KLK1*, *KLK3*) (180, 183). Among Major Histocompatibility Complex (MHC) genes, HLA-A1, B8, DR2 and DR3, have been linked to lupus (181, 208).

c. Epigenetics

Demethylation or hypomethylation of immune response-related genes in T cells or B cells may contribute to T and B cell hyperreactivity in SLE (209). Aberrant methylation patterns have been found in Gadd45a, CD11a, CD70, perforin and CD40L among other genes, leading to the overexpression of these molecules in T cells and promoting autoantibody production by B cells (180, 209). Regarding drug-induced lupus, it has been associated with inhibition of DNA methyltransferase 1 (Dnmt1) and activation of T cell genes, such as CD11a and CD70 (180).

Some studies in lupus-prone mice suggest that increased activity of histone deacetylases is involved in T cell hyperreactivity in murine lupus (210). Epigenetic mechanisms affecting activation-induced deaminase (AID) may directly contribute to the production of pathogenic anti-dsDNA IgG autoantibodies by B cells (211).

Differences in the methylation status of genes may explain, at least in part, why some identical twins are discordant for SLE. Taking into account that drugs known to induce lupus, such as procainamide and hydralazine may downregulate Dnmt1 levels by inhibiting ERK phosphorilation, epigenetic mechanisms may also represent the missing link between genetic and environmental risk factors (180, 183). Finally, 17β-estradiol downregulates Dnmt1 activity and enhances global DNA hypomethylation in female SLE $CD4^+$ T cells, partially explaining the gender differences in SLE prevalence (212).

d. Environmental factors: infections and drugs

Elevated IFN-α production, mainly by plasmacytoid dendritic cells (pDCs), is a common factor shared by SLE and viral infections (182, 183). The strongest candidate to be involved in SLE

etiopathogenesis is Epstein-Barr virus (EBV) (183, 213), due to its marked lymphotropism and the fact that 100% of multiple sclerosis patients are seropositive for EBV (214). Parvovirus B19, Cytomegalovirus (CMV), HHV-6, HHV-7, HHV-8, Human Papilloma Virus (HPV), among others, have also been associated with SLE (213, 215-220). In general, serological and molecular studies have found antibodies and PCR products related to these viruses at higher levels in SLE patients as compared to controls together with increased viral loads. In some cases, these phenomena have been correlated with disease activity (213).

In the case of EBV, the mechanisms proposed to participate in loss of tolerance and development of autoimmunity are some viral proteins involved in immune evasion and suppression of apoptosis of transformed infected lymphocytes, and molecular mimicry of viral antigens with self antigens (221).

It is well established that certain drugs induce autoantibodies in a significant number of patients, most of whom do not present previous signs of an autoantibody associated disease. Over 100 drugs have been reported to cause drug-induced lupus, including a number of the new biologics and antiviral agents (183).

e. Immune factors

Probably, the main characteristic of SLE is the aberrant immune response against endogenous nuclear antigens. The proposed mechanism regulating the loss of tolerance in SLE is the release of autoantigens by apoptotic cells, which are not successfully cleared and are captured and presented by DCs to T cells, leading to their activation (180, 181, 183) (Figure I5). T cell activation promotes antinuclear antibodies (ANAs) secretion by B cells. ANAs form complexes with nuclear antigens released from apoptotic cells, and deposition of such immune complexes in the capillary bed followed by local complement and leukocyte activation results in destructive tissue inflammation (222).

Autoantibodies

Antibodies directed against dsDNA are highly specific for lupus; constituting a hallmark in the diagnosis of this disease. They are present in 70-96% of patients with lupus but in less than 0.5% of healthy people or patients with other autoimmune diseases such as rheumatoid arthritis (183, 223), and levels of anti-dsDNA antibodies in serum have been correlated with disease activity (224).

Other autoantibodies that are frequently found in blood serum of SLE patients are anti-Sm and anti-RNP. Anti-Sm antibodies, directed against 7 proteins that constitute the common core of U1, U2, U4 and U5 small nuclear ribonucleoprotein (snRNP) particles, are detectable in a percentage of SLE patients ranging between 5 and 30%, or even higher frequencies (225, 226). Studies in North America generally cite a prevalence of around 30% (191), but European studies report lower frequencies of approximately 5% (225, 227). Anti-RNP antibodies react with proteins that are associated with U1 RNA and form U1snRNP. Anti-RNP antibodies are detectable in 13–47% of SLE patients (183, 226).

Additionally to anti-Sm and anti-RNP, other antibodies are commonly found in SLE patients sera, such as anti-Ro, anti-La, anti-phospholipid, anti-α-actinin, anti-NMDA and anti-C1q (181, 183, 228).

Cells and cytokines

The hallmark of SLE is the overproduction of IFN-α by pDCs, and it is considered to play a central role in the initiation and perpetuation of lupus (222). In fact, serologic levels of IFN-α are elevated in SLE patients and correlate with disease activity (229). TLR7 and TLR9, which are two innate endosomal sensors that are specialized in detecting single-stranded RNA and unmethylated CpG DNA, respectively (230); as well as some members of the IRF family (IRF7) are required for IFN-α synthesis by pDCs. Binding of IFN-α to its receptor leads to the upregulation of a large group of genes (more than 300): the α-interferon signature or interferon-stimulated genes (231, 232).

Thus, type I IFNs cause DC maturation and activation, with increased expression of major MHC class I and II molecules and co-stimulatory molecules such as CD80 and CD86 (233). Furthermore, type I IFN stimulates the production of several cytokines by natural killer (NK) cells and monocytes/macrophages/DCs, such as IFN-γ, IL-6, IL-10 and IL-15 (231). Type I IFNs also promote B-cell activation, differentiation, antibody production and Ig isotype class switching. Regarding B cells, B-lymphocyte stimulator (BLyS) and A proliferation-inducing ligand (APRIL) are also upregulated. This upregulation promotes development of both Th1 cells and cytotoxic T cells because of an increase in DC cross-presentation and inhibition of T-cell apoptosis.

Several cytokines have been implicated in lupus pathology. Elevated IL-6 (232, 234) and IL-17 (235-238) serum levels have been found in patients compared with healthy controls (239). Moreover, SLE patients present increased numbers of Th17 cells and double negative T cells (235, 237, 238), which are another important source of Il-17 (240). Elevated IL-6 levels are associated with B-cell hyperactivity and autoantibody production (241) and secretion of IgG anti-dsDNA antibodies. IL-17 is implicated in monocyte and neutrophil recruitment and migration, and also is able to promote B-cell differentiation and autoantibody production (242).

On the other hand, reduced numbers of Tregs, in parallel with reduced expression of IL-2 and IL-2R have been associated with SLE (243). Additionally, the tolerogenic functions of those Tregs are reported to be impaired in SLE patients (235, 244, 245).

Of note, a subset of pro-inflammatory DCs expressing PSGL-1 decorated with an especial 6-sulfo N-acetyl lactosamine (SLAN) modification that impairs selectin binding was described to produce high amounts of IL-12 and IL-23 in response to TLR7 and TLR8 ligands (246, 247). SlanDCs are increased in dermal biopsies of patients with cutaneous lupus and SLE (248), and have been described to enhance Th1 and Th17 responses in psoriasis skin lesions (249).

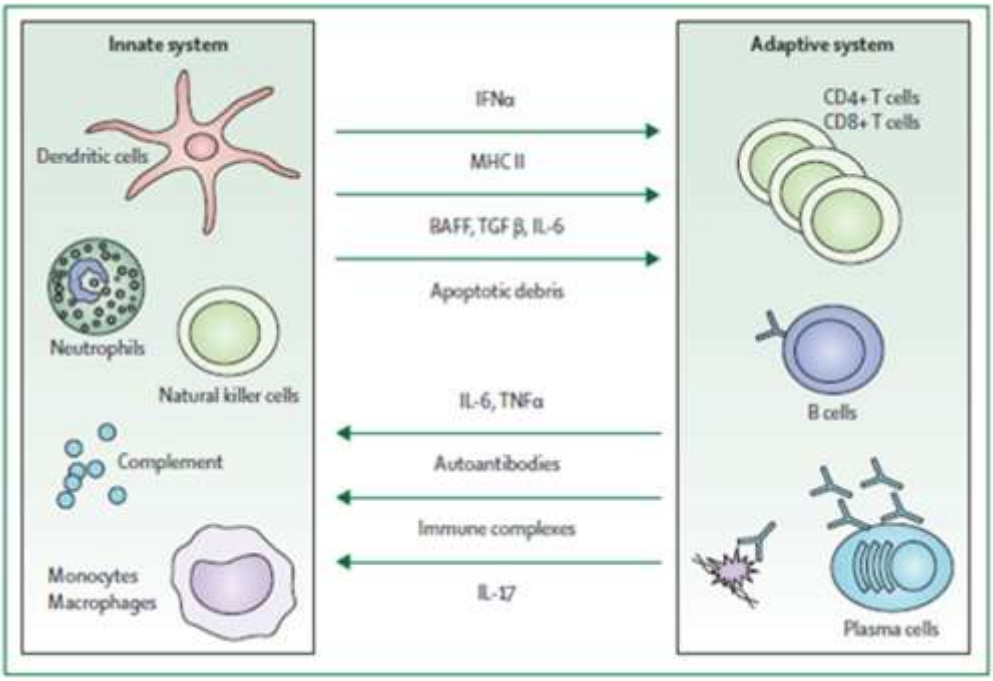

Figure I5. Interplay between innate and adaptive immune systems in SLE. Factors of the innate system activate T and B cells of the adaptive compartment, which feedback into the innate arm to promote and perpetuate immune activation. Central components of the innate system that feed into the adaptive system in SLE include type 1 interferon and other cytokines, MHC II, and apoptotic debris, while important factors from the adaptive system promoting innate responses include proinflammatory cytokines, autoantibodies, and immune complexes. BAFF=B-cell activating factor. IFN-α = Interferon-α. IL = interleukin. TGF-β = transforming growth factor β. TNF-α = tumour necrosis factor α. Adapted from *Lancet.* 2013;382 (9894): 819-31

3.3 Relationship between SLE and P-selectin

P-sel levels are elevated in the urine of SLE patients and correlate with disease severity (250). Genome-wide linkage studies in humans have suggested an important role for P-sel in SLE. Indeed, the P-sel gene is located in the SLE linkage region on human chromosome 1 (1q23) (251, 252). Moreover, variations in the upstream region of P-sel are a risk factor for SLE, and two risk alleles have been identified potentially affecting the transcription of P-sel and the binding to PSGL-1 (251).

3.4 P-selectin and mouse models of SLE

P-sel/PSGL-1 axis is involved in the generation of Treg (16). PSGL-1 null (*Psgl-1*$^{-/-}$) mice have altered tolerance/immunity balance in the colonic lamina propria and skin, and spontaneously develop an autoimmune syndrome similar to human scleroderma (43, 58). Experimental disease models indicate that although mice lacking P-sel, E-sel or both are significantly protected from neutrophil-dependent injury (32, 253, 254), selectin deficiency induces disease exacerbation in models of glomerulonephritis or collagen-induced arthritis, suggesting a protective role for endothelial P-sel in inflammation (32, 59, 255). Numerous murine models of SLE have been described such as MRL/MpJ^{faslpr} (MRL/lpr), BSXB and NZB mice crossed with NZW strains (NZB/W) (256), characterized by high levels of circulating autoantibodies, systemic vasculitis, lymphadenopathy, splenomegaly, skin and renal lesions and early death due to renal dysfunction, hypertension and spontaneous hemorrhage (256, 257). Studies performed with these SLE experimental models described that P-sel deficiency in lupus-prone mice resulted in more rapid development of glomerulonephritis and dermatitis and earlier death (56) and that P-sel levels appear elevated in the urine of lupus-prone mice (250).

Objectives

Objetives

1. To assess whether PSGL-1 deficient mice develop PAH and the molecular mechanisms implicated.

2. To evaluate whether P-selectin absence leads to PAH development.

3. To study the impact of P-selectin deficiency in the immune system homeostasis.

4. To characterize the autoimmune syndrome developed by P-selectin deficient mice.

5. To analyze the expression of P-selectin in patients with cutaneous lupus.

Materials and Methods

Materials and Methods

1. Mice

C57Bl/6 (WT) mice (The Jackson Laboratory) and C57BL/6 *PSGL-1* deficient and C57BL/6 *P-Sel* deficient mice, kindly provided by Dr. M. K. Wild and Dr. D. Vestweber (Max Planck Institute for Molecular Biomedicine, Münster, Germany), were maintained at the Conventional Animal Facility of the School of Medicine of the Universidad Autónoma de Madrid (UAM) (register number ES-28079-0000097) and the Animal Facility of the Centro Nacional de Investigaciones Cardiovasculares (CNIC; Madrid, Spain). Mice were sacrificed by cervical dislocation, and blood and internal organs were extracted for analysis. All experiments and breeding were performed in accordance with national and institutional guidelines for animal care (EU Directive 2010/63/EU for animal experiments). The experimental procedures were approved by the Dirección General de Medio Ambiente of Madrid (Ref: PROEX 69/14, PROEX 162/15 and PROEX375-15)

2. Hypoxia, echocardiography and vascular contractility assays

2.1 Hypoxia Experiments

Female *PSGL-1*$^{-/-}$ and WT mice were exposed to hypoxia (mixture of 10% O_2 and 90% of N_2) for 24 days in an airtight chamber with inflow and outflow valves. Mice were extracted from the chamber to undergo echocardiography at day 10, 18 and 22. At day 24, mice were sacrificed by cervical dislocation.

2.2 Transthoracic Doppler Echocardiography

All transthoracic echocadiography measurements were obtained with an echocardiography system (VEVO 2100, Visualsonics) and an 18-38 Hz ultrasound probe. Chest hair was removed with hypoallergenic depilatory cream and animals were kept anesthetized by continuous influx of 2% isofluorane with an oxygen flow rate of 1.5 l/min. The B-mode was used for morphometric measurement of right ventricle (RV) wall and the pulsed wave Doppler mode was used for measuring the pulmonary acceleration time (PAT) and the ejection time (ET) of blood flow in the pulmonary artery at the level of the pulmonary valve. The PAT/ET ratio was then calculated and used as an indirect evaluation of systolic pulmonary artery blood pressure. The ratio of RV weight to left ventricule (LV) weight plus septum (S) (RV/LV + S) was used as an index of RV hypertrophy (Fulton Index) (258).

2.3 Vascular contractility

Murine pulmonary arteries were carefully dissected free of surrounding tissue and cut into rings (1.8–2 mm length). Vessel segments were mounted on a wire myograph in Krebs physiological solution. Buffer solutions were continuously bubbled with 21% O_2, 5% CO_2, and 74% N_2 (pO2¼ 17–19 kPa)

(259), and stretched to a transmural pressure equivalent to 30 mmHg. Contractility was recorded by an isometric force transducer and a displacement device coupled with a digitalization and data acquisition system (PowerLab). To confirm smooth muscle viability, arteries were first stimulated by raising the K+ concentration of the buffer to 80 mmol/l and then allowed to recover. After washout, arteries were stimulated with serotonin (5-HT) (10^{-8}–10^{-5} mol/l; Sigma-Aldrich) in a concentration-response fashion performed by cumulative addition. Thereafter, concentration-response curves to acetylcholine (Ach) (10^{-9}–10^{-5} mol/l) and sodium nitroprusside (SNP, 10^{-11}–10^{-5} mol/l) were performed by cumulative addition to analyze the endothelium-dependent and endothelium-independent vasodilatation, respectively.

3. Autoantibody assays

Antinuclear antibodies (ANAs) were detected by indirect immunofluorescence. HEp-2 cells and *Crithidia* luciliae were previously fixed on glass slides (Inova Diagnostics). HEp-2 cells were employed for ANA screening and *Crithidia luciliae* were used for anti–double-stranded DNA (anti-dsDNA) antibody screening. Blood sera from WT and *PSGL-1*$^{-/-}$ mice were diluted 1:20 for HEp-2 incubation and 1:10 for *Crithidia luciliae* incubation. Diluted serum samples were incubated for 30 minutes with either HEp-2 cells or *C. luciliae*. Slides were incubated for 30 minutes with goat anti-mouse Alexa Fluor 488 (1:100) (Invitrogen). Circulating autoantibodies were measured by enzyme-linked immunosorbent assay (ELISA) with the specific Quanta Lite kits for SSA, U1 RNP, Sm, Jo-1, and Scl-70 antigens (Inova Diagnostics). Horseradish peroxidase–conjugated goat anti-mouse IgG (H#L) antibody from Pierce Antibodies (Thermo Scientific) diluted 1:2,500 was used as secondary antibody. The cut-off point for positivity on ELISA for a particular autoantibody was determined as the mean value (X) plus two standard deviations (SD) obtained from sera of at least 100 WT mice with an age ranging from1.5 to 24 months. At least 8 mice per group of age were analyzed.

4. UV radiation, histology and Immunohistochemistry

4.1 UV radiation protocol

Three month-old WT and *P-Sel*$^{-/-}$ mice were irradiated with an UVB lamp containing a set of six tubes (Phillips TL UV, 20 W; Royal Philips Electronics) (wavelength ranging from 290 nm to 320 nm), being the energy output at a distance of 15 cm, of 2.5 mW/cm^2. Mice received three doses of 0.306 J/cm^2 every other day for a week, and an additional dose of 0.12 J/cm^2 three days later. Mice were sacrificed 24 hours after the last dose and skin was dissected and processed.

4.2 Histopathological assessment of mouse tissue

Organs and tissues were fixed for 24 hours in 4% formaldehyde and then were preserved in 70% ethanol. Fixed tissues underwent a dehydration process consisting of serial incubations during 30 minutes in solutions with rising ethanol concentrations (70%, 95%, 100%) and liquid paraffin. After

that, processed samples were embedded in paraffin and sliced into 4-µm sections with a manual microtome.

Hematoxylin and eosin (H&E) staining was performed with Harris' hematoxylin (Merck) and Eosin Y (alcoholic solution; Leica Biosystems). Masson's trichrome staining was performed with the automatic Artisan Gomori's Green Trichrome Stain kit (Dako).

4.2.1 Skin: pathological index

Para-midline, upper back skin samples were evaluated blindly to obtain a semiquantitavive measurement by assigning a 3-criteria-based score (260): acanthosis (0, normal; 1, slight thickening of epidermis; 2 and 3, presence of two or three layers of stratum spinosum cells, respectively; 4, presence of four or more layers of stratum spinosum cells); hyperkeratosis (0, normal; 1, one layer of keratin; 2, two layer thick of keratin; 3, minimum three-layer thick of keratin; 4, minimum three-layer thick of keratin and formation of a keratin's plug); hypergrannulosis (0, normal; 1, moderate accumulation of granular dark material in the stratum granulosum; 2 and 3, two or more than three layers of granular dark material; 4, three or more layers of accumulated granular dark material overall section of skin). Finally, the total pathology score was calculated by adding the resulting values for the three criteria.

4.2.2 Kidney: infiltrates and ischemic events

The scouting for inflammatory infiltrates and architectural abnormalities in the mouse kidney was performed on H&E-stained slices. Inflammatory infiltrates were identified as accumulation of little, circular and reactive nuclei. The structural damage parameters considered were: enlargement of Bowmann's space, proliferation of mesothelial cells, glomerular sclerosis, and glomerular atrophy.

The presence of kidney ischemic events (infarcted areas) was assessed in Masson's trichrome-stained sections. Infarcted areas were identified by light blue-stained areas with tissue architecture disruption and fibrosis.

Images were obtained with a Leica DM2500 light microscope and a Leica DFC450 camera. All sections were examined by an observer unaware of sample origin.

4.2.3 Lung: evaluation of non specific interstitial pneumonia (NSIP)

Nonspecific interstitial pneumonia (NSIP) was evaluated in whole H&E-stained lung sections. Increment in interstitial cellularity, thickening of the alveolar walls and structure alteration of the lung parenchyma were considered as NSIP features. We differentiated between 3 stages of increasing NSIP severity: 1) focal NSIP affecting one lobule; 2) the presence of several NSIP foci affecting distinct lobules (generalized NSIP); 3) the presence of one or several large and widespread NSIP areas (diffuse NSIP).

4.3 Immunohistochemistry

4.3.1 Anti α-SMA immunohistochemistry in lung sections

Immunohistochemistry against murine α-smooth muscle actin (α-SMA) was performed in paraffin-embedded lung sections. Paraffin was removed with xylene, sections were rehydrated and antigen retrieval was performed with boiling sodium citrate buffer (10mM Sodium Citrate, 0.05% Tween 20, pH 6.0) during 2 minutes. Endogen peroxidase activity was inhibited by 30 minute incubation with 3% H_2O_2 in methanol. After blocking with phosphate buffered saline (PBS) 1x 4% bovine serum albumin (BSA), sections were incubated with anti-α-SMA 1:250 (Dako) for 2 hours at room temperature. For revealing, Universal LSAB+ Kit Rabbit/Mouse/Goat (DAB+) (Dako) was used. The small blood vessel (diameter of <50 µm) wall thickness was calculated by measuring, with ImageJ (NIH), the internal and total vessel diameter of anti–α-SMA–stained lungs, and calculating the vessel wall area. Then, the mean wall thickness area was calculated.

4.3.2 Anti-CD45 immunohistochemistry in lung sections

Paraffin-embedded lung sections were deparaffinated and rehydrated as described in the previous paragraph, and antigen retrieval was performed with boiling citrate buffer. Endogen peroxidase activity was inhibited by 30 minute incubation with 3% H_2O_2 in methanol. After blocking with PBS 1x 4% BSA, sections were incubated with anti-CD45 1:300 (BD Pharmingen) for 2 hours at room temperature. For revealing, Universal LSAB+ Kit Rabbit/Mouse/Goat (DAB+) (Dako) was used. At least 5 males and 5 females were evaluated per genotype and age.

4.3.3 Immunocomplex detection in skin and renal sections

Skin and glomerular immunoglobulin deposition were evaluated by IHC with an antibody cocktail against Fab regions of IgA, IgG, IgM (1:250) (Abcam). Tissue preparation and antigen retreavel was performed following the protocol described in the previous section, and the primary antibodies were incubated overnight at 4ºC. For revealing, Universal LSAB+ Kit Rabbit/Mouse/Goat (DAB+) (Dako) was used. At least 5 males and 5 females were evaluated per genotype and age.

5. Human skin samples

Skin biopsies from 4 chronic/subacute cutaneous lupus erythematosus (cLE) patients and from 4 aged-matched healthy controls were obtained from the Pathology Department, Hospital de la Princesa (Madrid, Spain). The investigations were conducted in accordance with the principles of the Declaration of Helsinki and were approved by the Clinical Research Ethics Committee of the Hospital de la Princesa, Madrid, Spain (Register number: PI-654, date of approval 07-02-2013). Informed consent was obtained from all the patients and healthy controls.

5.1 Immunohistochemistry of human skin sections

Consecutive tissue sections of sun-exposed skin biopsies underwent immunohistochemistry with the Dako REAL EnVision Detection System Peroxidase/DAB+ kit (Dako), using as primary antibodies anti-human P-selectin (10 µg/ml) (R&D Systems) and anti-human CD31 (1/50) (Abcam). Paraffin was removed with xylene, sections were rehydrated and antigen retrieval was performed with boiling sodium citrate buffer pH 6.0 during 2 minutes. Endogen peroxidase activity was inhibited by 30 minute incubation with 3% H_2O_2 in methanol. After blocking with PBS 1x 4% BSA, sections were incubated with either anti-P-selectin or anti-CD31 for 2 hours at room temperature. After washing, samples were incubated (15 minutes, room temperature) with horseradish peroxidase (HRP)-conjugated secondary antibodies directed against Fc regions of mouse and rabbit immunoglobulins. After washing, DAB (1/50) was added for signal detection. Samples were rehydrated, counterstained with hematoxylin (1 minute) and mounted with water-miscible resin (Eukitt).

The whole biopsies were scouted for blood vessels in a blinded manner. Vessels were identified by positive staining by CD31, localized in the consecutive P-selectin-stained section, and classified depending on the expression of P-selectin as follows:

1) Unstained, negative blood vessels.

2) Partially stained blood vessels.

3) Fully stained blood vessels.

6. Flow cytometry

6.1 Single-cell sample preparation

6.1.1 Spleen

Spleens were dissected and mechanically disrupted in PBS 1X, 0.5% BSA, 5 mM ethylenediaminetetraacetic acid (EDTA). Cell aggregates and undigested pieces of tissue were eliminated by using a 70 µm cell strainer (BD Falcon). Cells were then washed with 25 ml of PBS 1X, 0.5% BSA, 5 mM EDTA and concentrated in 700 µl. Then, samples were filtered again with a 30 µm cell strainer (BD Pharmingen).

6.1.2 Skin and Lung

Skin or lung samples were weighed, minced into ~1 mm^2 pieces and digested for 1 hour with RPMI1640 medium complemented with 1 mg/ml collagenase A (Sigma-Aldrich; San Luis, MI, USA), 2.5 mg/ml dispase II (Roche; Basel, Switzerland) and 40 µg/ml DNase (Sigma). Cell aggregates and undigested pieces of tissue were eliminated by using a 70 µm cell strainer (BD Falcon). Cells were then washed with 25 ml of PBS 1X, 0.5% BSA, 5 mM EDTA and concentrated in 700 µl. Then, samples were filtered again with a 30 µm cell strainer (BD Pharmingen).

6.1.3 Peripheral blood

Blood was extracted by intracardiac injection with a 25G x 5/8 needle (0.5mm x 16mm) (BD Pharmingen). 70 IU of heparin (Sigma) were used to prevent coagulation of 250 µl of blood.

6.2 Antibody staining

Before staining, samples were incubated with 1:200 Fc Block (BD Pharmingen) to saturate Fc receptors on the surface of myeloid cells. Then, samples were incubated with the mix of surface antibodies. After that, cells were permeabilized by 15 minute incubation with 2 ml of FACS Lysing Solution (BD Pharmingen). This solution also lyses erythrocytes and fixes cells. After centrifugation and washing, the cocktail of antibodies directed against intracellular cytokines was added and samples were incubated during 30 minutes at 4 ˚C. Finally, unbound antibody was eliminated by washing with 2ml of PBS 1X, 0.5% BSA, 5 mM EDTA. The list of antibodies used in this thesis is summarized in Table MM1.

Samples were analyzed with a FACSCanto II (BD Pharmingen) and FACS Diva Software (BD Pharmingen).

6.3 Gating strategy

6.3.1 Spleen

Immune cells were identified as $CD45^+$. T cells were identified as $CD3^+$ and were separated into $CD3^+CD4^+$ helper T (Th) cells and $CD3^+CD8^+$ cytotoxic T (Tc) cells.

Follicular Th cells were gated as $CD3^+CD4^+PD\text{-}1^{high}CXCR5^{high}$.

The subpopulations of T cells according to CD44 and CD62L expression were classified as:

- Naïve ($CD44^{neg}CD62L^+$)
- Central Memory ($CD44^+CD62L^+$)
- Effector Memory ($CD44^+CD62L^{neg}$)
- Effector ($CD44^{neg}CD62L^{neg}$)

B cells were identified as low complexity $CD11c^-B220^+$ cells. Among them, germinal centre B cells were gated as $CD11c^-B220^+FAS\text{-}L^+GL\text{-}7^+$. Plasma cells were gated as $CD19^+B220^-IgD^-CD138^+$.

6.3.2 Peripheral bllod

Low complexity $CD3^+$ and $B220^+$ cells were gated as T cells and B cells, respectively. T cell were then classified into $CD3^+CD4^+$ (Th) and $CD3^+CD8^+$ (Tc). $CD11c^-CD11b^+$ cells were gated as monocytes. $CD11c^+$ cells were gated as DC: $CD11c^+$ $CD11b^+$ $B220^-$ were gated as cDCs; and $CD11c^+$ $CD11b^-B220^+$ were gated as pDCs.

Antibody	Fluorochrome	Dilution	Reference	Manufacturer
GL-7	eFLUOR660	1:100	50-5902-82	eBioscience
CD3ε	PE-Cy7	1:100	25-0031-82	eBioscience
CD11c	PE-Cy7	1:100	25-0114-82	eBioscience
FOXp3	FITC	1:100	11-5773-82	eBioscience
IgD	Biotin	1:100	13-5993-82	eBioscience
F4/80	PE-Cy7	1:100	25-4801-82	eBioscience
CD11c	Biotin	1:100	553800	BD Pharmingen
FAS-L	Biotin	1:400	556998	BD Pharmingen
CD3ε	APC	1:100	553066	BD Pharmingen
CD25	APC	1:100	557192	BD Pharmingen
CD45R/B220	APC	1:100	553092	BD Pharmingen
IFN-γ	APC	1:100	554413	BD Pharmingen
IL-4	APC	1:100	554436	BD Pharmingen
IL-17A	APC-Cy7	1:100	560821	BD Pharmingen
CD45.2	BV421	1:100	562895	BD Pharmingen
CD62L	PE	1:100	553151	BD Pharmingen
CD11b	FITC	1:100	553310	BD Pharmingen
CD45.2	FITC	1:100	553772	BD Pharmingen
CD31	BV421	1:100	563356	BD Pharmingen
CD31	APC	1:100	551262	BD Pharmingen
CD138	PE	1:200	553714	BD Pharmingen
CD4	FITC	1:50	130-102-541	Miltenyi Biotec
CD8a	PerCP	1:50	130-102-468	Miltenyi Biotec
CD8a	FITC	1:50	130-102-490	Miltenyi Biotec
CD44	APC	1:50	130-102-563	Miltenyi Biotec
CD45R/B220	APC-Vio770	1:50	130-102-818	Miltenyi Biotec
CD19	VioBlue	1:50	130-103-139	Miltenyi Biotec
MHC-II	APC	1:50	130-102-898	Miltenyi Biotec
MHC-II	PE	1:50	130-102-186	Miltenyi Biotec
CD62P	PE	1:100	130-105-536	Miltenyi Biotec
CD62E	APC	1:100	130-105-468	Miltenyi Biotec
CD4	PE	1:50	22150044	Immunotools
CXCR5	PE/Dazzle594	1:100	145521	BioLegend
PD-1	BV421	1:100	135217	BioLegend
IL-10	PerCP-Cy5.5	1:100	505028	BioLegend
γδ TCR	PerCP-Cy5.5	1:100	118118	BioLegend
Streptavidin	PerCP	1:100	405213	BioLegend

Table MM1. Antibodies used for flow cytometry

6.3.3 Skin

Immune cells were identified as $CD45^+$. T cells were identified as $CD3^+$ and were separated into $CD3^+CD4^+$ (Th) and $CD3^+CD8^+$ (Tc). CD11c+ cells were gated as DC: $CD11c^+CD11b^+B220^-$ were gated as cDCs; and $CD11c^+CD11b^-B220^+$ were gated as pDCs. $CD11c^-B220^+$ cells, with low size/complexity index were considered B lymphocytes. $CD11c^-CD11b^+$ cells were gated as macrophages.

6.3.4 Lung

Immune cells were identified as $CD45^+$. T cells were identified as $CD3^+$ and were separated into $CD3^+CD4^+$ (Th) and $CD3^+CD8^+$ (Tc). Alveolar macrophages were gated as $F4/80^+CD11c^+$ cells. Interstitial macrophages were gated as $F4/80^+CD11c^-$. DCs were gated as $F4/80^-CD11c^+$ cells: cDCs were gated as $F4/80^-CD11c^+B220^-$; and pDCs were gated as $F4/80^-CD11c^+B220^+$. $CD11c^-B220^+$ cells were considered B lymphocytes. In other staining, B lymphocytes were gated as $CD3^-CD19^+$.

7. ELISA of lung samples

The left lung was mechanically disrupted in PBS 1X. After four freeze/thaw cycles to break cell membranes, samples were centrifuged at 5000g and supernatants were recovered. Then, AngII and ET-1 concentrations were measured with specific ELISA kits: Angiotensin II (ANG-II), Mouse, ELISA Kit CSB-E04495m (Cusabio) and Endothelin-1 ELISA kit #17165 (IBL).

8. Western blot

The right lung was frozen, pulverized and lysed in RIPA buffer (1% Triton X-100, 0.24M sodium deoxycolate 10%, 0.35M SDS in 1xTBS) complemented with phosphatase inhibitors. Samples were then centrifuged at 13000 rpm and supernatant was used for assays.

Antibody	Origin	Dilution	Reference	Manufacturer
Anti-ACE	Rabbit	1/1000	LS-C291661/61036	LifeSpan BioSciences
Anti-ACE2	Rabbit	1/1000	NBP1-76614	Novus Biologicals
Anti-AT1R	Rabbit	1/1000	NBP1-77078	Novus Biologicals
Anti-AT2R	Rabbit	1/1000	NBP1-77368	Novus Biologicals
Anti-ET_A	Rabbit	1/1000	NBP1-87467	Novus Biologicals
Anti-ET_B	Rabbit	1/1000	NBP2-16334	Novus Biologicals
Anti-β-actin	Rabbit	1/5000	V4505-100UL	Sigma Aldrich
Anti-Vinculin	Rabbit	1/2000	A5316-100UL	Sigma Aldrich
Anti-eNOS	Mouse	1/1000	610297	BD Pharmingen

Table MM2. Antibodies used for immunoblotting

50µg of protein were loaded in a 13% acrilamide-bisacrilamide gel, and then transferred to a nitrocellulose membrane. Membranes were blocked for nonspecific binding in TBS 1x 5% BSA 0.2% Tween 20 and primary antibodies were incubated overnight at 4ºC. HRP-conjugated goat anti rabbit IgG

secondary antibody was incubated during 1 hour and signal was detected by chemiluminiscence with the LuminataTM Forte Western HRP Substrate (Merck KGaA). Antibodies used for western blot are summarized in Table MM2.

Band intensity was analyzed with ImageJ and results were normalized to the expression of β-actin or vinculin considered as loading controls.

9. Statistical analysis

Statistical significance between two groups was calculated using two-tailed Student's *t* test for parametric variables and Mann-Whitney's U test for nonparametric variables. Statistical significance between three groups in parametric variables was calculated by one-way ANOVA with Bonferroni post hoc test. The chi-squared (df=1) test was used for statistical comparison of frequencies. Mantel-Cox chi-squared (df=1) test was used to analyze survival data. Differences were considered statistically significant with $p<0.05$ (*) and highly significant at $p<0.01$ (**) and $p<0.005$ (***). All statistical analyses were performed using SPSS 15.0 program (IBM). Graphic representations of skin pathology score and association between ENAs and urine parametres were performed with GraphPad Prism 6 (Graphpad).

Results

Results

1. Assessment of PAH development in PSGL-1 deficient mice and the molecular mechanisms implicated

1.1 *PSGL-1*$^{-/-}$ mice exhibit remodeling of pulmonary small vessels

Immunohistochemical staining of lung sections from wild-type (WT) and *PSGL-1*$^{-/-}$ mice with an antibody against α-smooth muscle actin (αSMA) revealed a thicker medial wall of small vessels in *PSGL-1*$^{-/-}$ lung (Figure R1A). Quantification demonstrated a significant increase of the relative wall area in almost all groups of *PSGL-1*$^{-/-}$ vessels independently of age (Figure R1B), becoming twice as thick in *PSGL-1*$^{-/-}$ animals as in WT, especially in aged animals (Figure R1B).

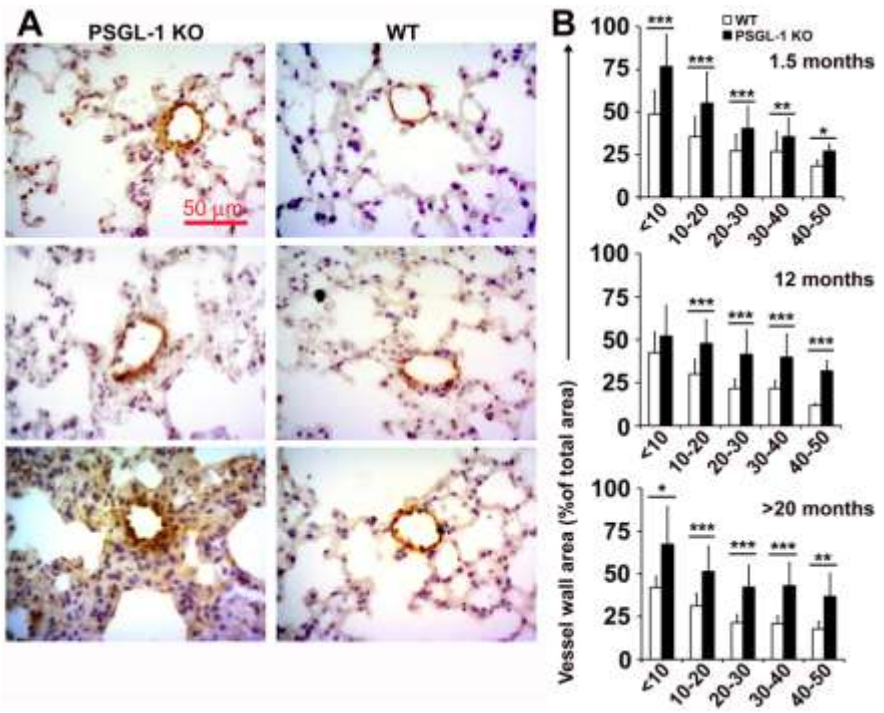

Figure R1. Vascular remodeling in pulmonary small vessels of *PSGL-1*$^{-/-}$ mice. (A) Representative microphotographs (40x) of anti-αSMA-immunostained lung sections of 1.5, 12 and >20-month-old mice (n = 5–6 per group). Scale bar = 50 µm. **(B)** Percentage of vessel wall area in <50 µm-diameter pulmonary blood vessels at 1.5, 12 and >20 months of age (>150 vessels analyzed for each group of age). Data are expressed as the mean ± SD. *P < 0.05, **P < 0.01, ***P < 0.005, by 2-tailed Student's t test.

1.2 *PSGL-1*$^{-/-}$ mice present altered echocardiographic parameters consistent with PAH

Given the remodeling observed in the lung small vessels and our previous observation of an elevated rate of death in *PSGL-1*$^{-/-}$ mice after reaching one year of age (58), echocardiography and Doppler were used to measure parameters that change to adapt RV to the increasing vascular load in high pulmonary pressure, including PAT/ET ratio and RV wall thickness. Follow-up transthoracic Doppler echocardiography performed on WT and *PSGL-1*$^{-/-}$ mice at the age of 14, 18 and 22 months showed an increased pulmonary artery pressure detected by a reduction in PAT/ET in 14-month aged female *PSGL-1*$^{-/-}$ mice as compared with WT mice, which was maintained throughout the longitudinal study (Figures R2A-C and R3A). Interestingly, this was not observed in male *PSGL-1*$^{-/-}$ mice (Figure R3A). Likewise, we found remodeling of RV consisted in an increased ventricular wall thickness in aged female *PSGL-1*$^{-/-}$ mice that was statistically significant at 14 months (Figure R3B).

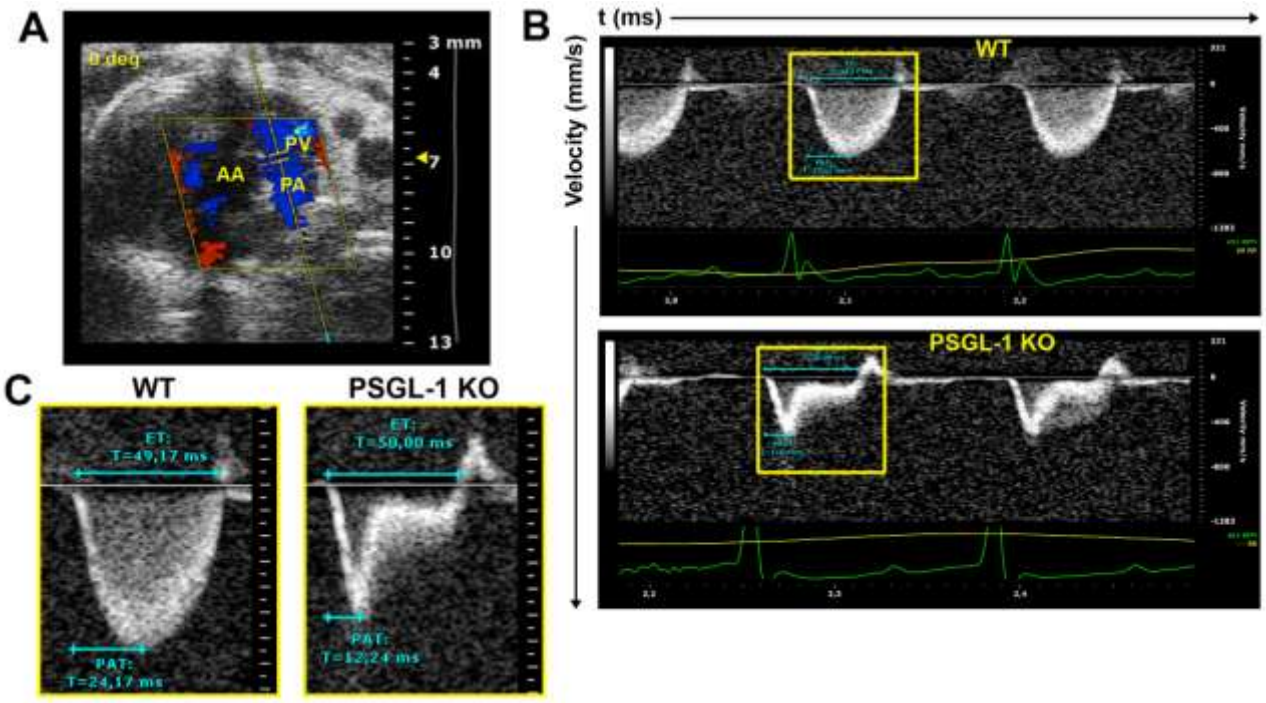

Figure R2. Echocardiographic plane for PAT/ET measurement. (A) B-Mode showing the echocardiographic plane used for Doppler pulmonary flow acquisition. PV=pulmonary valve; PA=pulmonary artery; AA=ascending aorta. **(B)** Representative Doppler pulmonary artery flow of aged female WT and *PSGL-1*$^{-/-}$ mice. **(C)** Magnification of a representative Doppler wave from WT and *PSGL-1*$^{-/-}$ mice. Data are expressed as the mean ± SD. **P* < 0.05, ***P* < 0.01, ****P* < 0.005, by 2-tailed Student's t test.

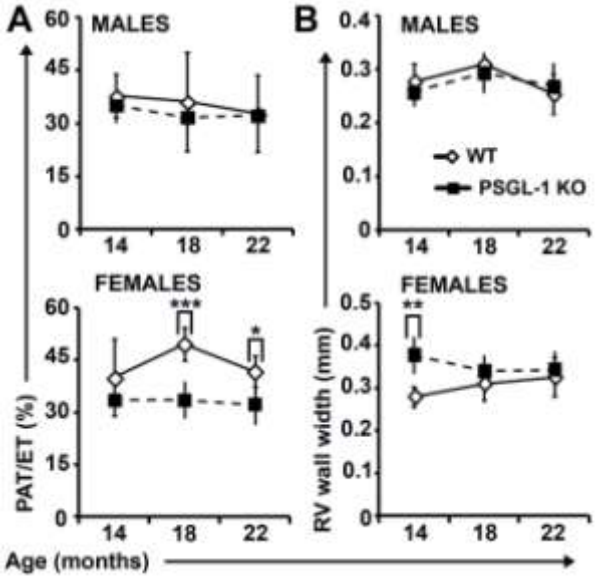

Figure R3. RV echocardiographic parameters of PAH in *PSGL-1*$^{-/-}$ mice. **(A-B)** Longitudinal study of PAT/ET **(A)** and RV wall thickness **(B)** in male and female WT and *PSGL-1*$^{-/-}$ mice at 14, 18 and 22 months of age (*n* = 5 mice per group). Data are expressed as the mean ± SD. **P* < 0.05, ***P* < 0.01, ****P* < 0.005, by 2-tailed Student's t test.

To determine the age at which the elevation in pulmonary artery pressure takes place, periodical echocardiography was performed on WT and *PSGL-1*$^{-/-}$ female littermates between the ages of 1.5 and 18 months. Recurrent tendency to reduced PAT/ET ratio was observed in animals from 3 months of age (Figure R4A). Because a group of three *PSGL-1*$^{-/-}$ females died between 15 and 18 months of age, we differentiated the dead and survivor groups. The group of *PSGL-1*$^{-/-}$ mice that died prematurely showed

increased pulmonary artery pressure detected by a reduced PAT/ET ratio as compared not only with WT mice, but also with the surviving group of *PSGL-1*$^{-/-}$ mice (Figure R4A). Surviving *PSGL-1*$^{-/-}$ mice maintained PAT/ET ratio below that observed in WT mice along their life. At 18 months, animals were sacrificed and the Fulton index was calculated for each mouse. Surviving female *PSGL-1*$^{-/-}$ mice presented a higher Fulton index than their female WT littermates (Figure R4B).

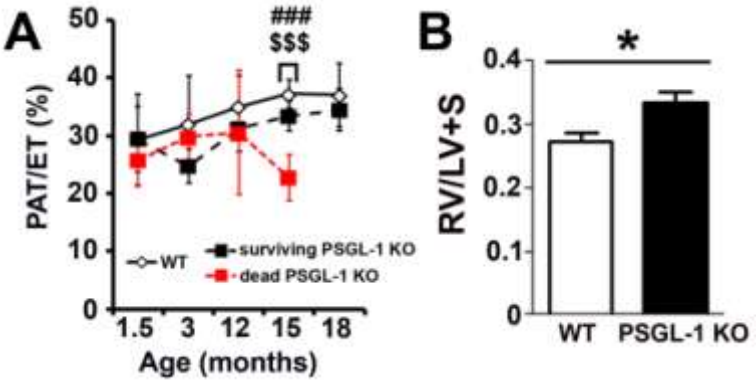

Figure R4. PAT/ET and Fulton index measurement in WT and *PSGL-1*$^{-/-}$ female mice. **(A)** Longitudinal study of PAT/ET between 1.5 and 18 months of age in WT mice (n = 4), surviving *PSGL-1*$^{-/-}$ mice (n = 6) and *PSGL-1*$^{-/-}$ mice dying prematurely (n = 3). **(B)** Fulton index (RV/LV+S) measured in WT and surviving *PSGL-1*$^{-/-}$ mice. Data are expressed as the mean ± SD. * WT vs surviving *PSGL-1*$^{-/-}$; # WT vs dead *PSGL-1*$^{-/-}$; $ surviving *PSGL-1*$^{-/-}$ vs dead *PSGL-1*$^{-/-}$ mice, by one-way ANOVA with Bonferroni *post hoc* test.

1.3 Decreased endothelial NO-dependent relaxing response in pulmonary arteries from *PSGL-1*$^{-/-}$ female mice

We next assessed vascular reactivity in pulmonary and mesenteric arterial rings using wire myography. When compared with littermates WT females, pulmonary arteries isolated from female *PSGL-1*$^{-/-}$ mice showed increased vasoconstriction in response to 80 mM KCl (Figure R5A), whereas the contractile response to serotonin (5-HT) was similar (Figure R5B). The vasodilating response to acetylcholine (Ach) was impaired in *PSGL-1*$^{-/-}$ arterial rings (Figure R5C); however, the addition of an external NO donor (SNP) was sufficient to fully relax both WT and *PSGL-1*$^{-/-}$ arterial rings (Figure R5D). Conversely, vascular reactivity was not different between mesenteric arterial rings of *PSGL-1*$^{-/-}$ and WT littermates (Figures R5E and R5F), suggesting that the endothelial dysfunction is not systemic.

1.4 Reduced pulmonary endothelial NO production in *PSGL-1*$^{-/-}$ mice

The percentage of NO-producing lung endothelial cells was reduced in aged *PSGL-1*$^{-/-}$ mice (Figures R6A and R6B), although this was significant only among the highest NO-producing endothelial cell subset (Figures R6A and R6C). Additionally, the mean fluorescence intensity (MFI) for the NO-sensing probe diaminorhodamine-4M acetoxymethyl ester (DAR-4M AM) was lower in lung endothelial cells of *PSGL-1*$^{-/-}$ than of WT mice (Figure R6D). These changes were not observed in 3-month-old mice

1.5 Unaltered eNOS expression in the lung of *PSGL-1*$^{-/-}$ mice

Given the reduced NO production by *PSGL-1*$^{-/-}$ lung endothelial cells, eNOS protein expression was measured in lung lysates and no differences were found between WT and *PSGL-1*$^{-/-}$ females (Figures R7A and R7B).

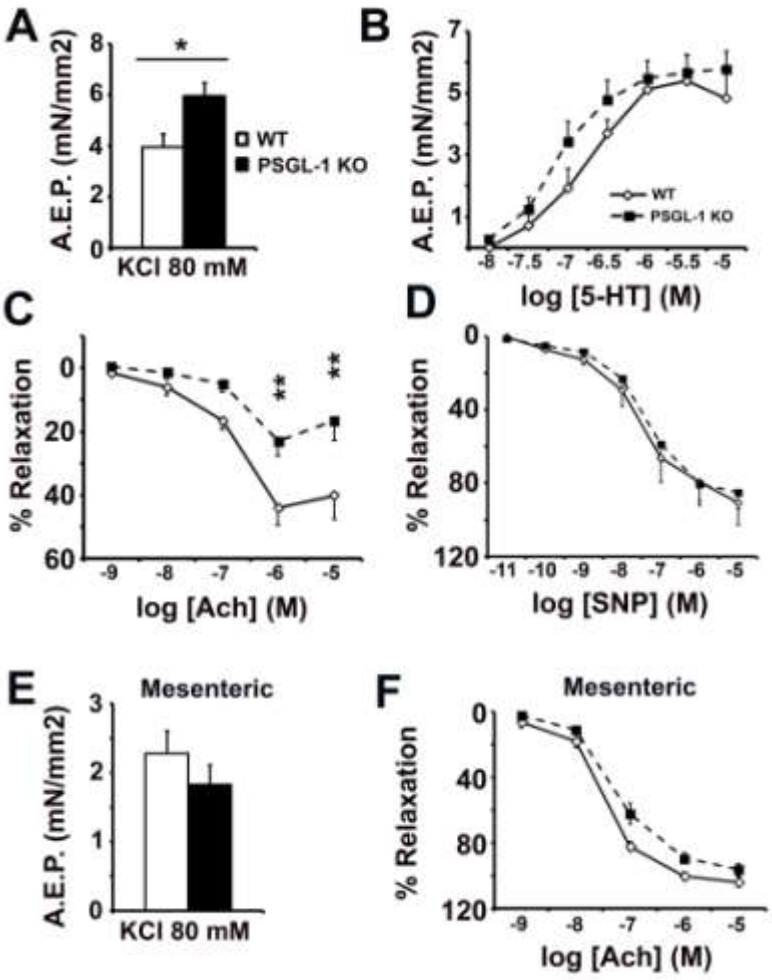

Figure R5. Vascular response to vasoconstrictor and vasodilator agents. (A-B) Contractile response to KCl **(A)** and serotonin **(B)** in pulmonary arterial rings obtained from 18-month-old female WT and *PSGL-1*$^{-/-}$ mice. A.E.P.: Active Effective Pressure. **(C-D)** Vasodilating response to acetylcholine **(C)** and SNP **(D)** in pulmonary arterial rings obtained from 18-month-old female WT and *PSGL-1*$^{-/-}$ mice. **(E** and **F)** Vascular response of mesenteric arterial rings to KCl **(E)** and acetylcholine **(F)** obtained from 18-month-old female WT and *PSGL-1*$^{-/-}$ mice. Data are expressed as the mean ± SD. **P* < 0.05, ***P* < 0.01 by 2-tailed Student's t test.

1.6 Impaired adaptation of *PSGL-1*$^{-/-}$ females to chronic hypoxia

Exposure to chronic hypoxia (10% O_2) killed 40% (2 out of 5 animals) of *PSLG-1*$^{-/-}$ mice during the first week, and surviving animals showed decreased PAT/ET ratio as compared with WT littermates (Figure R8A). The Fulton index at day 24 was similar between WT and *PSGL-1*$^{-/-}$ mice (Figure R8B). *PSGL-1*$^{-/-}$ lung arteries showed a trend toward a greater vasoconstriction response to 5-HT than those of WT animals, but differences did not reach statistical significance (Figure R8C). The relaxing response to Ach was lower in PA from WT mice exposed to hypoxia (Figure R8D) than from WT mice in normoxia (Figure R5C). Thus, after hypoxic exposure, the relaxation induced by Ach was similar between WT and *PSGL-1*$^{-/-}$ arteries (Figure R8D). Likewise, the relaxation in the presence of an external NO donor was similar in WT and *PSGL-1*$^{-/-}$ lung arteries (Figure R8E).

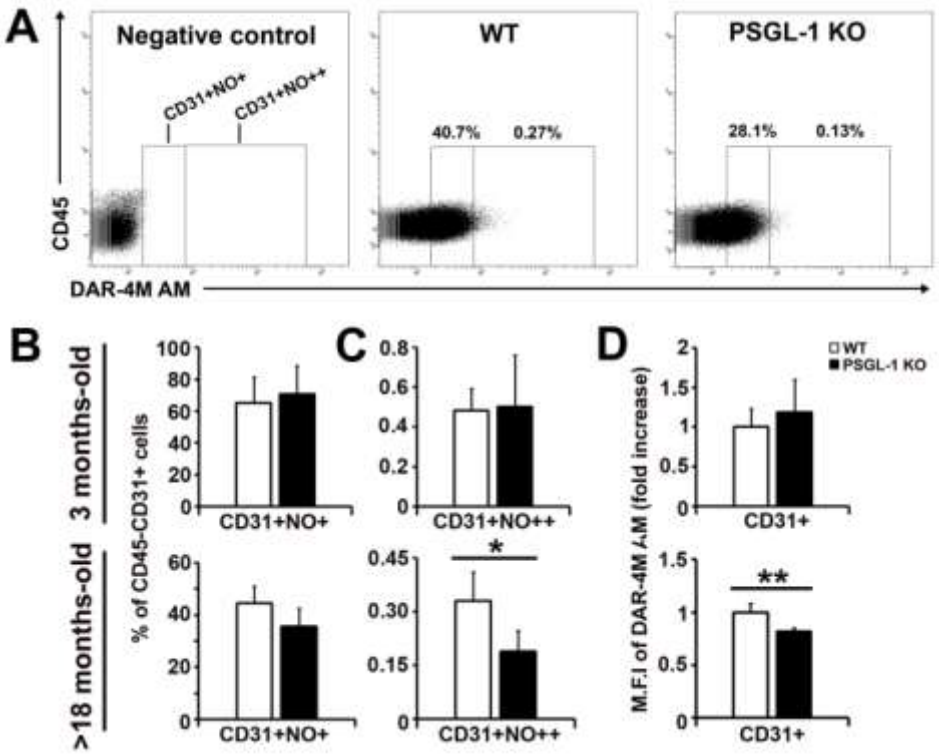

Figure R6. Quantification of NO production by lung endothelial cells. (A) Representative dot plots showing DAR-4M AM fluorescent lung endothelial cells ($CD45^{neg}CD31^{+}$) from WT and *PSGL-1*$^{-/-}$ female mice. **(B-C)** Percentage of lung endothelial cells producing moderate **(B)** or high **(C)** amounts of NO measured in 3 and >18-month-old female WT and *PSGL-1*$^{-/-}$ *mice*. **(D)** Fold change of medium fluorescence intensity (M.F.I.) for the NO-sensing probe DAR-4M AM measured in lung endothelial cells of 3 and >18-month-old female WT and *PSGL-1*$^{-/-}$ mice. Data are expressed as the mean ± SD. **P* < 0.05, ***P* < 0.01 by 2-tailed Student's t test.

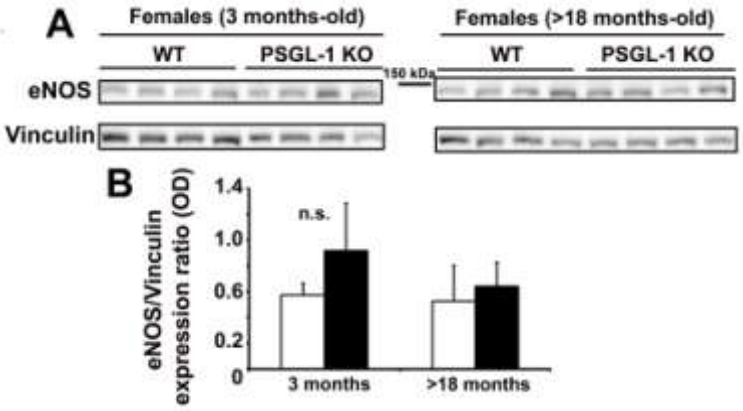

Figure R7. Quantification of pulmonary eNOS expression. (A-B) Western blot showing eNOS expression in the lungs of female WT (*n*=4) and *PSGL-1*$^{-/-}$ (*n*=4) mice **(A)** and its densitometry quantification **(B)**. Vinculin was used as loading control. Data are expressed as the mean ± SD. Non significant (n.s.) differences were found by Mann-Whitney's U test.

1.7 Reduced endothelin-1 concentration in the lung of aged *PSGL-1*$^{-/-}$ mice

As ET-1 is a key mediator involved in PH, we measured its level in lung tissue of young *PSGL-1*$^{-/-}$ and WT female mice and found no differences; however, it was reduced in aged male and female *PSGL-1*$^{-/-}$ mice (Figure R9). No significant differences were found for endothelin-1 receptor A (ETA) and B (ETB) protein expression between WT and *PSGL-1*$^{-/-}$ females (Figures R10A and R10B).

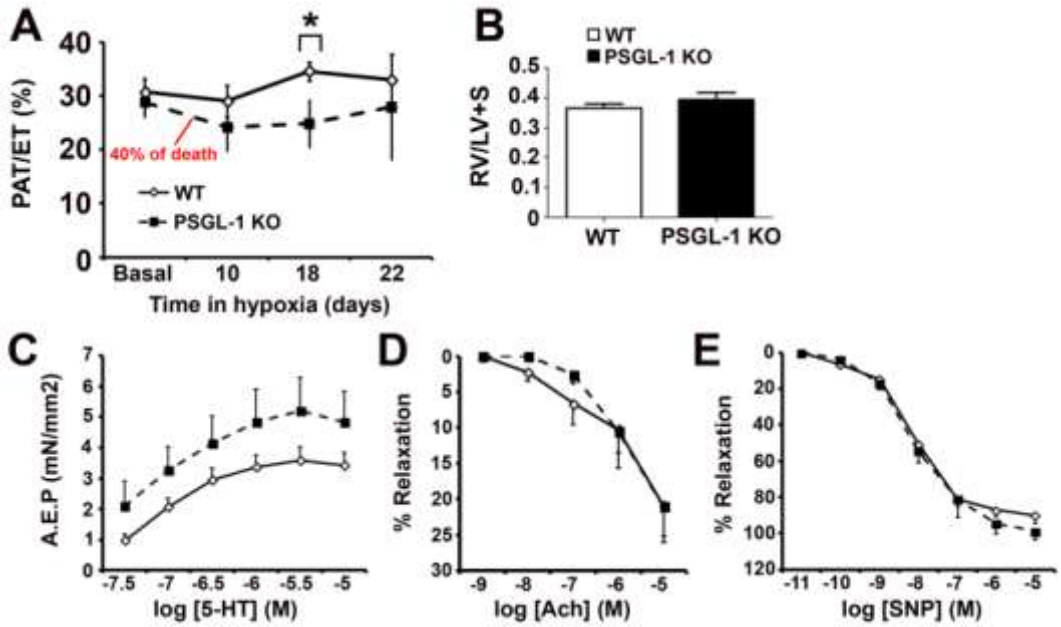

Figure R8. Effects of 24-day exposure to 10% O_2 on WT and *PSGL-1*$^{-/-}$ mice. (A) PAT/ET measures from basal to day 22 of hypoxia in female WT (n = 4) and surviving *PSGL-1*$^{-/-}$ (n = 5) mice. In red: percentage of dead *PSGL-1*$^{-/-}$ mice before day 10. **(B)** Fulton index calculated at day 24 of hypoxia. **(C)** Contractile response to serotonin of pulmonary arterial rings obtained from female WT and *PSGL-1*$^{-/-}$ mice exposed to hypoxia. **(D-E)** Vasodilating response to acetylcholine **(D)** and SNP **(E)** of pulmonary arterial rings obtained from female WT and surviving *PSGL-1*$^{-/-}$ mice exposed to hypoxia. Data are expressed as the mean ± SD. **P* < 0.05 by 2-tailed Student's t test.

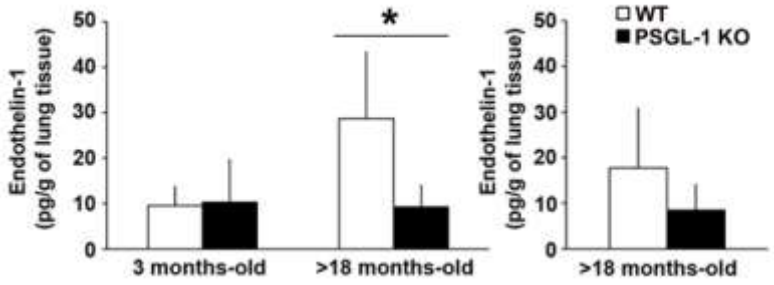

Figure R9. Endothelin-1 concentration in the lung of WT and *PSGL-1*$^{-/-}$ mice. ET-1 concentration in lung lysates of WT (n = 4) and *PSGL-1*$^{-/-}$ (n = 4) mice. Data are expressed as the mean ± SD. **P* < 0.05 by Mann-Whitney's U test.

1.8 Aged *PSGL-1*$^{-/-}$ female mice present increased pulmonary levels of AngII and reduced expression of AT2R

No differences were found in the pulmonary concentration of AngII between young WT and *PSGL-1*$^{-/-}$ females; however, AngII was significantly higher in aged *PSGL-1*$^{-/-}$ female mice (78.02±28.09 pg/g lung tissue) than in aged WT mice (48.70±5.13 pg/g lung tissue) (Figure R10, left panel). By contrast, AngII levels in aged males were similar between the two genotypes (Figure R11).

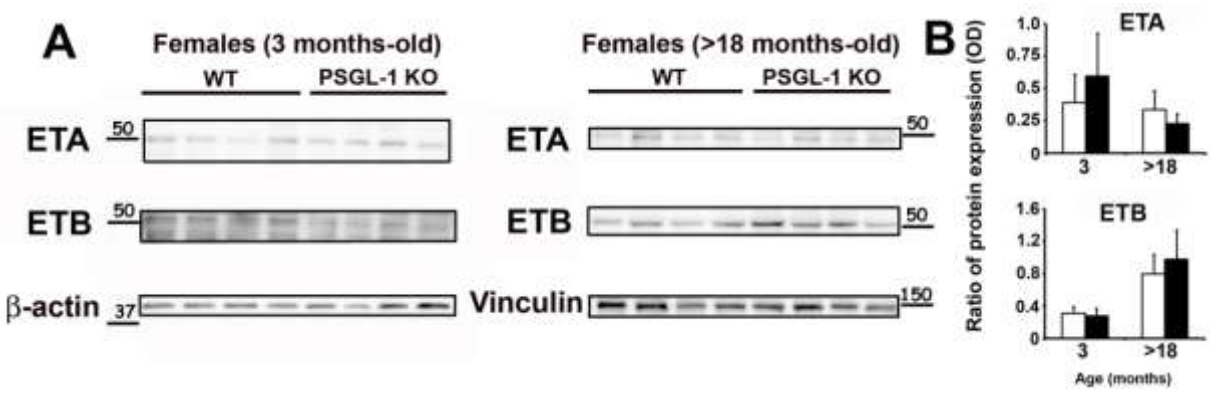

Figure R10. Expression of endothelin receptors in lungs of WT and *PSGL-1*$^{-/-}$ mice. (A) Western blot showing ETA and ETB expression in the lungs of female WT (n = 4) and *PSGL-1*$^{-/-}$ (n = 4) mice and **(B)** densitometry quantification. β-actin and vinculin were used as loading controls. Data are expressed as the mean ± SD. *P < 0.05 by Mann-Whitney's U test.

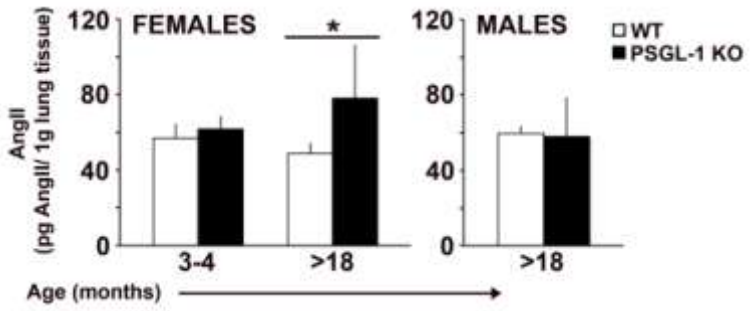

Figure R11. Angiotensin II concentration in the lung of WT and *PSGL-1*$^{-/-}$ mice. (A) AngII concentration in lung lysates of WT (n = 4) and *PSGL-1*$^{-/-}$ (n = 4) mice. Data are expressed as the mean ± SD. *P < 0.05 by Mann-Whitney's U test.

Although not statistically significant, the expression of ACE was lower both in young and aged *PSGL-1*$^{-/-}$ females than in WT (Figure R12A). Levels of ACE2 were similar between WT and *PSGL-1*$^{-/-}$ females (Figure R12B).

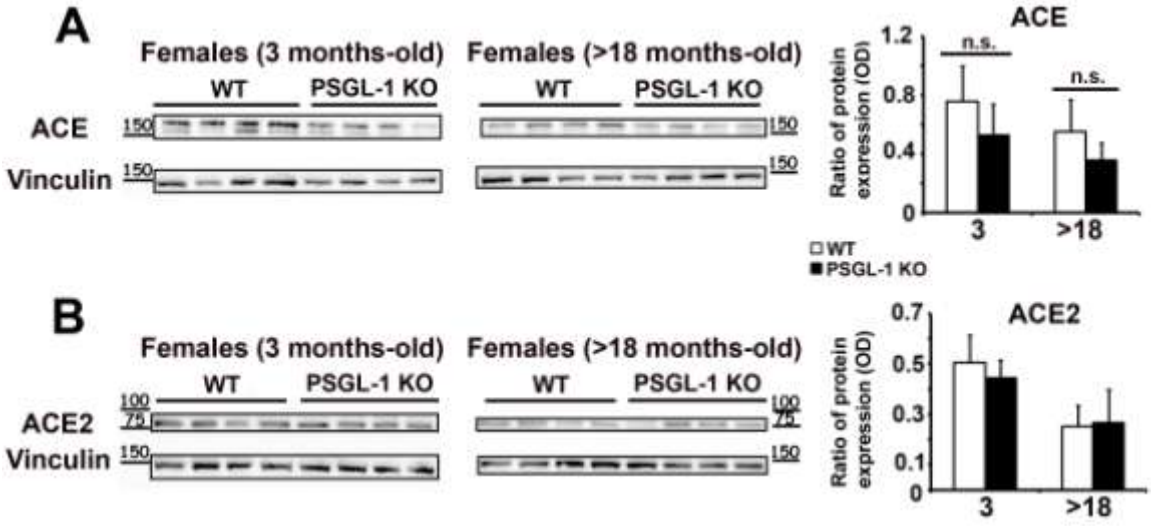

Figure 12. ACE and ACE2 expression in the lung of WT and *PSGL-1*$^{-/-}$ mice. (A-B) Immunoblots showing ACE **(A)** and ACE2 **(B)** levels in the lungs of female WT (n = 4) and *PSGL-1*$^{-/-}$ (n = 5) mice, and densitometric quantification (right panels). Vinculin was used as loading controls. Data are expressed as the mean ± SD. *P < 0.05 by Mann-Whitney's U test.

Regarding AngII receptors, the expression of AT2R was lower in young (WT: 0.227±0.088 vs KO: 0.089±0.024) and aged *PSGL-1*$^{-/-}$ females than in WT (WT: 0.337±0.094 vs KO: 0.189±0.072) (Figure R13A), whereas no differences were found for the expression of AT1R (Figure R13B).

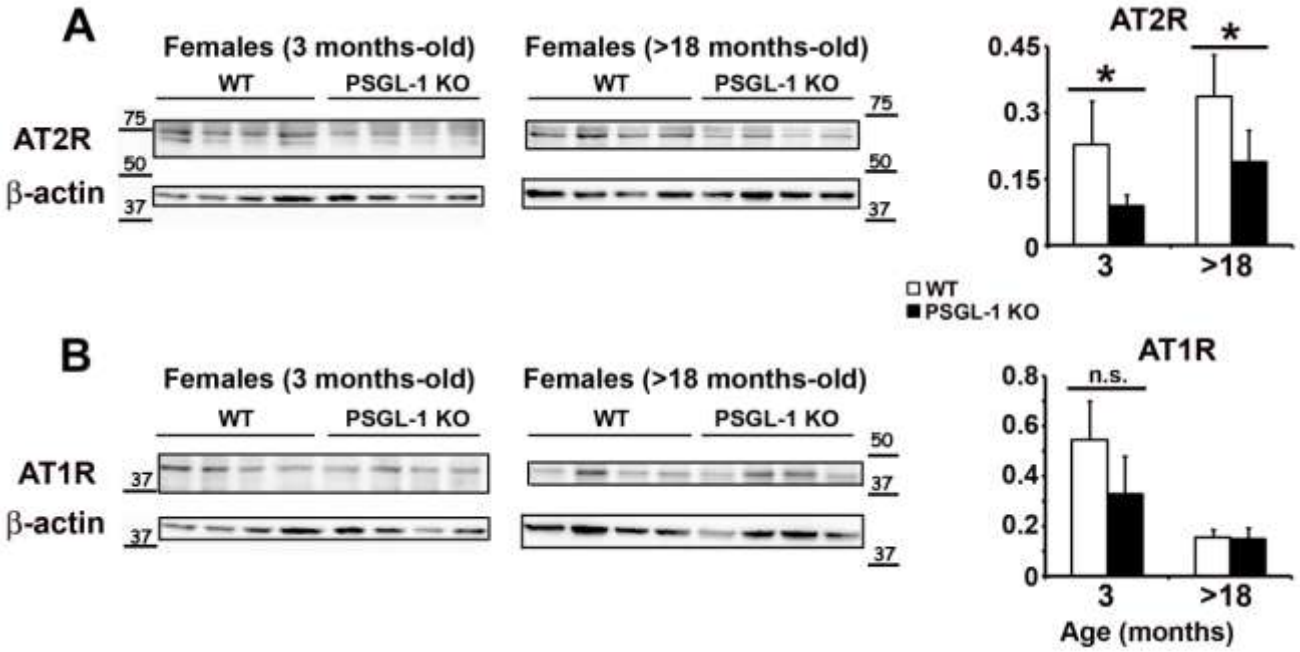

Figure R13. AT1R and AT2R expression in the lung of WT and *PSGL-1*$^{-/-}$ mice. (A-B) Immunoblots showing AT2R **(A)** and AT1R **(B)** levels in the lungs of female WT (n = 4) and *PSGL-1*$^{-/-}$ (n = 5) mice, and densitometric quantification (right panels). Vinculin was used as loading controls. Data are expressed as the mean ± SD. *P < 0.05 by Mann-Whitney's U test.

1.9 Gamma-interferon (IFN-γ) producing T cells, B cells and macrophages are overrepresented in the lung of aged *PSGL-1*$^{-/-}$ female mice

Analysis of the resident lung immune system in WT and *PSGL-1*$^{-/-}$ females revealed that the percentages of T and B cells producing IFN-γ were already higher (FigureS R14A and R14B) in young *PSGL-1*$^{-/-}$ females than in WT, becoming statistically significant in aged mice. IL-10^{+} T cells were reduced in *PSGL-1*$^{-/-}$ lungs, and IL-17^{+} T and B cell subpopulations were similar between WT and *PSGL-1*$^{-/-}$ females (Figures R14A and R14B).

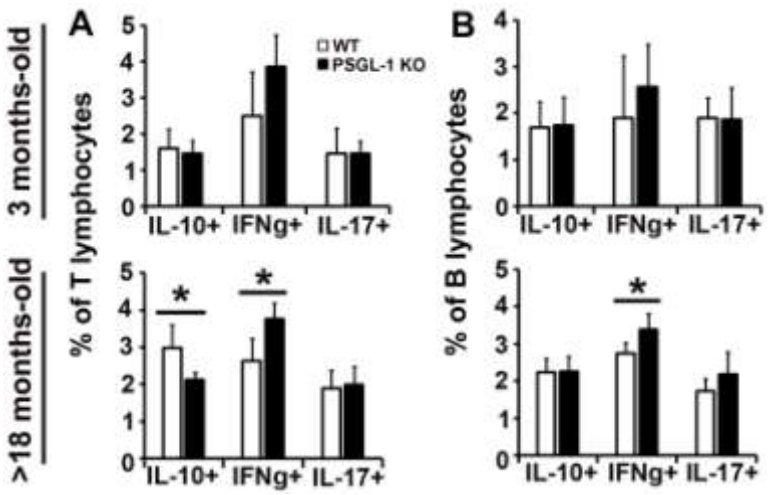

Figure R14. Cytokine production by pulmonary T and B cells of WT and *PSGL-1*$^{-/-}$ mice. (A) Percentage of T lymphocytes producing IL-10, IFN-γ, IL-17 in 3 and >18-month-old WT and *PSGL-1*$^{-/-}$ female mice. **(B)** Percentage of B lymphocytes producing IL-10, IFN-γ, IL-17 in 3 and >18-month-old WT and *PSGL-1*$^{-/-}$ mice. **P* < 0.05 by 2-tailed Student's t test.

Moreover, the percentage of IFN-γ^{+} cells in the alveolar macrophage subset was higher in young *PSGL-1*$^{-/-}$ females than in WT (Figures R15B and R15C) and a higher percentage of IFN-γ^{+} interstitial macrophages was found in aged *PSGL-1*$^{-/-}$ females as compared with WT mice (FigureS R15B and R15D).

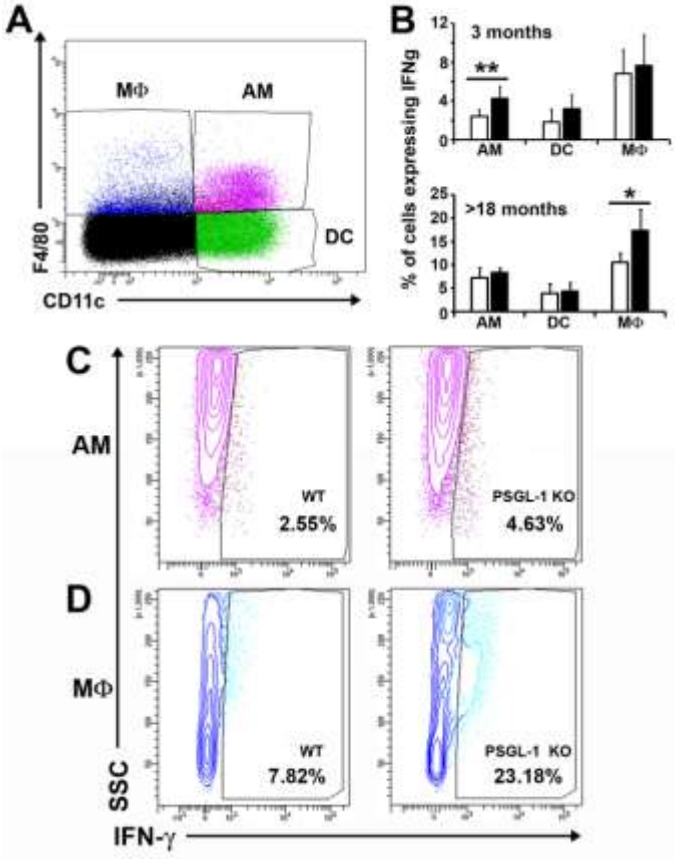

Figure R15. IFN-γ production by pulmonary DC and macrophage populations of WT and *PSGL-1*$^{-/-}$ mice. (A) Dot plot illustrating the classification of macrophage and DC populations according to the expression of F4/80 and CD11c markers. **(B)** Percentage of macrophages and dendritic cells producing IFN-γ in 3 and >18-month-old WT and *PSGL-1*$^{-/-}$ mice. **(C)** Representative dot plots showing IFN-γ producing AM and MΦ of aged WT and *PSGL-1*$^{-/-}$ female mice. AM: alveolar macrophages; DC: dendritic cells; MΦ: interstitial macrophages.**P* < 0.05, ***P* < 0.01 by 2-tailed Student's t test.

According to the increased IFN-g production by T cells, B cells and alveolar or interstitial macrophages, increased frequencies of P-sel and E-sel expressing cells were found among lung endothelial cells (CD45^{neg}CD31^{+}) (Figures R16B-D). However, the percentage of total endothelial cells was similar between WT and *PSGL-1*$^{-/-}$ female mice (Figure R16A).

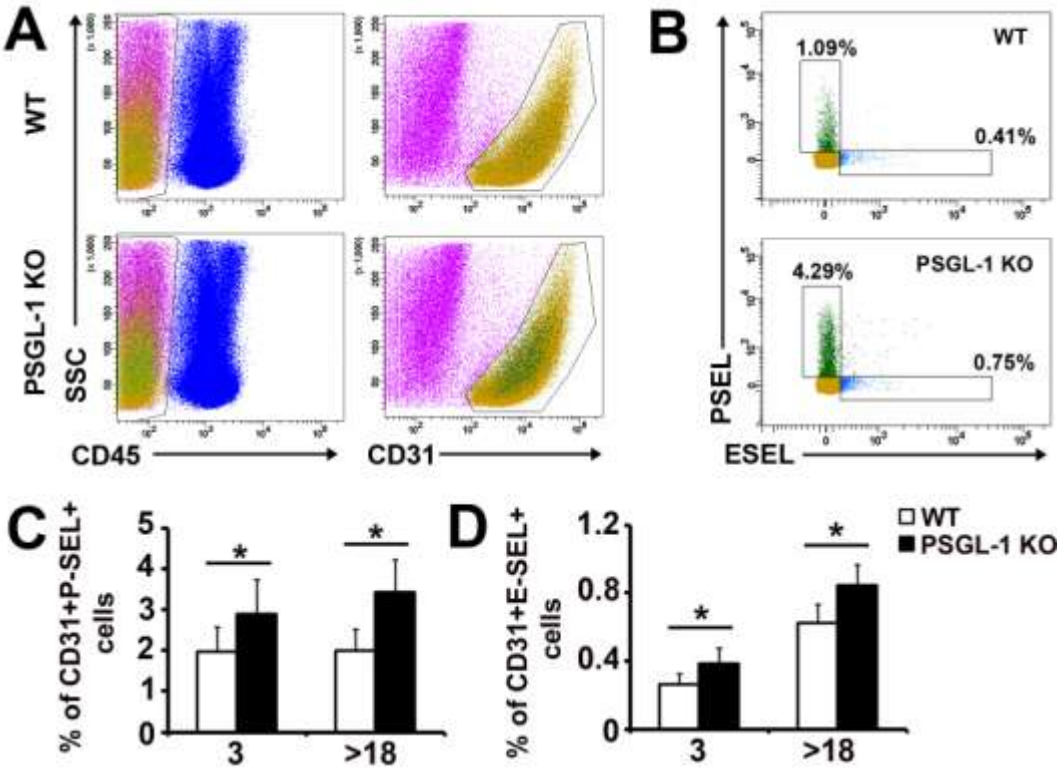

Figure R16. Lung endothelial cell expression of P- and E-selectin in WT and *PSGL-1*$^{-/-}$ mice. (A) Dot plots showing the gating strategy of CD45^{neg}CD31^{+} endothelial cells. (B) Representative dot plots of P- and E-selectin expression in lung endothelial cells of aged WT and *PSGL-1*$^{-/-}$ female mice. **(C-D)** Percentages of lung endothelial cells expressing P-selectin **(C)** or E-selectin **(D)** of 3 months-old and >18 months-old WT and and *PSGL-1*$^{-/-}$ female mice. **P* < 0.05, by 2-tailed Student's t test.

2. Evaluation of PAH development in P-selctin deficient mice

2.1 PAH development and low NO production by lung endothelial cells in aged P-selectin deficient female mice

As PSGL-1 requires binding to P-sel for triggering the tolerogenic program, we wondered whether P-selectin knockout mice (*P-sel*$^{-/-}$) also presented signs of PAH. To achieve this issue, follow-up transthoracic Doppler echocardiography was performed on WT and *P-sel*$^{-/-}$ mice at the age of 14, 18 and 22 months, revealing an increased pulmonary artery pressure detected by a reduction in PAT/ET in 18 and 22-month aged female *PSGL-1*$^{-/-}$ mice as compared with WT mice (Figure R17A). This reduction was observed in neither WT nor *P-sel*$^{-/-}$ male mice. At 18 months, 2 out of 5 female *P-sel*$^{-/-}$ mice had died, explaining the decrease in RV wall thickness from 14 to 18 month-old *P-sel*$^{-/-}$ female mice (Figure R17B).

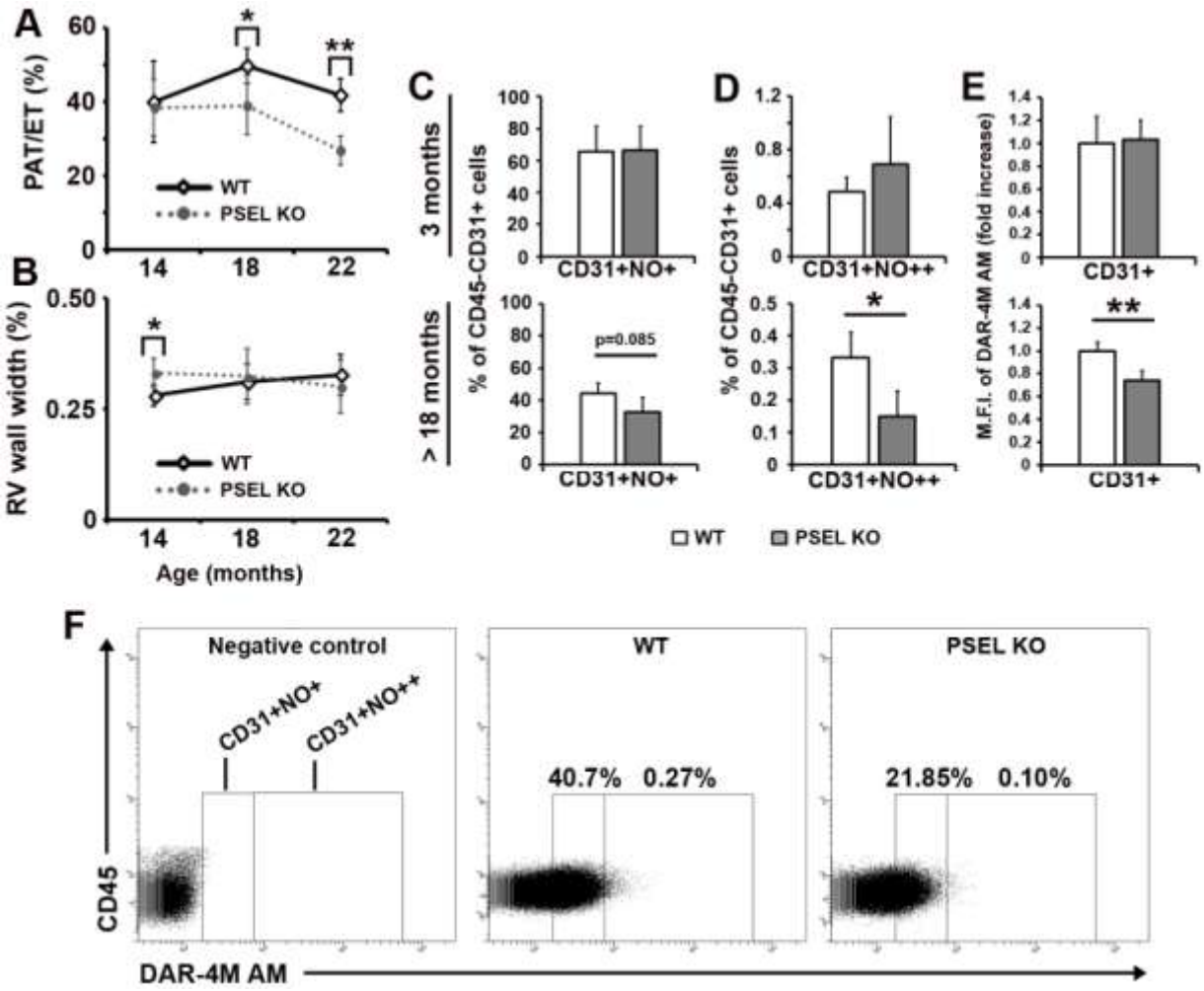

Figure R17. Echocardiographic PAH signs and reduced NO production by lung EC in aged *P-sel*$^{-/-}$ female mice. (A-B) Longitudinal study of PAT/ET **(A)** and RV wall thickness **(B)** in male and female WT and *P-sel*$^{-/-}$ mice at 14, 18 and 22 months of age (n = 5 mice per group). **(C-D)** Percentage of lung endothelial cells producing moderate **(C)** or high **(D)** amounts of NO measured in 3 and >18-month-old female WT and *P-sel*$^{-/-}$ *mice*. **(E)** Fold change of medium fluorescence intensity (M.F.I.) for the NO-sensing probe DAR-4M AM measured in lung endothelial cells of 3 and >18-month-old female WT and *P-sel*$^{-/-}$ mice. **(F)** Representative dot plots representing DAR-4M AM fluorescent lung endothelial cells ($CD45^{neg}CD31^{+}$) from WT and *P-sel*$^{-/-}$ female mice. Data are expressed as the mean ± SD. *P < 0.05, **P < 0.01 by 2-tailed Student's t test.

Coinciding with the reduction of PAT/ET, that indicates PAH, diminished levels of NO production by lung endothelial cells were found in aged *P-sel*$^{-/-}$ female mice (Figures R17C-F). As in *PSGL-1*$^{-/-}$ mice, reduced percentages of NO^{+} and NO^{++}endothelial cells were detected in lung single cell suspensions of aged *P-sel*$^{-/-}$ female mice (Figures R17C, R17D and R17F). Moreover, the mean fluorescence intensity for the NO-sensing probe was also reduced in *P-sel*$^{-/-}$ lung endothelial cells (Figure R17E).

3. Impact of P-selectin absence in the immune system homeostasis

In this thesis, we have previously described that, like *PSGL-1*$^{-/-}$ female mice, *P-sel*$^{-/-}$ females develop PAH and endothelial dysfunction with aging. As PAH is one of the most severe manifestations of connective tissue diseases, we wondered whether *P-sel*$^{-/-}$ presented some kind of connective tissue-related disease.

3.1 Presence of circulating autoantibodies in *P-sel*$^{-/-}$ mice

We first analyzed the presence of circulating autoantibodies and found that sera from *P-sel*$^{-/-}$ mice contained anti-cytoplasmic and anti-nuclear autoantibodies with a speckled or mitotic pattern (Figure R18A), but not anti-centromere autoantibodies. ELISA identified several extractable nuclear antigens (ENAs) recognized by these autoantibodies, including topoisomerase I (Scl-70), U1-RNP, Sm and t-RNA synthetase (Jo-1) (Figure R18B).

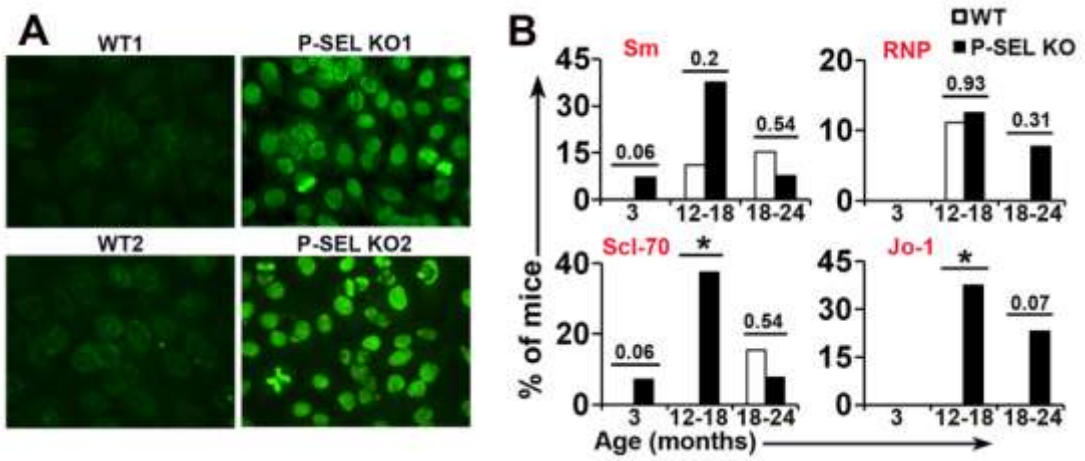

Figure R18. Spontaneous generation of autoantibodies related to CTD in *P-sel*$^{-/-}$ mice. (A) Representative immunofluorescence photomicrographs of HEp-2 cells incubated with serum from 2 independent wild-type (WT) and 2 independent *P-sel*$^{-/-}$ mice. **(B)** Percentage of mice positive for anti-Sm, RNP, Scl-70 and Jo-1 autoantibodies (n=8-10 animals per group); *p<0.05 by Chi-square test.

Sera were also positive in the Crithidia assay for anti-dsDNA autoantibodies (Figure R19), a hallmark of human lupus erythematosus (3, 32, 33). The anti-Sm, anti-topoisomerase I, and anti-dsDNA antibodies could be already detected at 3 months of age. The autoantibodies were co-expressed in the same animals and the percentage of mice with autoantibodies increased as a function of age, reaching a maximum at 12-18 months (Figure R18B) and decreasing at 18-24 months, especially anti-Sm and anti-Scl-70 (Figure R18B). The prevalence of anti-dsDNA autoantibodies increased gradually with ageing, from 10% in the 3-month-old group to 30% in the 18-24-month-old group (Figure R19).

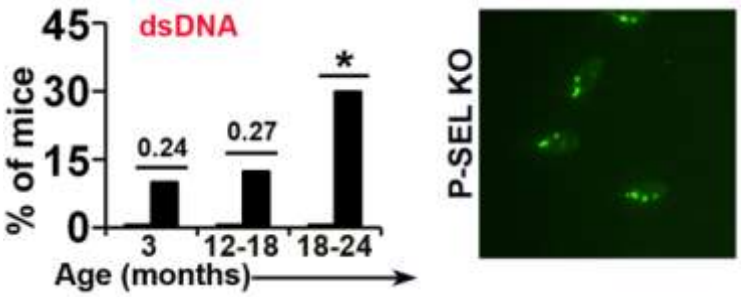

Figure R19. Presence of anti-dsDNA autoantibodies in *P-sel*$^{-/-}$ mice. Percentage of mice positive for anti-dsDNA autoantibodies (n=8-10 mice per group); *p<0.05 by Chi-square test. Immunofluorescence photomicrographs of *C. luciliae* incubated with serum of a *P-sel*$^{-/-}$ mouse (right panel).

3.2 Augmented splenic reactivity of *P-sel*$^{-/-}$ mice

Consistent with this exacerbation of humoral immunity, we observed a remarkable spleen enlargement in both male and female 1.5-3-month-old *P-sel*$^{-/-}$ mice (Figures R20A and R20B), which has been described previously in lupus-prone mouse strains (261, 262). Considering the increased cellularity and the increased number of splenic B cells of 3 month-old *P-sel*$^{-/-}$ spleens (Figures R20C and R20D), we analyzed by flow cytometry the follicular helper T cell (Tfh), the germinal centre (GC) B cell and the plasma cell subsets.

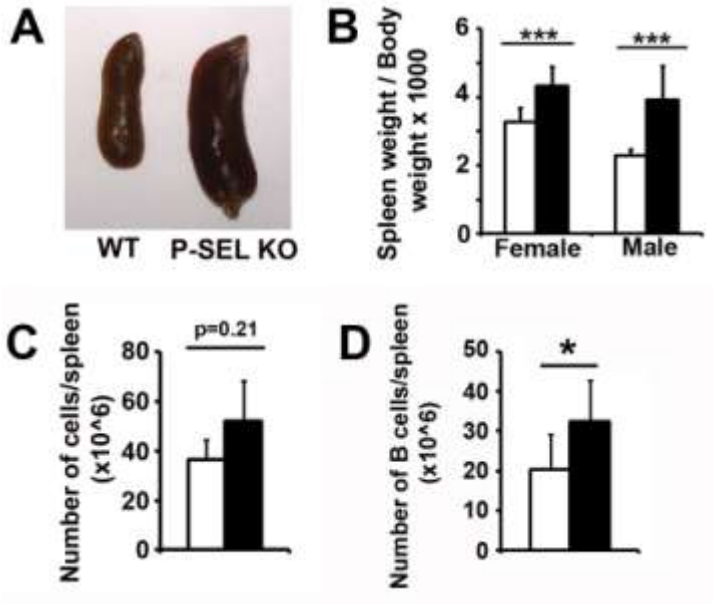

Figure R20. Splenomegaly in *P-sel*$^{-/-}$ mice. (A) Photograph of representative spleens of 1.5-3-month-old WT and *P-sel*$^{-/-}$ mice. **(B)** Spleen weight/body weight ratio of female and male 1.5-3-month-old WT and *P-sel*$^{-/-}$ mice (n=6 mice per group). **(C-D)** Total number of cells **(C)** and B cells **(D)** per spleen of WT and *P-sel*$^{-/-}$ mice. *p<0.05; ***p<0.005 by Student's two-tailed t-test. Bars show the mean±standard deviation (SD).

The Tfh cell compartment ($CD3^+CD4^+$PD-1highCXCR5high) was augmented in the spleen of *P-sel*$^{-/-}$ mice (Figures R21A-C), with a significant increase in the percentage (Figure R21B) and a tendency to increased total numbers (Figure R21C) of Tfh cells in knockout mice.

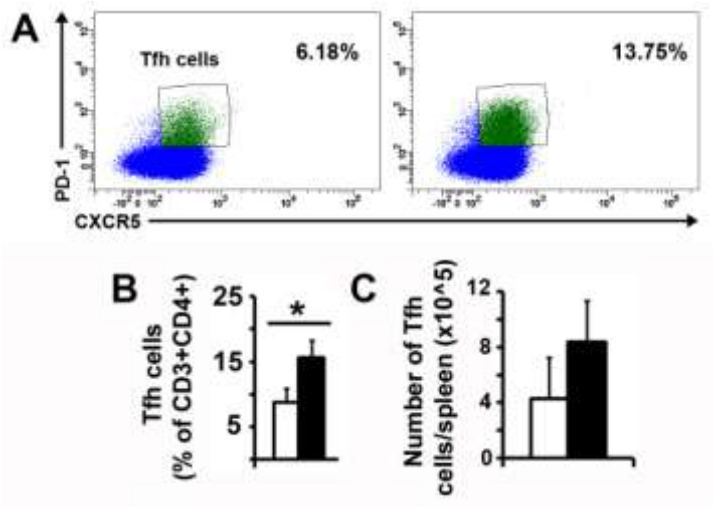

Figure R21. Increased percentage of Tfh cells in *P-sel*$^{-/-}$ mice. (A) Representative dot plots of follicular T helper (Tfh) cells in 1.5-3-month-old male WT and *P-sel*$^{-/-}$ mice. **(B-C)** Percentage **(B)** and total number **(C)** of splenic in 1.5-3-month-old male WT and *P-sel*$^{-/-}$ mice. n = 6. *p<0.05; ***p<0.005 by Student's two-tailed t-test. Bars show the mean±standard deviation (SD).

Likewise, both GC B cells and plasma cells were overrepresented in the spleen of young *P-Sel*$^{-/-}$ mice (Figures R22A-E). A significant increment in the frequency of GC B cells (CD11c^{-}B220^{+}FAS-L^{+}GL-7^{+}) was found in *P-sel*$^{-/-}$ mice (Figures R22A and R22B), whereas the total numbers were moderately increased (Figure R22C). In the case of the plasma cells (CD19^{+}B220^{-}IgD^{-}CD138^{+}), which are the antibody secreting cells, a tendency to increased percentage of plasma cells was detected (Figures R22D and R22E). Altogether, these data indicate a more reactive state of *P-sel*$^{-/-}$ spleens.

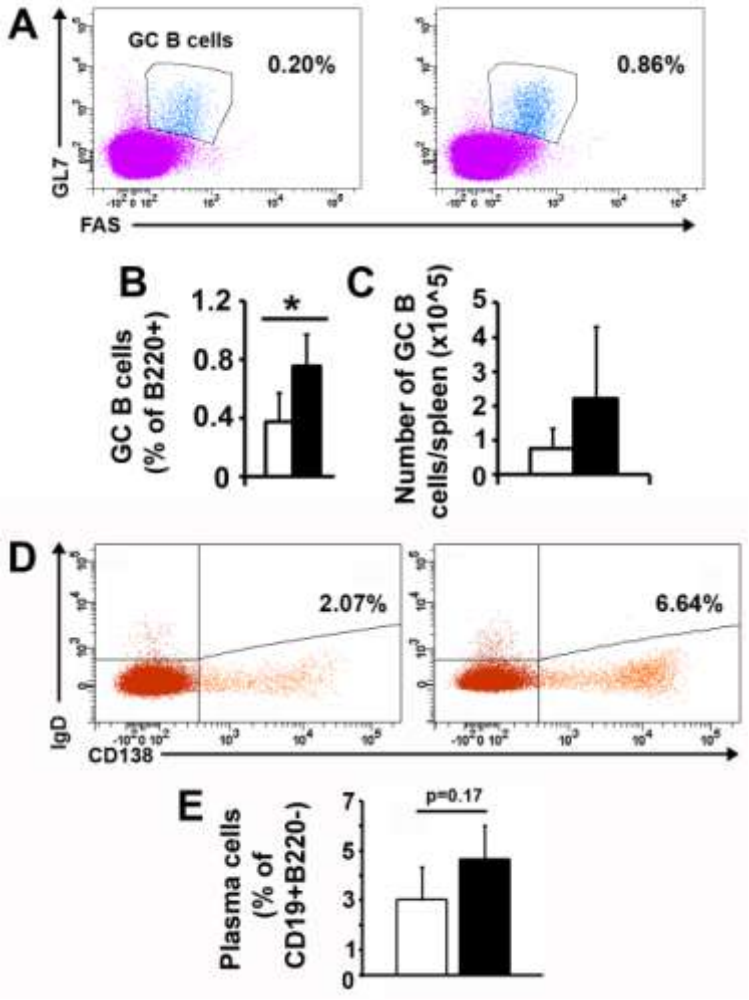

Figure R22. Increased percentages of GC B cells and plasma cells in *P-sel*$^{-/-}$ mice. (A) Representative dot plots of germinal center (GC) B cells in 1.5-3-month-old male WT and *P-sel*$^{-/-}$ mice. **(B-C)** Percentage **(B)** and total number **(C)** of splenic GC B cells in 1.5-3-month--old male WT and *P-sel*$^{-/-}$ mice. n = 4-6. **(D)** Representative dot plots of splenic plasma cells in 1.5-3-month-old male WT and *P-sel*$^{-/-}$ mice. **(E)** Percentage of splenic plasma cells 1.5-3-month-old male WT and *P-sel*$^{-/-}$ mice. n = 4.*p<0.05; ***p<0.005 by Student's two-tailed t-test. Bars show the mean±standard deviation (SD).

3.3 Altered circulating immune cell homeostasis in *P-sel*$^{-/-}$ mice

Taking the increased splenic reactivity of *P-sel*$^{-/-}$ mice, the distribution of peripheral blood leukocyte population was checked (Figures R23 and R24). 1.5-3-month-old male mice showed an important increase in the B cell compartment of *P-Sel*$^{-/-}$ mice (Figure R24A). In contrast, the T cell compartment was reduced, mainly because of the decrease in the CD4^{+} T cell subset (Figure R24A). Additionally, the monocytic population was also reduced in *P-sel*$^{-/-}$ animals (Figure R24A). However, in aged animals, only the granulocyte compartment was augmented (Figure R24B).

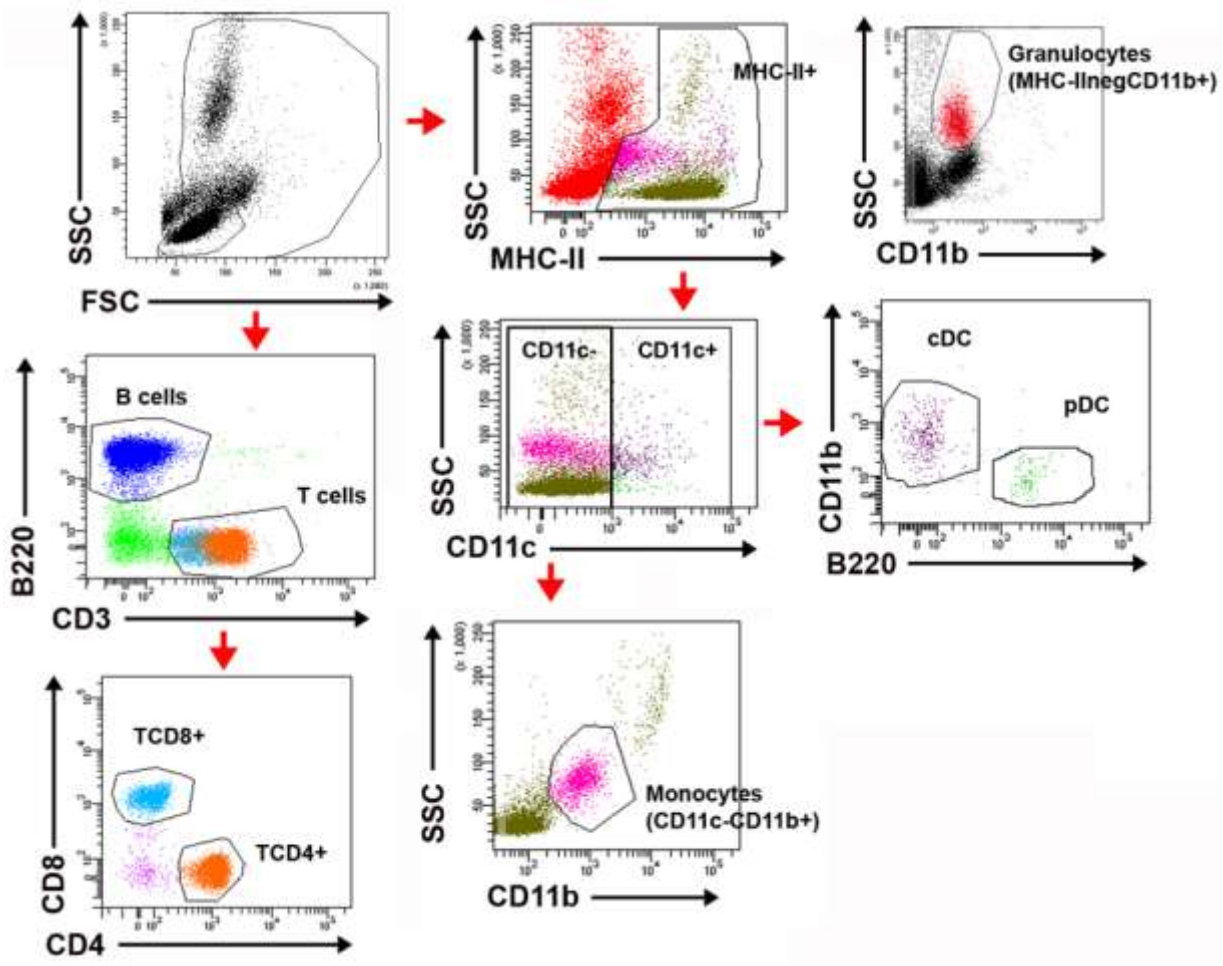

Figure R23. Peripheral blood immune system characterization in *P-sel*$^{-/-}$ mice. Gating strategy followed for the identification of the different immune cell subpopulations: B cells, CD4^{+} T cells, CD8^{+} T cells, granulocytes, monocytes, cDC and pDC**.**

Then, we studied the cytokine production of circulating immune populations and we found a reduction in the percentage of IL-10^{+} producing cells in 1.5-3-month-old *P-Sel*$^{-/-}$ mice, that was statistically significant among cDC and close to statistical significance in the B cell population (Figures R25A and R25B). Peripheral blood mononuclear cells of >18-month-old mice showed a statistically significant reduction in the percentage of IL-10^{+} producing monocytes and B cells (Figure R25B).

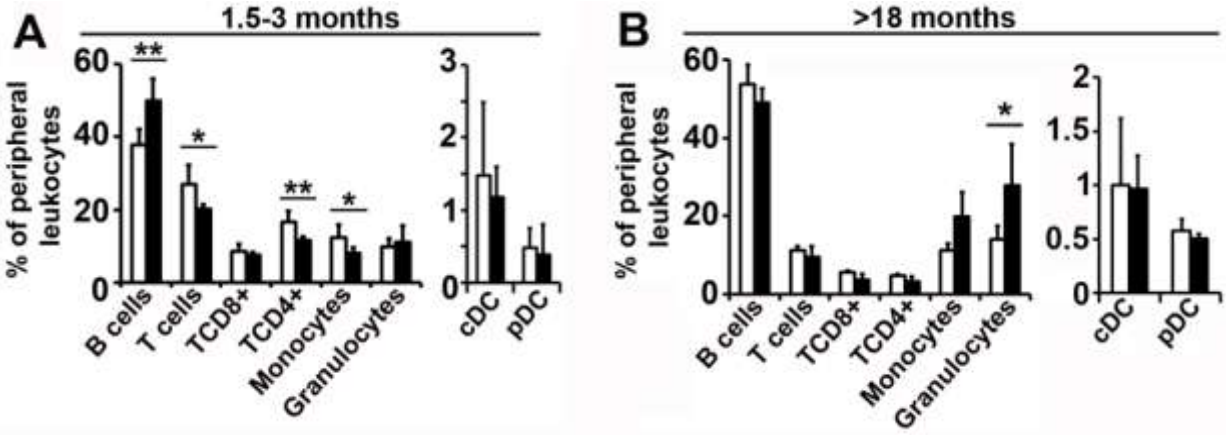

Figure R24. Peripheral blood immune system characterization in *P-sel*$^{-/-}$ mice. **(A-B)** Relative frequency of peripheral blood leukocyte populations of 1.5–3-month-old **(A)** and >18 months-old **(B)** WT and *P-sel*$^{-/-}$ mice. In all cases, n = 4 mice per group. Bars represent the mean ± SD. *p < 0.05; **p < 0.01; ***p < 0.005, by Student's two tailed t test.

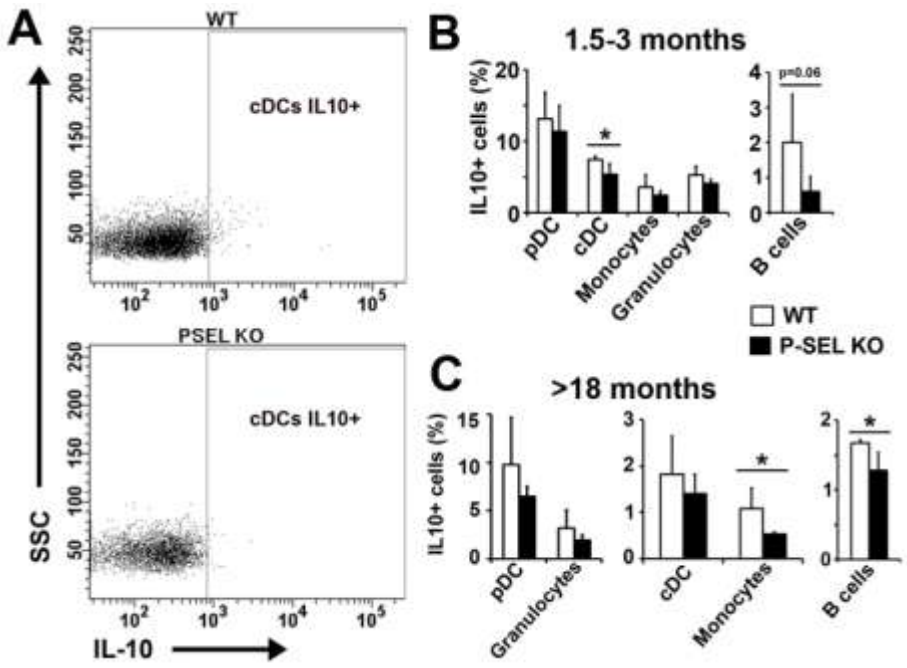

Figure R25. IL-10 production by peripheral immune cells of *P-sel*$^{-/-}$ mice. **(A)** Representative dot plots of IL-10^{+} cDC of 1.5-3-month-old WT and *P-sel*$^{-/-}$ mice. **(B-C)** Percentage of IL-10^{+} cDC, pDC, monocytes, granulocytes and B cells in 1.5-3-month-old **(B)** and > 18-month-old **(C)** WT and *P-sel*$^{-/-}$ mice. n = 4. Bars represent the mean ± SD. *p < 0.05; **p < 0.01; ***p < 0.005, by Student's two tailed t test.

Regarding T cells, a significant reduction in the TCD4^{+}IL-10^{+} compartment was found in 1.5-3 month-old *P-sel*$^{-/-}$ mice (Figures R26A and R26B), whereas WT and *P-sel*$^{-/-}$ mice showed no difference

in the percentage of IL-17^{+} T cells (Figures R26A and R26B). On the other hand, the IL-17^{+} CD4^{+} (Th17) population was increased in aged *P-sel*$^{-/-}$ mice (Figure R26C).

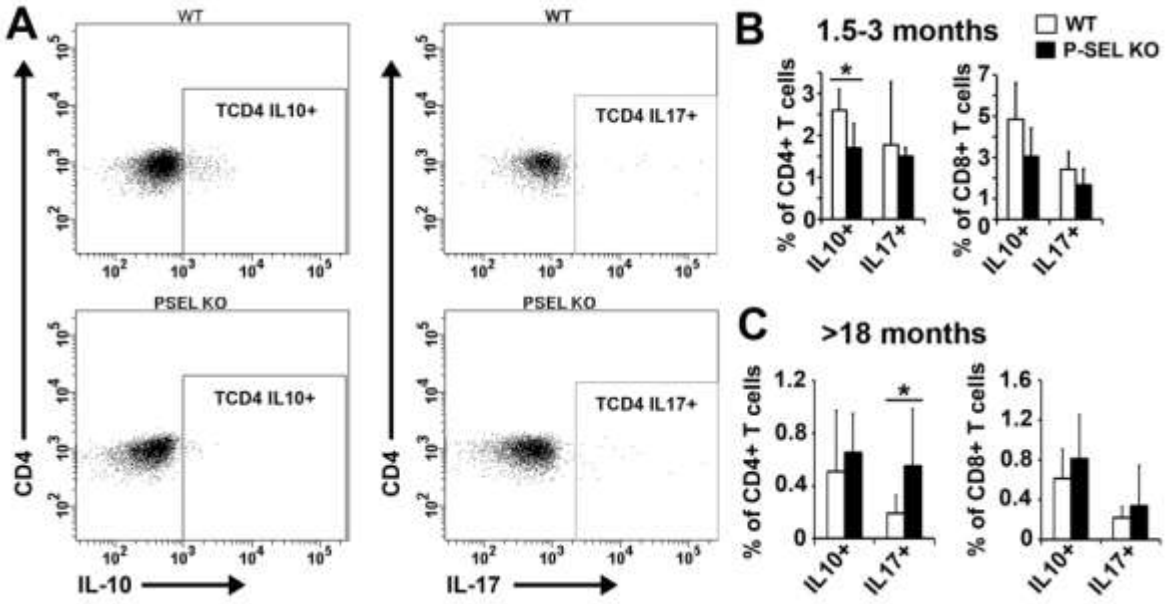

Figure R26. IL-10 and IL-17 production by T cells in *P-sel*$^{-/-}$ mice. (A) Representative dot plots of IL-10 and IL-17 producing CD4^{+} T cells in 1.5-months old WT and *P-sel*$^{-/-}$ mice. **(B-C)** frequency of IL-10 and IL-17 producing CD4^{+} and CD8^{+} T lymphocytes, in 1.5-month-old **(B)** and > 18-month-old **(C)** WT and *P-sel*$^{-/-}$ mice. n = 4. Bars represent the mean ± SD. *p < 0.05, by Student's two tailed t test.

3.4 Altered naïve/effector T lymphocyte balance in the spleen of *P-sel*$^{-/-}$ mice

To evaluate the effector and memory state of T cells, we analyzed the expression of CD62L and CD44 on splenic CD4^{+} and CD8^{+} T cells (Figures R27A and R27B). Naïve (CD62L^{+}CD44^{neg}) and central memory (CD62L^{+}CD44^{+}) subsets were decreased in 1.5-month-old *P-sel*$^{-/-}$ CD8^{+} splenic T cells, while effector (CD62L^{neg}CD44^{neg}) CD8^{+} T cells were augmented (Figures R27A and R27B). In the case of splenic CD4^{+} T cells, the naïve subset was severely diminished in the *P-sel*$^{-/-}$, while the effector (CD62L^{neg}CD44^{neg}) and effector memory (CD62L^{neg}CD44^{+}) compartments were highly increased (Figures R27A and R27B). Regarding >18-month-old mice, as compared with the WT mice, we found an increment in the percentages of CD8^{+} and CD4^{+} effector T lymphocytes, and a decrease of CD4^{+} central memory T lymphocytes in *P-sel*$^{-/-}$ mice (Figure R27A).

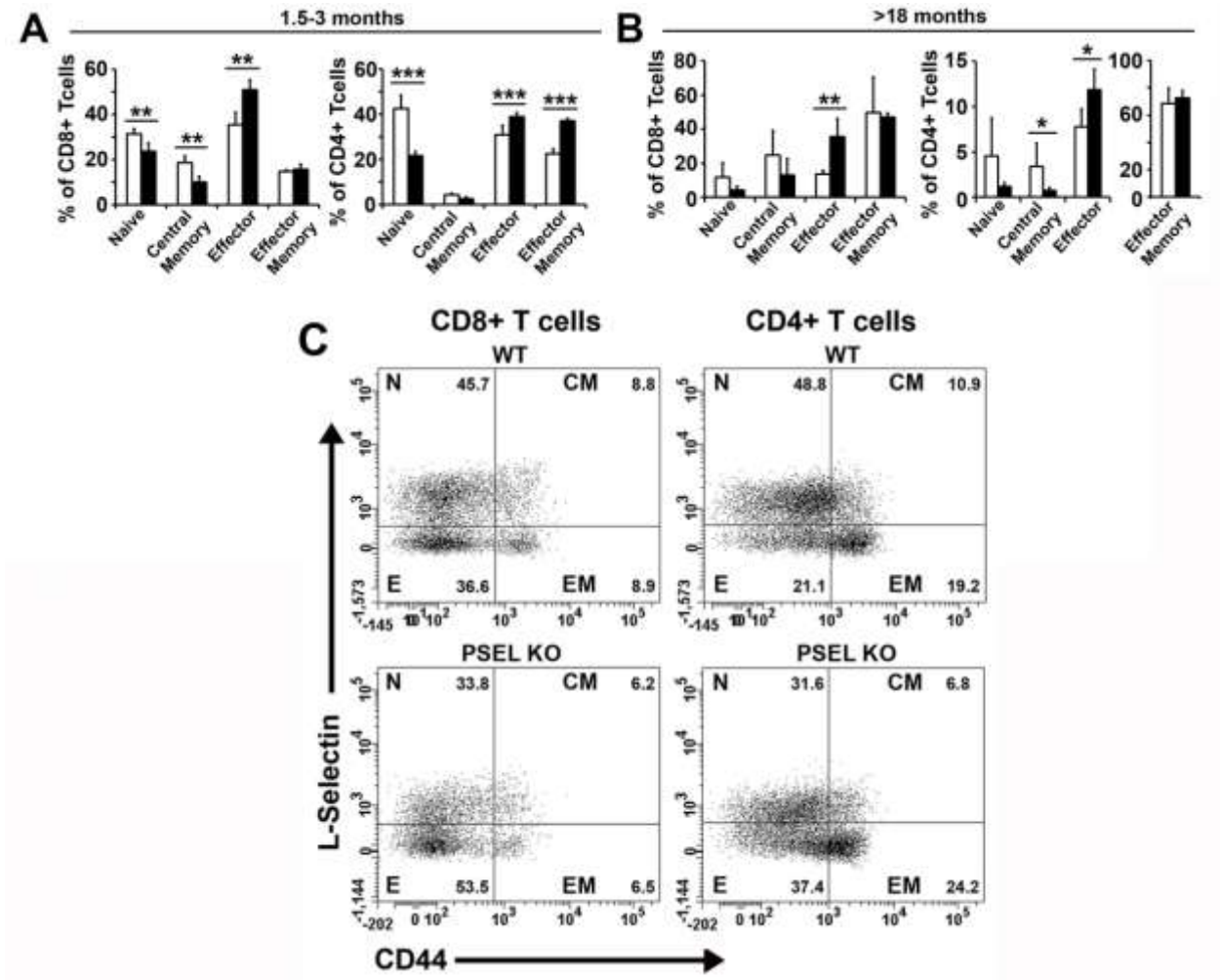

Figure R27. Spleen T cell characterization in *P-sel*$^{-/-}$ mice. (A) Phenotyping of CD4^{+} and CD8^{+} splenic T lymphocytes according to the expression of the naïve/memory/effector markers L-selectin (CD62L) and CD44 in 1.5–3-month-old and > 18 month-old WT and *P-sel*$^{-/-}$ mice. **(B)** Representative dot plots showing the distribution of 1.5–3-month-old mice splenic populations according to the expression of L-selectin and CD44. In all cases, n = 4 mice per group. Bars represent the mean±SD. *p < 0.05; **p < 0.01; ***p < 0.005, by Student's two tailed t test.

3.5 Altered skin homeostasis in *P-sel*$^{-/-}$ mice

Regarding the skin, one of the main organs affected in human lupus, we did not find significant changes in the different immune subpopulations in 1.5-3-month-old mice (Figures R28, R29 and R30) except from an increased percentage of pDC in *P-sel*$^{-/-}$ animals (Figure R29A). The frequencies of CD11b^{+} macrophages, cDC (Figure R28B and R28C), B cells (Figure R29B) and T cells (Figure R30C) remained unaltered in 1.5-3-month-old *P-sel*$^{-/-}$ mice.

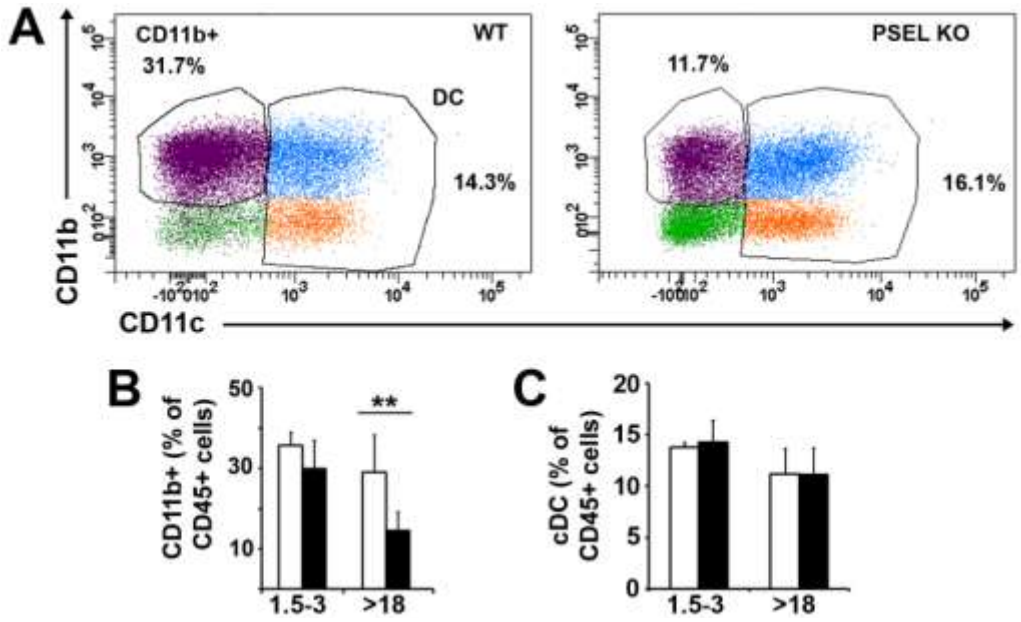

Figure R28. Frequency of CD11b+ and cDC in the skin of *P-sel*$^{-/-}$ mice. (A) Representative dot plots comparing the frequency of CD11b^{+} macrophages and DC between aged WT and and *P-sel*$^{-/-}$ mice. **(B-C)** Relative frequency of skin CD11b^{+} macrophages **(B)** and cDC **(C)** of 1.5–3-month-old and > 18-month-old WT and *P-sel*$^{-/-}$ mice. In all cases, n = 4 mice per group. Bars represent the mean±SD. *p < 0.05; **p < 0.01; ***p < 0.005, by Student's two tailed t test.

However, in aged animals, we found a reduced population of macrophages (Figures R28A and R28B), and a significant increment in the pDC (Figure R29A) and T cell subsets (Figures R30A and R30C). Among T cells, we did not find any difference in the percentage of gamma/delta (γδ) T cells either at 1.5-3 months or at >18 months (Figures R30B and R30D).

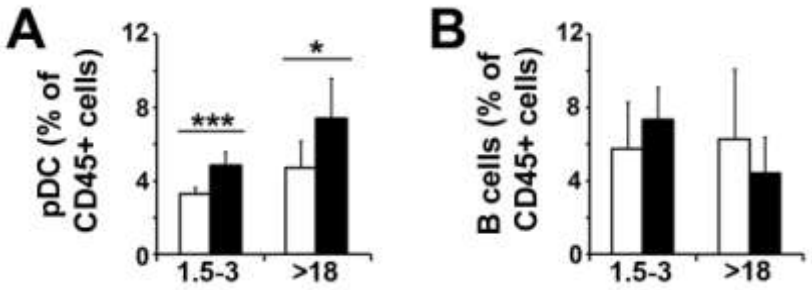

Figure R29. Frequency of pDC and B cells in the skin of *P-sel*$^{-/-}$ mice. (A-B) Relative frequency of skin pDc **(A)** and B cells **(B)** of 1.5–3-month-old and > 18-month-old WT and *P-sel*$^{-/-}$ mice. In all cases, n = 4 mice per group. Bars represent the mean±SD. *p < 0.05; **p < 0.01; ***p < 0.005, by Student's two tailed t test.

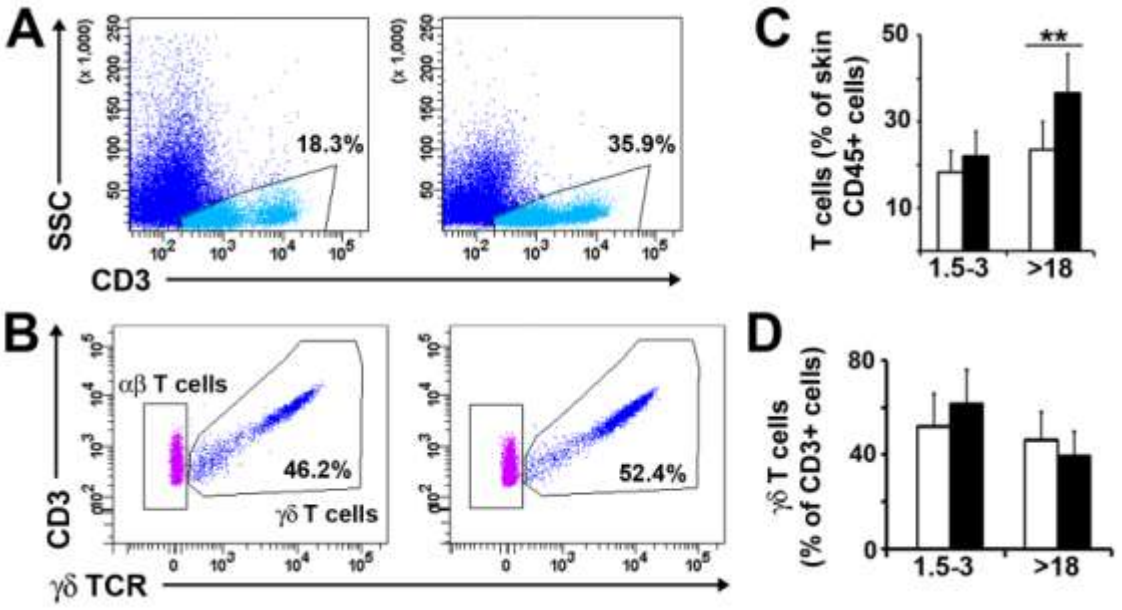

Figure R30. Frequency of T cells in the skin of *P-sel*$^{-/-}$ mice. (A-B) Representative dot plots comparing the frequency of T cells **(A)** and γδ T cells **(B)** between aged WT and and *P-sel*$^{-/-}$ mice. **(C)** Relative frequency of skin T cells in 1.5–3-month-old and > 18-month-old WT and *P-sel*$^{-/-}$ mice. **(D)** Relative frequency of skin γδ T cells in 1.5–3-month-old and > 18-month-old WT and *P-sel*$^{-/-}$ mice. In all cases, n = 4 mice per group. Bars represent the mean±SD. **p < 0.01, by Student's two tailed t test.

We also studied the cytokine production of the different populations, and only the >18-month-old *P-sel*$^{-/-}$ mice showed a reduction in the percentages of IL-10^{+} macrophages, cDC, pDC and B cells (Figures R31A and R31B). Accordingly, aged knockout mice displayed an increased IL-17^{+} (Figures R32A and R32B) and a reduced FOXP3^{+} (Figures R32C and R32D) T cell populations. We did not find significant differences in cytokine production in 1.5-3-month-old mice.

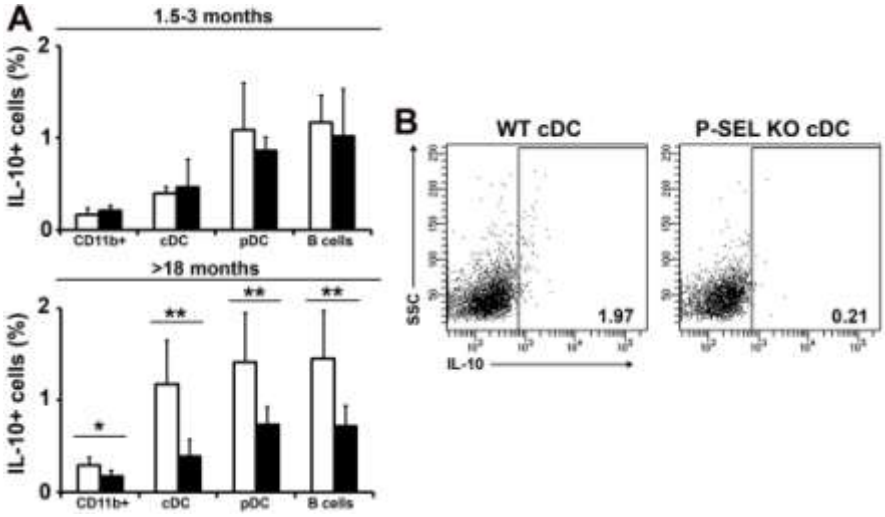

Figure R31. Frequency of T cells in the skin of *P-sel*$^{-/-}$ mice. (A) Percentage of IL-10^{+} macrophages (CD11b^{+}), conventional dendritic cells (cDC), plasmacytoid DC (pDC) and B cells, in 1.5–3-month-old and >18-month-old WT and *P-sel*$^{-/-}$ mice. (**B)** Representative dot plots of IL-10^{+} cDCs in >18-month-old WT and *P-sel*$^{-/-}$ mice. *p < 0.05; **p < 0.01 by Student's two tailed t test. n = 6 mice per genotype.

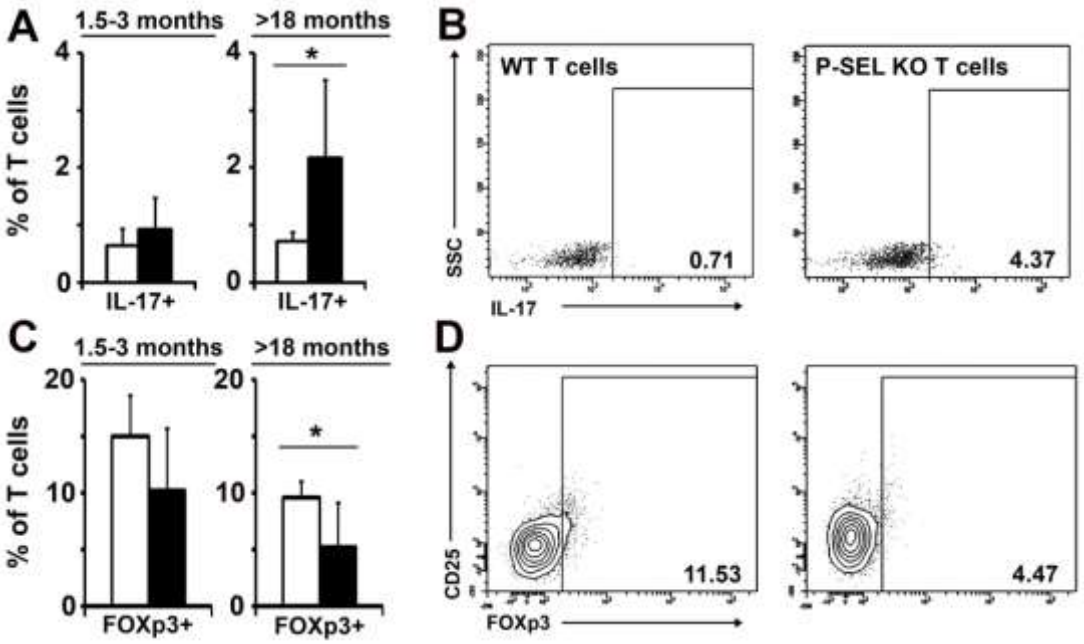

Figure R32. Frequency of T cells in the skin of *P-sel*$^{-/-}$ mice. (A) Percentage of IL-17^{+} T cells in 1.5–3-month-old and >18-month-old WT and *P-sel*$^{-/-}$ mice. (**B)** Representative dot plots of IL-17^{+} T cells in >18-month-old WT and *P-sel*$^{-/-}$ mice. (**C**) Percentage of FOXP3^{+} T cells in 1.5–3-month-old and >18-month-old WT and *P-sel*$^{-/-}$ mice. (**D)** Representative dot plots of FOXP3^{+} T cells in >18-month-old WT and *P-sel*$^{-/-}$ mice. *p < 0.05, by Student's two tailed t test. n = 6 mice per genotype.

4. Characterization of a lupus-like syndrome in P-selectin-deficient mice

Given the presence of circulating autoantibodies and the dermal and systemic immune system deregulation in *P-sel*$^{-/-}$, with an imbalance between the regulatory (IL-10^{+} cells and FOXP3^{+} T cells) and the pro-inflammatory compartment (IL-17^{+} T cells), we searched for tissue damage in target organs of SLE: skin, kidney and lung.

4.1 Histological alterations in the skin of *P-sel*$^{-/-}$ mice

Histological examination of the skin revealed that, compared with WT counterparts, male and female *P-sel*$^{-/-}$ mice had a reduced hypodermal layer (lipoatrophy), frequently infiltrated by leukocytes (panniculitis) (Figure R33). We also found that, apart from a remarkable infiltration, >18-month-old *P-sel*$^{-/-}$ mice presented hyperproliferation of the epidermal layer (acanthosis), accumulation of keratin in the corneal layer (hyperkeratosis) and keratin plugs inside hair follicles (Figure R34), described as murine lupus-like lesions (263-266).

.

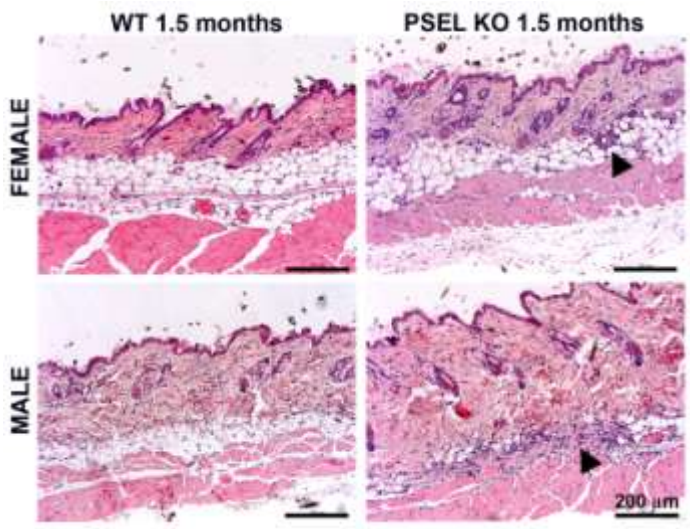

Figure R33. Lupus dermatitis in young *P-sel*$^{-/-}$ mice. Photomicrographs of representative H&E-stained skin sections (10x) of 1.5-3-month-old male and female WT or *P-sel*$^{-/-}$ mice. Black arrowheads point incipient panniculitis. n = 8-10. Scale bars represent 200 µm.

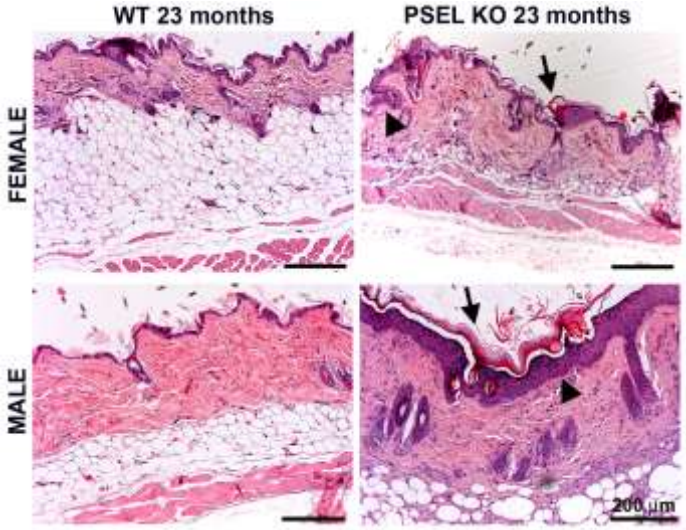

Figure R34. Lupus dermatitis in aged *P-sel*$^{-/-}$ mice. Photomicrographs of representative H&E-stained skin sections (10x) of 23-month-old male and female WT or *P-sel*$^{-/-}$ mice. Black arrowheads point acanthosis. Black arrows show hyperkeratosis. n = 8-10. Scale bars represent 200 µm.

Quantification of these observations by measuring the total thickness of the dermal, epidermal and corneal layers of WT and *P-sel*$^{-/-}$ mice showed that male and female *P-sel*$^{-/-}$ mice presented an enlarged dermis and incremented width of the epidermal and corneal layers in *P-sel*$^{-/-}$ mice that was more evident when mice were > 18 months-old (Figure R35).

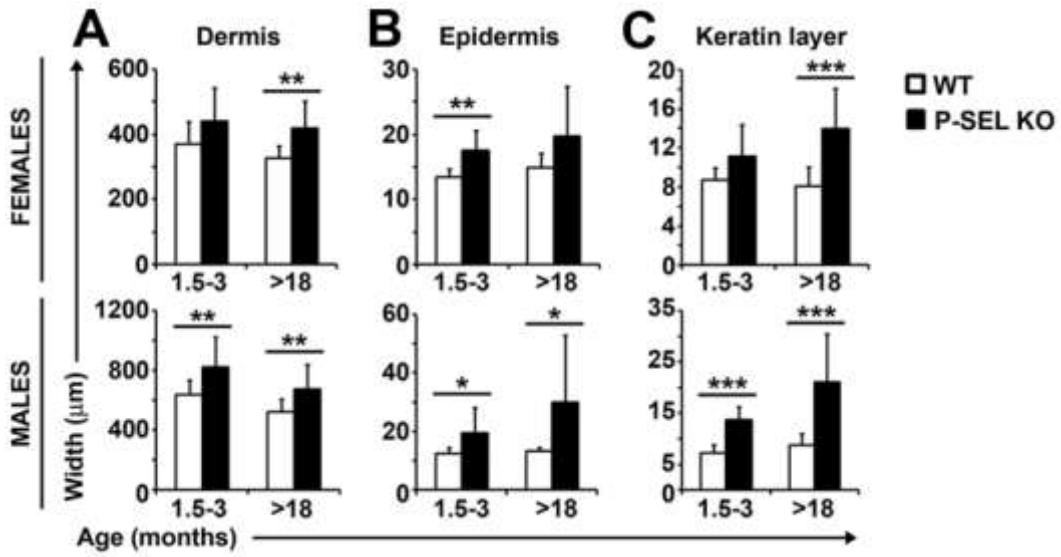

Figure R35. Quantification of dermal layers in WT and *P-sel*$^{-/-}$ mice. (A-C) Quantification of dermis **(A)**, epidermis **(B)** and corneal layer **(C)** width of WT and *P-sel*$^{-/-}$ mice. n = 8-10. Bars represent mean±SD. *p < 0.05; **p < 0.01; ***p < 0.001 by Student's two tailed t test.

Accordingly, the severity of the skin lesions estimated by grading scale was higher in young *P-Sel*$^{-/-}$ mice (female *P-sel*$^{-/-}$ 0.30±0.48 vs female WT 0.00±0.00; male *P-sel*$^{-/-}$ 0.73±1.44 vs male WT 0.00±0.00) and remarkably more severe in the aged mice (>18 months-old: female *P-sel*$^{-/-}$ 3.13±1.81 vs female WT 0.40±0.52; male *P-sel*$^{-/-}$ 4.57±4.83 vs male WT 0.00±0.00) (Figure R36).

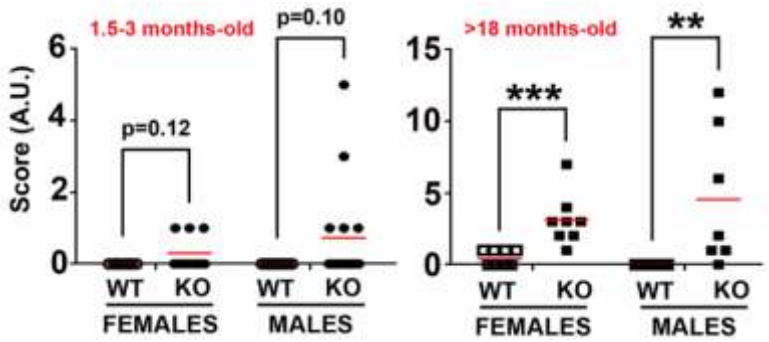

Figure R36. Semiquantitative evaluation of the lupus dermatitis of *P-sel*$^{-/-}$ mice. Pathological activity index of skin samples obtained from WT and *P-Sel*$^{-/-}$ mice. Graphs show the mean index value (red bar). n = 8-10. *p < 0.05; **p < 0.01; ***p < 0.001 by Student's two tailed t test.

4.2 Exposure to UV-B radiation

The exposure of 3-4-month-old female WT and *P-sel*$^{-/-}$ to UV radiation provoked an extensive dermatitis in *P-sel*$^{-/-}$ mice with ulcers in the exposed skin, but not in WT counterparts (Figure R37A). Histopathological analysis revealed a severe epidermal lesion in female *P-sel*$^{-/-}$ mice consisting of acanthosis and hyperkeratosis, immune infiltration in the dermis, and deposition of extracellular matrix components in the hypodermal layer (Figure R37B). Consequently, the severity of the lesions was significantly higher in UV-irradiated *P-sel*$^{-/-}$ mice (*P-sel*$^{-/-}$ 7.25±2.99 vs WT 3±1.41) (Figure R37C).

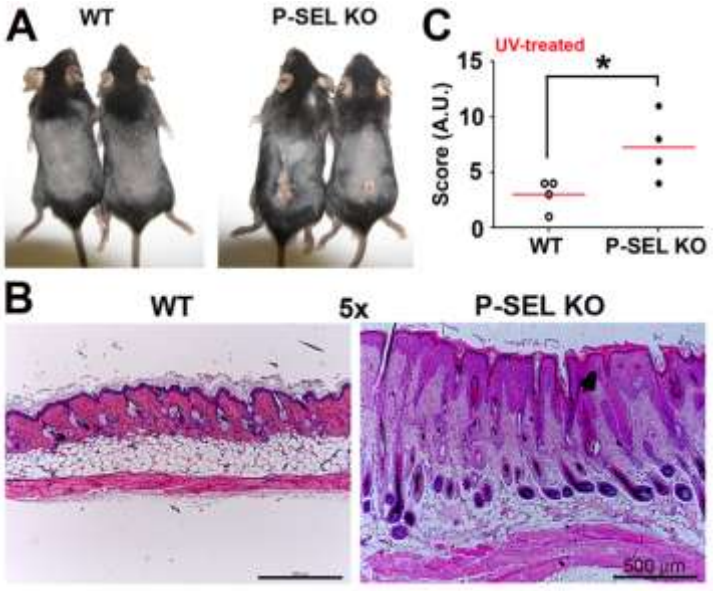

Figure R37. UV-induced lupus dermatitis in young *P-sel*$^{-/-}$ mice. (A) Lesions developed in the back of UV-irradiated 3-month-old female WT and *P-Sel*$^{-/-}$ mice. **(B)** Photomicrographs (5x) of representative H&E-stained skin sections of UV-irradiated 3-month-old female WT and *P-Sel*$^{-/-}$ mice. n = 4 mice per genotype. Representative experiment of three independent replicates. Scale bars represent 500 µm. **(C)** Pathological activity index of skin samples obtained from UV irradiated 3-month-old female WT and *P-Sel*$^{-/-}$ mice. Graph shows the mean index value (red bar). *p < 0.05; **p < 0.01; ***p < 0.005 by Student's two tailed t test.

4.3 Histological alterations in the kidney of *P-sel*$^{-/-}$ mice

Histological examination of kidney tissue of WT and *P-sel*$^{-/-}$ mice showed that *P-sel*$^{-/-}$ mice presented some glomerular alterations. Among them, we found a high proportion of glomeruli with a dilated Bowman's space (Figure R38A). Additionally, some glomeruli presented tubularization of the Bowman's capsule (Figure R38A). We also found some sclerotic glomeruli (Figure R38A).

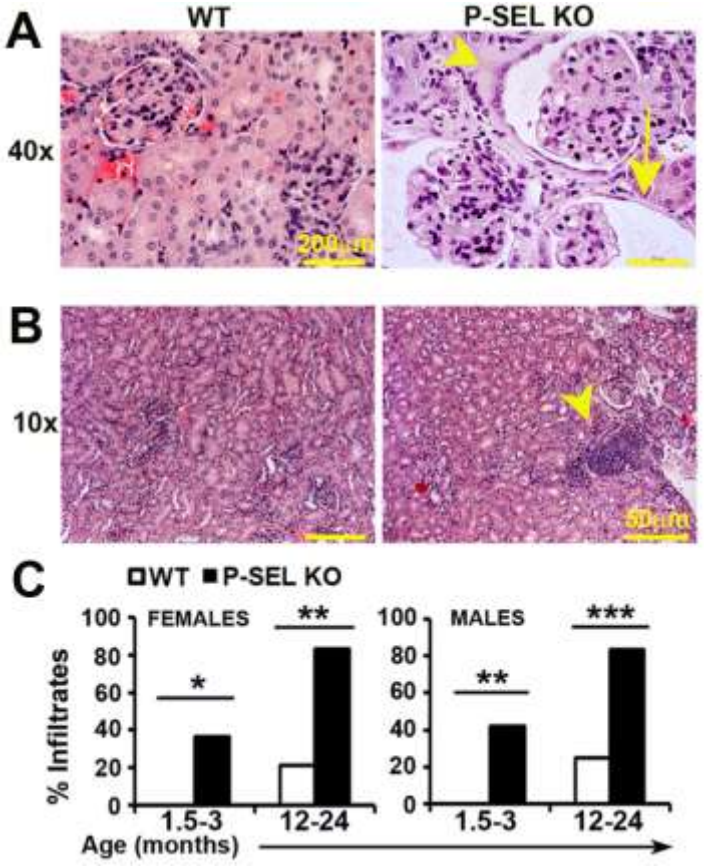

Figure R38. Glomerular damage and immune infiltration in kidney of *P-sel*$^{-/-}$ mice. (A) Representative photomicrographs (40x) of H&E stained kidney glomeruli of WT and *P-sel*$^{-/-}$ mice. Yellow arrow denotes a dilated Bowman's space. Yellow arrowhead denotes a tubularized glomerulus. **(B)** Photomicrographs (10x) of kidney sections showing an immune infiltrate (yellow arrowhead) in *P-sel*$^{-/-}$ mice. **(C)** Prevalence of immune infiltration in WT and *P-sel*$^{-/-}$ mice (n = 8–10 mice per group). *p < 0.05; **p < 0.01; ***p < 0.005 by Chi-square test.

We found also interstitial infiltrates in *P-sel*$^{-/-}$ mice (Figure R38B), whose prevalence increased from 40% at 1.5-3 months of age to 84% in mice older than one year (12-24 months-old) (Figure R38C), while only 20% of aged WT and none of the young WT mice presented interstitial infiltration.

We also observed that 30% of the 3-month-old *P-sel*$^{-/-}$ mice had infarcted foci (Figure R39A). The prevalence of infarcts increased as mice grew older (Figure R39B), reaching to 60% of females and 80% of males in the >18-month-old population of *P-sel*$^{-/-}$ mice.

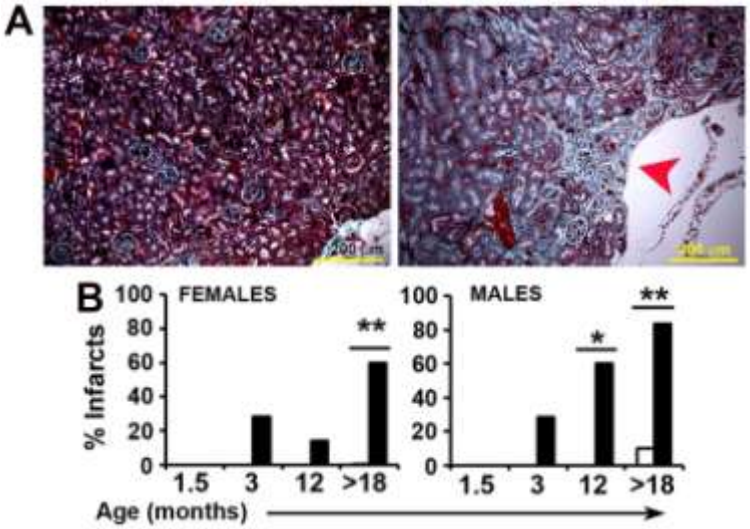

Figure R39. Renal infarcts in *P-sel*$^{-/-}$ mice. (**A**) Masson's trichrome-stained kidney sections of WT and *P-sel*$^{-/-}$ mice (10x), showing healthy and infarcted tissue (red arrowhead), respectively. (**B**) Prevalence of renal infarcts in WT and *P-sel*$^{-/-}$ mice (n = 8–10 mice per group). *p < 0.05; **p < 0.01; ***p < 0.005 by Chi-square test.

4.4 Biochemical analysis of renal failure parameters.

Although not statistically significant, we found increased levels of urea and creatinine and lower levels of albumin in the sera from >18-month-old *P-sel*$^{-/-}$ mice compared with equivalent WT mice (Figure R40). Conversely, the analysis of urine revealed that 13% and 38% of *P-sel*$^{-/-}$ mice had proteinuria and hematuria, respectively (Figure R41A).

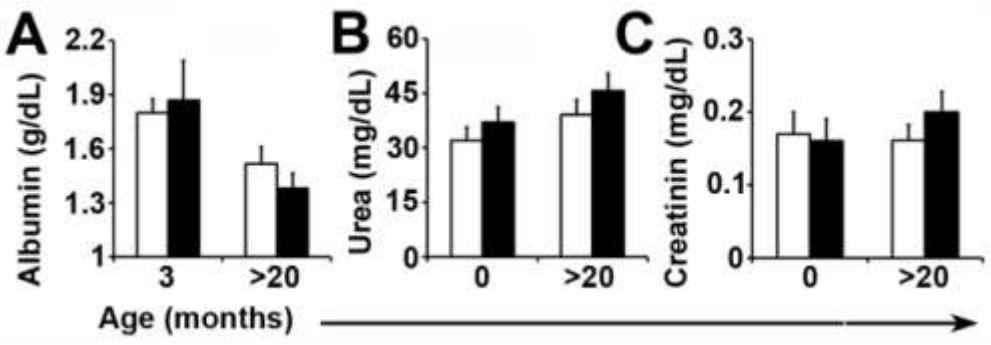

Figure R40. Biochemical analysis of renal failure parameters in *P-sel*$^{-/-}$ mice. (**A-C**) Quantification of albumin (A), urea (B) and creatinine (C) in serum of WT and *P-sel*$^{-/-}$ mice. n = 4 per group. Non significant differences were found by two-tailed Student's t test.

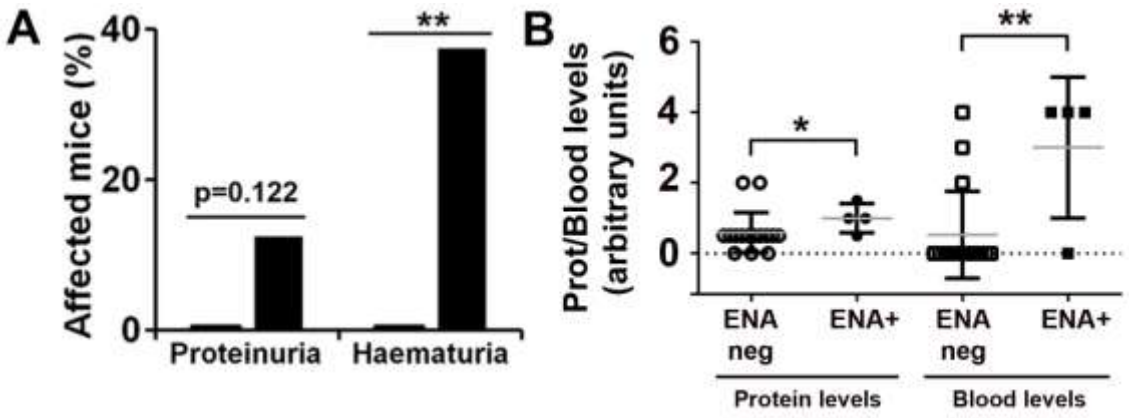

Figure R41. Urine evaluation in *P-sel*$^{-/-}$ mice. **(A)** Frequency of proteinuria and hematuria in >12-month-old WT and *P-Sel*$^{-/-}$ mice (n = 14–16 mice per group). **p < 0.01 by Chi-square test. **(B)** Association of higher levels of proteinuria and hematuria with the presence of serum extractable nuclear antigens (ENAs). Grey bars show the mean. *p < 0.05; **p < 0.01 by two-tailed Student's t test

Moreover, ENA+ *P-sel*$^{-/-}$ mice showed higher levels of proteinuria and hematuria than ENA negative knockout mice (Figure R41B), indicating the existence of an association between high titers of autoantibodies and more severe renal disease.

4.5 Immunocomplex deposition in the skin and kidney of *P-sel*$^{-/-}$ mice

We found deposits of immune complexes in the glomerular basal membrane in 100% of female and 25% of male *P-sel*$^{-/-}$ mice older than 18 months, but only in 25% of WT females and none in WT males (Figure 42). In the skin, we found deposits of immune complexes in 60% of male and 40% of female *P-sel*$^{-/-}$ mice over 18 months of age but in none of WT mice (Figure R42).

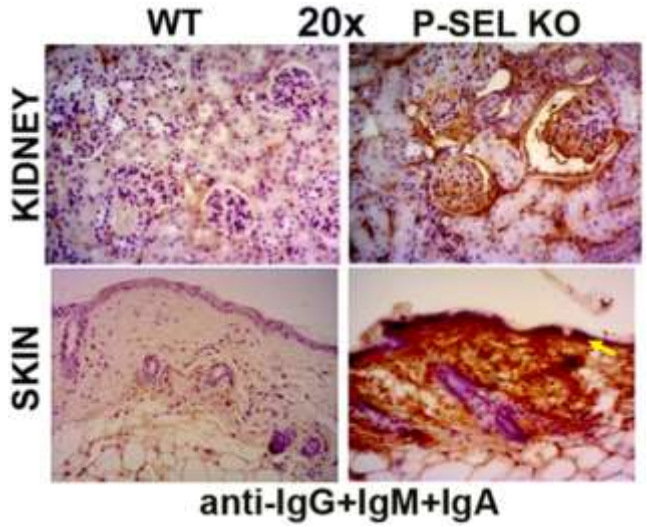

Figure R42. Urine evaluation in *P-sel*$^{-/-}$ mice. Representative photomicrographs of anti-IgM+IgA+IgG-stained kidney (upper panels) and skin (lower panels) sections (20x). n = 4–5 mice per group. Yellow arrow points to the dermoepidermal junction.

4.6 Histological alterations in the lungs of *P-sel*$^{-/-}$ mice

P-sel$^{-/-}$ mice presented structural lung abnormalities consisting of alveolar wall thickening and increased interstitial cellularity due to leukocyte infiltration (Figure R43A), characteristics of nonspecific interstitial pneumonia (NSIP). At 1.5-3 months of age, NSIP was found in approximately 30-40% of *P-sel*$^{-/-}$ but not in WT mice (Figure R43B). At 12-24 months, the presence of NSIP among *P-sel*$^{-/-}$ mice rose to 75% in females and 53% in males, while among WT animals, NSIP was found only in 15% of 12-24-month-old females (Figure R43B). At 1.5-3 months, NSIP was focal and restricted to a single lobule (Figure R43C). With ageing, the prevalence of NSIP increased and the lesion became generalized (affecting all the lung lobes) and more severe, increasing the presence of diffuse NSIP when mice were 12-24 months old (Figures R43A and R43C). CD45^{+} immune cell infiltration was confirmed by immunohistochemistry (Figure R44).

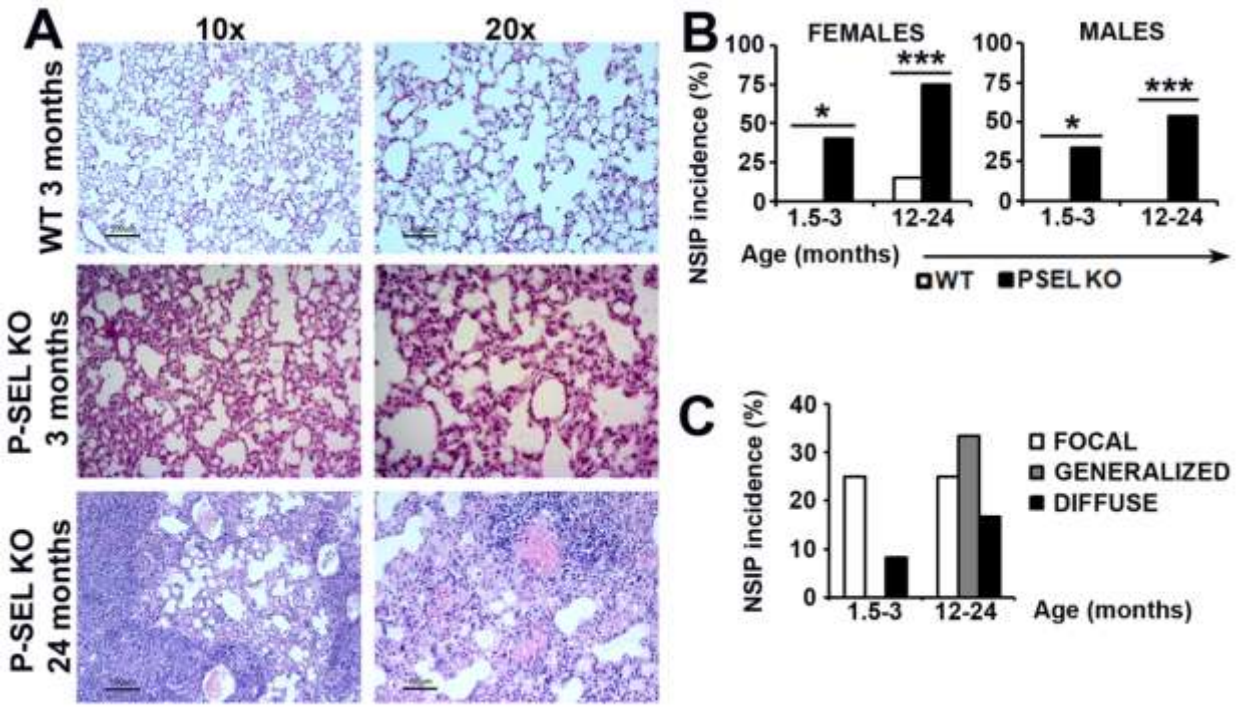

Figure R43. Nonspecific interstitial pneumonia (NSIP) in *P-sel*$^{-/-}$ mice. (A) Representative photomicrographs of H&E-stained lung sections from WT and *P-sel*$^{-/-}$ mice. **(B)** Incidence of NSIP in WT and *P-sel*$^{-/-}$ mice (n = 8-12 mice per group); ***p<0.005 by Chi-square test. **(C)** Incidence of NSIP according to the distribution a severity of the inflammation.

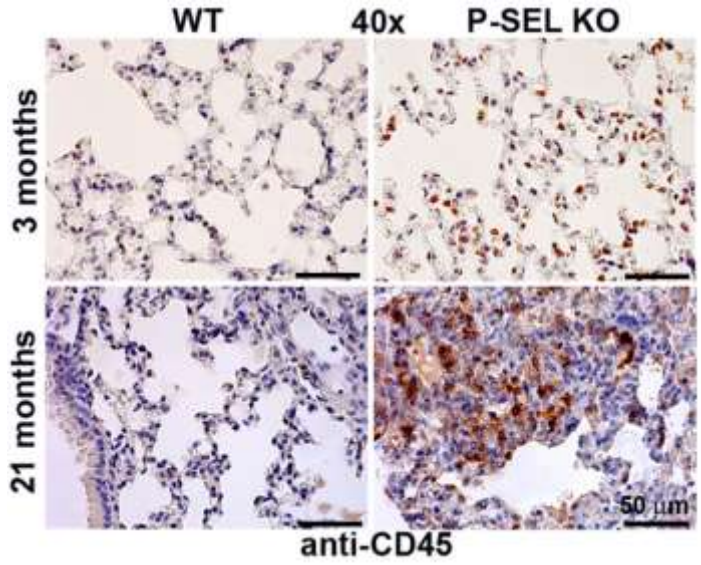

Figure 44. Immune cell infiltration in the lung of *P-sel*$^{-/-}$ mice. Representative photomicrographs (40x) of anti-CD45-stained lung sections of WT and *P-sel*$^{-/-}$ mice.

4.7 Reduced lifespan in *P-sel*$^{-/-}$ mice.

To analyze the impact of the autoimmune syndrome progression during the lifespan of *P-sel*$^{-/-}$ mice, we carried out a survival study with 20 WT and 23 *P-sel*$^{-/-}$ mice from 6 to 100 weeks of age. *P-sel*$^{-/-}$ mice started to die at week 47 and we observed a peak of mortality at around week 80. At week 100, 90% of WT mice remained alive whereas only 61% of the *P-sel*$^{-/-}$ mice were still alive (Figure R45).

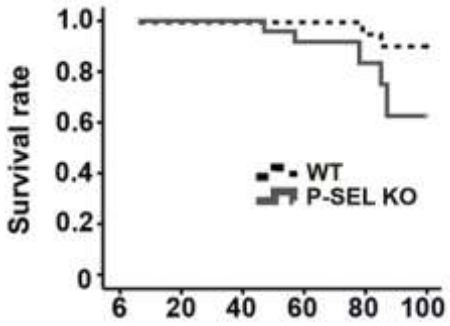

Figure R45. Increased mortality of *P-sel*$^{-/-}$ mice. Kaplan-Meier survival curves for WT and *P-sel*$^{-/-}$ mice (n = 20 WT and 23 *P-sel*$^{-/-}$ mice); p=0.033 by Mantel-Cox test.

5. Analysis of P-selectin expression in human cutaneous lupus

To assess the relevance of P-sel in human lupus, we compared by immunohistochemical staining the expression of P-sel in endothelial cells of the dermal vessels of skin biopsies obtained from cutaneous lupus erythematosus (cLE) patients and healthy controls. We identified all the blood vessels ($CD31^{+}$) in the whole biopsy and classified them into three categories depending on the expression of P-sel (Figures R46A and R46B): 1) unstained, 2) partially stained, and 3) fully stained.

We found a deep reduction of fully stained blood vessels in cLE biopsies, which were accompanied by a remarkable elevation in the percentage of negative vessels for P-sel expression (Figure R46C).

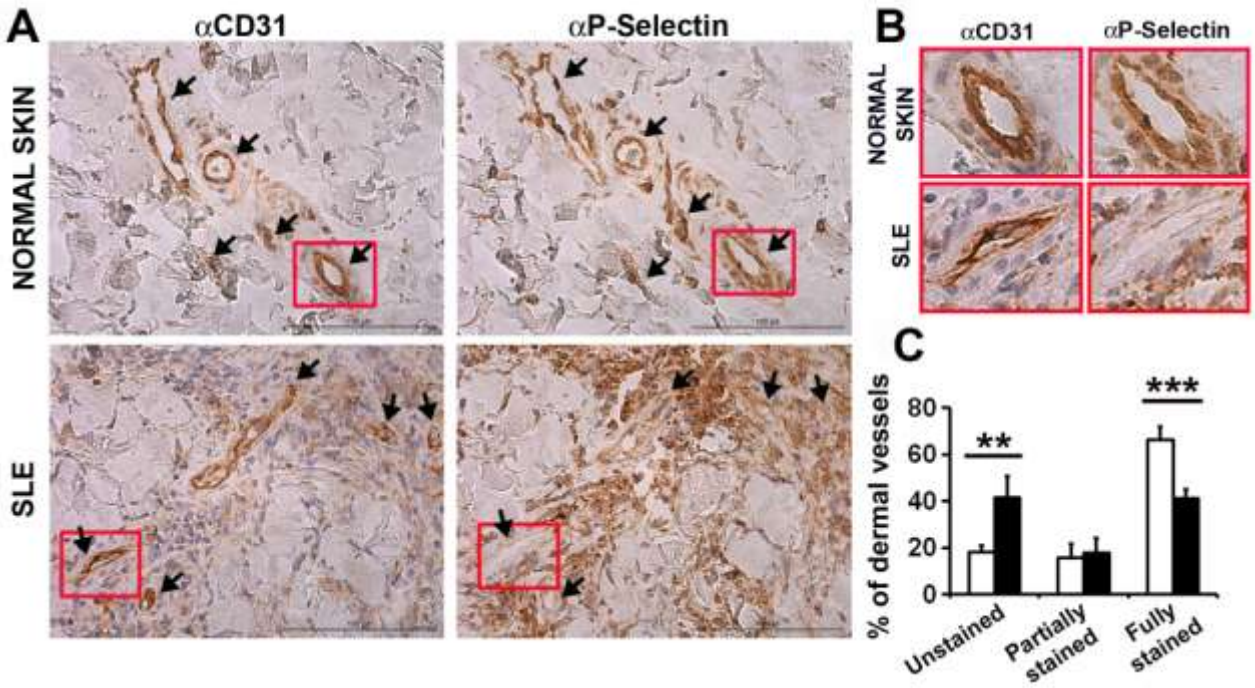

Figure R46. Decreased expression of P-sel in human cLE biopsies. (A) Representative photomicrographs (20x) of anti-CD31 and anti-P-sel stained skin biopsies of healthy donors and SLE patients. Black arrows point blood vessels. **(B)** 200% magnification of representative blood vessels from the original images are represented. **(C)** Classification and quantification of $CD31^+$ dermal blood vessels according to the expression level of P-sel (healthy controls, n = 4; cLE patients, n = 4); bars show the mean±SD. **p < 0.01; ***p < 0.001 by Student's two tailed t test.

We also found unspecific binding to infiltrating leukocytes, that has been already reported by other authors (267, 268).

Moreover, the expression of endothelial P-sel in human biopsies was also tested by immunofluorescence. The levels of P-sel were reduced in dermal small blood vessels of patients of cLE compared with age-matched controls (Figure R47).

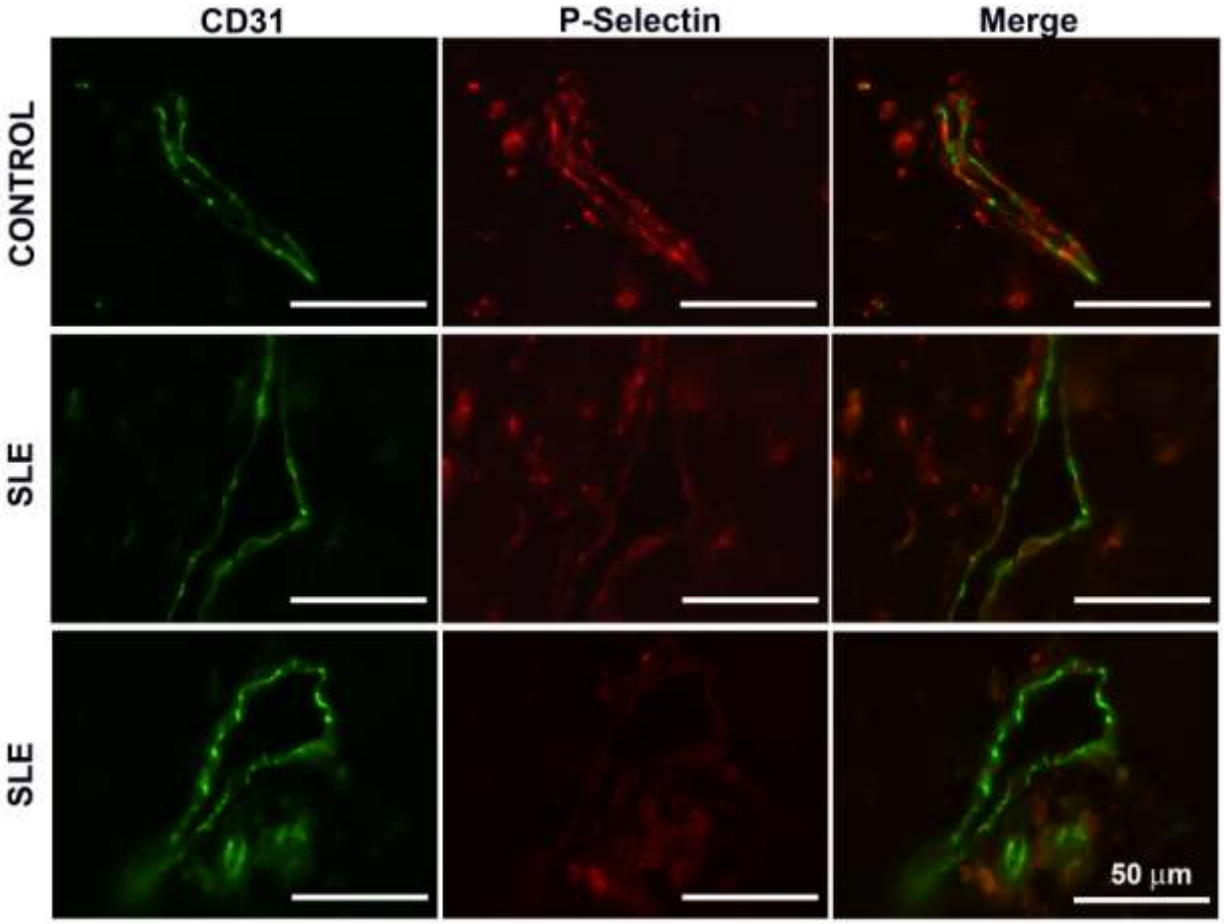

Figure R47. Decreased expression levels of P-sel in human cLE biopsies. (A) Representative photomicrographs (63x) of anti-CD31 (green) and anti-P-sel (red) stained skin biopsies of healthy donors and cLE patients. White scale bars represent 50 µm. Healthy controls, n = 4; cLE patients, n = 4.

Discussion

Discussion

PSGL-1 binding to endothelial selectins during the extravasation processes may trigger different regulatory signals depending on the immune cell type that contacts the endothelium. In dendritic cells and monocytes, PSGL-1 absence drives to the upregulation of costimulatory molecules such as MHC-II, CD80 and CD86, that together with the reduced expression of IL-10, TGF-β and IDO would lead to higher rate of differentiation of naïve T cells to pro-inflammatory effector T cells (16, 43). In the case of T cells, lack of PSGL-1 signalling would lead to decreased levels of the T cell exhaustion marker PD-1 (62) and increased $TCD8^{+}$ proliferation, contributing to a more robust and long-lasting immune response.

In this thesis, a relevant role for adhesion molecules in vascular and immune homeostasis has been highlighted. PSGL-1 arises as an immune checkpoint regulator for the immune system, controlling both dendritic cell (43, 58, 269) and T cell function (62). In this context, lack of PSGL-1 signalling on leukocytes lowers the threshold for autoimmunity, leading to an increased systemic humoral response with an augmented germinal centre reaction, and to a local cellular Th1 or Th17, depending on the target organ and the mouse model analyzed. Both *PSGL-1*$^{-/-}$ and *P-sel*$^{-/-}$ mice develop autoimmune syndromes sharing the reduction of the immunomodulatory cytokine IL-10 and lung endothelial dysfunction that ultimately leads to PAH and premature death.

Much less is known about the implication of P-sel in endothelial cell biology. Some studies pointed out that rolling and transmigration of neutrophils and monocytes could modify the integrity of endothelial cell tight junctions by the regulation of intracellular Ca^{2+} concentration (270, 271). Later, it was described that, in histamine-activated HUVEC, monoclonal antibodies against P-sel were able to trigger an increment of intracellular Ca^{2+} levels (272), indicating that P-sel can transduce external signals into second messenger in the cytoplasm. Recent studies with Pentraxin-3 (PTX3), a soluble glycoprotein that binds P-sel *in vitro* and *in vivo*, demonstrated that PTX3 can interfere with PSGL-1/P-sel (72, 273). The administration of PTX3 to wild-type mice induced endothelial dysfunction and increased blood pressure (273). Interestingly, PTX3 circulating levels were elevated in patients with hypertension (273) and SSc (274). These data suggest that, after binding to PSGL-1, signals transduced by P-sel on endothelial cells may by implicated in the maintenance of the correct endothelial function and integrity. The absence of P-sel signaling, due to either lack of PSGL-1 or P-sel itself, may lead to the endothelial dysfunction observed in both knockout models.

1. Pulmonary arterial hypertension and PSGL-1/P-selectin interaction

1.1 Spontaneous development of PAH in PSGL-1 and P-selectin deficient mice

PAH is a particularly severe, life-threatening complication of some CTDs that leads to RV remodeling, right heart failure and premature death (110). Although great effort has been invested in searching for an efficient treatment for PAH, no curative therapy is available. In the present study, we highlight the importance of leukocyte-endothelium interactions for the maintenance of vascular homeostasis and protection against PAH. Deficiency for leukocytic PSGL-1, which interacts with P-sel and E-sel on the surface of activated endothelium, induces reduced pulmonary AT2R expression and endothelial dysfunction characterized by reduced vasodilation response due to impaired NO production, coinciding with an increase in pulmonary AngII concentrations. This impairment in endothelial function drives to vascular remodeling, which would elevate flow resistance and lead to PAH and, ultimately, to premature death in mice. Our work contributes to the identification of new pathways and possible pharmaceutical targets for the treatment of PAH, which is crucial to improve the survival and the long-term prognosis of patients with this disease.

The increase in relative vessel wall area in lung vasculature has been described as a histological marker of PAH in both animal models and patients with PAH (77, 80, 110), and is considered as one of the first events occurring in the development of PAH (81, 114). We did not observe plexiform lesions (endothelial cell proliferation that reduce the blood vessel lumen) or intimal fibrosis in the lung of *PSGL-1*$^{-/-}$ mice, although these lesions do not appear in all the rodent models of PAH (275). In general terms, the animal models that reproduce the plexiform arteropathy are “second hit” models such as MCT + pneumonectomy in young rats (under 200 g of weight) and Sugen 5416 + hypoxia in rats and mice; or knock-in genetic models such as IL-6- and S100A4-overexpressing transgenic mice (275). Of note, only female *PSGL-1*$^{-/-}$ and *P-sel*$^{-/-}$ develop PAH with aging. In humans, PAH is a rare disease with a high sex-bias. In fact, women are more frequently affected by PAH (2:1) (75, 76). *PSGL-1*$^{-/-}$ male mice also presented lung vascular remodeling, but did not show either reduced expression of AT2R nor PAT/ET ratio. Other mouse models such as hypoxia or MCT did not reproduce the sex bias of PAH, showing similar affectation of male and female mice (275), thus constituting a relevant pathophysiological feature of *PSGL-1*$^{-/-}$ and *P-sel*$^{-/-}$ CTD-associated PAH mouse models.

The vascular remodeling observed in *PSGL-1*$^{-/-}$ mice might cause an increase in the lung vascular resistance to blood flow, the main consequence of which would be the elevation of the pressure in the pulmonary artery. Transthoracic Doppler echocardiography is a non-invasive diagnostic tool for patients with suspected PAH, giving information not only on diagnosis but also providing further information on the causes or consequences of the PAH (110, 276). This method has been validated for estimating pulmonary artery pressure (PAP) in patients with PAH and in rat and mouse models of PAH (277-279), and is becoming increasingly more relevant in the study of murine models of heart diseases (280). Using this echocardiography modality, and in accordance with the pulmonary vessel remodeling, we found a

reduced PAT/ET ratio in the pulmonary artery of *PSGL-1*$^{-/-}$ female mice. Our results from a longitudinal study show a consistently increased pulmonary artery pressure detected by a reduced PAT/ET ratio in *PSGL-1*$^{-/-}$ female mice from 3 months of age consistent with lung vascular remodeling, suggesting that *PSGL-1*$^{-/-}$ mice are already susceptible to PAH at young age.

1.2 Exposure to hypoxia and endothelial damage in *PSGL-1*$^{-/-}$ female mice

Chronic hypoxia killed 40% of *PSGL-1*$^{-/-}$ females during the first days of treatment, suggesting that some *PSGL-1*$^{-/-}$ mice are unable to adapt to reduced O_2 pressure. WT and surviving *PSGL-1*$^{-/-}$ females showed increased pulmonary artery pressure during the first week of hypoxia and both groups were able to partially compensate pulmonary artery pressure (increase PAT/ET ratio) during the next two weeks of exposure, although the recovery was slower for *PSGL-1*$^{-/-}$ mice. However, WT and *PSGL-1*$^{-/-}$ littermates showed a similar Fulton index and loss of NO-dependent relaxation, indicating that some hypoxia-induced changes are not additive to the endothelial dysfunction provoked by PSGL-1 absence after the 3-week exposure to low oxygen pressure. These data suggest that the endothelial dysfunction promoted by hypoxia in WT mice is already present in PSGL-1$^{-/-}$ females. Importantly, and in accordance with this hypothesis, we found that lung of aged *PSGL-1*$^{-/-}$ females, in addition to having a lower expression of AT2R, showed increased AngII concentration and reduced NO production by endothelial cells, which might explain the higher contractility and reduced relaxation capability of lung arteries at this age, ultimately leading to elevated flow resistance and hence to increased pulmonary pressure and reduced PAT/ET.

1.3 Implication of the RAAS in the development of PAH by *PSGL-1*$^{-/-}$ female mice

Molecular systems implicated in the control of vascular tone, such as ET-1, AngII and NO, have been described to be altered in several animal models and in patients with PAH (77, 110, 160). Thus, hypoxic and MCT-treated rats showed increased AngII and AT1R levels (159, 174, 281), and patients with iPAH showed higher levels of pulmonary AngII due to increased activity of ACE, as well as increased expression and signaling of AT1R, resulting in augmented VSMC proliferation (282). Inhibitors of the RAAS have been proven to have an effect in reducing mPAP and other PAH signs in some animal models and also in pilot studies with small patient cohorts, underscoring the role of RAAS in the pathology of PAH. For example, treatment with losartan (AT1R antagonist) or captopril (inhibitor of ACE) was able to reduce mPAP, RV hypertrophy and lung vascular remodeling in rats exposed to hypobaric hypoxia for 14 days (169, 282). Furthermore, treatment with captopril showed a clear effect in reducing PAP in some studies, whereas in others captopril was unable to lower mPAP (160).

Increased levels of AngII II are associated with the downregulation of miR-204 in PASMC (81). The reduction in the expression of miR-204 induces the upregulation and activation of STAT3, which in turns promotes PASMC proliferation and increases resistance to apoptosis (283). Moreover, the expression of miR-204 is decreased in both patients with PAH and MCT-treated rats (283). According

to these data, high AngII levels could directly induce vascular remodeling in aged *PSGL-1*$^{-/-}$ mice through the downregulation of miR-204. However, young female *PSGL-1*$^{-/-}$ mice did not present higher AngII titers in the lung, but showed reduced expression levels of AT2R, suggesting that the balance between AT1R/AT2R might be responsible for the lung vascular remodeling, modulating the expression of miR-204.

NO is a critical regulator of vascular homeostasis, not only by modulating vascular tone, but also by controlling VSMC proliferation and migration as well as leukocyte adhesion to the endothelium (103, 110). We found reduced NO production by *PSGL-1*$^{-/-}$ lung endothelial cells in aged females, but similar expression levels of eNOS. However, differences in eNOS activity due to changes in the post-translational modifications could account for the reduced NO levels of *PSGL-1*$^{-/-}$ lung endothelial cells (284). It has been previously reported that reduced levels of NO can trigger vascular remodeling, with increased proliferation of VSMC (174-177). However, in young female *PSGL-1*$^{-/-}$, pulmonary vascular remodeling was not associated with decreased NO production by lung endothelial cells, suggesting that other mechanisms could be mediating the first steps of endothelial dysfunction in *PSGL-1*$^{-/-}$ mice. The reduced expression levels of AT2R may account for an increased vascular tone and maintained vasoconstriction, and may contribute to the proliferation of the VSMC, as it was described to occur in patients with PAH (168, 171, 285).

The increased levels of pulmonary AngII found in aged *PSGL-1*$^{-/-}$ female mice might be explained by either an enhanced activity of ACE, which has been previously reported for patients with PAH and animal models (282, 286), or an overexpression/overactivity of chymase. Mast cell chymase, expressed mainly in kidney and heart tissue and also in endothelial cells, is an enzyme that cleaves both angiotensin(1-12) and angiotensinogen into AngII (164-166). It can be released by mast cell degranulation, and might account for the elevated AngII levels not only in inflammatory conditions such as atherosclerosis but also in heart failure (179). Interestingly, the chymase-dependent increase of cardiac AngII is related to aging (165) and aged *PSGL-1*$^{-/-}$ mice are massively infiltrated by immune cells, as previously reported (58).

1.4 Relationship between PAH, AngII and inflammation

Also, it has been reported that an increase in AngII could lead to eNOS uncoupling, which results in reduced NO production (287). In addition, several reports have highlighted the relevant role of inflammation and the immune system in endothelial dysfunction (275, 287, 288). In this context, vascular dysfunction in aortic endothelial cells can be mediated by inflammatory monocytes and NK cells producing IFN-γ and IL-12 in an AngII-dependent manner (287, 288). A similar mechanism could be operating in the pulmonary vasculature of female *PSGL-1*$^{-/-}$ mice, in which aging increases IFN-γ production in macrophages, B cells and T cells, and AngII pulmonary levels that can account for the endothelial dysfunction and eNOS uncoupling with the ensuing reduction in the endothelial NO.

Inflammation has emerged as a pivotal contributor to the development of PAH (151, 289, 290). Perivascular infiltration of mononuclear immune cells has been reported in almost all animal models, especially in rodents subjected to chronic hypoxia or MCT administration, and in IL-6 knock-in transgenic mice (275). Additionally, the upregulation of chemokines (CCL-2, CCL-5, RANTES, fractalkine) and pro-inflammatory cytokines (IL-6, IL-1, IFN-γ) has been described in patients with severe PAH (77, 146, 147, 291-293). In the case of CTD-associated PAH, it has been proposed that autoantibodies (anti-U1-RNP and anti-dsDNA) forming immune complexes could trigger the upregulation of endothelial ligands for leukocytes, such as ICAM-1 or E-sel, initiating or contributing to lung vasculopathology (294). Interestingly, *PSGL-1*$^{-/-}$ mice showed increased expression of P-sel and E-sel in lung endothelial cells. The activation of lung endothelium has been previously described for PAH patients. Plasma levels of soluble (s)P-sel, sE-sel, sICAM-1 and sVCAM-1 were reported to be higher in patients with PAH than in healthy controls (147, 151, 295). In another study, treatment with prostacyclin reduced the levels of sP-sel in a cohort of mainly iPAH patients(296). Similar results have been reported in MCT-induced PAH in rats, which present increased expression of pulmonary ICAM-1, VCAM-1 and E-sel (289). Moreover, it has been demonstrated by immunohistochemistry that infusion of AngII was able to induce the expression of P-sel, E-sel, ICAM-1 and VCAM-1 in mesenteric arterioles and venules in rats (178). Nevertheless, in this thesis we describe that the absence of P-selectin also drives to PAH development with ageing, coinciding with the increase of AngII in the lungs and reduction of NO production by pulmonary endocelial cells.

2. SLE-like syndrome in P-selectin knockout mice

In this thesis, we show that the absence of P-sel breaks immune tolerance and triggers the development of a progressive autoimmune lupus-like syndrome displaying most of the features previously described in lupus-prone mice. Importantly, we show that human biopsies of cLE have reduced number of P-sel stained vessels.

2.1 Autoantibody production and autoimmunity in *P-sel*$^{-/-}$ mice

Given that PSGL-1 deficient mice develop a scleroderma-like syndrome, we have analyzed whether the absence of P-sel, main ligand of PSGL-1, also triggered autoimmunity. We found the production of anti-dsDNA and anti-Sm autoandibodies, hallmarks of SLE in humans (297). Interestingly, anti-Sm and anti-dsDNA autoantibodies are detected at an early age in *P-sel*$^{-/-}$ mice. Despite the frequency of anti-dsDNA autoantibodies is not as high as in MLR/lpr strain, *P-sel*$^{-/-}$ and MLR/lpr mice are the two only murine models of spontaneous SLE expressing both anti-Sm and anti-U1 RNP. The frequency of appearance of anti-Sm in our cohort of mice is comparable with the prevalence described in humans (5-30% in patients versus 8-37% in *P-sel*$^{-/-}$ mice) (226, 228). It has also been reported that, in MLR/lpr mice, the frequency of a speckled autoantibody pattern in Hep-2 cell assay reaches 25% (261). This

pattern is traditionally associated with anti-ribonucleoprotein and anti-Sm antibodies, and, in our mice the combined frequency of mice bearing Sm or RNP is quite similar (31%). The high rate of autoantibodies probably favours, as in human SLE, the formation and deposition of immune complexes in anatomic sites characterized by high blood pressure including capillaries of the skin and glomeruli, among others. Accordingly, we found a high rate of immune complexes deposition in renal glomeruli and skin of aged *P-sel*$^{-/-}$ which is a characteristic of both human and murine lupus (56, 228, 263, 298).

To understand the autoantibody production, we studied the impact of P-sel absence in the homeostasis of the immune system and analyzed the effector and regulatory leukocyte subsets in blood, spleen and skin of WT and P-sel deficient mice, and found that the immune homeostasis is altered in *P-sel*$^{-/-}$ mice. We found higher percentage of germinal center B cell, plasma cells and Tfh subpopulations, indicating more reactive germinal centers in the spleen of young animals. The frequency of Tfh cells has been correlated with the number of plasma cells and disease activity in human SLE (299). In addition, SLE patients with active disease showed a marked expansion in plasma cells, and the frequency of circulating plasma cells correlated with disease activity scores, anti-dsDNA titers and serum immunoglobulin production (300, 301).

We also found reduced circulating CD4^{+} T cells and monocytic populations, in association with an increment in the B cell compartment in *P-sel*$^{-/-}$ mice. Interestingly, at young age we found a reduction in the circulating tolerogenic IL-10-producing cDC and monocyte subsets, as well as in the IL-10^{+} B cell compartment (Breg), whose reduction has been recently implicated in the development of human SLE (302). Although young *P-sel*$^{-/-}$ mice did not have alterations in Th1, Th2 and Th17 subsets, reduction in the IL-10-producing CD4^{+} T cells implies an imbalanced Teff/Treg ratio, as it has been described for both murine and human SLE (303). This reduction in IL-10^{+} cells could be explained by the lack of tolerogenic signal supplied by P-sel interaction with PSGL-1, as previously described (16). Remarkably, we found a shift through a Th17 response with aging in the blood of *P-sel*$^{-/-}$ mice coinciding with the worsening of the disease. Increased serum levels and numbers of Th17 cells have been found in patients with SLE, and the levels of serum IL-17 correlate with disease activity. In fact, IL-17 promotes the recruitment of T cells, monocytes and granulocytes to the inflammatory foci, activates B cells and contributes to the synthesis of IgG and anti-dsDNA autoantibodies (232). Accordingly, we report that, in *P-sel*$^{-/-}$ mice, the effector subpopulations of splenic CD4^{+} and CD8^{+} T cells were increased, with the consequent and relevant reduction among the naïve subset. SLE patients show reduced numbers of CD45RA^{+} naive T cells and increased numbers of CD45RO^{+} memory T cells (304). Interestingly, it has been described that mouse CD8^{+}CD122^{+} Treg have a central memory phenotype (CD44^{high}CD62L^{high}) (305) that could explain the reduction of this compartment in the *P-sel*$^{-/-}$ mice, as well as the reduced populations of IL-10 producing T cells. In addition, this subset has been described to regulate T cell homeostasis and to suppress both autoimmune and alloimmune responses (305).

2.2 Lupus dermatitis: immune and histological alterations

Given that the skin is one of the main organs affected in lupus patients, we have also analyzed whether the dermal immune system is also altered in *P-sel*$^{-/-}$ mice. Our results indicate that dermal pDC subpopulation is increased from youth and that aging also increases the T cell subset. Of note, increased numbers of pDC have been reported to infiltrate skin lesions of cLE patients, associated with an elevation in the production of IFN-α (306). pDC are the most important IFN-α producing cells in the organism, and IFN-α binds to its receptor in almost all leukocyte populations, inducing the expression of a large number of genes. This cluster of genes is called "lupus signature", and it has been found in patients with SLE and most of SLE murine models (286, 117).

Importantly, coinciding with the appearance of the lupus skin lesions, we have found a high reduction in dermal IL-10 producing immune cells and FOXP3^{+} Treg population, together with an important expansion of IL-17 producing T lymphocytes. Our data are in accordance with the expanded Th17 population and reduced Treg subset described for human patients (307). IL-17 producing cells can infiltrate skin, lung, and kidneys of SLE (235, 308-310) and contribute to organ damage by enhancing the recruitment of T cells, monocytes and neutrophils to the inflammed tissue. IL-17 can synergize with BAFF and IL-6 to activate B cells and potentiate the production of autoantibodies (242). It has been described that different mechanisms can be implicated in the breakage of immunological tolerance (311) and our work indicates that a defect in P-sel expression and function, probably through PSGL-1 interaction, could be implicated in maintaining the immune system immunity/tolerance balance. Dysfunction or low expression of P-sel and PSGL-1 could favor the use of alternative molecules for leukocyte extravasation and consequently, the loss of the tolerogenic signal triggered by PSGL-1/P-sel interaction. This hypothesis is supported by the fact that the number of SlanDCs is increased in skin biopsies of SLE and cLE patients (133). SlanDCs do express PSGL-1, but the SLAN glucidic group abrogates its binding to P-sel, conferring them a highly proinflammatory phenotype. Indeed, SlanDCs are strong producers of TNF-α, IL-12 and IL-23 after TLR7 or TLR8 signaling. SlanDC have found to play an important role in the pathogenesis of other autoimmune and inflammatory diseases, such as Crohn's disease, rheumatoid arthritis, , and psoriasis. In psoriatic skin, SlanDCs are important mediators of Th1 and Th17 responses (134).

The skin histological features described in this work for aged *P-sel*$^{-/-}$ mice, such as hyperkeratosis, acanthosis and immune cell infiltration, have been previously reported for MRL/lpr mice (264, 312). According to our data, it has been reported that P-sel or PSGL-1 deficiency in MRL/lpr mice results in an increase in the severity of dermatitis and glomerulonephritis (56). Apart from the lupus dermatitis features, in P-sel deficient mice, the overall frequency of dermal immunoglobulin deposition reached 50%, which is lower than that mentioned for MRL/lpr mice (313). However, in a model of cutaneous lupus induced by 5-fluorouracil plus UV-B light, the prevalence of IgG deposition in the dermoepidermal junction was only 66% (314).

We observed that UV irradiation could accelerate and intensify the appearance of the above mentioned lesions in 3-4-month-old *P-sel*$^{-/-}$ mice, whereas non lupus-prone strains are considered to be resistant to UV-induced DNA damage (297). Interestingly, more than 50% of SLE patients show photosensitivity (297, 315, 316).

2.3 Lupus nephritis and lung involvement

Glomerulonephritis and renal involvement are the most prevalent manifestations in SLE patients (40–70%) (183). Leukocyte infiltration is a common feature shared by humans and lupus-prone mice (317). Accordingly, we found leukocytic infiltration in both glomerular and tubulointerstitial compartments of the kidney in *P-sel*$^{-/-}$ mice. Additionally, *P-sel*$^{-/-}$ mice presented a high frequency of renal infarcts, indicating vascular dysfunction. Renal and systemic vasculitis have been described in patients and experimental models of SLE (256) and, together with immune infiltration, have been associated with loss of renal function (318). In agreement with our data, mice deficient for P-sel are more sensitive to glomerulonephritis (56, 319).

Anti-DNA autoantibodies have been traditionally associated with lupus nephritis (38). Accumulating data have suggested that anti-dsDNA could directly bind to different resident renal cells, such as podocytes and mesangial cells, and also to extracellular matrix components, inducing inflammation and imparing normal cell function (320). The increase in anti-dsDNA prevalence in *P-sel*$^{-/-}$ coincides with the worsening and the increased frequency of immune infiltration and ischemic events. Several autoantibodies have been reported to be potentially implicated in lupus nephritis pathogeny, such as anti-Ro/SSA and Sm, among others (181, 321, 322). Accordingly, the prevalence of Sm in our cohort of *P-sel*$^{-/-}$ mice rose to its maximum at 12-18 months. Moreover, we found an association between renal dysfunction and presence of circulating autoantibodies, with higher levels of proteinuria and hematuria among ENA^{+} P-sel deficient mice.

B cells and T cells have been shown to play a critical role in lupus nephritis (323). Th1 and Th17 responses have been reported in lupus nephritis (232, 324). Depletion of B cells could prevent from lupus nephritis in MRL/lpr lupus prone mice (325). The pathogenic effect of B cells in lupus nephritis is not limited to autoantibody production, as MRL/lpr unable to secrete antibodies were still able to develop lupus nephritis (326).

According to our results, it has been reported that the lack of either P-sel or PSGL-1 in murine lupus models enhances both skin and renal inflammation (56) and that the tissue expression of P- and E-sel in the MLR/lpr mice was not upregulated regarding the non-inflammed MRL$^{+/+}$ mice (327), giving further evidence that lack of selectins may potentiate the autoimmune phenotype in established mouse models of SLE, or that at least they are not necessary for the immune infiltration in both kidney and skin.

Lung involvement is more frequent in *P-sel*$^{-/-}$ mice than in SLE patients (183). In mice, more than 70% of *P-sel*$^{-/-}$ animals showed NISP, whereas lung involvement appears in up to 13% of patients with SLE (183). There is abundant evidence indicating that increased P-sel expression in lung post-capillary venules is crucial for leukocyte extravasation, particularly for neutrophils (328, 329). Considering the relevance of P-sel/PSGL-1 interaction for leukocyte trafficking in the lung, it would be reasonable to assume that the absence of P-sel could lead to the severe impairment of lung immune homeostasis found in *P-sel*$^{-/-}$ mice. Consistent with a previous report in MRL/lpr mice (330), mononuclear immune cell infiltrates were dispersed among the perivascular, peribronchiolar and the alveolar areas in *P-sel*$^{-/-}$ mice and promoted NSIP, whose severity increased with ageing.

As the lupus-like syndrome developed by P-sel deficient mice is progressive, together with the main features of the lupus-like syndrome, such as the severe and widespread form of NSIP, the highest frequency of renal infarcts, the most aggressive skin manifestations and immunoglobulin depositions, we found a rapid decrease of the body weight (caquexia) followed by sudden death when animals are over 18 months of age.

2.4 P-selectin implication in the pathology of human lupus erythematosus

According with our data in *P-sel*$^{-/-}$ mice, we found a reduction in the expression of P-sel in the dermal blood vessels of patients with cLE. This important result does not concur with the higher levels of P-sel that have been traditionally associated with other autoimmune and inflammatory diseases like glomerulonephritis, rheumatoid arthritis, psoriasis or atopic dermatitis (41, 268) (331). It has been reported that TNF-α and LPS can downregulate human P-sel. The increased levels of TNF-α in the serum of SLE patients are consistent with the low expression of P-sel that we found in the skin of lupus patients.

In summary, we show that P-sel expression is crucial for the immune system homeostasis and that its absence promotes the spontaneous development of a lupus-like syndrome in mice. Accordingly, patients with cutaneous lupus showed lower expression of P-sel in the endothelium of dermal vessels, suggesting that the reduced expression of P-selcould be implicated in the pathogenesis of this disease. As SLE pathogenesis is not well understood and there is not a universally curative treatment for lupus in humans, it would be very important to discover new molecules implicated in the development of the different forms of this disease that could be used as targets for new treatments. Importantly, our work in this thesis will contribute to the understanding of lupus pathogenesis and points that P-sel KO mice could be used as a new experimental model for in vivo assays to evaluate new treatments or combination of treatments against the progression of the disease that could prevent organ damage associated with SLE.

As a summary, the data presented in this thesis indicates that PSGL-1/P-selectin interaction plays an important role in controlling the immune and vascular homeostasis. The absence of either PSGL-1 or

P-selectin breaks immune tolerance and leads to the development of autoimmunity. Moreover, breakage of immune tolerance by lack of PSGL-1 or P-selectin induces endothelial dysfunction which promotes vascular remodeling in lungs and drives to pulmonary arterial hypertension, right ventricle dysfunction and death. Thus, this thesis highlights the relevance of leukocyte/endothelial communication and their interdependence for maintaining the immune system and cardiovascular homeostasis.

Conclusions

Conclusions

1. Female PSGL-1 deficient mice present lung vascular remodeling and incipient increment in the pulmonary pressure from 1.5 months.

2. Female PSGL-1 deficient mice, with aging, develop pulmonary arterial hypertension, associated with a reduction in the endothelial nitric oxide-dependent vasodilator response.

3. Female PSGL-1 deficient mice present reduced expression of the angiotensin II receptor 2 in lung lysates, from 1.5-3 months. Aging induces in females an increment in the angiotensin II levels in the lung, coinciding with a reduction in nitric oxide production by endothelial lung cells.

4. Aged female PSGL-1 deficient mice show enhanced levels of P-selectin and E-selectin in lung endotelial cells, and higher frequencies of IFN-γ producing macrophages, T cells and B cells in the lung.

5. With aging, female P-selectin deficient mice develop non specific interstitial pneumonia and pulmonary arterial hypertension, associated with a reduced production of nitric oxide by lung endothelial cells.

6. P-selectin deficient mice showed an increased Th17 circulating population, reduced expression of IL-10 by circulating leukocytes, increased splenic reactivity and an increase in the T cell effector compartment in the spleen. As a consequence, they develop a severe autoinmune syndrome that leads to premature death, characterized by the production of circulating autoantibodies related to human connective tissue diseases, incluing anti-dsDNA, and immune complex deposition. These mice

7. P-selectin deficient mice show lupus dermatitis, with a reduction in the percentages of IL-10 producing immune cells, a diminished Treg population and an augmented population of IL-17 producing T lymphocytes in the skin.

8. P-selectin deficient mice present lupus nephritis, with increased frequency of inflammatory infiltrates and ischemic events, and elevated levels of proteinuria and hematuria.

9. Patients with cutaneous lupus erythematosus present lower expression of P-selectin in dermal blood vessels. Futhermore, they show a reduced number of vessels expressing P-selectin in the skin.

10. Leukocyte/endothelial interaction through PSGL-1 and P-selectin is crucial for the maintenance of immune and vascular homeostasis, acting as a barrier for autoimmunity and pulmonary hypertension.

Conclusiones

Conclusiones

1. Los ratones hembra deficientes en PSGL-1 presentan una remodelación de los vasos sanguíneos del pulmón y un aumento incipiente de la presión pulmonar desde los 1,5 meses de edad.

2. Los ratones hembra deficientes en PSGL-1, con el envejecimiento, desarrollan hipertensión arterial pulmonar, asociada a una menor respuesta vasodilatadora dependiente de óxido nítrico endotelial.

3. Los ratones hembra deficientes en PSGL-1 presentan reducida la expresión del receptor 2 de la angiotensina II en lisados pulmonares, desde los 1,5-3 meses de edad. El envejecimiento induce en las hembras el aumento de la concentración de AngII en el pulmón, coincidiendo con la disminución en la producción de óxido nítrico por las células endoteliales pulmonares.

4. Las hembras envejecidas que carecen de PSGL-1 muestran niveles elevados de P-selectina y E-selectina en las células endoteliales pulmonares y un mayor porcentaje de macrófagos, linfocitos T y linfocitos B productores de IFN-γ en el pulmón.

5. Las hembras deficientes en P-selectina desarrollan, con el envejecimiento, neumonia intersticial no específica e hipertensión arterial pulmonar, asociada a una menor producción de óxido nítrico por las células endoteliales pulmonares.

6. Los ratones deficientes en P-selectina muestran un aumento de la población Th17 circulante, una reducción en la expresión de IL-10 por parte de los leucocitos de sangre periférica, mayor reactividad y aumento la población de linfocitos T efectores en el bazo. Como consecuencia, desarrollan un síndrome autoimmune severo que conduce a una muerte prematura, caracterizado por la producción de autoanticuerpos circulantes relacionados con enfermedades humanas de tejido conectivo, incluidos anti-dsDNA y depósito de inmunocomplejos.

7. Los ratones deficientes en P-selectina presentan dermatitis lúpica, con una reducción en los porcentajes de células que expresan IL-10, una disminución de la población de Treg disminuida y un aumento de linfocitos productores de IL-17 en la piel.

8. Los ratones deficientes en P-selectina muestran nefritis lúpica, con mayor frecuencia de infiltrados inflamatorios y eventos isquémicos, y elevados niveles de proteinuria y hematuria.

9. Los enfermos con lupus cutáneo presentan menor expresión de P-selectina en los vasos de la piel y, además, tienen reducido el número de vasos que expresan P-selectina.

10. La interacción leucocito/endotelio a través de PSGL-1y P-selectina es muy importante para el mantenimiento de la homeostasis del sistema inmune y el sistema vascular, actuando como una barrera frente a la autinmunidad y la hipertensión pulmonar.

References

References

1. Veldman, G., Bean, K., Cumming, D., Eddy, R., Sait, S., and Shows, T. 1995. Genomic organization and chromosomal localization of the gene encoding human P-selectin glycoprotein ligand. *J Biol Chem* 270:16470-16475.
2. Yang, J., Galipeau, J., Kozak, C., Furie, B., and Furie, B. 1996. Mouse P-selectin glycoprotein ligand-1: molecular cloning, chromosomal localization, and expression of a functional P-selectin receptor. *Blood* 87:4176-4186.
3. Zarbock, A., Ley, K., McEver, R.P., and Hidalgo, A. 2011. Leukocyte ligands for endothelial selectins: specialized glycoconjugates that mediate rolling and signaling under flow. *Blood* 118:6743-6751.
4. Carlow, D.A., Gossens, K., Naus, S., Veerman, K.M., Seo, W., and Ziltener, H.J. 2009. PSGL-1 function in immunity and steady state homeostasis. *Immunological Reviews* 230:75-96.
5. Afshar-Kharghan, V., Diz-Kucukkaya, R., Ludwig, E., Marian, A., and Lopez, J. 2001. Human polymorphism of P-selectin glycoprotein ligand 1 attributable to variable numbers of tandem decameric repeats in the mucinlike region. *Blood* 97:3306-3307.
6. McEver, R., and Cummings, R. 1997. Role of PSGL-1 binding to selectins in leukocyte recruitment. *J Clin Invest* 100:S97-S103.
7. Schachter, H., and Brockhausen, I. 1989. The biosynthesis of branched O-glycans. *Symp Soc Exp Biol* 43:1-26.
8. Somers, W., Tang, J., Shaw, G., and Camphausen, R. 2000. Insights into the molecular basis of leukocyte tethering and rolling revealed by structures of P- and E-selectin bound to SLe(X) and PSGL-1. *Cell* 103:467-479.
9. Beauharnois, M., Lindquist, K., Marathe, D., Vanderslice, P., Xia, J., Matta, K., and Neelamegham, S. 2005. Affinity and kinetics of sialyl Lewis-X and core-2 based oligosaccharides binding to L- and P-selectin *Biochemistry* 44:9507–9519.
10. Rossi, B., and Constantin, G. 2008. Anti-Selectin Therapy for the Treatment of Inflammatory Diseases. *Inflamm Allergy Drug Targets* 7:85-93.
11. Martinez, M., Joffraud, M., Giraud, S., Baïsse, B., Bernimoulin, M., Schapira, M., and Spertini, O. 2005. Regulation of PSGL-1 interactions with L-selectin, P-selectin, and E-selectin: role of human fucosyltransferase-IV and -VII. *J Biol Chem* 280:5378-5390.
12. Urzainqui, A., Serrador, J.M., Viedma, F., Yáñez-Mó, M., Rodríguez, A., Corbí, A.L., Alonso-Lebrero, J.L., Luque, A., Deckert, M., Vázquez, J., et al. 2002. ITAM-Based Interaction of ERM Proteins with Syk Mediates Signaling by the Leukocyte Adhesion Receptor PSGL-1. *Immunity* 17:401–412.
13. Alonso-Lebrero, J., Serrador, J., Domínguez-Jiménez, C., Barreiro, O., Luque, A., Pozo, M.d., Snapp, K., Kansas, G., Schwartz-Albiez, R., Furthmayr, H., et al. 2000. Polarization and

interaction of adhesion molecules P-selectin glycoprotein ligand 1 and intercellular adhesion molecule 3 with moesin and ezrin in myeloid cells. *Blood* 95:2413-2419.

14. Rivera-Nieves, J., Burcin, T., Olson, T., Morris, M., McDuffie, M., Cominelli, F., and Ley, K. 2006. Critical role of endothelial P-selectin glycoprotein ligand 1 in chronic murine ileitis. *J Exp Med* 203:907-917.
15. da Costa Martins, P., García-Vallejo, J., Thienen, J.v., Fernandez-Borja, M., Gils, J.v., Beckers, C., Horrevoets, A., Hordijk, P., and Zwaginga, J. 2007. P-selectin glycoprotein ligand-1 is expressed on endothelial cells and mediates monocyte adhesion to activated endothelium. *Arterioscler Thromb Vasc Biol* 27:1023-1029.
16. Urzainqui, A., Hoyo, G.M.d., Lamana, A., Fuente, H.d.l., Barreiro, O., Olazabal, I., Martin, P., Wild, M., Vestweber, D., González-Amaro, R., et al. 2007. Functional role of P-selectin glycoprotein ligand 1/P-selectin interaction in the generation of tolerogenic dendritic cells. *J Immunol* 179:7457-7465.
17. Frenette, P., Denis, C., Weiss, L., Jurk, K., Subbarao, S., Kehrel, B., Hartwig, J., Vestweber, D., and Wagner, D. 2000. P-Selectin glycoprotein ligand 1 (PSGL-1) is expressed on platelets and can mediate platelet-endothelial interactions in vivo. *J Exp Med* 191:1413-1422.
18. Domínguez-Luis, M., Lamana, A., Vazquez, J., García-Navas, R., Mollinedo, F., Sánchez-Madrid, F., Díaz-González, F., and Urzainqui, A. 2011. The metalloprotease ADAM8 is associated with and regulates the function of the adhesion receptor PSGL-1 through ERM proteins. *Eur J Immunol* 41:3436-3442.
19. van Genderen, H., Wielders, S., Lindhout, T., and Reutelingsperger, C. 2006. Rolling and adhesion of apoptotic monocytes is impaired by loss of functional cell surface-expressed P-selectin glycoprotein ligand-1. *J Thromb Haemost* 4:1611-1617.
20. Marsik, C., Mayr, F., Cardona, F., Schaller, G., Wagner, O., and Jilma, B. 2004. Endotoxin downmodulates P-selectin glycoprotein ligand-1 (PSGL-1, CD162) on neutrophils in humans. *J Clin Immunol* 24:62-65.
21. Jilma, B., Hergovich, N., Homoncik, M., Marsik, C., Kreuzer, C., and Jilma-Stohlawetz, P. 2002. Rapid down modulation of P-selectin glycoprotein ligand-1 (PSGL-1, CD162) by G-CSF in humans. *Transfusion* 42:328–333.
22. Knibbs, R., Craig, R., Natsuka, S., Chang, A., Cameron, M., Lowe, J., and Stoolman, L. 1996 The fucosyltransferase FucT-VII regulates E-selectin ligand synthesis in human T cells. *J Cell Biol. May;133(4):911-20* 133:911-920.
23. Braun, O., Slotta, J., Menger, M., Erlinge, D., and Thorlacius, H. 2008 Primary and secondary capture of platelets onto inflamed femoral artery endothelium is dependent on P-selectin and PSGL-1. *Eur J Pharmacol* 592:128-132.
24. Ley, K., and Kansas, G. 2004. Selectins in T-cell recruitment to non-lymphoid tissues and sites of inflammation. *Nat Rev Immunol* 4:325-335.

25. Austrup, F., Vestweber, D., Borges, E., Löhning, M., Bräuer, R., Herz, U., Renz, H., Hallmann, R., Scheffold, A., Radbruch, A., et al. 1997. P- and E-selectin mediate recruitment of T-helper-1 but not T-helper-2 cells into inflammed tissues. *Nature* 385:81-83.
26. Haddad, W., Cooper, C., Zhang, Z., Brown, J., Zhu, Y., Issekutz, A., Fuss, I., Lee, H., Kansas, G., and Barrett, T. 2003. P-selectin and P-selectin glycoprotein ligand 1 are major determinants for Th1 cell recruitment to nonlymphoid effector sites in the intestinal lamina propria. *J Exp Med* 198:369-377.
27. Watson, M.L., Kingsmore, S.F., Johnston, G.I., Siegelman, M.H., Beau, M.M.L., Lemons, R.S., Bora, N.S., Howard, T.A., Weissman, I.L., McEver, R.P., et al. 1990. Genomic Organization of the Selectin Family of Leukocyte Adhesion Molecules on Human and Mouse Chromosome 1. *J Exp Med* 172:263-272.
28. Johnston, G.I., Bliss, G.A., Newman, P.J., and McEver, R.P. 1990. Structure of the Human Gene Encoding Granule Membrane Protein-140, a Member of the Selectin Family of Adhesion Receptors for Leukocytes. *The Journal of Biological Chemistry* 265 21381-21385.
29. McEver, R.P., Beckstead, J.H., Moore, K.L., Marshall-Carlson, L., and Baintont, D.F. 1989. GMP-140, a Platelet a-Granule Membrane Protein, Is Also Synthesized by Vascular Endothelial Cells and Is Localized in Weibel-Palade Bodies. *J Clin Invest* 84:92-99.
30. Sanders, W., Wilson, R., Ballantyne, C., and Beaudet, A. 1992. Molecular cloning and analysis of in vivo expression of murine P-selectin. *Blood* 80:795-800.
31. Weller, A., Isenmann, S., and Vestweber, D. 1992. Cloning of the mouse endothelial selectins. Expression of both E- and P-selectin is inducible by tumor necrosis factor alpha. *J Biol Chem* 267:15176-15183.
32. Ley, K. 2003. The role of selectins in inflammation and disease. *Trends Mol Med* 9:263-268.
33. Vestweber, D., and Blanks, J. 1999. Mechanisms that regulate the function of the selectins and their ligands. *Physiol Rev* 79:181-213.
34. McEver, R.P., and Zhu, C. 2010. Rolling cell adhesion. *Annu Rev Cell Dev Biol* 26:363-396.
35. Schweitzer, K., Dräger, A., van der Valk, P., Thijsen, S., Zevenbergen, A., Theijsmeijer, A., van der Schoot, C., and Langenhuijsen, M. 1996. Constitutive expression of E-selectin and vascular cell adhesion molecule-1 on endothelial cells of hematopoietic tissues. *Am J Pathol* 148:165-175.
36. McEver, R. 2015. Selectins: initiators of leucocyte adhesion and signalling at the vascular wall. *Cardiovascular Research* 107:331–339.
37. Yao, L., Setiadi, H., Xia, L., Laszik, Z., Taylor, F., and McEver, R. 1999. Divergent inducible expression of P-selectin and E-selectin in mice and primates. *Blood* 94:3820-3828.
38. Liu, Z., Miner, J.J., Yago, T., Yao, L., Lupu, F., Xia, L., and McEver, R.P. 2010. Differential regulation of human and murine P-selectin expression and function in vivo. *J Exp Med* 207:2975-2987.

39. Kivisäkk, P., Mahad, D., Callahan, M., Trebst, C., Tucky, B., Wei, T., Wu, L., Baekkevold, E., Lassmann, H., Staugaitis, S., et al. 2003. Human cerebrospinal fluid central memory CD4+ T cells: evidence for trafficking through choroid plexus and meninges via P-selectin. *Proc Natl Acad Sci U S A* 100:8389-8394.
40. Vestweber, D. 2007. Adhesion and signaling molecules controlling the transmigration of leukocytes through endothelium. *Immunological Reviews* 218:178-196.
41. Angiari, S. 2015. Selectin-mediated leukocyte trafficking during the development of autoimmune disease. *Autoimmun Rev* 14:984–995.
42. Veerman, K.M., Williams, M.J., Uchimura, K., Singer, M.S., Merzaban, J.S., Naus, S., Carlow, D.A., Owen, P., Rivera-Nieves, J., Rosen, S.D., et al. 2007. Interaction of the selectin ligand PSGL-1 with chemokines CCL21 and CCL19 facilitates efficient homing of T cells to secondary lymphoid organs. *Nat Immunol* 8:532-539.
43. Nuñez-Andrade, N., Lamana, A., Sancho, D., Gisbert, J., Gonzalez-Amaro, R., Sanchez-Madrid, F., and Urzainqui, A. 2011. P-selectin glycoprotein ligand-1 modulates immune inflammatory responses in the enteric lamina propria. *J Pathol* 224:212-221.
44. Ainslie, M., McNulty, C., Huynh, T., Symon, F., and Wardlaw, A. 2002. Characterisation of adhesion receptors mediating lymphocyte adhesion to bronchial endothelium provides evidence for a distinct lung homing pathway. *Thorax* 57:1054–1059.
45. Rossi, F., Corbel, S., Merzaban, J., Carlow, D., Gossens, K., Duenas, J., So, L., Yi, L., and Ziltener, H. 2005. Recruitment of adult thymic progenitors is regulated by P-selectin and its ligand PSGL-1. *Nat Immunol* 6:626-634.
46. Kunkel, E., and Ley, K. 1996. Distinct phenotype of E-selectin-deficient mice. E-selectin is required for slow leukocyte rolling in vivo. *Circul Res* 79:1196-1204.
47. Luo, J., Xu, T., Li, C., Ba, X., Wang, X., Jiang, Y., and Zeng, X. 2013. p85-RhoGDI2, a novel complex, is required for PSGL-1-induced 1 integrin-mediated lymphocyte adhesion to VCAM-1. *Int J Biochem Cell Biol* 45:2764-2773.
48. Luo, J., Li, C., Xu, T., Liu, W., Ba, X., Wang, X., and Zeng, X. 2014. PI3K is involved in β1 integrin clustering by PSGL-1 and promotes β1 integrin-mediated Jurkat cell adhesion to fibronectin. *Mol Cell Biochem* 385:287-295.
49. Green, C., Pearson, D., Camphausen, R., Staunton, D., and Simon, S. 2004. Shear-dependent capping of L-selectin and P-selectin glycoprotein ligand 1 by E-selectin signals activation of high-avidity beta2-integrin on neutrophils. *J Immunol* 172:7780-7790.
50. Stadtmann, A., Brinkhaus, L., Mueller, H., Rossaint, J., Bolomini-Vittori, M., Bergmeier, W., Aken, H.V., Wagner, D., Laudanna, C., Ley, K., et al. 2011. Rap1a activation by CalDAG-GEFI and p38 MAPK is involved in E-selectin-dependent slow leukocyte rolling. *Eur J Immunol* 41:2074-2085.
51. Rose, D., Alon, R., and Ginsberg, M. 2007 Integrin modulation and signaling in leukocyte adhesion and migration. *Immunol Rev* 218:126-134.

52. Zarbock, A., Müller, H., Kuwano, Y., and Ley, K. 2009 PSGL-1-dependent myeloid leukocyte activation. *Journal of Leukocyte Biology* 86.

53. Zarbock, A., Abram, C., Hundt, M., Altman, A., Lowell, C., and Ley, K. 2008. PSGL-1 engagement by E-selectin signals through Src kinase Fgr and ITAM adapters DAP12 and FcR gamma to induce slow leukocyte rolling. *J Exp Med* 205:2339-2347.

54. Abbal, C., Lambelet, M., Bertaggia, D., Gerbex, C., Martinez, M., Arcaro, A., Schapira, M., and Spertini, O. 2006 Lipid raft adhesion receptors and Syk regulate selectin-dependent rolling under flow conditions. *Blood* 108:3352-3359.

55. Zarbock, A., Lowell, C.A., and Ley, K. 2007. Spleen tyrosine kinase Syk is necessary for E-selectin-induced alpha(L)beta(2) integrin-mediated rolling on intercellular adhesion molecule-1. *Immunity* 26:773-783.

56. He, X., Schoeb, T.R., Panoskaltsis-Mortari, A., Zinn, K.R., Kesterson, R.A., Zhang, J., Samuel, S., Hicks, M.J., Hickey, M.J., and Bullard, D.C. 2006. Deficiency of P-Selectin or P-Selectin Glycoprotein Ligand-1 Leads to Accelerated Development of Glomerulonephritis and Increased Expression of CC Chemokine Ligand 2 in Lupus-Prone Mice. *J Immunol* 177:8748-8756.

57. Yoshizaki, A., Yanaba, K., Iwata, Y., Komura, K., Ogawa, A., Akiyama, Y., Muroi, E., Hara, T., Ogawa, F., Takenaka, M., et al. 2010. Cell adhesion molecules regulate fibrotic process via Th1/Th2/Th17 cell balance in a bleomycin-induced scleroderma model. *J Immunol* 185:2502-2515.

58. Pérez-Frías, A., González-Tajuelo, R., Núñez-Andrade, N., Tejedor, R., García-Blanco, M., Vicente-Rabaneda, E., Castañeda, S., Gamallo, C., Silván, J., Esteban-Villafruela, A., et al. 2014. Development of an autoimmune syndrome affecting the skin and internal organs in P-selectin glycoprotein ligand 1 leukocyte receptor-deficient mice. *Arthritis Rheumatol* 66:3178-3189.

59. Rosenkranz, A., Mendrick, D., Cotran, R., and Mayadas, T. 1999. P-selectin deficiency exacerbates experimental glomerulonephritis: a protective role for endothelial P-selectin in inflammation. *J Clin Invest* 103:649-659.

60. Eto, T., Winkler, I., Purton, L.E., and Lévesque, J.-P. 2005. Contrasting effects of P-selectin and E-selectin on the differentiation of murine hematopoietic progenitor cells. *Experimental Hematology* 33:232-242.

61. Lévesque, J.-P., Zannettino, A.C., Pudney, M., Niutta, S., Haylock, D.N., Snapp, K.R., Kansas, G.S., Berndt, M.C., and Simmons, P.J. 1999. PSGL-1-Mediated Adhesion of Human Hematopoietic Progenitors to P-Selectin Results in Suppression of Hematopoiesis. *Immunity* 11:369–378.

62. Tinoco, R., Carrette, F., Barraza, M.L., Otero, D.C., Magaña, J., Bosenberg, M.W., Swain, S.L., and Bradley, L.M. 2016. PSGL-1 Is an Immune Checkpoint Regulator that Promotes T Cell Exhaustion. *Immunity* 44:1190-1203.

63. Matsumoto, M., Miyasaka, M., and Hirata, T. 2009. P-Selectin Glycoprotein Ligand-1 Negatively Regulates T-Cell Immune Responses. *J Immunol* 183:7204-7211.

64. Hirata, T., Furukawa, Y., Yang, B., Hieshima, K., Fukuda, M., Kannagi, R., Yoshie, O., and Miyasaka, M. 2004. Human P-selectin glycoprotein ligand-1 (PSGL-1) interacts with the skin-associated chemokine CCL27 via sulfated tyrosines at the PSGL-1 amino terminus. *J Biol Chem* 279:51775-51782.

65. Veldkamp, C.T., Kiermaier, E., Gabel-Eissens, S.J., Gillitzer, M.L., Lippner, D.R., DiSilvio, F.A., Mueller, C.J., Wantuch, P.L., Chaffee, G.R., Famiglietti, M.W., et al. 2015. Solution structure of CCL19 and identification of overlapping CCR7 and PSGL-1 binding sites. *Biochemistry* 54:4163–4166.

66. Nishimura, Y., Shimojima, M., Tano, Y., Miyamura, T., Wakita, T., and Shimizu, H. 2009. Human P-selectin glycoprotein ligand-1 is a functional receptor for enterovirus 71. *Nat Med* 15:794–797.

67. Nishimura, Y., Wakita, T., and Shimizu, H. 2010. Tyrosine Sulfation of the Amino Terminus of PSGL-1 Is Critical for Enterovirus 71 Infection. *PLoS Pathog* 6:e1001174.

68. Ramos-Sevillano, E., Urzainqui, A., Andrés, B.d., González-Tajuelo, R., Domenech, M., González-Camacho, F., Sánchez-Madrid, F., Brown, J.S., García, E., and Yuste, J. 2016. PSGL-1 on Leukocytes is a Critical Component of the Host Immune Response against Invasive Pneumococcal Disease. *PLoS Pathog* 12:e1005500.

69. Chung, M., Wines, B., Baker, H., Langley, R., Baker, E., and Fraser, J. 2007. The crystal structure of staphylococcal superantigen-like protein 11 in complex with sialyl Lewis X reveals the mechanism for cell binding and immune inhibition. *Mol Microbiol* 66:1342-1355.

70. Bestebroer, J., Poppelier, M., Ulfman, L., Lenting, P., Denis, C., van Kessel, K., van Strijp, J., and de Haas, C. 2007. Staphylococcal superantigen-like 5 binds PSGL-1 and inhibits P-selectin-mediated neutrophil rolling. *Blood* 109:2936-2943.

71. Pepin, M., Mezouar, S., Pegon, J., Muczynski, V., Adam, F., Bianchini, E.P., Bazaa, A., Proulle, V., Rupin, A., Paysant, J., et al. 2016. Soluble Siglec-5 associates to PSGL-1 and displays antiinflammatory activity. *Sci Rep* 6:37953.

72. Deban, L., Russo, R., Sironi, M., Moalli, F., Scanziani, M., Zambelli, V., Cuccovillo, I., Bastone, A., Gobbi, M., Valentino, S., et al. 2010. Regulation of leukocyte recruitment by the long pentraxin PTX3. *Nat Immunol* 11:328-334.

73. Aigner, S., Sthoeger, Z., Fogel, M., Weber, E., Zarn, J., Ruppert, M., Zeller, Y., Vestweber, D., Stahel, R., Sammar, M., et al. 1997. CD24, a Mucin-Type Glycoprotein, Is a Ligand for P-Selectin on Human Tumor Cells. *Blood* 89:3385-3395.

74. Ling, Y., Johnson, M., Kiely, D., Condliffe, R., Elliot, C., Gibbs, J., Howard, L., Pepke-Zaba, J., Sheares, K., Corris, P., et al. 2012 Changing demographics, epidemiology, and survival of incident pulmonary arterial hypertension: results from the pulmonary hypertension registry of the United Kingdom and Ireland. *Am J Respir Crit Care Med* 186:790-796.

75. Austin, E., and Loyd, J. 2007 Genetics and Mediators in Pulmonary Arterial Hypertension. *Clin Chest Med* 28:43-48.

76. Humbert, M., Sitbon, O., Chaouat, A., Bertocchi, M., Habib, G., Gressin, V., Yaici, A., Weitzenblum, E., Cordier, J., Chabot, F., et al. 2006. Pulmonary arterial hypertension in France: results from a national registry. *Am J Respir Crit Care Med* 173:1023-1030.

77. Montani, D., Günther, S., Dorfmüller, P., Perros, F., Girerd, B., Garcia, G., Jaïs, X., Savale, L., Artaud-Macari, E., Price, L.C., et al. 2013. Pulmonary arterial hypertension. *Orphanet Journal of Rare Diseases* 8.

78. Hachulla, E., and Coghlan, J. 2004. A new era in the management of pulmonary arterial hypertension related to scleroderma: endothelin receptor antagonism. *Ann Rheum Dis* 63:1009-1014.

79. Simonneau, G., Gatzoulis, M., Adatia, I., Celermajer, D., Denton, C., Ghofrani, A., Sanchez, M.G., Kumar, R.K., Landzberg, M., Machado, R., et al. 2013. Updated Clinical Classification of Pulmonary Hypertension. *J Am Coll Cardiol* 62:D34-41.

80. Farber, H., and Loscalzo, J. 2004. Pulmonary Arterial Hypertension. *N Engl J Med* 351:1655-1665.

81. Leopold, J.A., and Maron, B.A. 2016. Molecular Mechanisms of Pulmonary Vascular Remodeling in Pulmonary Arterial Hypertension. *Int J Mol Sci* 17.

82. Cogan, J., Pauciulo, M., Batchman, A., Prince, M., Robbins, I., Hedges, L., Stanton, K., Wheeler, L., 3rd, J.P., Loyd, J., et al. 2006. High Frequency of BMPR2 Exonic Deletions/Duplications in Familial Pulmonary Arterial Hypertension. *Am J Respir Crit Care Med* 174:590-598.

83. Aldred, M., Vijayakrishnan, J., James, V., Soubrier, F., Sanchez, M.G., Martensson, G., Galie, N., Manes, A., Corris, P., Simonneau, G., et al. 2006. BMPR2 gene rearrangements account for a significant proportion of mutations in familial and idiopathic pulmonary arterial hypertension. *Hum Mutat* 27:212-213.

84. Elliott, C. 2005 Genetics of pulmonary arterial hypertension: current and future implications. *Semin Respir Crit Care Med* 26:365-371.

85. International PPH Consortium, t., Lane, K., Machado, R., Pauciulo, M., Thomson, J., 3rd, J.P., Loyd, J., Nichols, W., and Trembath, R. 2000. Heterozygous germline mutations in BMPR2, encoding a TGF-beta receptor, cause familial primary pulmonary hypertension. *Nat Genet* 26:81-84.

86. Thomson, J., Machado, R., Pauciulo, M., Morgan, N., Humbert, M., Elliott, G., Ward, K., Yacoub, M., Mikhail, G., Rogers, P., et al. 2000. Sporadic primary pulmonary hypertension is associated with germline mutations of the gene encoding BMPR-II, a receptor member of the TGF-beta family. *J Med Genet* 37:741-745.

87. Machado, R., Aldred, M., James, V., Harrison, R., Patel, B., Schwalbe, E., Gruenig, E., Janssen, B., Koehler, R., Seeger, W., et al. 2006. Mutations of the TGF-beta type II receptor BMPR2 in pulmonary arterial hypertension. *Hum Mutat* 27:121-132.

88. Hamid, R., Cogan, J., Hedges, L., Austin, E., 3rd, J.P., Newman, J., and Loyd, J. 2009. Penetrance of pulmonary arterial hypertension is modulated by the expression of normal BMPR2 allele. *Hum Mutat* 30:649-654.

89. Harrison, R., Flanagan, J., Sankelo, M., Abdalla, S., Rowell, J., Machado, R., Elliott, C., Robbins, I., Olschewski, H., McLaughlin, V., et al. 2003. Molecular and functional analysis identifies ALK-1 as the predominant cause of pulmonary hypertension related to hereditary haemorrhagic telangiectasia. *J Med Genet* 40:865–871.

90. Chaouat, A., Coulet, F., Favre, C., Simonneau, G., Weitzenblum, E., Soubrier, F., and Humbert, M. 2004. Endoglin germline mutation in a patient with hereditary haemorrhagic telangiectasia and dexfenfluramine associated pulmonary arterial hypertension. *Thorax* 59:446–448.

91. Shintani, M., Yagi, H., Nakayama, T., Saji, T., and Matsuoka, R. 2009. A new nonsense mutation of SMAD8 associated with pulmonary arterial hypertension. *J Med Genet* 46:331-337.

92. Nasim, M., Ogo, T., Ahmed, M., Randall, R., Chowdhury, H., Snape, K., Bradshaw, T., Southgate, L., Lee, G., Jackson, I., et al. 2011. Molecular genetic characterization of SMAD signaling molecules in pulmonary arterial hypertension. *Hum Mutat* 32:1385-1389.

93. Austin, E., Ma, L., LeDuc, C., Rosenzweig, E., Borczuk, A., 3rd, J.P., Palomero, T., Sumazin, P., Kim, H., Talati, M., et al. 2012. Whole Exome Sequencing to Identify a Novel Gene (Caveolin-1) Associated with Human Pulmonary Arterial Hypertension. *Circ Cardiovasc Genet* 5:336-343.

94. Fishman, A. 2004. Primary Pulmonary Arterial Hypertension: A Look Back. *J Am Coll Cardiol* 43:2S-4S.

95. Savale, L., Chaumais, M.-C., Cottin, V., Bergot, E., Frachon, I., Prevot, G., Pison, C., Dromer, C., Poubeau, P., Lamblin, N., et al. 2012. Pulmonary hypertension associated with benfluorex exposure. *Eur Respir J* 40:1164-1172.

96. Garcia-Dorado, D., Miller, D., Garcia, E., Delcan, J., Maroto, E., and Chaitman, B. 1983. An epidemic of pulmonary hypertension after toxic rapeseed oil ingestion in Spain. *J Am Coll Cardiol* 1:1216-1222.

97. Chin, K., Channick, R., and Rubin, L. 2006. Is methamphetamine use associated with idiopathic pulmonary arterial hypertension? *Chest* 130:1657-1663.

98. Montani, D., Bergot, E., Günther, S., Savale, L., Bergeron, A., Bourdin, A., Bouvaist, H., Canuet, M., Pison, C., Macro, M., et al. 2012. Pulmonary arterial hypertension in patients treated by dasatinib. *Circulation* 125:2128-2137.

99. Förstermann, U., and Sessa, W. 2012. Nitric oxide synthases: regulation and function. *Eur Heart J* 33:829-837.

100. Gao, Y., Roman, L., Martásek, P., Panda, S., Ishimura, Y., and Masters, B. 2007. Oxygen Metabolism by Endothelial Nitric-oxide Synthase. *J Biol Chem* 282:28557-28565.

101. Palmer, R., Ferrige, A., and Moncada, S. 1987. Nitric oxide release accounts for the biological activity of endothelium-derived relaxing factor. *Nature* 327:524–526.

102. Kubes, P., Suzuki, M., and Granger, D. 1991. Nitric oxide: An endogenous modulator of leukocyte adhesion. *Proc Natl Acad Sci U S A* 88:4651-4655.

103. Martinelli, R., Gegg, M., Longbottom, R., Adamson, P., Turowski, P., and Greenwood, J. 2009 ICAM-1–mediated Endothelial Nitric Oxide Synthase Activation via Calcium and AMP-activated Protein Kinase Is Required for Transendothelial Lymphocyte Migration *Mol Biol Cell* 20:995–1005.

104. Mellion, B., Ignarro, L., Ohlstein, E., Pontecorvo, E., Hyman, A., and Kadowitz, P. 1981. Evidence for the inhibitory role of guanosine 3', 5'-monophosphate in ADP-induced human platelet aggregation in the presence of nitric oxide and related vasodilators. *Blood* 57:946-955.

105. Garg, U., and Hassid, A. 1989. Nitric oxide-generating vasodilators and 8-bromo-cyclic guanosine monophosphate inhibit mitogenesis and proliferation of cultured rat vascular smooth muscle cells. *J Clin Invest* 83:1774-1777.

106. Sarkar, R., Meinberg, E., Stanley, J., Gordon, D., and Webb, R. 1996. Nitric oxide reversibly inhibits the migration of cultured vascular smooth muscle cells. *Circ Res* 78:225-230.

107. Tsihlis, N., Oustwani, C., Vavra, A., Jiang, Q., Keefer, L., and Kibbe, M. 2011. Nitric oxide inhibits vascular smooth muscle cell proliferation and neointimal hyperplasia by increasing the ubiquitination and degradation of UbcH10. *Cell Biochem Biophys* 60:89-97.

108. Zuckerbraun, B., Stoyanovsky, D., Sengupta, R., Shapiro, R., Ozanich, B., Rao, J., Barbato, J., and Tzeng, E. 2007. Nitric oxide-induced inhibition of smooth muscle cell proliferation involves S-nitrosation and inactivation of RhoA. 292(2), C824–C831. *Am J Physiol Cell Physiol* 292:C824-C831.

109. Steudel, W., Scherrer-Crosbie, M., Bloch, K., Weimann, J., Huang, P., Jones, R., Picard, M., and Zapol, W. 1998. Sustained pulmonary hypertension and right ventricular hypertrophy after chronic hypoxia in mice with congenital deficiency of nitric oxide synthase 3. *J Clin Invest* 101:2468–2477.

110. Rabinovitch, M. 2012. Molecular pathogenesis of pulmonary arterial hypertension. *J Clin Invest* 122:4306-4313.

111. Giald, A., and Saleh, D. 1995. Reduced expression of endothelial nitric oxide synthase in the lungs of patients with pulmonary hypertension. *N Engl J Med* 333:214-221.

112. Gauthier, T., Davenpeck, K., and Lefer, A. 1994. Nitric oxide attenuates leukocyte-endothelial interaction via P-selectin in splanchnic ischemia-reperfusion *Am J Physiol Gastrointest Liver Physiol* 267:G562–G568.

113. Fagan, K., Fouty, B., Tyler, R., Jr, K.M., Hepler, L., Sato, K., LeCras, T., Abman, S., Weinberger, H., Huang, P., et al. 1999. The pulmonary circulation of homozygous or heterozygous eNOS-null mice is hyperresponsive to mild hypoxia. *J Clin Invest* 103:291-299.

114. Maron, B.A., and Loscalzo, J. 2013. Pulmonary Hypertension: Pathophysiology and Signaling Pathways. In *Pharmacotherapy of Pulmonary Hypertension*. Marc Humbert, O.V. Evgenov, and J.-P. Stasch, editors. Heidelberg: Springer.

115. Montani, D., Chaumais, M.-C., Guignabert, C., Günther, S., Girerd, B., Jaïs, X., Algalarrondo, V., Price, L.C., Savale, L., Sitbon, O., et al. 2014. Targeted therapies in pulmonary arterial hypertension. *Pharmacol Ther* 141:172–191.

116. Montani, D., Chaumais, M., Savale, L., Natali, D., Price, L., Jaïs, X., Humbert, M., Simonneau, G., and Sitbon, O. 2009. Phosphodiesterase type 5 inhibitors in pulmonary arterial hypertension. *Adv Ther* 26:813-825.

117. Gryglewski, R., Bunting, S., Moncada, S., Flower, R., and Vane, J. 1976. Arterialwalls are protected against deposition of platelet thrombi by a substance (prostaglandin X) which they make from prostaglandin endoperoxides. *Prostaglandins* 12:685-713.

118. Tuder, R., Cool, C., Geraci, M., Wang, J., Abman, S., Wright, L., Badesch, D., and Voelkel, N. 1999. Prostacyclin synthase expression is decreased in lungs from patients with severe pulmonary hypertension. *Am J Respir Crit Care Med* 159:1925-1932.

119. Christman, B., McPherson, C., Newman, J., King, G., Bernard, G., Groves, B., and Loyd, J. 1992. An imbalance between the excretion of thromboxane and prostacyclin metabolites in pulmonary hypertension. *N Engl J Med* 327:70-75.

120. Max, M., Kuhlen, R., Dembinski, R., and Rossaint, R. 1999. Effect of aerosolized prostacyclin and inhaled nitric oxide on experimental hypoxic pulmonary hypertension. *Intensive Care Med* 25:1147–1154.

121. Miyata, M., Ueno, Y., Sekine, H., Ito, O., Sakuma, F., Koike, H., Nishio, S., Nishimaki, T., and Kasukawa, R. 1996. Protective effect of beraprost sodium, a stable prostacyclin analogue, in development of monocrotalineinduced pulmonary hypertension *J Cardiovasc Pharmacol* 27:20-26.

122. Long, L., MacLean, M.R., Jeffery, T.K., Morecroft, I., Yang, X., Rudarakanchana, N., Southwood, M., James, V., Trembath, R.C., and Morrell, N.W. 2006. Serotonin Increases Susceptibility to Pulmonary Hypertension in BMPR2-Deficient Mice. *Circ Res* 98:818-827.

123. MacLean, M., Herve, P., Eddahibi, S., and Adnot, S. 2000. 5-hydroxytryptamine and the pulmonary circulation: receptors, transporters and relevance to pulmonary arterial hypertension. *British Journal of Pharmacology* 131:161-168.

124. Eddahibi, S., Raffestin, B., Pham, I., Launay, J., Aegerter, P., Sitbon, M., and Adnot, S. 1997. Treatment with 5-HT potentiates development of pulmonary hypertension in chronically hypoxic rats. *Am J Physiol* 272:H1173-1181.

125. Eddahibi, S., Hanoun, N., Lanfumey, L., Lesch, K., Raffestin, B., Hamon, M., and Adnot, S. 2000. Attenuated hypoxic pulmonary hypertension in mice lacking the 5-hydroxytryptamine transporter gene. *J Clin Invest* 105:1555-1562.

126. Markewitz, B., Farrukh, I., Chen, Y., Li, Y., and Michael, J. 2001. Regulation of endothelin-1 synthesis in human pulmonary arterial smooth muscle cells. Effects of transforming growth factor-beta and hypoxia. *Cardiovasc Res* 49:200–206.

127. Shi-Wen, X., Chen, Y., Denton, C., Eastwood, M., Renzoni, E., Bou-Gharios, G., Pearson, J., Dashwood, M., du Bois, R., Black, C., et al. 2004. Endothelin-1 promotes myofibroblast induction through the ETA receptor via a rac/phosphoinositide 3-kinase/Akt-dependent pathway and is essential for the enhanced contractile phenotype of fibrotic fibroblasts. *Mol Biol Cell* 15:2707–2719.

128. Yamashita, K., Discher, D., Hu, J., Bishopric, N., and Webster, K. 2001. Molecular regulation of the endothelin-1 gene by hypoxia. Contributions of hypoxia-inducible factor-1, activator protein-1, GATA-2, and p300/CBP. *J Biol Chem* 276:12645-12653.

129. Rodríguez-Pascual, F., Redondo-Horcajo, M., and Lamas, S. 2003. Functional cooperation between Smad proteins and activator protein-1 regulates transforming growth factor-beta-mediated induction of endothelin-1 expression. *Circ Res* 92:1288-1295.

130. Kanse, S., Takahashi, K., Lam, H., Rees, A., Warren, J., Porta, M., Molinatti, P., Ghatei, M., and Bloom, S. 1991. Cytokine stimulated endothelin release from endothelial cells. *Life Sci* 48:1379-1384.

131. Malek, A., Zhang, J., Jiang, J., Alper, S., and Izumo, S. 1999. Endothelin-1 gene suppression by shear stress: pharmacological evaluation of the role of tyrosine kinase, intracellular calcium, cytoskeleton, and mechanosensitive channels. *J Mol Cell Cardiol* 31:387-399.

132. Seo, B., Oemar, B., Siebenmann, R., von Segesser, L., and Luscher, T. 1994. Both ETA and ETB receptors mediate contraction to endothelin-1 in human blood vessels. *Circulation* 89:1203–1208.

133. Eguchi, S., Hirata, Y., Imai, T., and Marumo, F. 1993. Endothelin receptor subtypes are coupled to adenylate cyclase via different guanyl nucleotide-binding proteins in vasculature. *Endocrinology* 132:524–529.

134. Soma, S., Takahashi, H., Muramatsu, M., Oka, M., and Fukuchi, Y. 1999. Localization and Distribution of Endothelin Receptor Subtypes in Pulmonary Vasculature of Normal and Hypoxia-Exposed Rats. *Am J Respir Cell Mol Biol* 20:620-630.

135. Giaid, A., Yanagisawa, M., Langleben, D., Michel, R., Levy, R., Shennib, H., Kimura, S., Masaki, T., Duguid, W., Path, F., et al. 1993. Expression of endothelin-1 in the lungs of patients with pulmonary hypertension. *N Engl JMed* 328:1732-1739.

136. Janakidevi, K., Fisher, M., Del Vecchio, P., Tirupathi, C., Figge, J., and Malik, A. 1992. Endothelin-1 stimulates DNA synthesis and proliferation of pulmonary artery smooth muscle cells. *Am J Physiol Cell Physiol* 263:C1295–C1301.

137. Kelland, N., Kuc, R., McLean, D., Azfer, A., Bagnall, A., Gray, G., Gulliver-Sloan, F., Maguire, J., Davenport, A., Kotelevtsev, Y., et al. 2010. Endothelial cell-specific ETB receptor knockout: autoradiographic and histological characterization and crucial role in the clearance of endothelin-1. *Can J Physiol Pharmacol* 88:644–651.

138. Fukuroda, T., Fujikawa, T., Ozaki, S., Ishikawa, K., Yano, M., and Nishikibe, M. 1994. Clearance of circulating endothelin-1 by ETB receptors in rats. *Biochem Biophys Res Commun* 199:1461–1465.

139. Yorikane, R., Sakai, S., Miyauchi, T., Sakurai, T., Sugishita, Y., and Goto, K. 1993. Increased production of endothelin-1 in the hypertrophied rat heart due to pressure overload. *FEBS Lett* 332:31-34.

140. Elton, T., Oparil, S., Taylor, G., Hicks, P., Yang, R., Jin, H., and Chen, Y. 1992. Normobaric hypoxia stimulates endothelin-1 gene expression in the rat. *Am J Physiol* 263:R1260–1264.

141. Chen, S., Chen, Y., Opgenorth, T., Wessale, J., Meng, Q., Durand, J., DiCarlo, V., and Oparil, S. 1997. The orally active nonpeptide endothelin A-receptor antagonist A-127722 prevents and reverses hypoxia-induced pulmonary hypertension and pulmonary vascular remodeling in Sprague–Dawley rats. *J Cardiovasc Pharmacol* 29:713–725.

142. Chen, S., Chen, Y., Meng, Q., Durand, J., Dicarlo, V., and Oparil, S. 1995. Endothelin-receptor antagonist bosentan prevents and reverses hypoxic pulmonary hypertension in rats. *J Appl Physiol* 79:2122–2131.

143. Clozel, M., Breu, V., Gray, G., Kalina, B., Löffler, B., Burri, K., Cassal, J., Hirth, G., Müller, M., and Neidhart, W. 1994. Pharmacological characterization of bosentan, a new potent orally active nonpeptide endothelin receptor antagonist. *J Pharmacol Exp Ther* 270:228-235.

144. Galiè, N., Olschewski, H., Oudiz, R., Torres, F., Frost, A., Ghofrani, H., Badesch, D., McGoon, M., McLaughlin, V., Roecker, E., et al. 2008. Ambrisentan for the treatment of pulmonary arterial hypertension: results of the ambrisentan in pulmonary arterial hypertension, randomized, double-blind, placebo-controlled, multicenter, efficacy (ARIES) study 1 and 2. *Circulation* 117:3010–3019.

145. Wilkins, M. 2004. Selective or nonselective endothelin receptor blockade in pulmonary arterial hypertension. 169(4), 433–434. *Am J Respir Crit Care Med* 169:433-434.

146. Humbert, M., Monti, G., Brenot, F., Sitbon, O., Portier, A., Grangeot-Keros, L., Duroux, P., Galanaud, P., Simonneau, G., and Emilie, D. 1995. Increased interleukin-1 and interleukin-6 serum concentrations in severe primary pulmonary hypertension. *Am J Respir Crit Care Med* 151:1628–1631.

147. Balabanian, K., Foussat, A., Dorfmüller, P., Durand-Gasselin, I., Capel, F., Bouchet-Delbos, L., Portier, A., Marfaing-Koka, A., Krzysiek, R., Rimaniol, A., et al. 2002. CX(3)C chemokine fractalkine in pulmonary arterial hypertension. *Am J Respir Crit Care Med* 165:1419–1425.

148. Soon, E., Holmes, A., Treacy, C., Doughty, N., Southgate, L., Machado, R., Trembath, R., Jennings, S., Barker, L., Nicklin, P., et al. 2010. Elevated levels of inflammatory cytokines

predict survival in idiopathic and familial pulmonary arterial hypertension. *Circulation* 122:920-927.

149. de Cleva, R., Herman, P., Pugliese, V., Zilberstein, B., Saad, W., Rodrigues, J., and Laudanna, A. 2003 Prevalence of pulmonary hypertension in patients with hepatosplenic Mansonic schistosomiasis--prospective study. *Hepatogastroenterology* 50:2028-2030.
150. Cool, C., Rai, P., Yeager, M., Hernandez-Saavedra, D., Serls, A., Bull, T., Geraci, M., Brown, K., Routes, J., Tuder, R., et al. 2003. Expression of human herpesvirus 8 in primary pulmonary hypertension.
151. Dorfmüller, P., Perros, F., Balabanian, K., and Humbert, M. 2003. Inflammation in pulmonary arterial hypertension. *Eur Respir J* 22:358–363.
152. Vlachoyiannopoulos, P., Dafni, U., Pakas, I., Spyropoulou-Vlachou, M., Stavropoulos-Giokas, C., and Moutsopoulos, H. 2000. Systemic scleroderma in Greece: low mortality and strong linkage with HLA-DRB1*1104 allele. *Ann Rheum Dis* 59:359–367.
153. Wigley, F., Lima, J., Mayes, M., McLain, D., Chapin, J., and Ward-Able, C. 2005. The Prevalence of Undiagnosed Pulmonary Arterial Hypertension in Subjects With Connective Tissue Disease at the Secondary Health Care Level of Community-Based Rheumatologists (the UNCOVER Study). *Arthritis Rheum* 52:2125-2132.
154. Avouac, J., Airò, P., Meune, C., Beretta, L., Dieude, P., Caramaschi, P., Tiev, K., Cappelli, S., Diot, E., Vacca, A., et al. 2010. Prevalence of Pulmonary Hypertension in Systemic Sclerosis in European Caucasians and Metaanalysis of 5 Studies. *J Rheumatol* 37:2290–2298.
155. Mukerjee, D., St George, D., Coleiro, B., Knight, C., Denton, C., Davar, J., Black, C., and Coghlan, J. 2003. Prevalence and outcome in systemic sclerosis associated pulmonary arterial hypertension: application of a registry approach. *Ann Rheum Dis* 62:1088–1093.
156. Tedford, R., Mudd, J., Girgis, R., Mathai, S., Zaiman, A., Housten-Harris, T., Boyce, D., Kelemen, B., Bacher, A., Shah, A., et al. 2013. Right Ventricular Dysfunction in Systemic Sclerosis Associated Pulmonary Arterial Hypertension. *Circ Heart Fail* 6:953-963.
157. Derrett-Smith, E.C., Dooley, A., Gilbane, A.J., Trinder, S.L., Khan, K., Baliga, R., Holmes, A.M., Hobbs, A.J., Abraham, D., and Denton, C.P. 2013. Endothelial Injury in a Transforming Growth Factor β–Dependent Mouse Model of Scleroderma Induces Pulmonary Arterial Hypertension. *Arthritis Rheumatol* 65:2928–2939.
158. Rhee, R.L., Gabler, N.B., Praestgaard, A., Merkel, P.A., and Kawut, S.M. 2015. Adverse Events in Connective Tissue Disease–Associated Pulmonary Arterial Hypertension. *Arthritis Rheumatol* 67:2457–2465.
159. Becker, M.O., Kill, A., Kutsche, M., Guenther, J., Rose, A., Tabeling, C., Witzenrath, M., Kühl, A.A., Heidecke, H., Ghofrani, H.A., et al. 2014. Vascular receptor autoantibodies in pulmonary arterial hypertension associated with systemic sclerosis. *Am J Respir Crit Care Med* 190:808-817.

160. Maron, B.A., and Leopold, J.A. 2014. The role of the renin-angiotensin-aldosterone system in the pathobiology of pulmonary arterial hypertension *Pulm Circ* 4:200-210.

161. Bruce, E., Shenoy, V., Rathinasabapathy, A., Espejo, A., Horowitz, A., Oswalt, A., Francis, J., Nair, A., Unger, T., Raizada, M.K., et al. 2015. Selective activation of angiotensin AT2 receptors attenuates progression of pulmonary hypertension and inhibits cardiopulmonary fibrosis. *British Journal of Pharmacology* 172:2219–2231.

162. Briet, M., and Schiffrin, E. 2010. Aldosterone: effects on the kidney and cardiovascular system. *Nat Rev Nephrol* 6:261–273.

163. Batt, J., Ahmed, S., Correa, J., Bain, A., and Granton, J. 2014. Skeletal muscle dysfunction in idiopathic pulmonary arterial hypertension. *Am J Respir Cell Mol Biol* 50:74–86.

164. Ahmad, S., Varagic, J., VonCannon, J.L., Groban, L., Collawn, J.F., Dell'Italia, L.J., and Ferrario, C.M. 2016. Primacy of cardiac chymase over angiotensin converting enzyme as an angiotensin-(1-12) metabolizing enzyme. *Biochem Biophys Res Commun* 478:559–564.

165. Froogh, G., Pinto, J.T., Le, Y., Kandhi, S., Aleligne, Y., Huang, A., and Sun, D. 2016. Chymase-dependent production of angiotensin II: an old enzyme in old hearts. *Am J Physiol Heart Circ Physiol*.

166. Jessup, J.A., Trask, A.J., Chappell, M.C., Nagata, S., Kato, J., Kitamura, K., and Ferrario, C.M. 2008. Localization of the novel angiotensin peptide, angiotensin-(1-12), in heart and kidney of hypertensive and normotensive rats *Am J Physiol Heart Circ Physiol* 294:H2614–H2618.

167. Santos, R.A., Ferreira, A.J., and Simoes, E. 2008. Recent advances in the angiotensin-converting enzyme 2-angiotensin(1-7)-Mas axis. *Exp Physiol* 93:519-527.

168. de Man, F., Tu, L., Handoko, M.L., Rain, S., Ruiter, G., François, C., Schalij, I., Dorfmüller, P., Simonneau, G., Fadel, E., et al. 2012. Dysregulated Renin–Angiotensin–Aldosterone System Contributes to Pulmonary Arterial Hypertension. *Am J Respir Crit Care Med* 186:780–789.

169. Morrell, N., Morris, K., and Stenmark, K. 1995. Role of angiotensin-converting enzyme and angiotensin II in development of hypoxic pulmonary hypertension. *Am J Physiol* 269:1186-1894.

170. Morrell, N., Atochina, E., Morris, K., Danilov, S., and Stenmark, K. 1995. Angiotensin converting enzyme expression is increased in small pulmonary arteries of rats with hypoxia induced pulmonary hypertension. *J Clin Invest* 96:1823–1833.

171. Orte, C., Polak, J., Haworth, S., Yacoub, M., and Morrell, N. 2000. Expression of pulmonary vascular angiotensin-converting enzyme in primary and secondary plexiform pulmonary hypertension. *J Pathol* 192:379–384.

172. Xie, L., Lin, P., Xie, H., and Xu, C. 2010. Effects of atorvastatin and losartan on monocrotaline-induced pulmonary artery remodeling in rats. *Clin Exp Hypertens* 32:547-554.

173. Kanno, S., Wu, Y., Lee, P., Billiar, T., and Ho, C. 2001. Angiotensin-converting enzyme inhibitor preserves p21 and endothelial nitric oxide synthase expression in monocrotaline-induced pulmonary arterial hypertension in rats. *Circulation* 104:945-950.

174. Li, G., Liu, Y., Zhu, Y., Liu, A., Xu, Y., Li, X., Li, Z., Su, J., and Sun, L. 2013. ACE2 Activation Confers Endothelial Protection and Attenuates Neointimal Lesions in Prevention of Severe Pulmonary Arterial Hypertension in Rats. *Lung* 191:327-336.

175. Johnson, J., West, J., Maynard, K., and Hemnes, A. 2011. ACE2 improves right ventricular function in a pressure overload model. *PLoS ONE* 6:e20828.

176. Yamazato, Y., Ferreira, A., Hong, K., Sriramula, S., Francis, J., Yamazato, M., Yuan, L., Bradford, C., Shenoy, V., Oh, S., et al. 2009. Prevention of Pulmonary Hypertension by Angiotensin-Converting Enzyme 2 Gene Transfer. *Hypertension* 54:365-371.

177. Gaddam, R.R., Chambers, S., and Bhatia, M. 2014. ACE and ACE2 in Inflammation: A Tale of Two Enzymes. *Inflammation & Allergy - Drug Targets* 13:224-234.

178. Álvarez, Á., Cerdá-Nicolás, M., Nabah, Y.N.A., Mata, M., Issekutz, A.C., Panés, J., Lobb, R.R., and Sanz, M.-J. 2004. Direct evidence of leukocyte adhesion in arterioles by angiotensin II. *Blood* 104:402-407.

179. Company, C., Piqueras, L., Nabah, Y.N.A., Escudero, P., Blanes, J.I., Jose, P.J., Morcillo, E.J., and Sanz, M.-J. 2011. Contributions of ACE and mast cell chymase to endogenous angiotensin II generation and leucocyte recruitment in vivo. *Cardiovascular Research* 92:48-56.

180. Perl, A. 2010. Pathogenic mechanisms in systemic lupus erythematosus. *Autoimmunity* 43:1-6.

181. Rahman, A., and Isenberg, D.A. 2008. Systemic Lupus Erythematosus. *N Engl J Med* 358:929-939.

182. Laxminarayana, D. 2014. Molecular insights into systemic lupus erythematosus pathogenesis. *Clin Med Insights Pathol* 7:7-9.

183. Bertsias, G., Cervera, R., and Boumpas, D.T. 2012. Systemic Lupus Erythematosus: Pathogenesis and Clinical Features. In *EULAR 2012*. E. 2012, editor. Berlin.

184. Somers, E., Marder, W., Cagnoli, P., Lewis, E., DeGuire, P., Gordon, C., Helmick, C., Wang, L., Wing, J., Dhar, J., et al. 2014. Population-based incidence and prevalence of systemic lupus erythematosus: the Michigan Lupus Epidemiology and Surveillance program. *Arthritis Rheumatol* 66:369-378.

185. Samanta, A., Feehally, J., Roy, S., Nichol, F.E., Sheldon, P.J., and Walls, J. 1991. High prevalence of systemic disease and mortality in Asian subjects with systemic lupus erythematosus. *Ann Rheum Dis* 50:490-492.

186. Pons-Estel, G.J., Alarcón, G.S., Scofield, L., Reinlib, L., and Cooper, G.S. 2010. Understanding the Epidemiology and Progression of Systemic Lupus Erythematosus. *Semin Arthritis Rheum* 39:257-280.

187. Johnson, A., Gordon, C., Palmer, R., and Bacon, P. 1995. The prevalence and incidence of systemic lupus erythematosus in Birmingham, England: relationship to ethnicity and country of birth. *Arthritis Rheum* 38:551-558.

188. Lichtnekert, J., Rupanagudi, K., Kulkarni, O., Darisipudi, M., Allam, R., and Anders, H. 2011. Activated protein C attenuates systemic lupus erythematosus and lupus nephritis in MRL-Fas(lpr) mice. *J Immunol* 187:3413-3421.

189. Wallace, D.J. 2015. The evolution of drug discovery in systemic lupus erythematosus. *Nat Rev Rheumatol* 11:616-620.

190. Cohen, A., Reynolds, W., Franklin, E., Kulka, J., Ropes, M., Shulman, L., and Wallace, S. 1971. Preliminary criteria for the classification of systemic lupus erythematosus. *Bull Rheum Dis* 21:643-648.

191. Tan, E.M., Cohen, A.S., Fries, J.F., Masi, A.T., McShane, D.J., Rothfield, N.F., Schaller, J.G., Talal, N., and Winchester, R.J. 1982. The 1982 revised criteria for the classification of systemic lupus erythematosus. *Arthritis & Rheumatism* 25:1271-1277.

192. Hochberg, M.C. 1997. Updating the American College of Rheumatology Revised Criteria for the Classification of Systemic Lupus Erythematosus. *Arthritis & Rheumatism* 40:1725.

193. Petri, M., Orbai, A., Alarcón, G., Gordon, C., Merrill, J., Fortin, P., Bruce, I., Isenberg, D., Wallace, D., Nived, O., et al. 2012. Derivation and validation of the Systemic Lupus International Collaborating Clinics classification criteria for systemic lupus erythematosus. *Arthritis Rheum* 64:2677-2686.

194. Gladman, D., Ibañez, D., and Urowitz, M. 2002. Systemic lupus erythematosus disease activity index 2000. *J Rheumatol* 29:288-291.

195. Bengtsson, A., and Rönnblom, L. 2017. Systemic lupus erythematosus: still a challenge for physicians. *J Intern Med* 281:52-64.

196. Khamashta, M., Merrill, J., Werth, V., Furie, R., Kalunian, K., Illei, G., Drappa, J., Wang, L., Greth, W., and investigators, C.s. 2016. Sifalimumab, an anti-interferon-α monoclonal antibody, in moderate to severe systemic lupus erythematosus: a randomised, double-blind, placebo-controlled study. *Ann Rheum Dis* 75:1909-1916.

197. Furie, R., Khamashta, M., Merrill, J., Werth, V., Kalunian, K., Brohawn, P., Illei, G.G., Drappa, J., Wang, L., Yoo, S., et al. 2015. Anifrolumab, an Anti-Interferon-Alpha Receptor Monoclonal Antibody, in Moderate to Severe Systemic Lupus Erythematosus. *Arthritis Rheumatol* 67.

198. Pierdominici, M., and Ortona, E. 2013. Estrogen Impact on Autoimmunity Onset and Progression: the Paradigm of Systemic Lupus Erythematosus. *Int Trends Immun* 1:24-34.

199. Zandman-Goddard, G., Peeva, E., and Shoenfeld, Y. 2007. Gender and autoimmunity. *Autoimmun Rev* 6:366-372.

200. Rubtsova, K., Marrack, P., and Rubtsov, A. 2015. Sexual dimorphism in autoimmunity. *J Clin Invest* 125:2187-2193.

201. Jørgensen, K., Rostgaard, K., Bache, I., Biggar, R., Nielsen, N., Tommerup, N., and Frisch, M. 2010. Autoimmune diseases in women with Turner's syndrome. *Arthritis Rheum* 62:658-666.

202. Scofield, R.H., Bruner, G.R., Namjou, B., Kimberly, R.P., Ramsey-Goldman, R., Petri, M., Reveille, J.D., Alarcon, G.S., Vila, L.M., Reid, J., et al. 2008. Klinefelter's Syndrome, 47,XXY,

in Male Systemic Lupus Erythematosus Supports a Gene Dose Effect from the X Chromosome. *Arthritis & Rheumatism*.

203. Prieto, G., and Rosenstein, Y. 2006. Oestradiol potentiates the suppressive function of human CD4 CD25 regulatory T cells by promoting their proliferation. *Immunology* 118:58-65.
204. Shelly, S., Boaz, M., and Orbach, H. 2012. Prolactin and autoimmunity. *Autoimmun Rev* 11:A465-A470.
205. Trigunaite, A., Dimo, J., and Jørgensen, T.N. 2015. Suppressive effects of androgens on the immune system. *Cell Immunol* 294:87-94.
206. Lindqvist, A., and Alarcón-Riquelme, M. 1999. The Genetics of Systemic Lupus Erythematosus. *Scand J Immunol* 50:562-571.
207. Sullivan, K. 2000. Genetics of systemic lupus erythematosus: clinical implications. *Rheum Dis Clin North Am* 26:229-256.
208. Dai, C., Deng, Y., Quinlan, A., Gaskin, F., Tsao, B.P., and Fu, S.M. 2014. Genetics of systemic lupus erythematosus: immune responses and end organ resistance to damage. *Curr Opin Immunol* 0.
209. Chen, S., Lv, Q., Hu, L., Peng, M., Wang, G., and Sun, B. 2016. DNA methylation alterations in the pathogenesis of lupus. *Clin Exp Immunol* 187:185-192.
210. Mishra, N., Reilly, C., Brown, D., Ruiz, P., and Gilkeson, G. 2003. Histone deacetylase inhibitors modulate renal disease in the MRL-lpr/lpr mouse. *J Clin Invest* 111:539–552.
211. Zan, H., Zhang, J., Ardeshna, S., Xu, Z., Park, S., and Casali, P. 2009. Lupus-prone MRL/faslpr/lpr mice display increased AID expression and extensive DNA lesions, comprising deletions and insertions, in the immunoglobulin locus: Concurrent up-regulation of somatic hypermutation and class switch DNA recombination. *Autoimmunity* 42:89-103.
212. Wu, Z., Sun, Y., Mei, X., Zhang, C., Pan, W., and Shi, W. 2014. 17beta-oestradiol enhances global DNA hypomethylation in CD4-positive T cells from female patients with lupus, through overexpression of oestrogen receptor-alpha-mediated downregulation of DNMT1. *Clin Exp Dermatol* 39:525-532.
213. Nelson, P., Rylance, P., Roden, D., Trela, M., and Tugnet, N. 2014. Viruses as potential pathogenic agents in systemic lupus erythematosus. *Lupus* 23:596-605.
214. Hanlon, P., Avenell, A., Aucott, L., and Vickers, M.A. 2014. Systematic review and meta-analysis of the sero-epidemiological association between Epstein-Barr virus and systemic lupus erythematosus. *Arthritis Res Ther* 16:R3.
215. Rasmussen, N., Draborg, A., Nielsen, C., Jacobsen, S., and Houen, G. 2015. Antibodies to early EBV, CMV, and HHV6 antigens in systemic lupus erythematosus patients. *Scand J Rheumatol* 44:143-149.
216. Varani, S., and Landini, M. 2011. Cytomegalovirus-induced immunopathology and its clinical consequences. *Herpesviridae* 2:6.

217. Pavlovic, M., Kats, A., Cavallo, M., and Shoenfeld, Y. 2010. Clinical and molecular evidence for association of SLE with parvovirus B19. *Lupus* 19:783-792.

218. Broccolo, F., Fusetti, L., and Ceccherini-Nelli, L. 2013. Possible Role of Human Herpesvirus 6 as a Trigger of Autoimmune Disease. *ScientificWorldJournal* 2013:867389.

219. Sun, Y., Sun, S., Li, W., Li, B., and Li, J. 2011. Prevalence of human herpesvirus 8 infection in systemic lupus erythematosus. *Virol J* 8:210.

220. Khalifa, M., Kaabia, N., Bahri, F., Jazia, E., Bouajina, E., and Letaief, A. 2007. Infection in systemic lupus erythematosus. *Med Maladies Infect* 37:792-795.

221. Draborg, A.H., Duus, K., and Houen, G. 2013. Epstein-Barr Virus in Systemic Autoimmune Diseases. *Clin Dev Immunol* 2013:535738.

222. Günther, C., Kind, B., Reijns, M.A., Berndt, N., Martinez-Bueno, M., Wolf, C., Tüngler, V., Chara, O., Lee, Y.A., Hübner, N., et al. 2015. Defective removal of ribonucleotides from DNA promotes systemic autoimmunity. *J Clin Invest* 125:413-424.

223. Isenberg, D., Shoenfeld, Y., Walport, M., Mackworth-Young, C., Dudeney, C., Todd-Pokropek, A., Brill, S., Weinberger, A., and Pinkas, J. 1985. Detection of cross-reactive anti-DNA antibody idiotypes in the serum of systemic lupus erythematosus patients and of their relatives. *Arthritis Rheum* 28:999-1007.

224. ter Borg, E., Horst, G., Hummel, E., Limburg, P., and Kallenberg, C. 1990. Measurement of increases in anti-double-stranded DNA antibody levels as a predictor of disease exacerbation in systemic lupus erythematosus. A long-term, prospective study. *Arthritis Rheum* 33:634-643.

225. Zieve, G., and Khusial, P. 2003. The anti-Sm immune response in autoimmunity and cell biology. *Autoimmun Rev* 2:235-240.

226. Migliorini, P., Baldini, C., Rocchi, V., and Bombardieri, S. 2005. Anti-Sm and anti-RNP antibodies. *Autoimmunity* 38:47-54.

227. Clotet, B., Guardia, J., Pigrau, C., Lience, E., Murcia, C., Pujol, R., and Bacardí, R. 1984. Incidence and clinical significance of anti-ENA antibodies in systemic lupus erythematosus. Estimation by counterimmunoelectrophoresis. *Scand J Rheumatol* 13:15-20.

228. Rottman, J., and Willis, C. 2010. Mouse models of systemic lupus erythematosus reveal a complex pathogenesis. *Vet Pathol* 47:664-676.

229. Baechler, E., Batliwalla, F., Karypis, G., Gaffney, P., Ortmann, W., Espe, K., Shark, K., Grande, W., Hughes, K., Kapur, V., et al. 2003. Interferon-inducible gene expression signature in peripheral blood cells of patients with severe lupus. *Proc Natl Acad Sci U S A* 100:2610-2615.

230. Cao, W. 2014. Pivotal Functions of Plasmacytoid Dendritic Cells in Systemic Autoimmune Pathogenesis. *J Clin Cell Immunol* 5:212.

231. Rönnblom, L., and Pascual, V. 2008. The innate immune system in SLE: type I interferons and dendritic cells. *Lupus* 17:394-399.

232. Ohl, K., and Tenbrock, K. 2011. Inflammatory Cytokines in Systemic Lupus Erythematosus. *J Biomed Biotechnol* 2011.

233. Wahren-Herlenius, M., and Dörner, T. 2013. Immunopathogenic mechanisms of systemic autoimmune disease. *Lancet* 382:819-831.

234. Linker-Israeli, M., Deans, R., Wallace, D., Prehn, J., Ozeri-Chen, T., and Klinenberg, J. 1991. Elevated levels of endogenous IL-6 in systemic lupus erythematosus. A putative role in pathogenesis. *J Immunol* 147:117-123.

235. Yang, J., Chu, Y., Yang, X., Gao, D., Zhu, L., Yang, X., Wan, L., and Li, M. 2009. Th17 and natural Treg cell population dynamics in systemic lupus erythematosus. *Arthritis Rheum* 60:1472-1483.

236. Wong, C., Ho, C., Li, E., and Lam, C. 2000. Elevation of proinflammatory cytokine (IL-18, IL-17, IL-12) and Th2 cytokine (IL-4) concentrations in patients with systemic lupus erythematosus. *Lupus* 9:589-593.

237. Wong, C., Lit, L., Tam, L., Li, E., Wong, P., and Lam, C. 2008. Hyperproduction of IL-23 and IL-17 in patients with systemic lupus erythematosus: implications for Th17-mediated inflammation in auto-immunity. *Clin Immunol* 127:385-393.

238. Nalbandian, A., Crispín, J., and Tsokos, G. 2009. Interleukin-17 and systemic lupus erythematosus: current concepts. *Clin Exp Immunol* 157:209-215.

239. Munroe, M.E., Vista, E.S., Guthridge, J.M., Thompson, L.F., Merrill, J.T., and James, J.A. 2014. Proinflammatory Adaptive Cytokine and Shed Tumor Necrosis Factor Receptor Levels Are Elevated Preceding Systemic Lupus Erythematosus Disease Flare. *Arthritis Rheumatol* 66:1888-1899.

240. Crispín, J., Oukka, M., Bayliss, G., Cohen, R., Van Beek, C., Stillman, I., Kyttaris, V., Juang, Y., and Tsokos, G. 2008 Expanded double negative T cells in patients with systemic lupus erythematosus produce IL-17 and infiltrate the kidneys. *J Immunol* 181:8761-8766.

241. Tackey, E., Lipsky, P., and Illei, G. 2004. Rationale for interleukin-6 blockade in systemic lupus erythematosus. *Lupus* 13:339-343.

242. Mitsdoerffer, M., Lee, Y., Jäger, A., Kim, H., Korn, T., Kolls, J., Cantor, H., Bettelli, E., and Kuchroo, V. 2010. Proinflammatory T helper type 17 cells are effective B-cell helpers. *Proc Natl Acad Sci U S A* 107:14292-14297.

243. Miyara, M., Amoura, Z., Parizot, C., Badoual, C., Dorgham, K., Trad, S., Nochy, D., Debré, P., Piette, J., and Gorochov, G. 2005. Global natural regulatory T cell depletion in active systemic lupus erythematosus. *J Immunol* 175:8392-8400.

244. Valencia, X., Yarboro, C., Illei, G., and Lipsky, P. 2007. Deficient CD4+CD25high T regulatory cell function in patients with active systemic lupus erythematosus. *J Immunol* 178:2579-2588.

245. Crispín, J., and Tsokos, G. 2010. IL-17 in systemic lupus erythematosus. *J Biomed Biotechnol* 2010:943254.

246. Schäkel, K., Mayer, E., Federle, C., Schmitz, M., Riethmüller, G., and Rieber, E. 1998. A novel dendritic cell population in human blood: one-step immunomagnetic isolation by a specific mAb (M-DC8) and in vitro priming of cytotoxic T lymphocytes. *Eur J Immunol* 28:4084-4093.

247. Schäkel, K., von Kietzell, M., Hänsel, A., Ebling, A., Schulze, L., Haase, M., Semmler, C., Sarfati, M., Barclay, A.N., Randolph, G.J., et al. 2006. Human 6-Sulfo LacNAc-Expressing Dendritic Cells Are Principal Producers of Early Interleukin-12 and Are Controlled by Erythrocytes. *Immunity* 24:767–777.

248. Hänsel, A., Günther, C., Baran, W., Bidier, M., Lorenz, H.-M., Schmitz, M., Bachmann, M., Döbel, T., Enk, A.H., and Schäkel, K. 2013. Human 6-sulfo LacNAc (slan) dendritic cells have molecular and functional features of an important pro-inflammatory cell type in lupus erythematosus. *J Autoimmun* 40 1-8.

249. Hänsel, A., Günther, C., Ingwersen, J., Starke, J., Schmitz, M., Bachmann, M., Meurer, M., Rieber, E., and Schäkel, K. 2011. Human slan (6-sulfo LacNAc) dendritic cells are inflammatory dermal dendritic cells in psoriasis and drive strong TH17/TH1 T-cell responses. *J Allergy Clin Immunol* 127:787-794.

250. Wu, T., Xie, C., Wang, H., Zhou, X., Schwartz, N., Calixto, S., Mackay, M., Aranow, C., Putterman, C., and Mohan, C. 2007. Elevated urinary VCAM-1, P-selectin, soluble TNF receptor-1, and CXC chemokine ligand 16 in multiple murine lupus strains and human lupus nephritis. *J Immunol* 179:7166-7175.

251. Morris, D., Graham, R., Erwig, L.-P., Gaffney, P., Moser, K., Behrens, T., Vyse, T., and Graham, D. 2009. Variation in the upstream region of P-Selectin (SELP) is a risk factor for SLE. *Genes Immun*:404-413.

252. Herrmann, S., Ricard, S., Nicaud, V., Mallet, C., Evans, A., Ruidavets, J., Arveiler, D., Luc, G., and Cambien, F. 1998. The P-selectin gene is highly polymorphic: reduced frequency of the Pro715 allele carriers in patients with myocardial infarction. *Human Molecular Genetics* 7:1277-1284.

253. Singbartl, K., Green, S., and Ley, K. 2000. Blocking P-selectin protects from ischemia/reperfusion-induced acute renal failure. *FASEB J* 14:48-54.

254. Singbartl, K., and Ley, K. 2000. Protection from ischemia-reperfusion induced severe acute renal failure by blocking E-selectin. *Crit Care Med* 28:2507-2514.

255. Bullard, D., Mobley, J., Justen, J., Sly, L., Chosay, J., Dunn, C., Lindsey, J., Beaudet, A., and Staite, N. 1999. Acceleration and increased severity of collagen-induced arthritis in P-selectin mutant mice. *J Immunol* 163:2844-2849.

256. Hickey, M.J. 2003. Alterations in leucocyte trafficking in lupus-prone mice: an examination of the MRL/faslpr mouse. *Immunol Cell Biol* 81:390-396.

257. Kinoshita, K., Yoo, B.-S., Nozaki, Y., Sugiyama, M., Ikoma, S., Ohno, M., Funauchi, M., and Kanamaru, A. 2003. Increases Survival in NZB/W F1 Mice. *J Immunol* 170:5793-5798.

258. Morales-Cano, D., Menendez, C., Moreno, E., Moral-Sanz, J., Barreira, B., Galindo, P., Pandolfi, R., Jimenez, R., Moreno, L., Cogolludo, A., et al. 2014. The Flavonoid Quercetin Reverses Pulmonary Hypertension in Rats. *PLoS ONE* 9.

259. Cogolludo, A., Frazziano, G., Briones, A., Cobeño, L., Moreno, L., Lodi, F., Salaices, M., Tamargo, J., and Perez-Vizcaino, F. 2007 The dietary flavonoid quercetin activates BKCa currents in coronary arteries via production of H2O2. Role in vasodilatation. *Cardiovasc Res* 73:424-431.

260. Bribes, E., Galiegue, S., Bourrie, B., and Casellas, P. 2003. Involvement of the peripheral benzodiazepine receptor in the development of cutaneous pathology in Mrl/Lpr mice. *Immunol Lett* 85:13-18.

261. Christensen, S., Shupe, J., Nickerson, K., Kashgarian, M., Flavell, R., and Shlomchik, M. 2006. Toll-like receptor 7 and TLR9 dictate autoantibody specificity and have opposing inflammatory and regulatory roles in a murine model of lupus. *Immunity* 25:417-428.

262. Rowland, S.L., Riggs, J.M., Gilfillan, S., Bugatti, M., Vermi, W., Kolbeck, R., Unanue, E.R., Sanjuan, M.A., and Colonna, M. 2014. Early, transient depletion of plasmacytoid dendritic cells ameliorates autoimmunity in a lupus model. *J Exp Med* 211:1977-1991.

263. Furukawa, F., and Yoshimasu, T. 2005. Animal models of spontaneous and drug-induced cutaneous lupus erythematosus. *Autoimmun Rev* 4:345-350.

264. Furukawa, F., Tanaka, H., Sekita, K., Nakamura, T., Horiguchi, Y., and Hamashima, Y. 1984. Dermatopathological studies on skin lesions of MRL mice. *Arch Dermatol Res* 276:186-194.

265. Guiducci, C., Tripodo, C., Gong, M., Sangaletti, S., Colombo, M.P., Coffman, R.L., and Barrat, F.J. 2010. Autoimmune skin inflammation is dependent on plasmacytoid dendritic cell activation by nucleic acids via TLR7 and TLR9. *J Exp Med* 207:2931-2942.

266. Choi, J.-Y., Gao, W., Odegard, J., Shiah, H.-S., Kashgarian, M., McNiff, J.M., Baker, D.C., Cheng, Y.-C., and Craft, J. 2006. Abrogation of Skin Disease in Lupus-Prone MRL/Faslpr Mice By Means of a Novel Tylophorine Analog. *Arthritis Rheumatol* 54:3277-3283.

267. Dreßler, J., Bachmann, L., Koch, R., and Müller, E. 1998. Enhanced expression of selectins in human skin wounds. *Int J Legal Med* 112:39-44.

268. Miyazaki, Y., Satoh, T., Nishioka, K., and Yokozeki, H. 2006. STAT-6-Mediated Control of P-Selectin by Substance P and Interleukin-4 in Human Dermal Endothelial Cells. *Am J Pathol* 169.

269. González-Tajuelo, R., Silván, J., Pérez-Frías, A., Fuente-Fernández, M.d.l., Tejedor, R., Espartero-Santos, M., Vicente-Rabaneda, E., Juarranz, Á., Muñoz-Calleja, C., Castañeda, S., et al. 2017. P-Selectin preserves immune tolerance in mice and is reduced in human cutaneous lupus. *Scientific Reports* 7:41841.

270. Huang, A., Manning, J., Bandak, T., Ratau, M., Hanser, K., and Silverstein, S. 1993. Endothelial cell cytosolic free calcium regulates neutrophil migration across monolayers of endothelial cells. *J Cell Biol* 120:1371-1380.

271. Ziegelstein, R., Corda, S., Pili, R., Passaniti, A., Lefer, D., Zweier, J., Fraticelli, A., and Capogrossi, M. 1994. Initial contact and subsequent adhesion of human neutrophils or monocytes to human aortic endothelial cells releases an endothelial intracellular calcium store. *Circulation* 90:1899-1907.

272. Lorenzon, P., Vecile, E., Nardon, E., Ferrero, E., Harlan, J., Tedesco, F., and Dobrina, A. 1998. Endothelial Cell E- and P-Selectin and Vascular Cell Adhesion Molecule-1 Function as Signaling Receptors. *J Cell Biol* 142:1381–1391.

273. Carrizzo, A., Lenzi, P., Procaccini, C., Damato, A., Biagioni, F., Ambrosio, M., Amodio, G., Remondelli, P., Giudice, C.D., Izzo, R., et al. 2015. Pentraxin 3 Induces Vascular Endothelial Dysfunction Through a P-selectin/Matrix Metalloproteinase-1 Pathway. *Circulation* 131:1495-1505.

274. Ílgen, U., Yayla, M., and Düzgün, N. 2017. Low serum fibroblast growth factor 2 levels not accompanied by increased serum pentraxin 3 levels in patients with systemic sclerosis. *Clin Rheumatol* 36:367-372.

275. Stenmark, K., Meyrick, B., Galie, N., Mooi, W.J., and McMurtry, I.F. 2009. Animal models of pulmonary arterial hypertension: the hope for etiological discovery and pharmacological cure. *Am J Physiol Lung Cell Mol Physiol* 297:L1013-L1032.

276. Bleeker, G.B., Steendijk, P., Holman, E.R., Yu, C.-M., Breithardt, O.A., Kaandorp, T.A.M., Schalij, M.J., Wall, E.E.v.d., Nihoyannopoulos, P., and Bax, J.J. 2006. Assessing right ventricular function: the role of echocardiography and complementary technologies. *Heart* 92:i19-i26.

277. Urboniene, D., Haber, I., Fang, Y., Thenappan, T., and Archer, S. 2010. Validation of high-resolution echocardiography and magnetic resonance imaging vs. high-fidelity catheterization in experimental pulmonary hypertension. *Am J Physiol Lung Cell Mol Physiol* 299:401-412.

278. Brittain, E., Penner, N.L., West, J., and Hemnes, A. 2013. Echocardiographic Assessment of the Right Heart in Mice. *J Vis Exp* 81:e50912.

279. Thibault, H., Kurtz, B., Raher, M., Shaik, R., Waxman, A., Derumeaux, G., Halpern, E., Bloch, K., and Scherrer-Crosbie, M. 2010 Noninvasive assessment of murine pulmonary arterial pressure: validation and application to models of pulmonary hypertension. *Circ Cardiovasc Imaging* 3:157-163.

280. Chen, G., Li, Y., Tian, J., Zhang, L., Jean-Charles, P., Gobara, N., Nan, C., Jin, J., and Huang, X.P. 2012. Application of Echocardiography on TransgenicMice with Cardiomyopathies. *Biochemistry Research International*.

281. Yuan, Y.-M., Luo, L., Guo, Z., Yang, M., Ye, R.-S., and Luo, C. 2015. Activation of renin–angiotensin–aldosterone system (RAAS) in the lung of smoking-induced pulmonary arterial hypertension (PAH) rats. *Journal of the Renin-Angiotensin-Aldosterone System* 16:249-253.

282. Man, F.S.d., Tu, L., Handoko, M.L., Rain, S., Ruiter, G., François, C., Schalij, I., Dorfmüller, P., Simonneau, G., Fadel, E., et al. 2012. Dysregulated Renin–Angiotensin–Aldosterone System Contributes to Pulmonary Arterial Hypertension. *Am J Respir Crit Care Med* 186:780–789.

283. Courboulin, A., Paulin, R., Giguère, N., Saksouk, N., Perreault, T., Meloche, J., Paquet, E., Biardel, S., Provencher, S., Côté, J., et al. 2011. Role for miR-204 in human pulmonary arterial hypertension. *J Exp Med* 208:535-548.

284. Siragusa, M., and Fleming, I. 2016. The eNOS signalosome and its link to endothelial dysfunction. *Eur J Physiol* 468:1125–1137.

285. Michel, M., Brunner, H., Foster, C., and Huo, Y. 2016. Angiotensin II type 1 receptor antagonists in animal models of vascular, cardiac, metabolic and renal disease. *Pharmacol Ther* 164:1-81.

286. Shenoy, V., Qi, Y., Katovich, M.J., and Raizada, M.K. 2011. ACE2, a Promising Therapeutic Target for Pulmonary Hypertension. *Curr Opin Pharmacol* 11:150–155.

287. Kossmann, S., Hu, H., Steven, S., Schönfelder, T., Fraccarollo, D., Mikhed, Y., Brähler, M., Knorr, M., Brandt, M., Karbach, S.H., et al. 2014. Inflammatory Monocytes Determine Endothelial Nitric-oxide Synthase Uncoupling and Nitro-oxidative Stress Induced by Angiotensin II. *J Biol Chem* 289:27540–27550.

288. Kossmann, S., Schwenk, M., Hausding, M., Karbach, S.H., Schmidgen, M.I., Brandt, M., Knorr, M., Hu, H., Kröller-Schön, S., Schönfelder, T., et al. 2013. Angiotensin II–Induced Vascular Dysfunction Depends on Interferon-γ–Driven Immune Cell Recruitment and Mutual Activation of Monocytes and NK-Cells. *Arterioscler Thromb Vasc Biol* 33:1313-1319.

289. Zhao, H., Xue, Y., Guoa, Y., Sun, Y., Liu, D., and Wang, X. 2017. Inhibition of endocan attenuates monocrotaline-induced connective tissue disease related pulmonary arterial hypertension. *International Immunopharmacology* 42: 115–121.

290. Steiner, M.K., Syrkina, O.L., Kolliputi, N., Mark, E.J., Hales, C.A., and Waxman, A.B. 2009. Interleukin-6 Overexpression Induces Pulmonary Hypertension. *Circ Res* 104:236-244.

291. Savai, R., Pullamsetti, S.S., Kolbe, J., Bieniek, E., Voswinckel, R., Fink, L., Scheed, A., Ritter, C., Dahal, B.K., Vater, A., et al. 2012. Immune and Inflammatory Cell Involvement in the Pathology of Idiopathic Pulmonary Arterial Hypertension. *Am J Respir Crit Care Med* 186:897-908.

292. Dorfmüller, P., Zarka, V., Durand-Gasselin, I., Monti, G., Balabanian, K., Garcia, G., Capron, F., Coulomb-Lherminé, A., Marfaing-Koka, A., Simonneau, G., et al. 2002. Chemokine RANTES in severe pulmonary arterial hypertension. *Am J Respir Crit Care Med* 165:534–539.

293. Sanchez, O., Marcos, E., Perros, F., Fadel, E., Tu, L., Humbert, M., Dartevelle, P., Simonneau, G., Adnot, S., and Eddahibi, S. 2007. Role of endothelium-derived cc chemokine ligand 2 in idiopathic pulmonary arterial hypertension. *Am J Respir Crit Care Med* 176:1041–1047.

294. Okawa-Takatsuji, M., Aotsuka, S., Fujinami, M., Uwatoko, S., Kinoshita, M., and Sumiya, M. 1999. Up-regulation of intercellular adhesion molecule-1 (ICAM-1), endothelial leucocyte

adhesion molecule-1 (ELAM-1) and class II MHC molecules on pulmonary artery endothelial cells by antibodies against U1-ribonucleoprotein. *Clin Exp Immunol* 116:174-180.

295. Iannone, F., Riccardi, M.T., Guiducci, S., Bizzoca, R., Cinelli, M., Matucci-Cerinic, M., and Lapadula, G. 2008. Bosentan regulates the expression of adhesion molecules on circulating T cells and serum soluble adhesion molecules in systemic sclerosis-associated pulmonary arterial hypertension. *Ann Rheum Dis* 67:1121-1126.
296. Sakamaki, F., Kyotani, S., Nagaya, N., Sato, N., Oya, H., Satoh, T., and Nakanishi, N. 2000. Increased plasma P-selectin and decreased thrombomodulin in pulmonary arterial hypertension were improved by continuous prostacyclin therapy. *Circulation* 102:2720–2725.
297. Furukawa, F. 2003. Photosensitivity in cutaneous lupus erythematosus: lessons from mice and men. *J Dermatol Sci* 33:81-89.
298. Savarese, E., Steinberg, C., Pawar, R.D., Reindl, W., Akira, S., Anders, H.-J., and Krug, A. 2008. Requirement of Toll-like Receptor 7 for Pristane-Induced Production of Autoantibodies and Development of Murine Lupus Nephritis. *Arthritis Rheumatol* 58:1107-1115.
299. Feng, X., Wang, D., Chen, J., Lu, L., Hua, B., Li, X., Tsao, B., and Sun, L. 2012. Inhibition of aberrant circulating Tfh cell proportions by corticosteroids in patients with systemic lupus erythematosus. *PLoS ONE* 7:e51982.
300. Odendahl, M., Jacobi, A., Hansen, A., Feist, E., Hiepe, F., Burmester, G., Lipsky, P., Radbruch, A., and Dörner, T. 2000. Disturbed Peripheral B Lymphocyte Homeostasis in Systemic Lupus Erythematosus. *J Immunol* 165:5970-5979.
301. Jacobi, A., Odendahl, M., Reiter, K., Bruns, A., Burmester, G., Radbruch, A., Valet, G., Lipsky, P., and Dörner, T. 2003. Correlation between circulating CD27high plasma cells and disease activity in patients with systemic lupus erythematosus. *Arthritis Rheum* 48:1332-1342.
302. Menon, M., Blair, P.A., Isenberg, D.A., and Mauri, C. 2016. A Regulatory Feedback between Plasmacytoid Dendritic Cells and Regulatory B Cells Is Aberrant in Systemic Lupus Erythematosus. *Immunity* 44:683–697.
303. Shah, K., Lee, W.-W., Lee, S.-H., Kim, S.H., Kang, S.W., Craft, J., and Kang, I. 2010. Dysregulated balance of Th17 and Th1 cells in systemic lupus erythematosus. *Arthritis Res Ther* 12.
304. Fritsch, R.D., Shen, X., Illei, G.G., Yarboro, C.H., Prussin, C., Hathcock, K.S., Hodes, R.J., and Lipsky, P.E. 2006. Abnormal Differentiation of Memory T Cells in Systemic Lupus Erythematosus. *Arthritis Rheumatol* 54:2184-2197.
305. Liu, J., Chen, D., Nie, G.D., and Dai, Z. 2015. CD8+CD122+ T-cells: a newly emerging regulator with central memory cell phenotypes. *Front Immunol* 6.
306. Gilliet, M., Cao, W., and Liu, Y. 2008. Plasmacytoid dendritic cells: sensing nucleic acids in viral infection and autoimmune diseases. *Nat Rev Immunol* 8:594–606.
307. Mak, A., and Kow, N.Y. 2014. The pathology of T cells in systemic lupus erythematosus. *J Immunol Res*.

308. Crispín, J., and Tsokos, G. 2009. Human TCR-αβ+CD4−CD8− T cells can derive from CD8+ T cells and display an inflammatory effector phenotype. *J Immunol* 183:4675–4681.

309. Wang, Y., Ito, S., Chino, Y., Goto, D., Matsumoto, I., Murata, H., Tsutsumi, A., Hayashi, T., Uchida, K., Usui, J., et al. 2010. Laser microdissection-based analysis of cytokine balance in the kidneys of patients with lupus nephritis. *Clin Exp Immunol* 159:1-10.

310. Kwan, B., Tam, L., Lai, K., Lai, F., Li, E., Wang, G., Chow, K., Li, P., and Szeto, C. 2009. The gene expression of type 17 T-helper cell-related cytokines in the urinary sediment of patients with systemic lupus erythematosus. *Rheumatology (Oxford)* 48:1491-1497.

311. Hoffman, R. 2004. T cells in the pathogenesis of systemic lupus erythematosus. *Clin Immunol* 113:4-13.

312. Deng, G., Liu, L., Bahjat, F., Pine, P., and Tsokos, G. 2010. Suppression of skin and kidney disease by inhibition of spleen tyrosine kinase in lupus-prone mice. *Arthritis Rheumatol* 62:2086-2092.

313. Furukawa, F., Kanauchi, H., Wakita, H., Tokura, Y., Tachibana, T., Horiguchi, Y., Imamura, S., Ozaki, S., and Takigawa, M. 1996. Spontaneous autoimmune skin lesions of MRL/n mice: autoimmune disease-prone genetic background in relation to Fas-defect MRL/1pr mice. *J Invest Dermatol* 107:95-100.

314. Yoshimasu, T., Nishide, T., Seo, N., Hiroi, A., Ohtani, T., Uede, K., and Furukawa, F. 2004. Susceptibility of T cell receptor-a chain knock-out mice to ultraviolet B light and fluorouracil: a novel model for drug-induced cutaneous lupus erythematosus. *Clin Exp Immunol* 136:245-254.

315. Barbhaiya, M., and Costenbader, K. 2014. Ultraviolet radiation and systemic lupus erythematosus. *Lupus* 23:588-595.

316. Ghoreishi, M., and Dutz, J.P. 2009. Murine models of cutaneous involvement in lupus erythematosus. *Autoimmun Rev* 8:484-487.

317. Bignon, A., Gaudin, F., Hémon, P., Tharinger, H., Mayol, K., Walzer, T., Loetscher, P., Peuchmaur, M., Berrebi, D., and Balabanian, K. 2014. CCR1 Inhibition Ameliorates the Progression of Lupus Nephritis in NZB/W Mice. *J Immunol* 192:886-896.

318. Hamidou, M.A., Audrain, M.A., Masseau, A., Agard, C., and Moreau, A. 2006. Anti-topoisomerase I antibodies in systemic lupus erythematosus as a marker of severe nephritis. *Clin Rheumatol* 25:542-543.

319. Holdsworth, S., and Tipping, P. 2007. Leukocytes in glomerular injury. *Semin Immunopathol* 29:355-374.

320. Yap, D., and Lai, K. 2015. Pathogenesis of Renal Disease in Systemic Lupus Erythematosus—The Role of Autoantibodies and Lymphocytes Subset Abnormalities. *Int J Mol Sci* 16:7917-7931.

321. Korbet, S., Schwartz, M., Evans, J., Lewis, E., and Group, C.S. 2007. Severe lupus nephritis: racial differences in presentation and outcome. *J Am Soc Nephrol* 18:244-254.

322. Doria, A., and Gatto, M. 2012. Nephritogenic-antinephritogenic antibody network in lupus glomerulonephritis. *Lupus* 21:1492-1496.

323. Lech, M., and Anders, H. 2013. The pathogenesis of lupus nephritis. *J Am Soc Nephrol* 24:1357-1366.

324. Kulkarni, O., Pawar, R., Purschke, W., Eulberg, D., Selve, N., Buchner, K., Ninichuk, V., Segerer, S., Vielhauer, V., Klussmann, S., et al. 2007. Spiegelmer inhibition of CCL2/MCP-1 ameliorates lupus nephritis in MRL-(Fas)lpr mice. *J Am Soc Nephrol* 18.

325. Chan, O., Madaio, M., and Shlomchik, M. 1999. B cells are required for lupus nephritis in the polygenic, Fas-intact MRL model of systemic autoimmunity. *J Immunol* 163:3592-3596.

326. Chan, O., Hannum, L., Haberman, A., Madaio, M., and Shlomchik, M. 1999. A novel mouse with B cells but lacking serum antibody reveals an antibody-independent role for B cells in murine lupus. *J Exp Med* 189:1639-1648.

327. Harari, O.A., Marshall, D., McHale, J.F., Ahmed, S., and Haskard, D.O. 2001. Limited endothelial E- and P-selectin expression in MRL/lpr lupus-prone mice. *Rheumatology* 40:889-895.

328. Moldobaeva, A., Rentsendorj, O., Jenkins, J., and Wagner, E.M. 2014. Nitric Oxide Synthase Promotes Distension-Induced Tracheal Venular Leukocyte Adherence. *PLoS One* 9:e106092.

329. Moldobaeva, A., Jenkins, J., and Wagner, E.M. 2008. Effects of distension on airway inflammation and venular P-selectin expression. ***Am J Physiol Lung Cell Mol Physiol*** 295:L941-L948.

330. Shiozawa, F., Kasama, T., Yajima, N., Odai, T., Isozaki, T., Matsunawa, M., Yoda, Y., Negishi, M., Ide, H., and Adachi, M. 2004. Enhanced expression of interferon-inducible protein 10 associated with Th1 profiles of chemokine receptor in autoimmune pulmonary inflammation of MRL/lpr mice. *Arthritis Research & Therapy* 6:R78-R86.

331. Segawa, C., Wada, T., Takaeda, M., Furuichi, K., Matsuda, I., Hisada, Y., Ohta, S., Takasawa, K., Takeda, S., Kobayashi, K., et al. 1997. In situ expression and soluble form of P-selectin in human glomerulonephritis. *Kidney Int* 52:1054-1063.

Annexes

Annexes

Publications related to this Thesis work:

- González-Tajuelo, R., Silván, J., Pérez-Frías, A., de la Fuente-Fernández, M., Tejedor, R., Espartero-Santos, M., Vicente-Rabaneda, E., Juarranz, A., Muñoz-Calleja, C., Castañeda, S., Gamallo, C. and Urzainqui, A. (2017). P-Selectin preserves immune tolerance in mice and is reduced in human cutaneous lupus. *Scientific Reports*, *7*, 41841. http://doi.org/10.1038/srep41841
- González-Tajuelo, R., De la Fuente-Fernández, M., Morales-Cano, D., Barreira, B., Silván, J., Gamallo, C., Vicente-Rabaneda, E., Castañeda, S., Pérez-Vizcaíno, F., Cogolludo, A., Jiménez-Borreguero, L.J. and Urzainqui, A. AngII involvement in lung endothelial dysfunction and spontaneous PAH development in PSGL-1 deficient female mice. *Circulation Research.* Submitted.

Other publications:

- Pérez-Frías, A. *, González-Tajuelo, R.*, Núñez-Andrade, N., Tejedor, R., García-Blanco, M. J., Vicente-Rabaneda, E., Castañeda, S., Gamallo, C., Silván, J., Esteban-Villafruela, A., Cubero-Rueda, L., García-García, C., Muñoz-Calleja, C., García-Diez, A. and Urzainqui, A. (2014). Development of an Autoimmune Syndrome Affecting the Skin and Internal Organs in P-Selectin Glycoprotein Ligand 1 Leukocyte Receptor–Deficient Mice. *Arthritis & Rheumatology*, 66: 3178–3189. http://doi.org/10.1002/art.38808
  *Equal contribution
- Ramos-Sevillano, E., Urzainqui, A., de Andrés, B., González-Tajuelo, R., Domenech, M., González-Camacho, F., Sánchez-Madrid, F., Brown, J.S., García, E. and Yuste, J. (2016). PSGL-1 on Leukocytes is a Critical Component of the Host Immune Response against Invasive Pneumococcal Disease. *PLoS Pathogens*, *12*(3), e1005500. http://doi.org/10.1371/journal.ppat.1005500

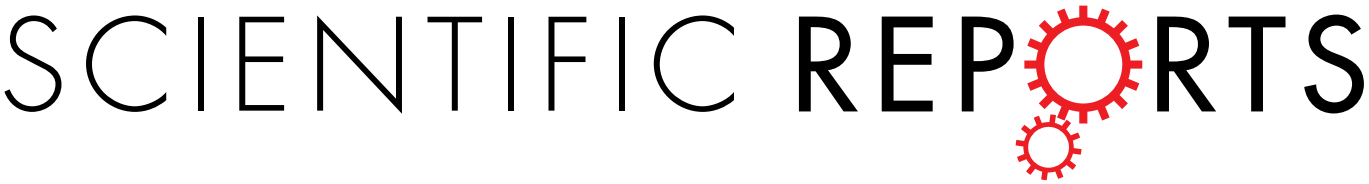

OPEN

P-Selectin preserves immune tolerance in mice and is reduced in human cutaneous lupus

Received: 26 September 2016
Accepted: 30 December 2016
Published: 02 February 2017

Rafael González-Tajuelo[1], Javier Silván[1,*], Alicia Pérez-Frías[1,*], María de la Fuente-Fernández[1], Reyes Tejedor[2], Marina Espartero-Santos[1], Esther Vicente-Rabaneda[3,4], Ángeles Juarranz[4], Cecilia Muñoz-Calleja[2], Santos Castañeda[3], Carlos Gamallo[5] & Ana Urzainqui[1]

Mice deficient in P-Selectin presented altered immunity/tolerance balance. We have observed that the absence of P-Selectin promotes splenomegaly with reduced naïve T cell population, elevated activated/effector T cell subset, increased germinal center B and Tfh populations and high production of autoreactive antibodies. Moreover, 1.5-3-month-old P-selectin KO mice showed reduced IL-10-producing leukocytes in blood and a slightly reduced Treg population in the skin. With aging and, coinciding with disease severity, there is an increase in the IL17$^+$ circulating and dermal T cell subpopulations and reduction of dermal Treg. As a consequence, P-Selectin deficient mice developed a progressive autoimmune syndrome showing skin alterations characteristic of lupus prone mice and elevated circulating autoantibodies, including anti-dsDNA. Similar to human SLE, disease pathogenesis was characterized by deposition of immune complexes in the dermoepidermal junction and renal glomeruli, and a complex pattern of autoantibodies. More important, skin biopsies of cutaneous lupus erythematosus patients did not show increased expression of P-Selectin, as described for other inflammatory diseases, and the number of vessels expressing P-Selectin was reduced.

Selectins (E-, L- and P-Selectin) mediate leukocyte rolling during their extravasation through interactions of their N-terminal lectin domains with a sialyl Lewis x (sLex) capping structure on leukocytic P-Selectin glycoprotein ligand-1 (PSGL-1)[1,2]. P-Selectin is stored in the α-granules of platelets and Weibel-Palade bodies of endothelial cells, and is rapidly mobilized to the membrane upon activation by complement, oxygen-derived free radicals or thrombin[3–6], without requiring new protein synthesis. Additionally, TNF, IL-1β, or LPS increase also murine P-Selectin mRNA and protein in endothelial cells[7–10].

Systemic lupus erythematosus (SLE) is a chronic, inflammatory autoimmune disease characterized by the production of autoantibodies against double strand DNA (dsDNA) and nuclear antigens, immune complex deposition, complement activation and polyclonal expansion of autorreactive lymphocytes[11,12]. SLE predominantly affects women (6–10:1 ratio of women to men) in the childbearing years[12,13]. Clinical manifestations of SLE include inflammation of the skin and internal organs, which are translated into non-specific symptoms like fever, arthralgia, skin rashes and anemia[12]. P-Selectin levels are elevated in the urine of SLE patients and correlate with disease severity[14]. Genome-wide linkage studies in humans have suggested an important role for P-Selectin in SLE. Indeed, the P-Selectin gene is located in the SLE linkage region on human chromosome 1 (1q23)[15,16]. Moreover, variations in the upstream region of P-Selectin are a risk factor for SLE, and two risk alleles have been identified potentially affecting the transcription of P-Selectin and the binding to P-Selectin glycoprotein ligand-1 (PSGL-1)[15], the main ligand for P-Selectin expressed on all leukocyte subsets, and also a ligand for E- and L-Selectin[3,17–19].

[1]1Fundación de Investigación Biomédica (FIB), Instituto de Investigación Sanitaria-Princesa (IIS-Princesa), Hospital de la Princesa, Immunology Department, C/Diego de León 62, 28006, Madrid, Spain. [2]FIB, IIS-Princesa, Hospital de la Princesa, Cytometry and Autoimmunity Unit, C/Diego de León 62, 28006, Madrid, Spain. [3]FIB, IIS-Princesa, Hospital de la Princesa, Rheumatology Department, C/Diego de León 62, 28006, Madrid, Spain. [4]Biology Department, Facultad de Ciencias, Universidad Autónoma de Madrid and Instituto Ramón y Cajal de Investigaciones Sanitarias (IRYCIS), C/Francisco Tomás y Valiente 7, 28049, Madrid, Spain. [5]Pathology Department, Facultad de Medicina, Universidad Autónoma de Madrid, C/Arzobispo Morcillo 4, 28029, Madrid, Spain. *These authors contributed equally to this work. Correspondence and requests for materials should be addressed to A.U. (email: ana.urzainqui@salud.madrid.org)

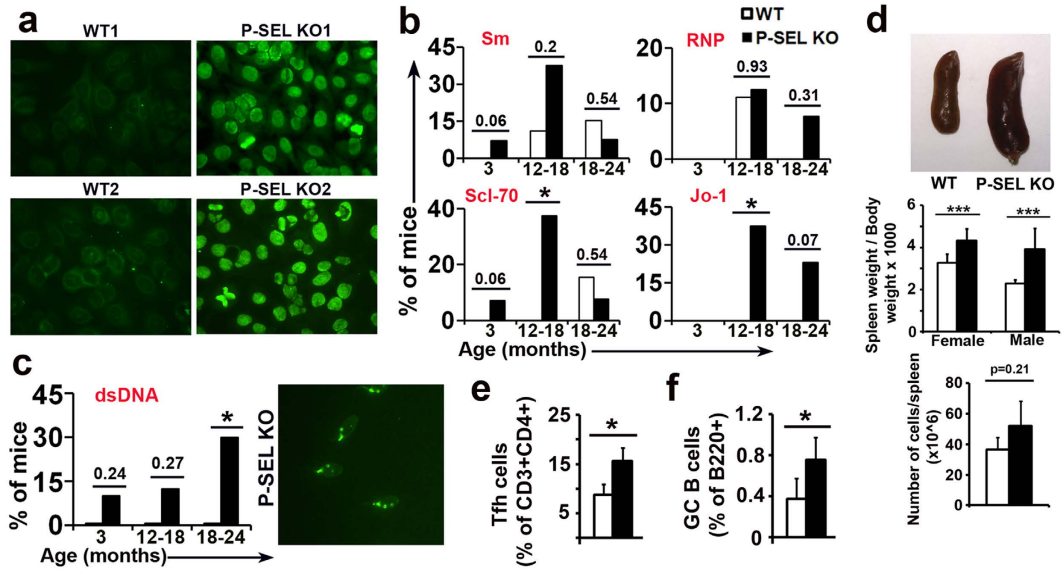

Figure 1. Spontaneous generation of autoantibodies related to connective tissue autoimmune diseases in *P-Sel*$^{-/-}$ mice. (**a**) Representative immunofluorescence photomicrographs of HEp-2 cells incubated with serum from 2 independent wild-type (WT) and 2 independent *P-Sel*$^{-/-}$ mice. (**b**) Percentage of mice positive for anti-Sm, RNP, Scl-70 and Jo-1 autoantibodies (n = 8–10 animals per group); *$p < 0.05$ by Chi-square test. (**c**) Percentage of mice positive for anti-dsDNA autoantibodies (n = 8–10 animals per group); *$p < 0.05$ by Chi-square test. Immunofluorescence photomicrographs of *C. luciliae* incubated with serum of a *P-Sel*$^{-/-}$ mouse (right panel). (**d**) Photograph of representative spleens of 3-month-old WT and *P-Sel*$^{-/-}$ mice (upper panel). Spleen weight/body weight ratio of female and male 3-month-old WT and *P-Sel*$^{-/-}$ mice (middle panel) (n = 6 mice per group). Total number of cells per spleen of WT and *P-Sel*$^{-/-}$ mice (lower panel). (**e**,**f**) Percentage of splenic follicular T helper (Tfh) cells (**e**) and germinal center (GC) B cells (**f**) in 3-month-old male WT and *P-Sel*$^{-/-}$ mice. *$p < 0.05$; ***$p < 0.005$ by Student's two-tailed t-test. Bars show the mean ± standard deviation (SD).

P-Selectin/PSGL-1 axis is involved in the generation of regulatory T (Treg) cells[20]. PSGL-1 null (*Psgl-1*$^{-/-}$) mice have altered tolerance/immunity balance in the colonic lamina propria and skin, and spontaneously develop an autoimmune syndrome similar to human scleroderma[21,22]. Experimental disease models indicate that although mice lacking P-Selectin, E-Selectin or both are significantly protected from neutrophil-dependent injury[5,23,24], selectin deficiency induced disease exacerbation in models of glomerulonephritis or collagen-induced arthritis, suggesting a protective role for endothelial P-Selectin in inflammation[5,25,26]. Numerous murine models of SLE have been described such as MRL/Mpj^{faslpr} (MRL/lpr), BSXB and NZB mice crossed with NZW strains (NZB/W)[27], characterized by high levels of circulating autoantibodies, systemic vasculitis, lymphadenopathy, splenomegaly, skin and renal lesions and early death due to renal dysfunction, hypertension and spontaneous hemorrhage[27,28]. Studies performed with this SLE experimental models described that P-Selectin deficiency in lupus-prone mice resulted in more rapid development of glomerulonephritis and dermatitis and earlier death[29] and that P-Selectin levels appear elevated in the urine of lupus-prone mice[14].

Given all these data, we sought to determine whether *P-Sel*$^{-/-}$ mice develop a connective tissue-related autoimmune syndrome sharing some characteristics with *Psgl-1*$^{-/-}$ mice.

Results

Presence of circulating autoantibodies and augmented splenic reactivity in *P-Sel*$^{-/-}$ mice. Sera from *P-Sel*$^{-/-}$ mice contained anti-cytoplasmic and anti-nuclear autoantibodies with a speckled or mitotic pattern (Fig. 1a), but not anti-centromere autoantibodies. ELISA identified several antigens recognized by these autoantibodies, including topoisomerase I (Scl-70), U1-RNP, Sm and t-RNA synthetase (Jo-1) (Fig. 1b). Sera were also positive in the Crithidia assay for anti-dsDNA autoantibodies (Fig. 1c), a hallmark of human lupus erythematosus[1,3,5], whereas none of the WT sera were positive in the same conditions. The anti-Sm, anti-topoisomerase I, and anti-dsDNA antibodies could be already detected at 3 months of age. The autoantibodies were co-expressed in the same animals and the percentage of mice with autoantibodies increased as a function of age, reaching a maximum at 12–18 months (Fig. 1b) and decreasing at 18–24 months, especially anti-Sm and anti-Scl-70 (Fig. 1b). The prevalence of anti-dsDNA autoantibodies increased gradually with ageing, from 10% in the 3-month-old group to 30% in the 18–24-month-old group (Fig. 1c). Consistent with this exacerbation of humoral immunity, we observed a remarkable spleen enlargement in both male and female 1.5-3-month-old *P-Sel*$^{-/-}$ mice (Fig. 1d), which has been described previously in lupus-prone mouse strains[30,31]. Considering the increased cellularity of 3 month-old *P-Sel*$^{-/-}$ spleens (Fig. 1d, lower panel), we analyzed the germinal centre (GC) B cell and the follicular helper T cell subsets (Tfh). We found an increase in both lymphocytic populations, indicating a more reactive state of *P-Sel*$^{-/-}$ spleens (Fig. 1e,f).

Immune homeostasis imbalance in *P-Sel*$^{-/-}$ mice blood and spleen. The study of the peripheral blood leukocyte populations of 1.5-3-month-old male mice showed an important increase in the B cell compartment of *P-Sel*$^{-/-}$ mice. In contrast, the T cell compartment was reduced, mainly due to the decrease of the CD4$^+$ T cell subset. Additionally, the monocytic population was also reduced in *P-Sel*$^{-/-}$ animals (Fig. 2a).

We studied the cytokine production of the circulating immune populations and we found a reduction in the percentage of IL-10$^+$ producing cells of 1.5-3-month-old *P-Sel*$^{-/-}$ mice, that was statistically significant among cDC and CD4$^+$ T lymphocytes and close to the statistical signification in the B cell population (Fig. 2b,c, left panels). Circulating leukocytes of >18-month-old mice showed a statistically significant reduction in the percentage of IL-10$^+$ producing monocytes and B cells (Fig. 2d, left and middle panels). Interestingly, the IL-17$^+$ CD4$^+$ (Th17) population was increased in aged *P-Sel*$^{-/-}$ mice (Fig. 2d, right panels).

To evaluate the effector and memory state of T cells, we analyzed the expression of CD62L and CD44 splenic CD4$^+$ and CD8$^+$ T cells (Fig. 2e,f). Naïve (CD62L$^+$CD44^{neg}) and central memory (CD62L$^+$CD44$^+$) subsets were decreased in 1.5-month-old *P-Sel*$^{-/-}$ CD8$^+$ splenic T cells, while effector (CD62L^{neg}CD44^{neg}) CD8$^+$ T cells were augmented. In the case of splenic CD4$^+$ T cells, the naïve subset was severely diminished in the *P-Sel*$^{-/-}$, while the effector (CD62L^{neg}CD44^{neg}) and effector memory (CD62L^{neg}CD44$^+$) compartments were highly increased (Fig. 2e, upper panels). Regarding >18-month-old mice, as compared with the WT mice, we found an increment in the rates of effector TCD8$^+$ and TCD4$^+$ lymphocytes, and a decrease of central memory TCD4$^+$ lymphocytes in *P-Sel*$^{-/-}$ mice (Fig. 2e, lower panels and 2f).

Immune homeostasis imbalance in the skin of *P-Sel*$^{-/-}$ mice. Regarding the skin, one of the main organs affected in human lupus, we did not find significant changes in the different immune subpopulations in 1.5-3-month-old mice, except from an increased percentage of plasmacytoid DC (pDC) in *P-Sel*$^{-/-}$ animals (Fig. 3a, upper panels). However, in aged animals, we found a reduced population of macrophages and a significant increment in the T cell and pDC subsets (Fig. 3a, lower panels). Among T cells, we did not find any difference in the percentage of gamma/delta (γδ) T cells (Fig. 3a, right panels). We studied the cytokine production of the different populations, and only the >18-month-old *P-Sel*$^{-/-}$ mice showed a reduction in the percentages of IL-10$^+$ macrophages, cDC, pDC and B cells (Fig. 3b, lower panels; Fig. 3c). Accordingly, aged knocked-out mice displayed a reduced FOXP3$^+$ (Fig. 3d and e) and an increased Il-17$^+$ T cell populations (Fig. 3f and g). We did not found significant differences in cytokine production in 1.5-3-month-old mice.

Histological alterations in the skin of *P-Sel*$^{-/-}$ mice. Histological examination of the skin revealed that, compared with WT counterparts, male and female *P-Sel*$^{-/-}$ mice had a reduced hypodermal layer (lipoatrophy), frequently infiltrated by leukocytes (panniculitis) (Fig. 4a). We also found that, apart from a remarkable infiltration, >18-month-old *P-Sel*$^{-/-}$ mice presented hyperproliferation of the epidermal layer (acanthosis), accumulation of keratin in the corneal layer (hyperkeratosis) and keratin plugs inside hair follicles (Fig. 4a, lower panels), described as murine lupus-like lesions[32–35]. Quantification of these observations by measuring the total thickness of the dermal, epidermal and corneal layers of WT and *P-Sel*$^{-/-}$ mice showed that male and female *P-Sel*$^{-/-}$ mice presented an enlarged dermis and incremented width of the epidermal and corneal layers in *P-Sel*$^{-/-}$ mice that was more evident when mice were >18 months-old (Fig. 4b). Accordingly, the severity of the skin lesions estimated by grading scale was higher in young *P-Sel*$^{-/-}$ mice (female *P-Sel*$^{-/-}$ 0.30 ± 0.48 vs female WT 0.00 ± 0.00; male *P-Sel*$^{-/-}$ 0.73 ± 1.44 vs male WT 0.00 ± 0.00) and remarkably more severe in the aged mice (>18 months-old: female *P-Sel*$^{-/-}$ 3.13 ± 1.81 vs female WT 0.40 ± 0.52; male *P-Sel*$^{-/-}$ 4.57 ± 4.83 vs male WT 0.00 ± 0.00) (Fig. 4c).

The exposure of 3–4-month-old female WT and *P-Sel*$^{-/-}$ to UV radiation provoked an extensive dermatitis in *P-Sel*$^{-/-}$ mice with ulcers in the exposed skin, but not in WT counterparts (Fig. 4d). Histopathological analysis revealed a severe epidermal lesion in female *P-Sel*$^{-/-}$ mice consisting of acanthosis and hyperkeratosis, immune infiltration in the dermis, and deposition of extracellular matrix components in the hypodermal layer (Fig. 4e). Consequently, the severity of the lesions was significantly higher in UV-irradiated *P-Sel*$^{-/-}$ mice (*P-Sel*$^{-/-}$ 7.25 ± 2.99 vs WT 3.00 ± 1.41) (Fig. 4f).

Kidney alterations and deposits of immune complexes in skin and kidneys of *P-Sel*$^{-/-}$ mice. Histological examination of kidney sections of WT and *P-Sel*$^{-/-}$ mice showed that *P-Sel*$^{-/-}$ mice had a high proportion of glomeruli with a dilated Bowman's space (Fig. 5a). Additionally, some glomeruli presented tubularization of the Bowman's capsule (Fig. 5a). We found also interstitial infiltrates in *P-Sel*$^{-/-}$ mice (Fig. 5b), whose prevalence increased from 40% at 1.5–3 months of age to 84% in mice older than one year (12–24 months-old) (Fig. 5c), while only 20% of aged WT and none of the young WT mice presented interstitial infiltration.

We also observed that 30% of the 3-month-old *P-Sel*$^{-/-}$ mice had infarcted foci (Fig. 5d). The prevalence of infarcts increased as mice grew older (Fig. 5e), reaching to 60% of females and 80% of males in the >18-month-old population of *P-Sel*$^{-/-}$ mice.

We found deposits of immune complexes in the glomerular basal membrane in 100% of female and 25% of male *P-Sel*$^{-/-}$ mice older than 18 months, but only in 25% of WT females and none in WT males (Fig. 5f). In the skin, we found deposits of immune complexes in 60% of male and 40% of female *P-Sel*$^{-/-}$ mice over 18 months of age but in none of WT mice (Fig. 5f).

According to the structural renal damage and the immune complex deposition, we found that 13% of >18 months *P-Sel*$^{-/-}$ mice developed proteinuria, while 38% of *P-Sel*$^{-/-}$ mice develop hematuria (Fig. 5g).

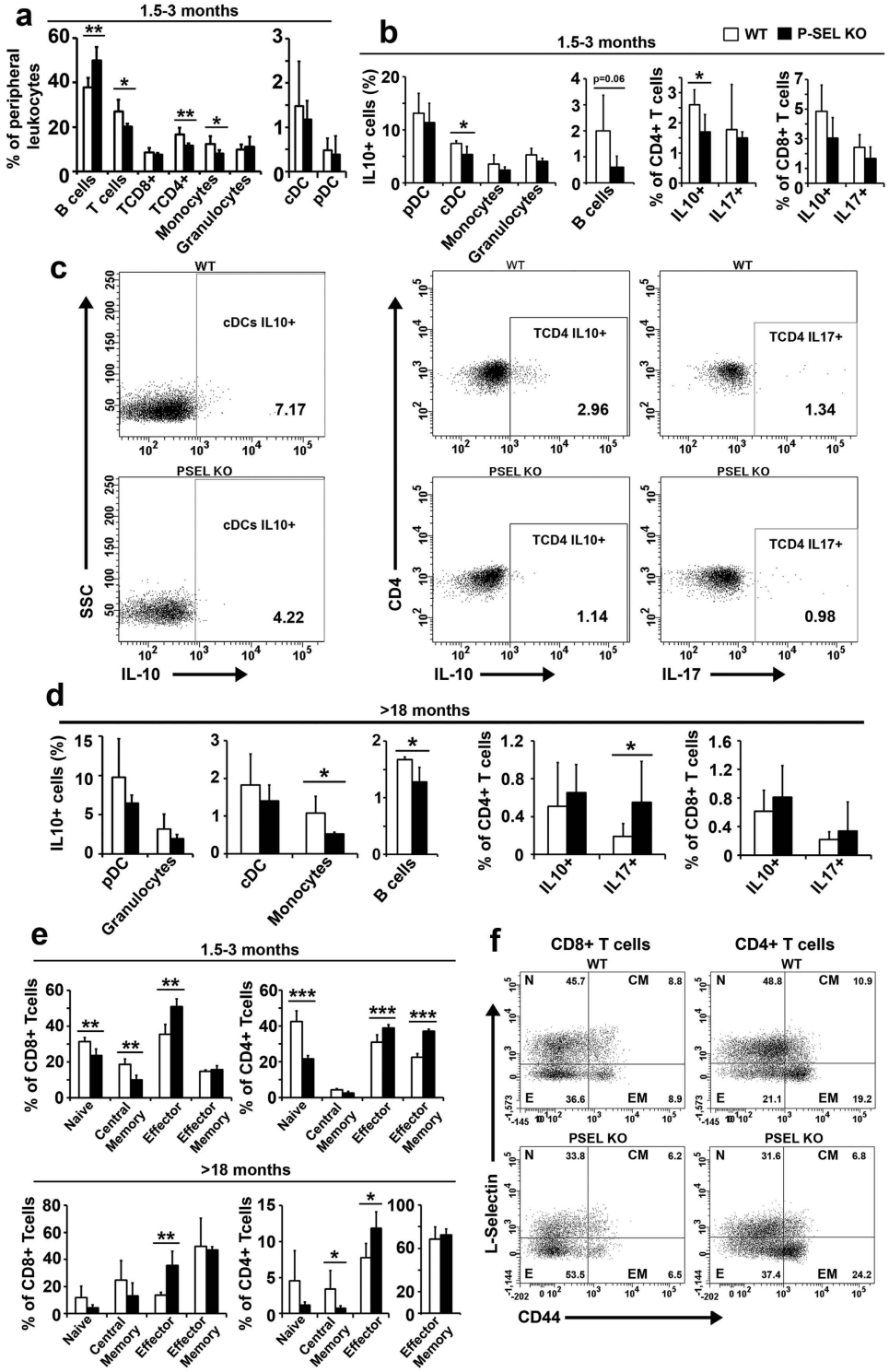

Figure 2. Peripheral blood and spleen immune system characterization in *P-Sel*$^{-/-}$ mice. (**a**) Relative frequency of peripheral blood leukocyte populations of 1.5–3 month-old WT and *P-Sel*$^{-/-}$ mice. (**b**,**d**) Percentage of IL-10^{+} conventional dendritic cells (cDC), plasmacytoid DC (pDC), monocytes, granulocytes and B cells; and frequency of IL-10 and IL-17 producing CD4^{+} and CD8^{+} T lymphocytes, in 1.5-month-old (**b**) and >18-month-old (**d**) WT and *P-Sel*$^{-/-}$ mice. (**c**) Representative dot plots of IL-10^{+} cDCs and IL-10 and IL-17 producing CD4^{+} T cells in 1.5-months old WT and *P-Sel*$^{-/-}$ mice. (**e**) Phenotyping of CD4^{+} and CD8^{+} splenic T lymphocytes according to the expression of the naïve/memory/effector markers CD62L and CD44 in 1.5–3 months-old (upper panels) and >18 month-old (lower panels) WT and *P-Sel*$^{-/-}$ mice. (**f**) Representative dot plots showing the distribution of 1.5–3-month-old mice splenic populations according to the expression of L-Selectin and CD44. In all cases, n = 4 mice per group. In all cases, n = 4 mice per group. Bars represent the mean ± SD. *$p < 0.05$; **$p < 0.01$; ***$p < 0.005$, by Student's two tailed t test.

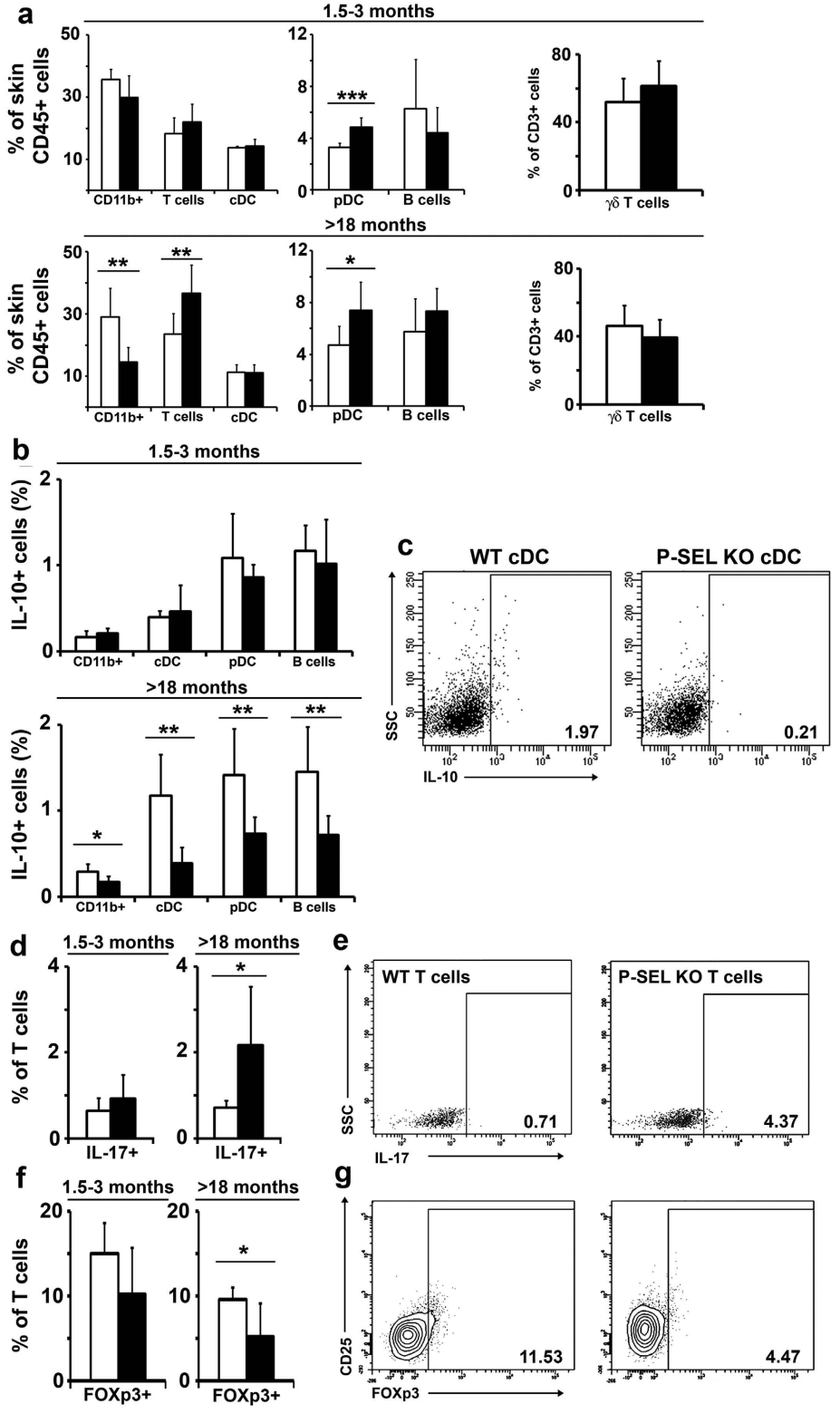

Figure 3. Characterization of the skin immune system of *P-Sel*$^{-/-}$ mice. (**a**) Relative frequency of skin leukocyte populations of 1.5–3 month-old and >18-month-old WT and *P-Sel*$^{-/-}$ mice. (**b**) Percentage of IL-10^{+} macrophages (CD11b^{+}), conventional dendritic cells (cDC), plasmacytoid DC (pDC) and B cells, in 1.5–3-month-old and >18-month-old WT and *P-Sel*$^{-/-}$ mice. (**c**) Representative dot plots of IL-10^{+} cDCs in >18-month-old WT and *P-Sel*$^{-/-}$ mice. (**d**) Percentage of IL-17^{+} T cells in 1.5–3-month-old and >18-month-old WT and *P-Sel*$^{-/-}$ mice. (**e**) Representative dot plots of IL-17^{+} T cells in >18-month-old WT and *P-Sel*$^{-/-}$ mice. (**f**) Percentage of FOXP3^{+} T cells in 1.5–3-month-old and >18-month-old WT and *P-Sel*$^{-/-}$ mice. (**g**) Representative dot plots of FOXP3^{+} T cells in >18-month-old WT and *P-Sel*$^{-/-}$ mice. *$p < 0.05$; **$p < 0.01$ by Student's two tailed t test. n = 6 mice per genotype.

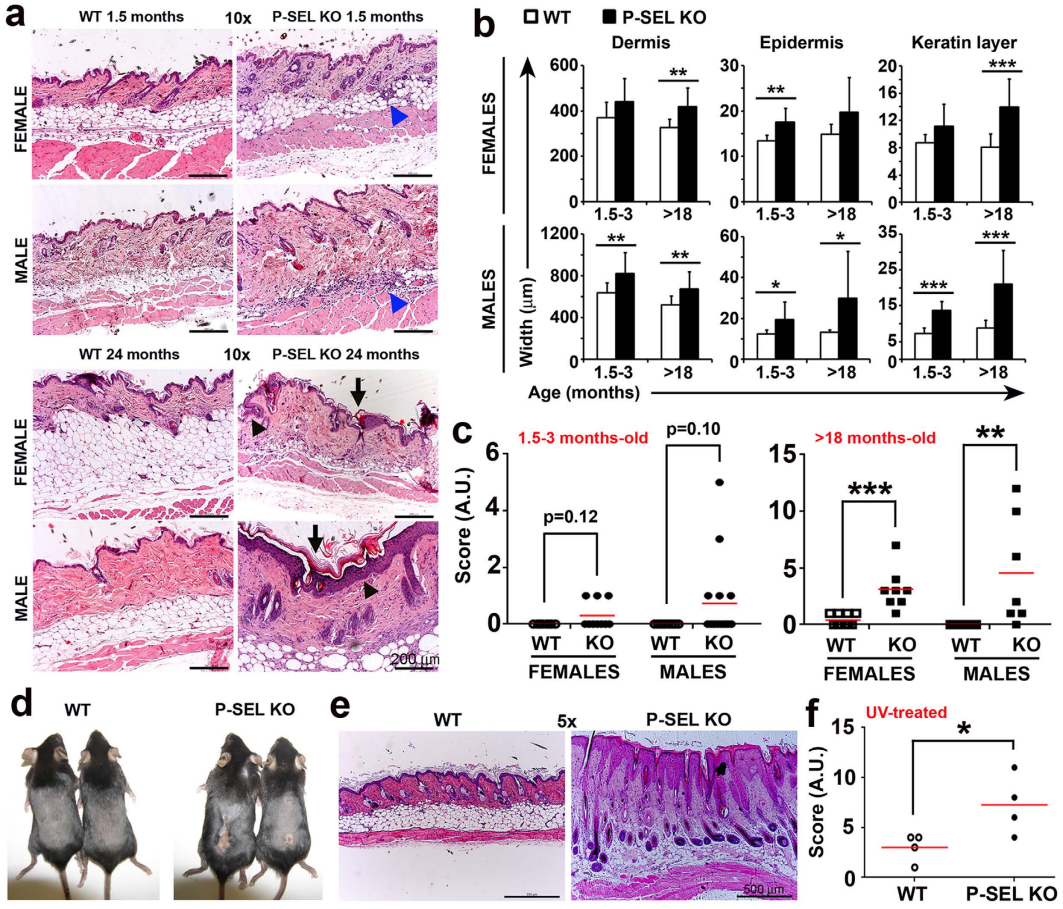

Figure 4. Histological alterations in the skin of *P-Sel*$^{-/-}$ mice. (**a**) Photomicrographs (10×) of hematoxylin and eosin (H&E)-stained skin sections of 1.5 month-old (upper panels) and 24-month-old female and male WT and *P-Sel*$^{-/-}$ mice (lower panels). Blue arrowheads show panniculitis. Black arrowheads show acanthosis; arrows show hyperkeratosis and keratin plugs. Scale bars represent 200 µm. (**b**) Quantification of dermis, epidermis and corneal layer width of WT and *P-Sel*$^{-/-}$ mice. (**c**) Pathological activity index of skin samples obtained from WT and *P-Sel*$^{-/-}$ mice. (**d**) Lesions developed in the back of UV-irradiated 3-month-old female WT and *P-Sel*$^{-/-}$ mice. (**e**) Photomicrographs (5×) of representative skin sections of UV-irradiated 3-month-old female WT and *P-Sel*$^{-/-}$ mice. n = 4 mice per genotype. Representative experiment of three independent replicates. Scale bars represent 500 µm. (**f**) Pathological activity index of skin samples obtained from UV-irradiated 3-month-old female WT and *P-Sel*$^{-/-}$ mice. (**b,c,f**) Bars show the mean ± SD *$p < 0.05$; **$p < 0.01$; ***$p < 0.005$ by Student's two tailed t test. n = 8–10 mice per genotype.

Reduced lifespan of *P-Sel*$^{-/-}$ mice. To analyze the impact of the autoimmune syndrome progression during the lifespan of *P-Sel*$^{-/-}$ mice, we carried out a survival study with 20 WT and 23 *P-Sel*$^{-/-}$ mice from 6 to 100 weeks of age. *P-Sel*$^{-/-}$ mice started to die at week 47 and we observed a peak of mortality at around week 80. At week 100, 90% of WT mice remained alive whereas only 61% of the *P-Sel*$^{-/-}$ mice were still alive (Fig. 5h).

Decreased expression of P-Selectin in SLE skin biopsies. To assess the relevance of P-Selectin in human lupus, we compared by immunohistochemical staining the expression of P-Selectin in endothelial cells of the dermal vessels of skin biopsies obtained from cutaneous lupus erythematosus (cLE) patients and healthy controls. We identified all the blood vessels ($CD31^+$) in the whole biopsy and classified them into three categories depending on the expression of P-Selectin (Fig. 6a and b): (1) unstained, (2) partially stained, and 3) fully stained. We found a deep reduction of fully stained blood vessels in cLE biopsies, which were accompanied by a remarkable elevation in the percentage of negative vessels for P-Selectin expression (Fig. 6c). We also found unspecific binding to infiltrating leukocytes, that has been already reported by other authors[36,37].

Discussion

In this work, we show that the absence of P-Selectin breaks the immune tolerance and triggers the development of a progressive autoimmune lupus-like syndrome displaying most of the features previously described in lupus-prone mice. Importantly, we show that human biopsies of cutaneous lupus have reduced number of P-Selectin stained vessels.

Given that PSGL-1 deficient mice develop a scleroderma-like syndrome, we have analyzed whether the absence of P-Selectin, main ligand of PSGL-1, also triggered autoimmunity. We found the production of

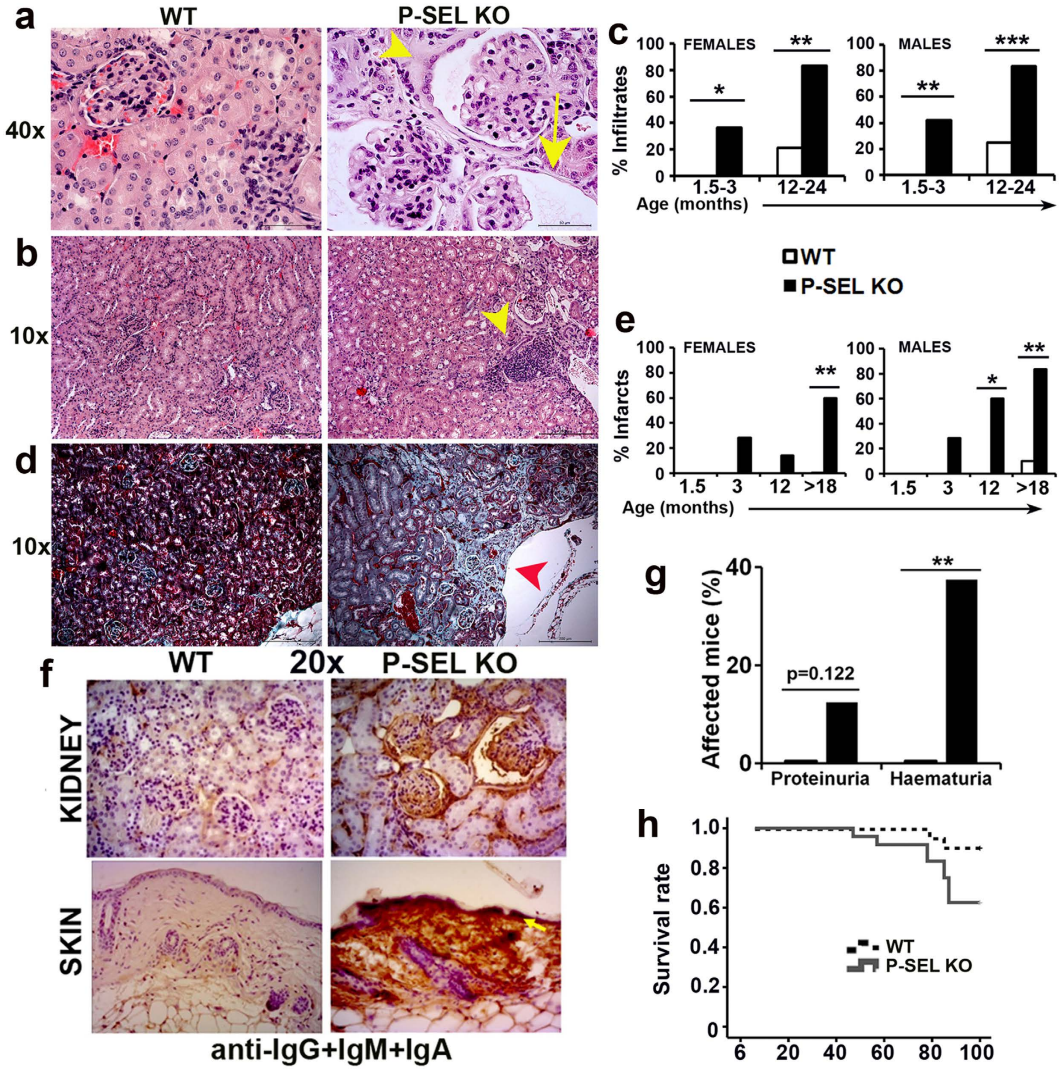

Figure 5. Kidney alterations and deposits of immune complexes in skin and kidneys of *P-Sel*$^{-/-}$ mice. (**a**) Representative photomicrographs (40×) of H&E-stained kidney glomeruli of WT and *P-Sel*$^{-/-}$ mice. Yellow arrow denotes a dilated Bowman's space. Yellow arrowhead denotes a tubularized glomerulus. (**b**) Photomicrographs (10×) of kidney sections showing an immune infiltrate (yellow arrowhead) in *P-Sel*$^{-/-}$ mice. (**c**) Prevalence of immune infiltration in WT and *P-Sel*$^{-/-}$ mice (n = 8–10 mice per group). (**d**) Masson's trichrome-stained kidney sections of WT and *P-Sel*$^{-/-}$ mice (10×), showing healthy and infarcted tissue (red arrowhead), respectively. (**e**) Prevalence of renal infarcts in WT and *P-Sel*$^{-/-}$ mice (n = 8–10 mice per group). (**f**) Representative photomicrographs of anti-IgM+ IgA+ IgG-stained kidney (upper panels) and skin (lower panels) sections (20×). n = 4–5 mice per group. Yellow arrow points to the dermoepidermal junction. (**g**) Frequency of proteinuria and hematuria in >12-month-old WT and *P-Sel*$^{-/-}$ mice (n = 14–16 mice per group). (**h**) Kaplan-Meier survival curves for WT and *P-Sel*$^{-/-}$ mice (n = 20 WT and 23 *P-Sel*$^{-/-}$ mice); p = 0.033 by Mantel-Cox test. (**c,e,g**) *$p < 0.05$; **$p < 0.01$; ***$p < 0.005$ by Chi-square test.

anti-dsDNA and anti-Sm autoandibodies, hallmarks of SLE in humans[38]. Interestingly, anti-Sm and anti-dsDNA autoantibodies are detected at an early age in *P-Sel*$^{-/-}$ mice. The high rate of autoantibodies probably favours, as in human SLE, the formation and deposition of immune complexes in anatomic sites characterized by high blood pressure including capillaries of the skin and glomeruli, among others. Accordingly, we found a high rate of immune complexes deposition in renal glomeruli and skin of aged *P-Sel*$^{-/-}$ which is a characteristic of both human and murine lupus[29,32,39,40].

To understand the autoantibody production, we studied the impact of P-Selectin absence in the homeostasis of the immune system and analyzed the effector and regulatory leukocyte subsets in blood, spleen and skin of WT and KO mice, and found that the immune homeostasis is altered in *P-Sel*$^{-/-}$ mice. We found higher percentage of germinal center B cell and Tfh subpopulations, indicating more reactive germinal centers in the spleen of young animals as well as reduced circulating TCD4^{+} and monocytic populations, in association with an increment in the B cell compartment. Interestingly, at the young age we found a reduction in the circulating tolerogenic IL-10-producing cDC and monocyte subsets, as well as in the IL-10^{+} B cell compartment (Breg), whose reduction

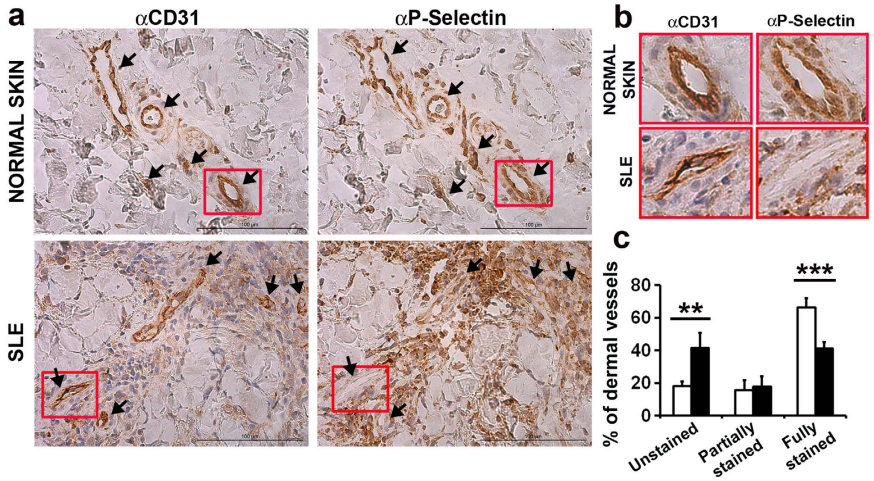

Figure 6. Decreased expression of P-Selectin in human SLE biopsies. (**a**) Representative photomicrographs (20×) of anti-CD31 and anti-P-Selectin stained skin biopsies of healthy donors and SLE patients (upper panels). Black arrows point blood vessels. (**b**) 200% magnification of representative blood vessels from the original images are represented (lower panels). (**c**) Classification and quantification of CD31+ dermal blood vessels according to the expression level of P-Selectin (healthy controls, n = 4; SLE patients, n = 4); bars show the mean ± SD. **$p < 0.01$ by Student's two tailed t test.

has been recently implicated in the development of human SLE[41]. Although young *P-Sel*$^{-/-}$ mice did not have altered the presence of Th1, Th2 and Th17 populations, reduction in the IL-10-producing CD4$^+$ T cells implies an imbalanced Teff/Treg ratio, as it has been described for both murine and human SLE[42]. This reduction in IL-10$^+$ cells could be explained by the lack of tolerogenic signal supplied by P-Selectin interaction with PSGL-1, as previously described[20]. Remarkably, we found a shift through a Th17 response with aging in the blood of *P-Sel*$^{-/-}$ mice coinciding with the worsening of the disease, in agreement with the described role of PSGL-1 expression on Treg in the attenuation of persistent T cell activation during the immune response[43]. In fact, IL-17 promotes the recruitment of T cells, monocytes and granulocytes to the inflammatory foci, activates B cells and contributes to the synthesis of IgG and anti-dsDNA autoantibodies[44]. Accordingly, we report that, in *P-Sel*$^{-/-}$ mice, the effector subpopulations of splenic CD4$^+$ and CD8$^+$ T cells were increased, with the consequent and relevant reduction among the naïve subset. SLE patients show reduced numbers of CD45RA$^+$ naïve T cells and increased numbers of CD45RO$^+$ memory T cells[45]. Interestingly, it has been described that mouse CD8$^+$ CD122$^+$ Treg have a central memory phenotype (CD44^{high}CD62L^{high})[46] what could explain the reduction of this compartment in the *P-Sel*$^{-/-}$ mice, as well as the reduced populations of IL-10 producing T cells. In addition, this subset has been described to regulate T cell homeostasis and to suppress both autoimmune and alloimmune responses[46].

Given that the skin is one of the main organs affected in lupus patients, we have also analyzed whether the dermal immune system is also altered in *P-Sel*$^{-/-}$ mice. Our results indicate that dermal pDC subpopulation is increased from youth and that aging also increases the T cell subset. Importantly, coinciding with the appearance of the lupus skin lesions, we have found a high reduction in the dermal IL-10 producing immune cells and the FOXP3$^+$ Treg population, together with an important expansion of the IL-17 producing T lymphocytes. Our data are in accordance with the expanded Th17 population and reduced Treg subset described for human patients[47]. It has been described that different mechanisms can be implicated in the breakage of the immunological tolerance[48] and our work indicates that a defect in P-Selectin expression and function, probably through PSGL-1 interaction, could be implicated in maintaining the immune system immunity/tolerance balance. Dysfunction or low expression of P-Selectin and PSGL-1 could favor the use of alternative molecules for leukocyte extravasation and consequently, the loss of the tolerogenic signal triggered by PSGL-1/P-Selectin interaction.

The skin histological features described in this work for aged *P-Sel*$^{-/-}$ mice, such as hyperkeratosis, acanthosis and immune cell infiltration, have been previously reported for MRL/lpr mice[33,49]. According with our data, it has been reported that P-Selectin or PSGL-1 deficiency in MRL/lpr mice results in an increase in the severity of dermatitis and glomerulonephritis[29]. We observed that UV irradiation could accelerate and intensify the appearance of the above mentioned lesions in 3–4-month-old *P-Sel*$^{-/-}$ mice, whereas non lupus-prone strains are considered to be resistant to UV-induced DNA damage[38]. Interestingly, more than 50% of SLE patients show photosensitivity[38,50,51].

Glomerulonephritis and renal involvement are the most common manifestations in SLE patients (40–70%)[52]. Leukocyte infiltration is a common feature shared by humans and lupus-prone mice[11]. Accordingly, we found leukocytic infiltration in both glomerular and tubulointerstitial compartments of the kidney in *P-Sel*$^{-/-}$ mice. Additionally, *P-Sel*$^{-/-}$ mice presented a high frequency of renal infarcts, indicating vascular dysfunction. Renal and systemic vasculitis have been described in patients and experimental models of SLE[27] and, together with immune infiltration, have been associated with loss of renal function[53]. In agreement with our data, mice deficient for P-Selectin are more sensitive to glomerulonephritis[29,54]. Importantly, as a consequence of the renal damage, we found increased prevalence of proteinuria and hematuria in *P-Sel*$^{-/-}$ mice.

We also report that the lifespan of *P-Sel*$^{-/-}$ mice is reduced compared to WT animals, showing an augmented death rate at approximately 1 year of age (47 weeks), which is sharply increased at 80 weeks coinciding with disease worsening. This increased death along *P-Sel*$^{-/-}$ mice could underestimate the prevalence of some clinical observations such as anti-DNA autoantibodies, skin lesions or proteinuria.

Finally, it has been reported that the lack of either P-Selectin or PSGL-1 in murine lupus models enhances both skin and renal inflammation[29] and that the tissue expression of P- and E-Selectin in the MLR/lpr mice was not upregulated regarding the non-inflammed MRL$^{+/+}$ mice[55]. Importantly, when analyzed in patients, although E-selectin expression was increased in skin biopsies[56], according with our data in *P-Sel*$^{-/-}$ mice, we found a reduction in the expression of P-Selectin in the dermal blood vessels of patients with cutaneous lupus. This important result does not concur with the higher levels of P-Selectin that have been traditionally associated with other autoimmune and inflammatory diseases like glomerulonephritis, rheumatoid arthritis, psoriasis or atopic dermatitis[37,57,58]. It has been reported that TNFα and LPS downregulated human P-Selectin[7]. The increased levels of TNFα in the serum of SLE patients are consistent with the low expression of P-Selectin that we found in the skin of lupus patients.

In summary, we show that P-Selectin expression is crucial for the immune system homeostasis and that its absence promotes the spontaneous development of a lupus-like syndrome in mice. Accordingly, patients with cutaneous lupus showed lower expression of P-Selectin in the endothelium of the dermal vessels, suggesting that the reduced expression of P-Selectin could be implicated in the pathogenesis of this disease. As SLE pathogenesis is not well understood and there is not a universally curative treatment for lupus in humans, it is very important to discover new molecules implicated in the development of the different forms of this disease that could be used as targets for new treatments. Our work will contribute to the understanding of lupus pathogenesis, and our future research will explore the role of P-Selectin in the development of human lupus and other autoimmune diseases. In addition, our work suggests that P-Selectin KO mice could be used as a new experimental model for *in vivo* assays to evaluate new treatments or combination of treatments against the progression of the disease that could prevent organ damage associated with SLE.

Methods

Mice. C57Bl/6 (WT) mice (The Jackson Laboratory) and C57Bl/6-*P-Sel*$^{-/-}$ mice, kindly provided by Dr. D. Vestweber (Max Planck Institute for Molecular Biomedicine, Münster, Germany), were maintained at the Conventional Animal Facility of the School of Medicine of the Universidad Autónoma de Madrid (UAM) (register number ES-28079-0000097). Mice were sacrificed by cervical dislocation, and blood and internal organs were extracted for analysis. All experiments and breeding were performed in accordance with national and institutional guidelines for animal care (EU Directive 2010/63/EU for animal experiments). The experimental procedures were approved by the Director General de Medio Ambiente of Madrid (Ref: PROEX 69/14 and PROEX 162/15).

UV radiation protocol. Three month-old WT and *P-Sel*$^{-/-}$ mice were irradiated with an UVB lamp containing a set of six tubes (Phillips TL UV, 20 W; Royal Philips Electronics, Amsterdam, Netherlands) (ranging from 290 nm to 320 nm), being the energy output, at a distance of 15 cm, of 2.5 mW/cm^2. Mice received three doses of 0.306 J/cm^2 every other day for a week and an additional dose of 0.12 J/cm^2 three days later. Skin was processed 24 hours after the last dose.

Autoantibody assays. The presence of anti-nuclear antibodies (ANAs), the Crithidia assay for anti-dsDNA and the characterization and quantification of circulating autoantibodies were performed as previously described[22]. The cut-off point for positivity on ELISA for a particular autoantibody was determined as the mean value (X) plus two standard deviations (SD) obtained from sera of at least 100 WT mice with an age ranging from1.5 to 24 months. At least 8 mice per group of age were analyzed.

Histopathological assessment and immunohistochemical (IHC) staining of mouse skin and kidney. Masson's trichrome staining was performed with the Artisan Gomori's Green Trichrome Stain kit (Dako; Glostrup, Denmark). Images were obtained with a Leica DM2500 light microscope and a Leica DFC450 camera. All sections were examined by a pathologist blinded to the sample origin.

Para-midline, upper back skin samples were evaluated blindly to obtain a semiquantitavive measurement by assigning a 3-criteria-based score[59]: acanthosis (0, normal; 1, slight thickening of epidermis; 2 and 3, presence of two or three layers of stratum spinosum cells, respectively; 4, presence of four or more layers of stratum spinosum cells); hyperkeratosis (0, normal; 1, one layer of keratin; 2, two layer thick of keratin; 3, minimum three-layer thick of keratin; 4, minimum three-layer thick of keratin and formation of a keratin's plug); hypergrannulosis (0, normal; 1, moderate accumulation of granular dark material in the stratum granulosum; 2 and 3, two or more than three layers of granular dark material; 4, three or more layers of accumulated granular dark material overall section of skin). Finally, the total pathology score was calculated by adding the resulting values for the three criteria.

The presence of kidney ischemic events (infarcted areas) was assessed in Masson's trichrome-stained sections.

Skin and glomerular immunoglobulin deposition were evaluated by IHC with an antibody cocktail against Fab regions of IgA, IgG, IgM (1/250) (Abcam; Cambridge, UK), following manufacturer's instructions of the Universal LSAB+ Kit Rabbit/Mouse/Goat (DAB+) (Dako). At least 5 males and 5 females were evaluated per genotype and age.

Urine analyses. Urinary protein and haemoglobin were determined using Combur Test M dipsticks (Roche; Basel, Switzerland). The cut-off for positivity in the proteinuria test was the lowest value in *P-Sel*$^{-/-}$ mice not reached by any of the WT mice analyzed.

Human skin samples. Skin biopsies from 4 chronic/subacute cutaneous lupus erythematosus patients and from 4 aged-matched healthy controls were obtained from the Pathology Department, Hospital de la Princesa (Madrid, Spain). The investigations were conducted in accordance with the principles of the Declaration of Helsinki and were approved by the Clinical Investigation Ethical Committee of the Hospital de la Princesa, Madrid, Spain (Register number: PI-654, date of approval 07-02-2013). Informed consent was obtained from all the patients and healthy controls.

Immunohistochemistry of human skin sections. Consecutive tissue sections of sun-exposed skin biopsies underwent immunohistochemistry with the Dako REAL EnVision Detection System Peroxidase/DAB+kit (Dako), using as primary antibodies anti-human P-Selectin (10 μg/ml) (R&D Systems; Minneapolis, MN, USA) and anti-human CD31 (1/50) (Abcam). The whole biopsies were scouted for blood vessels in a blinded manner. Vessels were identified by positive staining by CD31, localized in the consecutive P-Selectin-stained section, and classified depending on the expression of P-Selectin as follows: 1) unstained, negative vessels; 2) partially stained; 3) fully stained blood vessels.

Flow cytometry. Blood, skin and spleens from 1.5–3 month and >18 month-old male WT and *P-Sel*$^{-/-}$ were analyzed. Spleens were dissected and mechanically disrupted in PBS 1X, 0.5% BSA, 5 mM EDTA. Skin samples were minced into ~1 mm^2 pieces and digested with RPMI1640 medium complemented with 1 mg/ml collagenase A (Sigma-Aldrich; San Luis, MI, USA), 2.5 mg/ml dispase II (Roche; Basel, Switzerland) and 40 μg/ml DNase (Sigma). Cells were blocked with 1:200 Fc Block (BD Pharmingen; San Jose, CA, USA), labelled with the mix of antibodies recognising surface cell markers for 10 minutes at 4 °C and analyzed with a FACSCanto II (BD Pharmingen). For intracellular cytokine staining, after surface labelling, cells were fixed/permeabilized by 15 minute incubation with 2 ml of FACS Lysing Solution (BD Pharmingen), washed, incubated during 30 minutes at 4 °C with the cocktail of antibodies directed against intracellular cytokines and analyzed with a FACSCanto II.

Reagents: GL-7-eFLUOR660, CD3e-PE-Cy7 and CD11c-PE-Cy7 (eBioscience, San Diego, CA, USA); FAS-L-Biotin, CD3-APC, CD25-APC, CD45R/B220-APC, IFNg-APC, IL-4-APC, IL-17A-APC-Cy7, CD45.2-BV421, CD62L-PE and CD11b-FITC (BD Pharmingen); CD4-FITC, CD8a-PerCP, CD44-APC, CD8a-FITC, B220-APC-Vio770, MHC II-APC, and MHC II-PE (Miltenyi Biotec, Cologne, Germany); CD4-PE (Immunotools, Friesoythe; Germany); CXCR5-PE/Dazzle594, PD-1-BV421, IL-10-PerCP/Cy5.5, Gamma/delta TCR-PerCP/Cy5.5 and Streptavidin-PerCP (BioLegend, San Diego, CA, USA).

Gating strategy: in tissues, immune cells were identified as $CD45^+$. $CD11c^-CD11b^+$ cells were gated as monocytes (peripheral blood) or macrophages (skin). $CD11c^+$ cells were gated as DC: $CD11c^+$ $CD11b^+$ $B220^-$ were gated as cDCs; and $CD11c^+$ $CD11b^-B220^+$ were gated as pDCs. $CD11c^-B220^+$ cells, with low size/complexity index were considered B lymphocytes. T lymphocytes were gated as $CD3^+$ cells. Follicular Th cells were gated as $CD3^+$ $CD4^+$ PD-$1^{high}CXCR5^{high}$. Germinal centre B cells were gated as $CD11c^-B220^+$ FAS-L^+ GL-7^+. Gamma/delta T cells were gated as $CD3^+\gamma\delta^+$.

Statistical analysis. Statistical significance between two groups was calculated using two-tailed Student's *t* test for parametric variables and Mann-Whitney's U test for nonparametric variables. The chi-squared (df = 1) test was used for statistical comparison of frequencies. Mantel-Cox chi-squared (df = 1) test was used to analyze survival data. Differences were considered statistically significant with $p < 0.05$ (*) and highly significant at $p < 0.01$ (**) and $p < 0.005$ (***). All statistical analyses were performed using SPSS 15.0 program (IBM, Armonk, NY, USA). Skin pathology score graphic representation was performed with GraphPad Prism 6 (La Jolla, CA, USA).

References

1. Zarbock, A., Ley, K., McEver, R. P. & Hidalgo, A. Leukocyte ligands for endothelial selectins: specialized glycoconjugates that mediate rolling and signaling under flow. *Blood* **118,** 6743–6751 (2011).
2. McEver, R. P. & Zhu, C. Rolling cell adhesion. *Annu Rev Cell Dev Biol* **26,** 363–396 (2010).
3. Vestweber, D. & Blanks, J. Mechanisms that regulate the function of the selectins and their ligands. *Physiol Rev* **79,** 181–213 (1999).
4. Wagner, J. G. & Roth, R. A. Neutrophil Migration Mechanisms, with an Emphasis on the Pulmonary Vasculature. *Pharmacol Rev* **52,** 349–374 (2000).
5. Ley, K. The role of selectins in inflammation and disease. *Trends Mol Med* **9,** 263–268 (2003).
6. Zhou, C. *et al.* α1G T-type calcium channel selectively regulates P-selectin surface expression in pulmonary capillary endothelium. *Am J Physiol Lung Cell Mol Physiol* **299,** L86–L97 (2010).
7. Liu, Z. *et al.* Differential regulation of human and murine P-selectin expression and function *in vivo*. *J Exp Med* **207,** 2975–2987 (2010).
8. Sanders, W., Wilson, R., Ballantyne, C. & Beaudet, A. Molecular cloning and analysis of *in vivo* expression of murine P-selectin. *Blood* **80,** 795–800 (1992).
9. Weller, A., Isenmann, S. & Vestweber, D. Cloning of the mouse endothelial selectins. Expression of both E- and P-selectin is inducible by tumor necrosis factor alpha. *J Biol Chem* **267,** 15176–15183 (1992).
10. Hahne, M., Jäger, U., Isenmann, S., Hallmann, R. & Vestweber, D. Five tumor necrosis factor-inducible cell adhesion mechanisms on the surface of mouse endothelioma cells mediate the binding of leukocytes. *J Cell Biol* **121,** 655–664 (1993).
11. Bignon, A. *et al.* CCR1 Inhibition Ameliorates the Progression of Lupus Nephritis in NZB/W Mice. *J Immunol* **192,** 886–896 (2014).
12. Lichtnekert, J. *et al.* Activated protein C attenuates systemic lupus erythematosus and lupus nephritis in MRL-Fas(lpr) mice. *J Immunol* **187,** 3413–3421 (2011).
13. Laxminarayana, D. Molecular insights into systemic lupus erythematosus pathogenesis. *Clin Med Insights Pathol* **7,** 7–9 (2014).
14. Wu, T. *et al.* Elevated urinary VCAM-1, P-selectin, soluble TNF receptor-1, and CXC chemokine ligand 16 in multiple murine lupus strains and human lupus nephritis. *J Immunol* **179,** 7166–7175 (2007).
15. Morris, D. *et al.* Variation in the upstream region of P-Selectin (SELP) is a risk factor for SLE. *Genes Immun*, 404–413 (2009).
16. Herrmann, S. *et al.* The P-selectin gene is highly polymorphic: reduced frequency of the Pro715 allele carriers in patients with myocardial infarction. *Human Molecular Genetics* **7,** 1277–1284 (1998).
17. Xia, L. *et al.* P-selectin glycoprotein ligand-1-deficient mice have impaired leukocyte tethering to E-selectin under flow. *J Clin Invest* **109,** 939–950 (2002).

18. Rivera-Nieves, J. *et al.* Critical role of endothelial P-selectin glycoprotein ligand 1 in chronic murine ileitis. *J Exp Med* **203,** 907–917 (2006).
19. McEver, R. P., Moore, K. & Cummings, R. Leukocyte trafficking mediated by selectin-carbohydrate interactions. *J Biol Chem* **270,** 11025–11028 (1995).
20. Urzainqui, A. *et al.* Functional role of P-selectin glycoprotein ligand 1/P-selectin interaction in the generation of tolerogenic dendritic cells. *J Immunol* **179,** 7457–7465 (2007).
21. Nuñez-Andrade, N. *et al.* P-selectin glycoprotein ligand-1 modulates immune inflammatory responses in the enteric lamina propria. *J Pathol* **224,** 212–221 (2011).
22. Pérez-Frías, A. *et al.* Development of an autoimmune syndrome affecting the skin and internal organs in P-selectin glycoprotein ligand 1 leukocyte receptor-deficient mice. *Arthritis Rheumatol* **66,** 3178–3189 (2014).
23. Singbartl, K., Green, S. & Ley, K. Blocking P-selectin protects from ischemia/reperfusion-induced acute renal failure. *FASEB J* **14,** 48–54 (2000).
24. Singbartl, K. & Ley, K. Protection from ischemia-reperfusion induced severe acute renal failure by blocking E-selectin. *Crit Care Med* **28,** 2507–2514 (2000).
25. Rosenkranz, A., Mendrick, D., Cotran, R. & Mayadas, T. P-selectin deficiency exacerbates experimental glomerulonephritis: a protective role for endothelial P-selectin in inflammation. *J Clin Invest* **103,** 649–659 (1999).
26. Bullard, D. *et al.* Acceleration and increased severity of collagen-induced arthritis in P-selectin mutant mice. *J Immunol* **163,** 2844–2849 (1999).
27. Hickey, M. J. Alterations in leucocyte trafficking in lupus-prone mice: an examination of the MRL/faslpr mouse. *Immunol Cell Biol* **81,** 390–396 (2003).
28. Kinoshita, K. *et al.* Increases Survival in NZB/W F1 Mice. *J Immunol* **170,** 5793–5798 (2003).
29. He, X. *et al.* Deficiency of P-Selectin or P-Selectin Glycoprotein Ligand-1 Leads to Accelerated Development of Glomerulonephritis and Increased Expression of CC Chemokine Ligand 2 in Lupus-Prone Mice. *J Immunol* **177,** 8748–8756 (2006).
30. Christensen, S. *et al.* Toll-like receptor 7 and TLR9 dictate autoantibody specificity and have opposing inflammatory and regulatory roles in a murine model of lupus. *Immunity* **25,** 417–428 (2006).
31. Rowland, S. L. *et al.* Early, transient depletion of plasmacytoid dendritic cells ameliorates autoimmunity in a lupus model. *J Exp Med* **211,** 1977–1991 (2014).
32. Furukawa, F. & Yoshimasu, T. Animal models of spontaneous and drug-induced cutaneous lupus erythematosus. *Autoimmun Rev* **4,** 345–350 (2005).
33. Furukawa, F. *et al.* Dermatopathological studies on skin lesions of MRL mice. *Arch Dermatol Res* **276,** 186–194 (1984).
34. Guiducci, C. *et al.* Autoimmune skin inflammation is dependent on plasmacytoid dendritic cell activation by nucleic acids via TLR7 and TLR9. *J Exp Med* **207,** 2931–2942 (2010).
35. Choi, J.-Y. *et al.* Abrogation of Skin Disease in Lupus-Prone MRL/Faslpr Mice By Means of a Novel Tylophorine Analog. *Arthritis Rheumatol* **54,** 3277–3283 (2006).
36. Dreßler, J., Bachmann, L., Koch, R. & Müller, E. Enhanced expression of selectins in human skin wounds. *Int J Legal Med* **112,** 39–44 (1998).
37. Miyazaki, Y., Satoh, T., Nishioka, K. & Yokozeki, H. STAT-6-Mediated Control of P-Selectin by Substance P and Interleukin-4 in Human Dermal Endothelial Cells. *Am J Pathol* **169** (2006).
38. Furukawa, F. Photosensitivity in cutaneous lupus erythematosus: lessons from mice and men. *J Dermatol Sci* **33,** 81–89 (2003).
39. Savarese, E. *et al.* Requirement of Toll-like Receptor 7 for Pristane-Induced Production of Autoantibodies and Development of Murine Lupus Nephritis. *Arthritis Rheumatol* **58,** 1107–1115 (2008).
40. Rottman, J. & Willis, C. Mouse models of systemic lupus erythematosus reveal a complex pathogenesis. *Vet Pathol* **47,** 664–676 (2010).
41. Menon, M., Blair, P. A., Isenberg, D. A. & Mauri, C. A Regulatory Feedback between Plasmacytoid Dendritic Cells and Regulatory B Cells Is Aberrant in Systemic Lupus Erythematosus. *Immunity* **44,** 683–697 (2016).
42. Shah, K. *et al.* Dysregulated balance of Th17 and Th1 cells in systemic lupus erythematosus. *Arthritis Res Ther* **12** (2010).
43. Angiari, S. *et al.* Regulatory T cells suppress the late phase of the immune response in lymph nodes through P-selectin glycoprotein ligand-1. *J Immunol* **191,** 5489–5500 (2013).
44. Ohl, K. & Tenbrock, K. Inflammatory Cytokines in Systemic Lupus Erythematosus. *J Biomed Biotechnol* **2011** (2011).
45. Fritsch, R. D. *et al.* Abnormal Differentiation of Memory T Cells in Systemic Lupus Erythematosus. *Arthritis Rheumatol* **54,** 2184–2197 (2006).
46. Liu, J., Chen, D., Nie, G. D. & Dai, Z. CD8+ CD122+ T-cells: a newly emerging regulator with central memory cell phenotypes. *Front Immunol* **6** (2015).
47. Mak, A. & Kow, N. Y. The pathology of T cells in systemic lupus erythematosus. *J Immunol Res* (2014).
48. Hoffman, R. T cells in the pathogenesis of systemic lupus erythematosus. *Clin Immunol* **113,** 4–13 (2004).
49. Deng, G., Liu, L., Bahjat, F., Pine, P. & Tsokos, G. Suppression of skin and kidney disease by inhibition of spleen tyrosine kinase in lupus-prone mice. *Arthritis Rheumatol* **62,** 2086–2092 (2010).
50. Barbhaiya, M. & Costenbader, K. Ultraviolet radiation and systemic lupus erythematosus. *Lupus* **23,** 588–595 (2014).
51. Ghoreishi, M. & Dutz, J. P. Murine models of cutaneous involvement in lupus erythematosus. *Autoimmun Rev* **8,** 484–487 (2009).
52. Bertsias, G., Cervera, R. & Boumpas, D. T. In *EULAR 2012* (ed. EULAR 2012) (Berlin, 2012).
53. Hamidou, M. A., Audrain, M. A., Masseau, A., Agard, C. & Moreau, A. Anti-topoisomerase I antibodies in systemic lupus erythematosus as a marker of severe nephritis. *Clin Rheumatol* **25,** 542–543, doi: 10.1007/s10067-005-0061-9 (2006).
54. Holdsworth, S. & Tipping, P. Leukocytes in glomerular injury. *Semin Immunopathol* **29,** 355–374 (2007).
55. Harari, O. A., Marshall, D., McHale, J. F., Ahmed, S. & Haskard, D. O. Limited endothelial E- and P-selectin expression in MRL/lpr lupus-prone mice. *Rheumatology* **40,** 889–895 (2001).
56. Belmont, H., Buyon, J., Giorno, R. & Abramson, S. Up-regulation of endothelial cell adhesion molecules characterizes disease activity in systemic lupus erythematosus. The Shwartzman phenomenon revisited. *Arthritis & Rheumatism* **37,** 376–383 (1994).
57. Angiari, S. Selectin-mediated leukocyte trafficking during the development of autoimmune disease. *Autoimmun Rev* **14,** 984–995 (2015).
58. Segawa, C. *et al. In situ* expression and soluble form of P-selectin in human glomerulonephritis. *Kidney Int* **52,** 1054–1063 (1997).
59. Bribes, E., Galiegue, S., Bourrie, B. & Casellas, P. Involvement of the peripheral benzodiazepine receptor in the development of cutaneous pathology in Mrl/Lpr mice. *Immunol Lett* **85,** 13–18 (2003).

Acknowledgements

We thank the UAM animal facility for animal breeding and care. We also thank the Cytometry Unit and Statistical and Methodological Support Unit of the Hospital de la Princesa for technical support. We want to express our deepest gratitude to Dr Javier Fraga, Head of the Pathology Department of the Hospital de la Princesa, for providing the human tissue samples. We also wish to thank the Histopathology Unit at the CNIC for IHC assays. We thank Manuel Gómez Gutierrez and Kenneth McCreath for manuscript editing. This work was supported by Spanish Ministry of Health and ISCIII (cofinanced by Fondos FEDER) (FIS-PI11-01418, FIS-PI14-01698,

FIS-PI12-01578, Proyecto Coordinado de Excelencia PIE13-00041 and Red Cardiovascular RD12/0042/0065), by the Fundación Ramon Areces (CIVP16A1855, 2012-2015) and by Comunidad de Madrid (S2010/BMD-2359). Rafael González-Tajuelo is supported by the Proyecto Coordinado de Excelencia PIE13/00041.

Author Contributions

A.U. conceived and supervised the study. R.G.-T. and A.U. designed and interpreted the experiments presented in this manuscript and analyzed the data. R.G.-T. performed most of the experiments and wrote the manuscript. A.P.-F., J.S., M.F.-F., M.E.-S. and R.T. performed experiments. A.J. contributed to the design and performance of the photosensitivity assay. E.V., S.C., C.G. and C.M.-C. gave clinical advice. C.G. analyzed and interpreted histological samples. All the authors contributed to discuss the data and revised the manuscript.

Additional Information

Competing financial interests: The authors declare no competing financial interests.

How to cite this article: González-Tajuelo, R. *et al.* P-Selectin preserves immune tolerance in mice and is reduced in human cutaneous lupus. *Sci. Rep.* **7**, 41841; doi: 10.1038/srep41841 (2017).

Publisher's note: Springer Nature remains neutral with regard to jurisdictional claims in published maps and institutional affiliations.

ARTHRITIS & RHEUMATOLOGY
Vol. 66, No. 11, November 2014, pp 3178–3189
DOI 10.1002/art.38808

Development of an Autoimmune Syndrome Affecting the Skin and Internal Organs in P-selectin Glycoprotein Ligand 1 Leukocyte Receptor–Deficient Mice

A. Pérez-Frías, R. González-Tajuelo, N. Núñez-Andrade, R. Tejedor, M. J. García-Blanco, E. Vicente-Rabaneda, S. Castañeda, C. Gamallo, J. Silván, A. Esteban-Villafruela, L. Cubero-Rueda, C. García-García, C. Muñoz-Calleja, A. García-Diez, and A. Urzainqui

Objective. **To define and characterize the progression of the spontaneous autoimmune disease that develops in mice in the absence of the leukocyte adhesion receptor P-selectin glycoprotein ligand 1 (PSGL-1).**

Methods. **Skin-resident immune cells from PSGL-1–deficient mice and C57BL/6 control mice of different ages were isolated and analyzed by flow cytometry. Biochemical parameters were analyzed in mouse serum and urine, and the presence of serum autoantibodies was investigated. Skin and internal organs were extracted, and their structure was analyzed histologically.**

Results. **Skin-resident innate and adaptive immune cells from PSGL-1$^{-/-}$ mice had a proinflammatory phenotype with an imbalanced T effector cell:Treg cell ratio. Sera from PSGL-1$^{-/-}$ mice had circulating autoantibodies commonly detected in connective tissue–related human autoimmune diseases. Biochemical and histologic analysis of skin and internal organs revealed skin fibrosis and structural and functional abnormalities in the lungs and kidneys. Furthermore, PSGL-1$^{-/-}$ mice exhibited vascular alterations, showing loss of dermal vessels, small vessel medial layer remodeling in the lungs and kidneys, and ischemic processes in the kidney that promote renal infarcts.**

Conclusion. **Our study demonstrates that immune system overactivation due to PSGL-1 deficiency triggers an autoimmune syndrome with characteristics similar to systemic sclerosis, including skin fibrosis, vascular alterations, and systemic organ involvement. These results suggest that PSGL-1 expression contributes to the maintenance of the homeostasis of the immune system and could act as a barrier for autoimmunity in mice.**

Systemic sclerosis (SSc; scleroderma) is a rare disease that affects mainly women (3–14 females:1 male) of ~50 years of age. SSc is characterized by widespread fibrosis of the skin and internal organs, noninflammatory small vessel vasculopathy, and immunologic activation with production of disease-specific autoantibodies. These abnormalities lead to a disruption in tissue architecture and loss of functional integrity of affected internal organs. The survival expectancy for SSc patients depends on disease subtype, and the main causes of death are pulmonary arterial hypertension (PAH) and pulmonary fibrosis (1).

Several factors are implicated in SSc development, such as environmental, chemical, or genetic factors, immune system dysfunction, or infectious agents (2–4). SSc pathophysiology includes immune system and fibroblast activation and endothelial cell dysfunction, resulting in extracellular matrix protein accumulation, vascular injury, autoantibody production, and overproduction of inflammatory and profibrotic cytokines (5,6).

Supported by the Spanish Ministry of Health (grants FIS-PI080894 and FIS-PI11-01418) and the Fundación Ramón Areces (grant 2012-2015). Mr. González-Tajuelo's work was supported by a grant from the Fundación Ramón Areces.

A. Pérez-Frías, BSc, R. González-Tajuelo, BSc, N. Núñez-Andrade, BSc, R. Tejedor, M. J. García-Blanco, MD, E. Vicente-Rabaneda, MD, PhD, S. Castañeda, MD, PhD, C. Gamallo, MD, PhD, J. Silván, BSc, A. Esteban-Villafruela, BSc, L. Cubero-Rueda, BSc, C. García-García, MD, C. Muñoz-Calleja, MD, PhD, A. García-Diez, MD, PhD, A. Urzainqui, PhD: Fundación de Investigación Biomédica, Instituto de Investigación Sanitaria-Princesa, and Hospital de la Princesa, Madrid, Spain.

Ms Pérez-Frías and Mr. González-Tajuelo contributed equally to this work.

Address correspondence to A. Urzainqui, PhD, Fundación de Investigación Biomédica, Instituto de Investigación Sanitaria-Princesa, Hospital de la Princesa, Diego de León 62, 28006 Madrid, Spain. E-mail: ana.urzainqui@salud.madrid.org.

Submitted for publication January 28, 2014; accepted in revised form July 29, 2014.

Fibroblasts activated by proinflammatory factors are the principal effector cells, while activated innate immune system, matrix-mediated signaling, hypoxia, and oxidative stress are the main perpetuating factors of fibrosis (7). Though diagnosis of SSc is straightforward once the disease is established, it is difficult to make an early diagnosis, which is crucial for the application of early treatments to prevent tissue damage and loss of organ function. Immunosuppressive therapies can control the disease and minimize organ damage in the short term, but disease remission has not been achieved with any therapy available thus far (8). Some patients with severe disease have experienced improvement with autologous bone marrow (BM) transplantation (9,10), suggesting a role of the immune system in disease initiation. However, very little is known about the immune mechanisms involved in the onset of SSc.

The leukocyte adhesion receptor P-selectin glycoprotein ligand 1 (PSGL-1) interacts with P-, E- and L-selectins (11) and is responsible for the initial interactions of leukocytes with activated endothelium (12) and their recruitment to sites of inflammation (13). PSGL-1 is also important for the homeostatic homing and entry of leukocytes into different tissues and organs (14–17). PSGL-1 expression is regulated by the metalloproteinase ADAM-8 (18), and PSGL-1–P-selectin interactions can be modulated by PSGL-1 modification with epitopes such as M-DC8 (19,20), indicating the importance of PSGL-1–P-selectin interaction in immune system homeostasis.

PSGL-1 signaling through Syk induces human monocyte-derived dendritic cells (DCs) to become tolerogenic and promotes the generation of Treg cells. Accordingly, PSGL-$1^{-/-}$ mice produce less CD4+ natural Treg cells in the thymus and PSGL-$1^{-/-}$ mouse DCs are more immunogenic than PSGL-$1^{+/+}$ mouse DCs (21–23). Deficiency in P-selectin or PSGL-1 leads to accelerated development of glomerulonephritis in lupus-prone mice and exacerbated disease in several animal models, for example, bleomycin-induced scleroderma, Dextran sulfate sodium–induced ulcerative colitis, and experimental autoimmune encephalomyelitis (24–27). Moreover, DCs isolated from systemic lupus erythematosus patients are unable to generate Treg cells after P-selectin interaction (28), and SSc patients show high serum levels of selectins (29,30), suggesting a connection between PSGL-1 and these autoimmune diseases. Taken together, these data suggest that homeostatic PSGL-1–selectin interactions during leukocyte recirculation and tissue replenishment are important for the control of autoimmune reactivity and maintain immune tolerance.

Several animal models have been developed to study the signaling pathways involved in fibrosis development and to identify new therapeutic target molecules. However, none of them completely mimics the human disease (31,32). Our work shows that PSGL-$1^{-/-}$ mice present increased basal activation of the immune system and spontaneously develop an autoimmune disease similar to SSc, featuring autoantibodies, skin fibrosis, vascular alterations, kidney disease, nonspecific interstitial pneumonia, and a high mortality rate, establishing the possibility that PSGL-1 could be an important molecule in the pathogenesis of this disease.

MATERIALS AND METHODS

Mice. C57BL/6 PSGL-$1^{-/-}$ mice were kindly provided by Dr. M. K. Wild and Dr. D. Vestweber (Max Planck Institute for Molecular Biomedicine, Münster, Germany). Wild-type (WT) C57BL/6 mice were obtained from The Jackson Laboratory and were backcrossed with PSGL-$1^{-/-}$ mice. Mice were kept in pathogen-free conditions at the Animal Facility of the School of Medicine, Universidad Autónoma de Madrid (UAM; Madrid, Spain) and the Animal Facility of the Centro Nacional de Investigaciones Cardiovasculares (CNIC; Madrid, Spain). Mice were killed by cervical dislocation at 1.5 months old (young), 3, 6, and 9 months old (adult), and 12, 15, 18, and $>$20 months old (old), and blood and internal organs were extracted for analysis. All experiments and breeding were performed in accordance with national and institutional guidelines for animal care. The experimental procedures were approved by the Veterinarian Committee of the UAM (register number ES-28079-0000097).

Autoantibody assays. Antinuclear antibodies (ANAs) were detected by indirect immunofluorescence. Serum from WT and PSGL-$1^{-/-}$ mice was incubated for 30 minutes with HEp-2 cells for ANA screening and *Crithidia luciliae* for anti–double-stranded DNA (anti-dsDNA) antibody screening, and fixed on slides (Inova Diagnostics). Sera were diluted 1:20 for HEp-2 incubation and 1:10 for *Crithidia luciliae* incubation. Slides were incubated for 30 minutes with goat anti-mouse Alexa Fluor 488 (1:100) (Invitrogen). Circulating autoantibodies were measured by enzyme-linked immunosorbent assay (ELISA) with the specific Quanta Lite kits for SSA, U1 RNP, Sm, Jo-1, and Scl-70 antigens (Inova Diagnostics). Horseradish peroxidase–conjugated goat anti-mouse IgG (H+L) antibody from Pierce Antibodies (Thermo Scientific) diluted 1:2,500 was used as secondary antibody. The cutoff for positivity on ELISA for a particular autoantibody was determined as the mean value plus 2 SD obtained from the sera of at least 100 WT mice ages 1.5–24 months. At least 25 mice per age group were analyzed.

Histologic staining. Organs and tissues were embedded in paraffin and sliced into 4-μm sections. Hematoxylin and eosin (H&E) staining was performed with Harris' hematoxylin (Merck) and Eosin Y (alcoholic solution; Leica Biosystems). Masson's trichrome staining was performed with Artisan Gomori's Green Trichrome Stain kit (Dako). Picrosirius red staining was performed in the Pathology Unit at the CNIC. All

images were obtained with a Leica DM2500 light microscope and a Leica DFC450 camera. All sections were examined by a pathologist (CG) who was blinded with regard to the sample origin.

Collagen quantification. Sircol assay was carried out to measure tissue collagen concentration using the Sircol kit (Biocolor).

Histopathologic assessment of dermal fibrosis in mice. All mouse skin sections were obtained from the para-midline, upper back region to minimize regional variations in thickness. Dermal thickness, analyzed using ImageJ software (National Institutes of Health [NIH]), was defined as the thickness of the skin from the granular layer to the junction between the dermis and the subcutaneous fat (hypodermis). The thickest and the thinnest sections of at least 3 different skin areas were measured per mouse. At least 5 males and 5 females of each genotype and age were analyzed.

Histopathologic assessment of renal damage in mice. Mice were assessed for the presence of tubular interstitial infiltrates in whole H&E-stained kidney sections, and for the presence of ischemic events (infarcted areas) in whole H&E- and Masson's trichrome–stained kidney sections. At least 5 males and 5 females were evaluated per genotype.

Histopathologic assessment of pulmonary damage in mice. Whole H&E-stained mouse lung sections were evaluated for nonspecific interstitial pneumonia. Interstitial cellularity, thickening of the alveolar walls, and structure alteration of the lung parenchyma were considered to be features of nonspecific interstitial pneumonia.

Immunohistochemical staining of mouse skin, kidney, and lung and evaluation of vascular alteration. Immunohistochemical staining was performed in the Pathology Unit at the CNIC with an Autostainer Plus Staining System (Dako). Skin vascular damage was evaluated by staining skin sections (from 4 males and 4 females per genotype) with a polyclonal rabbit anti-mouse CD31 antibody (Abcam). The total number of dermal blood vessels in a total of 10 consecutive 40×-objective fields (total length of section 1,727 μm) was counted for each mouse. The mean value was calculated for each group of mice. All CD31-stained structures with an internal lumen, without diameter restrictions, were considered blood vessels.

Lung interstitial leukocyte infiltration was evaluated by immunohistochemical staining with a rat anti-mouse CD45 antibody (Becton Dickinson). Lung sections were evaluated in 18–24-month-old mice (5 males and 5 females per genotype).

The small blood vessel (diameter of <50 μm in the lungs and <20 μm in the kidneys) wall thickness was calculated by measuring, with ImageJ (NIH), the internal and total vessel diameter of anti–α-smooth muscle actin (anti–α-SMA)–stained kidneys and lungs, and calculating the vessel wall area. The mean wall thickness area was calculated for at least 4 males and 4 females of each genotype.

Urine and serum biochemical analyses. Urinary protein and hemoglobin measurements were determined with Combur Test M dipsticks (Roche). The cutoff for positivity in the proteinuria test was the lowest value in knockout (KO) mice not reached in any of the WT mice analyzed. Serum levels of urea, creatinine, and albumin were measured on a Dimension RxL Max analyzer (Siemens).

Flow cytometric analysis. Rat anti-mouse CD3, CD4, CD8, CD25, CD11c, F4/80, B220, CD49b, interleukin-12 (IL-12), IL-10, IL-4, IL-17, interferon-γ (IFNγ), Gr1, CD62L, CD69, major histocompatibility complex (MHC) class II, CD86, and CD40 directly labeled with a fluorochrome or biotin and streptavidin–PerCP were obtained from Becton Dickinson. The mouse Th1/Th2 10-plex FlowCytomix kit was purchased from eBioscience.

Tissue sections (1 mm^2) were incubated in RPMI medium supplemented with 4% fetal calf serum (FCS), 1 mg/ml collagenase IA, 50 μg/ml Dispase, and 40 μg/ml DNAse (all enzymes from Sigma-Aldrich) in a shaking bath at 37°C and 100 rpm for at least 1 hour. Cells were then filtered, washed, immunostained, and analyzed with a FACSCanto II flow cytometer. Tissue proteins were extracted with T-PER tissue protein extraction buffer (Thermo Scientific) and quantified with the BCA Protein Assay Kit (Pierce). Tissue cytokines were detected with the FlowCytomix kit (Bender MedSystems).

Macrophage generation from mouse BM precursors. Fresh mouse BM cells were flushed from the tibia and cultured in petri dishes (BD Biosciences) with differentiation medium containing RPMI 1640 (Invitrogen) supplemented with 10% FCS (HyClone), 100 units/ml penicillin, 100 μg/ml streptomycin, 2 m*M* L-glutamine and 15% L929-conditioned medium (containing macrophage colony-stimulating factor). Fresh differentiation medium was added every 3 days. Macrophages were phenotyped on days 8–10. Efficiency of differentiation was assessed by measuring the expression of F4/80 surface antigen by flow cytometry.

Statistical analysis. Student's 2-tailed *t*-test for 2 groups was used for parametric variables, and the Mann-Whitney U test was used for nonparametric data. For statistical comparison of frequencies, the chi-square test (1df) was performed. For the survival assay, the Mantel-Cox chi-square test (1df) was performed. *P* values less than 0.05 were considered significant, and *P* values less than 0.01 were considered highly significant. All statistical analyses were performed using SPSS software version 15.0.

RESULTS

Development of skin fibrosis in PSGL-1$^{-/-}$ mice. We observed a high rate of spontaneous skin lesions on the backs of adult PSGL-1$^{-/-}$ mice. Such lesions were absent in WT mice. Raising the hair on the backs of the 3-month-old PSGL-1$^{-/-}$ mice, we detected red skin zones with circumscribed nonspecific small and sterile superficial ulcers that were diffuse and more severe in older mice (Figure 1A). Histologic analysis of lesions from 3-month-old mice demonstrated small superficial ulcers with epidermal necrosis and cell debris and a minimal inflammatory infiltrate in the underlying dermis. In contrast, lesions from older mice presented large ulcers with epidermal necrosis and cell debris, and horizontally positioned fibroblasts and marked fibrosis in the underlying dermis (Figure 1A).

Histologic analysis of the skin revealed dermal thickening with lipoatrophy in both male and female KO

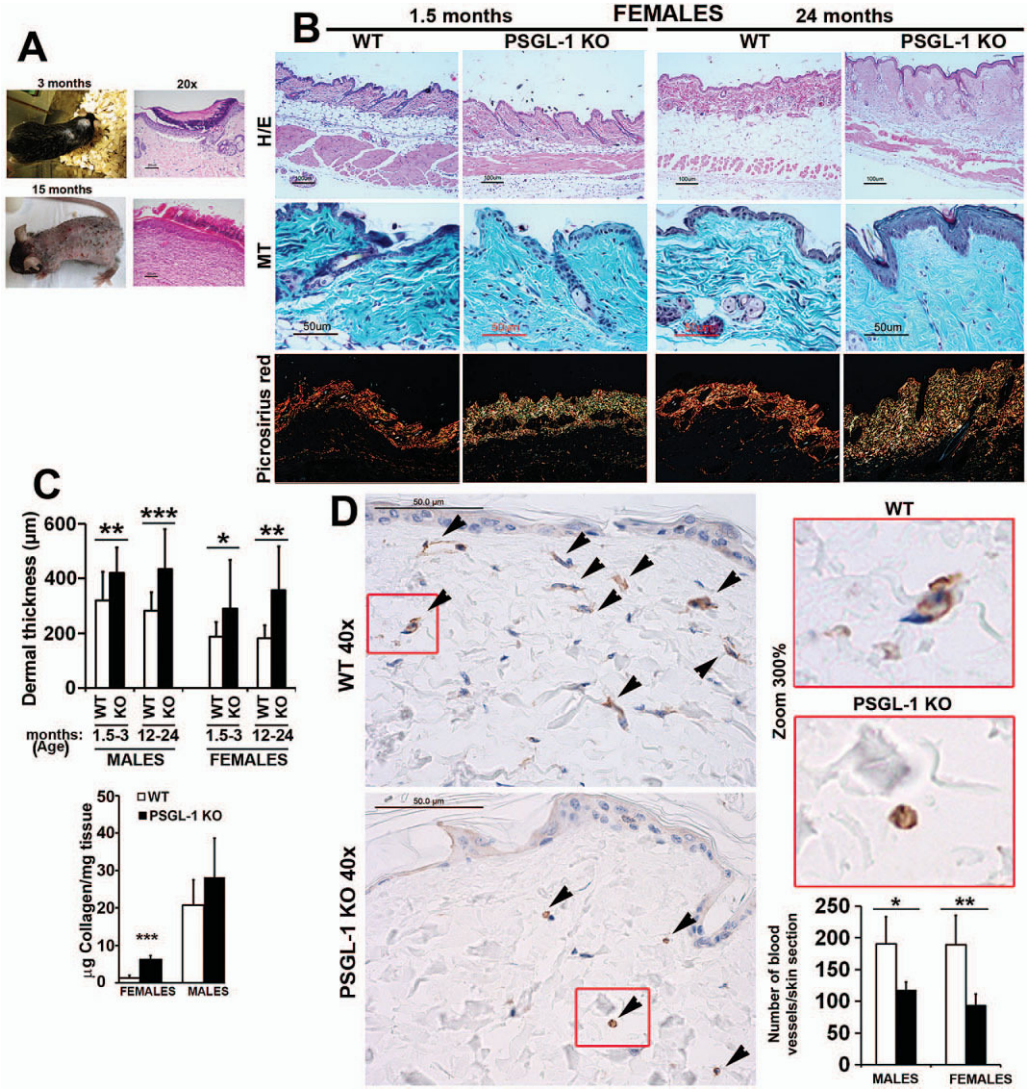

Figure 1. Development of skin fibrosis, lipoatrophy, and peripheral vascular alterations in P-selectin glycoprotein ligand 1–knockout (PSGL-1–KO) mice. **A,** Left, Photographs of a 3-month-old PSGL-1–KO mouse and a 15-month-old PSGL-1–KO mouse, showing skin lesions. Right, Photomicrographs of hematoxylin and eosin (H&E)–stained sections of representative skin wounds from young and old mice. **B,** Photomicrographs of representative skin sections from 1.5-month-old and 24-month-old female wild-type (WT) and PSGL-1–KO mice, stained with H&E, Masson's trichrome (MT), and picrosirius red. Original magnification × 10 in top panels; × 40 in middle panels; × 5 in bottom panels. **C,** Top, Dermal thickness in 1.5–3-month-old and 12–24-month-old male and female WT and PSGL-1–KO mice (n = 8 mice per group). Bottom, Collagen content in the dermis of 1.5–3-month-old WT and PSGL-1–KO mice (n = 4 mice per group). **D,** Photomicrographs of representative upper dermis sections from WT and PSGL-1–KO mice immunostained with anti-CD31 antibody. Boxed areas in the left panels are shown at a higher-magnification view in the right panels to better visualize the vessel architecture. **Arrowheads** indicate blood vessels. The bar graph shows the number of CD31+ blood vessels in a 1,727-μm long dermis section from male and female WT mice (open bars) and PSGL-1–KO mice (solid bars) (n = 4 mice per group). In **C** and **D,** bars represent the mean ± SD. $* = P < 0.05$; $** = P < 0.01$; $*** = P < 0.005$, by Student's 2-tailed t-test.

mice, which was due to increased collagen deposition (fibrosis), as indicated by Masson's trichrome staining (Figure 1B) and a higher collagen content (Figure 1C). Measurement of dermal thickness revealed enhanced thickness in PSGL-$1^{-/-}$ mice compared with WT mice, and this difference was accentuated in 12–24-month-old mice (Figure 1C). Moreover, picrosirius red staining indicated that PSGL-$1^{-/-}$ mice had increased amounts of type III collagen–like fibers (thinner collagen fibers shown in yellow and green in Figure 1B), including type

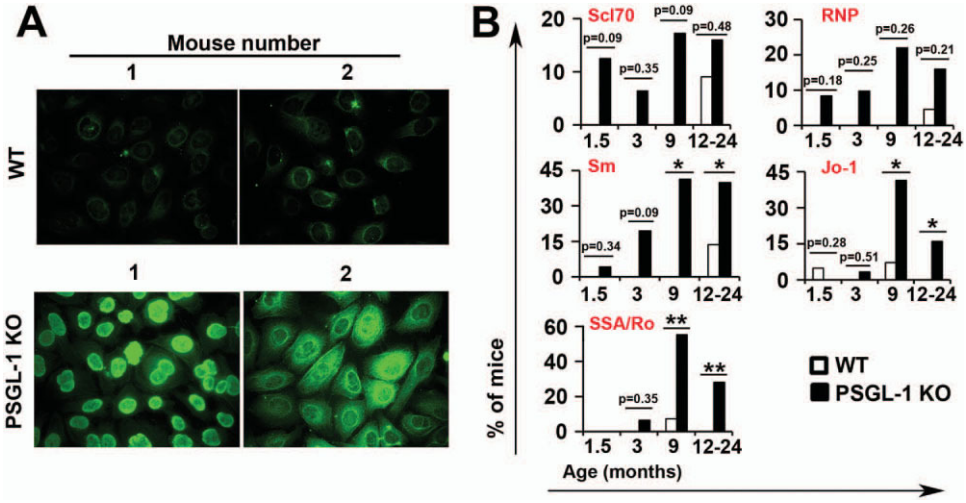

Figure 2. Spontaneous generation of autoantibodies related to connective tissue autoimmune diseases in P-selectin glycoprotein ligand 1–knockout (PSGL-1–KO) mice. **A,** Representative immunofluorescence photomicrographs of HEp-2 cells incubated with serum from 2 independent wild-type (WT) mice and 2 independent PSGL-1–KO mice. **B,** Percentage of mice positive for Scl-70, U1 RNP, Sm, Jo-1, and SSA/Ro autoantibodies (n = 25 or more mice per age group). $* = P < 0.05$; $** = P < 0.01$. *P* values were determined by chi-square test.

III collagen and newly formed type I fibers, than type I collagen–like fibers (thicker collagen shown in fibers in orange and red in Figure 1B). Additionally, CD31 staining showed that the number of blood vessels in the dermis of PSGL-$1^{-/-}$ mice was significantly lower than in WT mice, particularly in the upper dermis (Figure 1D).

Generation of autoantibodies associated with connective tissue autoimmune diseases in PSGL-$1^{-/-}$ mice. Immunofluorescence analysis of sera revealed antinuclear and anticytoplasmic autoantibodies in PSGL-$1^{-/-}$ mice that were absent in WT mice (Figure 2A), whereas anticentromere and anti-dsDNA autoantibodies (*Crithidia luciliae* assay) were not detected in either group. ELISAs indicated that the sera from PSGL-$1^{-/-}$ mice recognized several autoantigens related to connective tissue diseases, including topoisomerase I, U1 RNP, Sm, tRNA synthetase (Jo-1), and SSA/Ro (Figure 2B). By studying different groups of mice at different ages, we found that these autoantibodies were coexpressed in the same animals and that their levels increased with the age of the animal. Indeed, anti–topoisomerase I, anti–U1 RNP, and anti-Sm antibodies were detected in the youngest animals, and antitopoisomerase was the most prevalent antibody detected in 1.5-month-old mice (12.5%). In a followup study using 15 mice, we performed ELISAs at 1.5 months and again at 3 months. We found that the 1.5-month-old mice that were positive for antitopoisomerase antibodies died before reaching 3 months of age. Consequently, the number of mice with anti–topoisomerase I antibodies decreased in the 3-month-old group, increasing again to 15% in the elderly population (Figure 2B).

Kidney disease in PSGL-$1^{-/-}$ mice. Histologic analysis of H&E-stained kidney sections revealed that 12–24-month-old PSGL-$1^{-/-}$ mice had perivascular infiltrates (Figure 3A). Quantification of these infiltrates showed that at 1.5–3 months of age, only female PSGL-$1^{-/-}$ mice had interstitial infiltrates (30%), but at 12–24 months, 80% of both male and female KO mice had developed infiltrates (Figure 3A). Closer inspection of the histologic features (Figure 3A) revealed glomerular damage as sclerotic glomeruli and tubularization of Bowman's capsule in PSGL-$1^{-/-}$ mice. Additionally, Masson's trichrome staining of kidney sections revealed the presence of infarcted areas in KO mice (Figure 3B), indicating ischemic events. Quantification showed that almost 50% of male and 28% of female PSGL-$1^{-/-}$ mice ages 18 months and older had kidney infarcts, while in the WT group only 10% of the older males showed infarcts (Figure 3B). Notably, α-SMA staining revealed a thickening of the kidney small vessel medial layer in KO mice (Figure 3C), which was calculated to be 10% thicker in both young and old mice, indicating sustained kidney vascular alteration (Figure 3C).

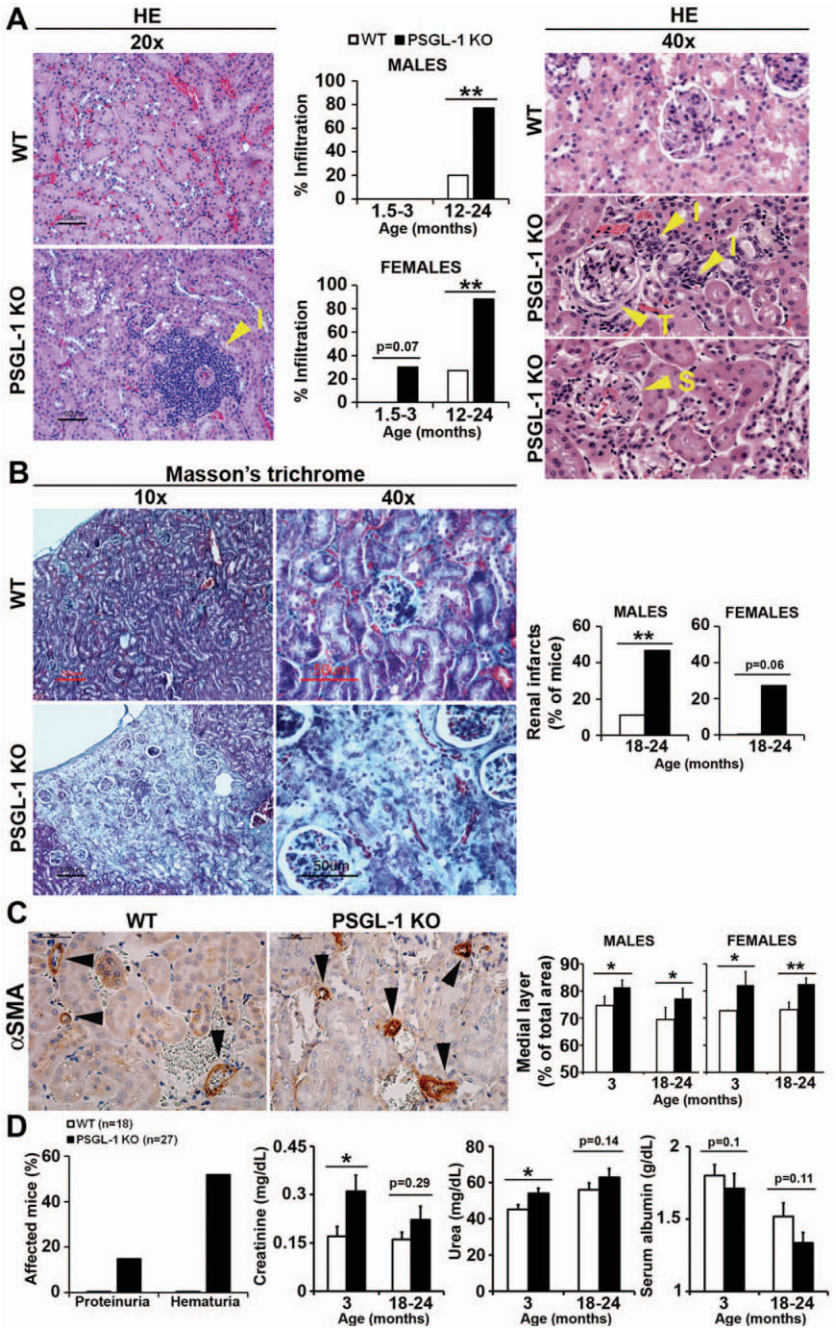

Figure 3. Renal dysfunction in PSGL-1–KO mice. **A,** Left, Interstitial infiltration (**I**) in H&E–stained kidney sections from 23-month-old WT and PSGL-1–KO mice. Middle, Frequency of interstitial immune infiltrates among WT and PSGL-1–KO mice (n = 7–17 mice per group). Right, Glomeruli in kidney sections from 23-month-old WT and PSGL-1–KO mice, showing tubularized (**T**) and sclerotic (**S**) glomeruli. **B,** Left, Masson's trichrome–stained kidney sections from 23-month-old WT and PSGL-1–KO mice, showing healthy and infarcted tissue. Right, Frequency of renal infarcts in 18–24-month-old WT mice (open bars) and PSGL-1–KO mice (solid bars) (n = 11 or more mice per group). **C,** Left, Anti–α-smooth muscle actin (anti–α-SMA)–stained kidney sections from 3-month-old WT and PSGL-1–KO mice. **Arrowheads** denote stained vessels. Original magnification × 40. Right, Percentage of blood vessel wall area in blood vessels of <20 μm in diameter in 3-month-old and 18–24-month-old WT mice (open bars) and PSGL-1–KO mice (solid bars). Bars show the mean ± SD (n = 4 mice per group). **D,** Frequency of proteinuria and hematuria in 18–24-month-old WT and PSGL-1–KO mice, and creatinine, urea, and albumin levels in the serum of WT and PSGL-1–KO mice. Bars in the middle panels and the right panel show the mean ± SEM (n = 8–12 mice per group). * = $P < 0.05$; ** = $P < 0.01$, by chi-square test in **A** and **B** and by Student's 2-tailed *t*-test in **C** and **D**. See Figure 1 for other definitions.

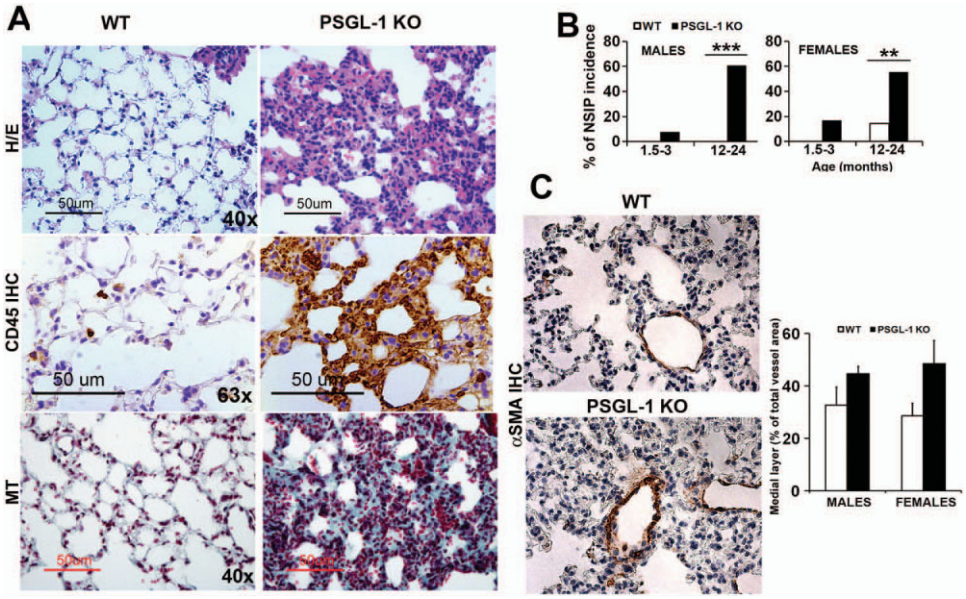

Figure 4. Nonspecific interstitial pneumonia (NSIP) and lung small vessel remodeling in PSGL-1–KO mice. **A,** Representative photomicrographs of H&E-stained, anti-CD45–stained, and Masson's trichrome–stained lung sections from WT and PSGL-1–KO mice. **B,** Incidence of nonspecific interstitial pneumonia in WT and PSGL-1–KO mice (n = 9 mice per group). ** = $P < 0.01$; *** = $P < 0.005$, by chi-square test. **C**, Left, Representative photomicrographs of anti–α-smooth muscle actin (anti–α-SMA)–stained lung sections from 3-month-old WT and PSGL-1–KO mice. Right, Vessel wall area with respect to the total vessel area in vessels of <50 μm in diameter in the lungs of 3-month-old WT and PSGL-1–KO mice. Bars show the mean ± SD. Statistical significance was determined by Student's 2-tailed *t*-test. IHC = immunohistochemistry (see Figure 1 for other definitions).

An evaluation of biochemical parameters in urine and serum revealed proteinuria in 15% of the 18–24-month-old PSGL-$1^{-/-}$ mice and hematuria in 50% of the 18–24-month-old PSGL-$1^{-/-}$ mice (Figure 3D). In addition, serum analysis showed higher levels of creatinine and urea and a tendency toward lower levels of albumin in the sera of 3-month-old PSGL-$1^{-/-}$ mice compared with WT mice. Taken together, these data indicate renal dysfunction in PSGL-$1^{-/-}$ mice at 18 months of age and older.

Promotion of nonspecific interstitial pneumonia by PSGL-1 deficiency. Histologic analysis of lung sections showed that, in comparison with WT mice, old PSGL-$1^{-/-}$ mice had increased interstitial cellularity and thickening of the interstitial space (Figure 4A). Immunohistochemical staining for CD45 identified the interstitial cells as infiltrating leukocytes (Figure 4A), and Masson's trichrome staining revealed a substantial increase in the thickness of the interalveolar septa (Figure 4A). Quantification of nonspecific interstitial pneumonia lesions in mice showed that at 1.5–3 months 7.8% of male and 16.7% of female PSGL-$1^{-/-}$ mice, but no WT mice, had nonspecific interstitial pneumonia. At

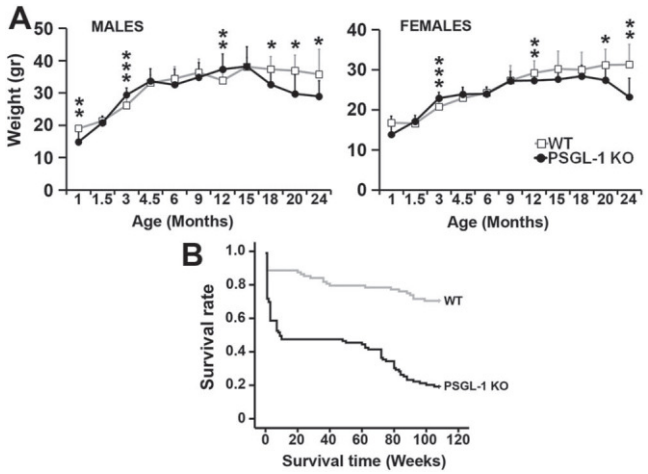

Figure 5. Body weight analysis and mortality in P-selectin glycoprotein ligand 1–knockout (PSGL-1–KO) mice. **A,** Changes in body weight in male and female wild-type (WT) and PSGL-1–KO mice. Values are the mean ± SD (n = 6 or more animals per age and genotype group). * = $P < 0.05$; ** = $P < 0.01$; *** = $P < 0.005$, by Student's 2-tailed *t*-test. **B,** Kaplan-Meier survival curves for WT and PSGL-1–KO mice (n = 87 WT and 99 PSGL-1–KO mice). $P = 5.2466 \times 10^{-13}$ by Mantel-Cox test.

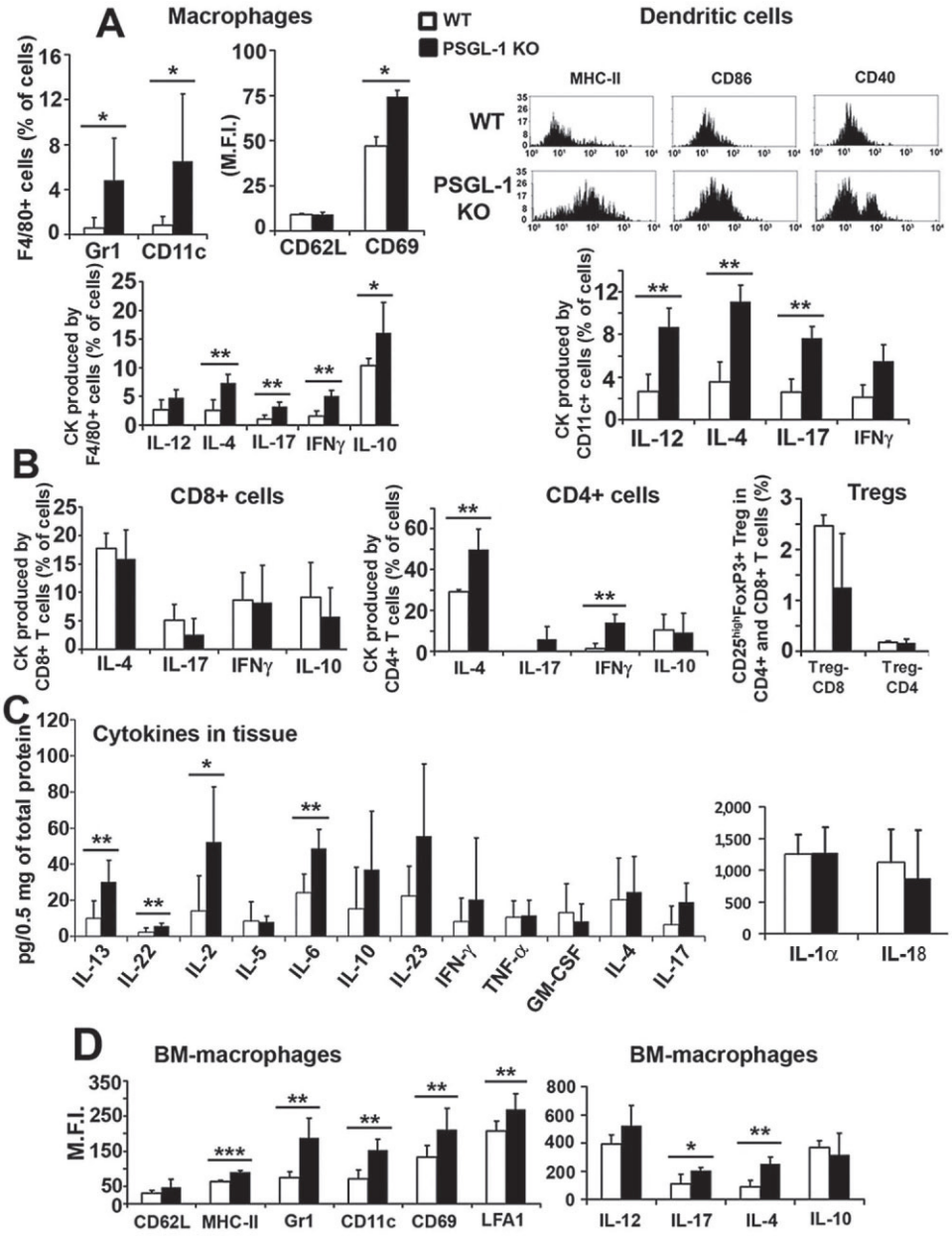

Figure 6. Skin-resident immune system activation in P-selectin glycoprotein ligand 1–knockout (PSGL-1–KO) mice. **A,** Left, Percentage of Gr1+ and CD11c+ cells, mean fluorescence intensity (MFI) of CD62L and CD69 molecules (top), and intracellular cytokine (CK) staining (bottom) in the F4/80+ subpopulation in the skin of wild-type (WT) and PSGL-1–KO mice. Right, Histograms showing expression levels of major histocompatibility complex (MHC) class II, CD86, and CD40 on dendritic cells (DCs) obtained from the skin of a representative WT mouse and a representative PSGL-1–KO mouse (of 4 examined per group) (top) and MFI of intracellular cytokine staining of CD11c+ DCs from WT and PSGL-1–KO mice (bottom). **B,** Left and middle, Percentage of CD8+ (left) and CD4+ (middle) T cells expressing interleukin-4 (IL-4; Th2), IL-17 (Th17), interferon-γ (IFNγ; Th1), and IL-10. Right, Percentage of Treg cells ($CD25^{high}FoxP3+$) in the CD4+ and CD8+ subpopulations. **C,** Cytokine concentration in 0.5 mg of skin tissue protein. **D,** Surface expression of molecular markers (left) and intracellular cytokine expression (right) on macrophages derived from precursors isolated from the bone marrow (BM) of WT and PSGL-1 KO mice. Bars show the mean ± SD (n = 4 mice per group in **A, B,** and **D**; n = 6 mice per group in **C**). ∗ = $P < 0.05$; ∗∗ = $P < 0.01$; ∗∗∗ = $P < 0.005$, by Student's 2-tailed *t*-test. TNFα = tumor necrosis factor α; GM-CSF = granulocyte–macrophage colony-stimulating factor; LFA-1 = lymphocyte function–associated antigen 1.

12–24 months of age, nonspecific interstitial pneumonia was found in 64.7% of male and 53.8% of female PSGL-$1^{-/-}$ mice, but only in 14.3% of female WT mice (Figure 4B). In addition, we found that lung small vessels had a thickened medial layer, as denoted by α-SMA staining (Figure 4C), which was almost 50% thicker in PSGL-$1^{-/-}$ mice than in WT mice.

Increased mortality rate in PSGL-$1^{-/-}$ mice. Analysis of body weights over a 24-month period showed that during the first year of life, male and female WT and PSGL-$1^{-/-}$ mice gradually increased their body weight. However, during the second year of life, while WT mice continued to gain weight, male PSGL-$1^{-/-}$ mice started to lose weight at 15 months of age (Figure 5A) and female PSGL-$1^{-/-}$ mice stopped gaining weight at 12 months and began losing weight at ~18 months (Figure 5A). At 2 years of age, PSGL-$1^{-/-}$ mice had lost 20% of their body mass, a sign of cachexia and premature death.

A survival study showed that, whereas WT mice had a low rate of mortality during the first 2 years of life, PSGL-$1^{-/-}$ mice had 2 significant peaks of mortality. The first peak occurred between birth and 3 months of age, during which time 50% of newborns died, although neonates did not present with kidney or lung structural or developmental problems (data not shown). The second peak occurred during the second year of life, with 30% of deaths occurring before mice reached 2 years of age. As a consequence, while 70% of the WT mice reached 2 years of age, only 20% of the PSGL-$1^{-/-}$ mice reached this age (Figure 5B).

Altered skin immunity in PSGL-$1^{-/-}$ mice. Since PSGL-1 is a leukocyte receptor, we assessed whether it plays a role in maintaining skin immune tolerance. Thus, we studied the phenotype of different innate and adaptive skin-resident immune cell populations. We found that most PSGL-$1^{-/-}$ mouse skin macrophages were proinflammatory (Gr1+, CD11c+), with higher expression levels of CD69, indicating an increased activation state (Figure 6A). Similarly, PSGL-$1^{-/-}$ mouse skin DCs expressed higher levels of MHC class II, CD86, and CD40 (Figure 6A), revealing a more activated state than corresponding WT mouse DCs. The percentage of skin macrophages and DCs producing proinflammatory cytokines was also significantly higher in PSGL-$1^{-/-}$ mice (Figure 6A). Examination of skin T effector (Teff) cells revealed above-normal numbers of CD4+ Teff cells producing IL-4, IL-17, and IFNγ in PSGL-$1^{-/-}$ mice. In contrast, numbers of IL-10–producing T lymphocytes and Treg cells were normal, indicating an imbalanced Teff cell:Treg cell ratio in the skin of PSGL-$1^{-/-}$ mice (Figure 6B). Accordingly, we found elevated levels of IL-2, IL-6, IL-13, and IL-22 in the pool of tissue proteins, and a tendency toward increased levels of IL-10, IL-17, and IL-23 (Figure 6C), confirming a proinflammatory and profibrotic microenvironment in the skin of PSGL-$1^{-/-}$ mice.

Proinflammatory phenotype of PSGL-$1^{-/-}$ mouse BM-derived macrophages (BMMs). To investigate whether PSGL-$1^{-/-}$ mouse skin–resident macrophages become proinflammatory and activated once they enter the tissue, or if they are generated in the BM with this phenotype, we obtained macrophages in vitro from WT and PSGL-$1^{-/-}$ mouse BM precursors and analyzed markers of inflammation. PSGL-$1^{-/-}$ mouse BMMs had a proinflammatory phenotype ($Gr1^{high}CD11c^{high}$) and higher expression of CD69 and MHC class II (Figure 6D). Further, cytokine profiling showed that PSGL-$1^{-/-}$ mouse BMMs produced higher levels of IL-17, IL-4, and IL-12 than corresponding macrophages derived from WT mouse BM precursors (Figure 6D), indicating that they are generated with a proinflammatory and more activated phenotype.

DISCUSSION

We have demonstrated that PSGL-1 deficiency in mice results in the development of a progressive autoimmune syndrome characterized by skin fibrosis with involvement of several internal organs and microvasculature alterations. These pathologic events are similar to SSc, but there are important differences compared to the human disease, including the nonspecific skin ulcers, the wide range of autoantibodies, and the kidney pathology found in the PSGL-$1^{-/-}$ mice. Clearly, these differences could be due to different organ structures—and thus to different expression of autoimmune diseases—in mice and humans, but they could also be due to the complete absence of PSGL-1 in KO mice. PSGL-1 is a crucial molecule for skin homing of leukocytes and we show that it also contributes to skin homeostasis. Hence, it is perhaps not surprising that the skin is the first organ to be highly affected in PSGL-$1^{-/-}$ mice.

SSc is a progressive autoimmune disease characterized by fibrosis and vasculopathy. While fibroblasts, endothelial cells, and the immune system have been implicated in the development of SSc, the initial trigger remains unknown (7). All risk genes related to SSc susceptibility are immune-related genes. Several studies have demonstrated that the innate and adaptive immune systems may participate in SSc pathogenesis, and weak perivascular infiltrates appear in the skin in early SSc,

pointing to a role for the immune system in the initiation of fibrosis (5,33,34). Moreover, increased numbers of circulating Th1, Th17, and transforming growth factor β–producing CD4+ T cells can be used to distinguish different SSc subtypes, and the affected skin in SSc patients has altered immune cell populations (35–37).

Our findings suggest that PSGL-1 is essential for maintaining skin immune homeostasis in mice. PSGL-$1^{-/-}$ mouse skin has increased levels of IL-6, IL-13, and IL-22 and a tendency toward increased levels of IL-10, IFNγ, and IL-17, as expected for a sclerotic skin disorder; further, PSGL-$1^{-/-}$ mouse skin has increased Th1, Th2, and Th17 populations, which could explain the exacerbation of disease developed by PSGL-$1^{-/-}$ mice after treatment with bleomycin (27). Interestingly, during the acute inflammation phase induced by bleomycin, Th1 recruitment to the skin was impaired in PSGL-$1^{-/-}$ mice. However, in the progressive scleroderma-like disease developed by PSGL-$1^{-/-}$ mice, the Th1 population is also increased in the skin of 3-month-old animals. The percentage of skin macrophages and DCs with an activated proinflammatory phenotype is increased in PSGL-$1^{-/-}$ mice, contributing to the tissue proinflammatory microenvironment. Importantly, PSGL-$1^{-/-}$ mouse BMMs display a proinflammatory phenotype and a higher activated state compared with PSGL-$1^{+/+}$ mouse BMMs, as described for PSGL-$1^{-/-}$ mouse DCs (22). These findings suggest that PSGL-$1^{-/-}$ mouse macrophages and DCs arrive activated to the skin and contribute to the generation of a proinflammatory environment leading to skin fibroblast activation and increased collagen deposition.

It has previously been demonstrated that the generation of natural Treg cells, responsible for the control of self tolerance (38), was reduced in PSGL-$1^{-/-}$ mice (22). We found an imbalanced Teff cell:Treg cell ($CD25^{high}$FoxP3+) ratio in the skin of PSGL-$1^{-/-}$ mice. This imbalance is involved in the development of autoimmune diseases (39,40) and could explain the generation of chronic inflammation and autoimmunity in PSGL-$1^{-/-}$ mice, thus suggesting a role for PSGL-1 in the control of the immunity–autoimmunity barrier. Autoimmune disorders are characterized by the generation of numerous autoantibodies. The most prevalent autoantibody in 1.5-month-old PSGL-$1^{-/-}$ mice was anti–topoisomerase I, which has been shown to be almost exclusively associated with diffuse cutaneous SSc (41), while 24-month-old mice had a complex pattern of coexisting autoantibodies related to other connective tissue diseases. However, none of the animals had detectable levels of anticentromere antibodies, which characterize limited cutaneous SSc (42), or anti-dsDNA antibody, the serologic marker of SLE (43,44). In humans, anti–topoisomerase I antibodies are associated with diffuse skin involvement, pulmonary fibrosis, poor prognosis, and SSc-related mortality (41). Accordingly, we found that 1.5-month-old PSGL-$1^{-/-}$ mice positive for antitopoisomerase autoantibodies died before reaching 3 months of age.

Renal dysfunction in SSc patients is characterized by the onset of malignant hypertension that progresses to renal failure (45), with arterial thrombosis associated with glomerular ischemic collapse. Aged PSGL-$1^{-/-}$ mice develop ischemic events that promote kidney infarcts and have sclerotic glomeruli, but also have tubulointerstitial nephritis, present in many autoimmune disorders, and a high frequency of glomeruli with tubularization of Bowman's capsule. These findings, together with the wide range of autoantibodies, could reflect the development of an autoimmune disorder similar to some overlapping syndromes in humans (46).

One of the hallmarks of SSc is vasculopathy, with loss of arteries and capillaries that is not compensated due to defects in angiogenesis and vasculogenesis (47,48). These vascular complications induce the generation of ulcers in the skin and dysfunction of internal organs. SSc-associated renal crisis and SSc-associated PAH are due to microvascular injury that leads to restricted blood flow and subsequent organ failure (48). We found that PSGL-1 deficiency resulted in a 50% reduction in blood vessels in the dermis, ischemic events in the kidneys, and thickening of the small vessel medial layer in kidney and lung, suggesting that PSGL-1 may contribute to maintaining vascular homeostasis in mice. Importantly, thickening of the lung small vessel medial layer could produce PAH, the main cause of premature death among SSc patients (49).

Histologic examination of PSGL-$1^{-/-}$ mice demonstrated that, at 1.5 months, these mice already had skin fibrosis, and some animals showed nonspecific interstitial pneumonia, tubulointerstitial infiltrates, and thickening of the arteriolar medial layer. These findings suggested that the SSc-like disease was already established and that, similar to human disease, it progresses with age, leading to renal and pulmonary failure which may be the main causes of death in these animals. SSc incidence is higher in women than in men and may be related to hormone production or hormone receptor expression. Interestingly, no differences in fibrosis, autoantibody production, or effects on internal organs were found between male and female PSGL-$1^{-/-}$ mice, but a higher incidence of infarcts was apparent in males.

PSGL-$1^{-/-}$ mice did not receive any external insult to trigger or accelerate disease progression, suggesting that the basally activated innate immune system, together with an increased accumulation of effector lymphocytes, culminates in the rupture of organ structure and function. These events almost certainly contribute to weight loss, multiorgan failure, and the high mortality rate during the second year of life. Interestingly, almost 40% of PSGL-$1^{-/-}$ mice died in the perinatal period, but did not show lung or kidney developmental problems.

In summary, we show that the absence of PSGL-1 triggers the spontaneous development of a systemic autoimmune disease with characteristics that resemble SSc. Given that preclinical findings in current SSc animal models have failed to deliver clinical results in SSc patients (50), it is important to discover new molecules that can increase our understanding of the pathogenesis of SSc. SSc-like pathogenesis can be studied using PSGL-$1^{-/-}$ mice. Future research will explore the role of PSGL-1 in the development of human SSc and other autoimmune diseases.

ACKNOWLEDGMENTS

We thank Dr. Dietmar Vestweber and Dr. Mark Wild for providing PSGL-1–deficient mice. We also wish to thank the Universidad Autónoma de Madrid and the Centro Nacional de Investigaciones Cardiovasculares (CNIC) animal facilities for animal care and breeding. We thank the Cytometry Unit and Statistical and Methodological Support Unit of the Hospital de la Princesa for technical support and Margarita García Marcos for advice and discussion on biochemical assays. We also thank the Histopathology and the Microscopy Units at the CNIC for immunohistochemistry assays and help in image processing and quantification, respectively. We thank Manuel Gómez Gutiérrez, Lawrence Baron, Kenneth McCreath, and Simon Bartlett for manuscript editing and Javier Fraga for histopathology help and advice.

AUTHOR CONTRIBUTIONS

All authors were involved in drafting the article or revising it critically for important intellectual content, and all authors approved the final version to be published. Dr. Urzainqui had full access to all of the data in the study and takes responsibility for the integrity of the data and the accuracy of the data analysis.

Study conception and design. Pérez-Frías, González-Tajuelo, Vicente-Rabaneda, Castañeda, Gamallo, Muñoz-Calleja, García-Diez, Urzainqui.

Acquisition of data. Pérez-Frías, González-Tajuelo, Núñez-Andrade, Tejedor, Silván, Esteban-Villafruela, Cubero-Rueda, Urzainqui.

Analysis and interpretation of data. Pérez-Frías, González-Tajuelo, Núñez-Andrade, García-Blanco, Vicente-Rabaneda, Castañeda, Gamallo, Silván, García-García, Muñoz-Calleja, García-Diez, Urzainqui.

REFERENCES

1. Mayes MD. Scleroderma epidemiology. Rheum Dis Clin North Am 2003;29:239–54.
2. Barnes J, Mayes MD. Epidemiology of systemic sclerosis: incidence, prevalence, survival, risk factors, malignancy, and environmental triggers. Curr Opin Rheumatol 2012;24:165–70.
3. Grossman C, Dovrish Z, Shoenfeld Y, Amital H. Do infections facilitate the emergence of systemic sclerosis? Autoimmun Rev 2011;10:244–7.
4. Roberts-Thomson PJ, Walker JG. Stochastic processes in the aetiopathogenesis of scleroderma. Intern Med J 2012;42:235–42.
5. Chizzolini C, Brembilla NC, Montanari E, Truchetet ME. Fibrosis and immune dysregulation in systemic sclerosis. Autoimmun Rev 2011;10:276–81.
6. Gabrielli A, Avvedimento EV, Krieg T. Scleroderma. N Engl J Med 2009;360:1989–2003.
7. Bhattacharyya S, Wei J, Varga J. Understanding fibrosis in systemic sclerosis: shifting paradigms, emerging opportunities. Nat Rev Rheumatol 2011;8:42–54.
8. Opitz C, Klein-Weigel PF, Riemekasten G. Systemic sclerosis: a systematic overview. Part 2. Immunosuppression, treatment of SSc-associated vasculopathy, and treatment of pulmonary arterial hypertension. Vasa 2011;40:20–30.
9. Passweg J, Tyndall A. Autologous stem cell transplantation in autoimmune diseases. Semin Hematol 2007;44:278–85.
10. Henes JC, Schmalzing M, Vogel W, Riemekasten G, Fend F, Kanz L, et al. Optimization of autologous stem cell transplantation for systemic sclerosis—a single-center longterm experience in 26 patients with severe organ manifestations. J Rheumatol 2012;39:269–75.
11. Spertini O, Cordey AS, Monai N, Giuffre L, Schapira M. P-selectin glycoprotein ligand 1 is a ligand for L-selectin on neutrophils, monocytes, and CD34+ hematopoietic progenitor cells. J Cell Biol 1996;135:523–31.
12. Ley K, Laudanna C, Cybulsky M, Nourshargh S. Getting to the site of inflammation: the leukocyte adhesion cascade updated. Nat Rev Immunol 2007;7:678–89.
13. Walcheck B, Moore KL, McEver RP, Kishimoto TK. Neutrophil-neutrophil interactions under hydrodynamic shear stress involve L-selectin and PSGL-1: a mechanism that amplifies initial leukocyte accumulation of P-selectin in vitro. J Clin Invest 1996;98:1081–7.
14. Fuhlbrigge RC, Kieffer JD, Armerding D, Kupper TS. Cutaneous lymphocyte antigen is a specialized form of PSGL-1 expressed on skin-homing T cells. Nat Rev Rheumatol 1997;389:978–81.
15. Kieffer JD, Fuhlbrigge RC, Armerding D, Robert C, Ferenczi K, Camphausen RT, et al. Neutrophils, monocytes, and dendritic cells express the same specialized form of PSGL-1 as do skin-homing memory T cells: cutaneous lymphocyte antigen. Biochem Biophys Res Comm 2001;285:577–87.
16. Rossi FM, Corbel SY, Merzaban JS, Carlow DA, Gossens K, Duenas J, et al. Recruitment of adult thymic progenitors is regulated by P-selectin and its ligand PSGL-1. Nat Immunol 2005;6:626–34.
17. Veerman KM, Williams MJ, Uchimura K, Singer MS, Merzaban JS, Naus S, et al. Interaction of the selectin ligand PSGL-1 with chemokines CCL21 and CCL19 facilitates efficient homing of T cells to secondary lymphoid organs. Nat Immunol 2007;8:532–9.
18. Dominguez-Luis M, Lamana A, Vazquez J, Garcia-Navas R, Mollinedo F, Sanchez-Madrid F, et al. The metalloprotease ADAM8 is associated with and regulates the function of the adhesion receptor PSGL-1 through ERM proteins. Eur J Immunol 2011;41:3436–42.
19. Hansel A, Gunther C, Ingwersen J, Starke J, Schmitz M, Bachmann M, et al. Human slan (6-sulfo LacNAc) dendritic cells are inflammatory dermal dendritic cells in psoriasis and drive

strong T_H17/T_H1 T-cell responses. J Allergy Clin Immunol 2011; 127:787–94.e9.
20. Schakel K, Kannagi R, Kniep B, Goto Y, Mitsuoka C, Zwirner J, et al. 6-Sulfo LacNAc, a novel carbohydrate modification of PSGL-1, defines an inflammatory type of human dendritic cells. Immunity 2002;17:289–301.
21. Spertini C, Baisse B, Spertini O. Ezrin-radixin-moesin-binding sequence of PSGL-1 glycoprotein regulates leukocyte rolling on selectins and activation of extracellular signal-regulated kinases. J Biol Chem 2012;287:10693–702.
22. Urzainqui A, Martinez del Hoyo G, Lamana A, de la Fuente H, Barreiro O, Olazabal IM, et al. Functional role of P-selectin glycoprotein ligand 1/P-selectin interaction in the generation of tolerogenic dendritic cells. J Immunol 2007;179:7457–65.
23. Urzainqui A, Serrador JM, Viedma F, Yanez-Mo M, Rodriguez A, Corbi AL, et al. ITAM-based interaction of ERM proteins with Syk mediates signaling by the leukocyte adhesion receptor PSGL-1. Immunity 2002;17:401–12.
24. Angiari S, Rossi B, Piccio L, Zinselmeyer BH, Budui S, Zenaro E, et al. Regulatory T cells suppress the late phase of the immune response in lymph nodes through P-selectin glycoprotein ligand-1. J Immunol 2013;191:5489–500.
25. He X, Schoeb TR, Panoskaltsis-Mortari A, Zinn KR, Kesterson R, Zhang J, et al. Deficiency of P-selectin or P-selectin glycoprotein ligand-1 leads to accelerated development of glomerulonephritis and increased expression of CC chemokine ligand 2 in lupus-prone mice. J Immunol 2006;177:8748–56.
26. Nunez-Andrade N, Lamana A, Sancho D, Gisbert JP, Gonzalez-Amaro R, Sanchez-Madrid F, et al. P-selectin glycoprotein ligand-1 modulates immune inflammatory responses in the enteric lamina propria. J Pathol 2011;224:212–21.
27. Yoshizaki A, Yanaba K, Iwata Y, Komura K, Ogawa A, Akiyama Y, et al. Cell adhesion molecules regulate fibrotic process via Th1/Th2/Th17 cell balance in a bleomycin-induced scleroderma model. J Immunol 2010;185:2502–15.
28. Estrada-Capetillo L, Hernandez-Castro B, Monsivais-Urenda A, Alvarez-Quiroga C, Layseca-Espinosa E, Abud-Mendoza C, et al. Induction of Th17 lymphocytes and Treg cells by monocyte-derived dendritic cells in patients with rheumatoid arthritis and systemic lupus erythematosus. Clin Dev Immunol 2013;2013: 584303.
29. Dunne JV, van Eeden SF, Keen KJ. L-selectin and skin damage in systemic sclerosis. PLoS One 2012;7:e44814.
30. Iversen LV, Ostergaard O, Ullman S, Nielsen CT, Halberg P, Karlsmark T, et al. Circulating microparticles and plasma levels of soluble E- and P-selectins in patients with systemic sclerosis. Scand J Rheumatol 2013;42:473–82.
31. Yamamoto T. Animal model of systemic sclerosis. J Dermatol 2010;37:26–41.
32. Beyer C, Schett G, Distler O, Distler JH. Animal models of systemic sclerosis: prospects and limitations [review]. Arthritis Rheum 2010;62:2831–44.
33. Lafyatis R, York M. Innate immunity and inflammation in systemic sclerosis. Curr Opin Rheumatol 2009;21:617–22.
34. Stummvoll GH, Aringer M, Grisar J, Steiner CW, Smolen JS, Knobler R, et al. Increased transendothelial migration of scleroderma lymphocytes. Ann Rheum Dis 2004;63:569–74.
35. Guiducci S, Giacomelli R, Cerinic MM. Vascular complications of scleroderma. Autoimmun Rev 2007;6:520–3.
36. Hasegawa M. B lymphocytes: shedding new light on the pathogenesis of systemic sclerosis. J Dermatol 2010;37:3–10.
37. Hussein MR, Hassan HI, Hofny ER, Elkholy M, Fatehy NA, Abd Elmoniem AE, et al. Alterations of mononuclear inflammatory cells, CD4/CD8+ T cells, interleukin 1β, and tumour necrosis factor α in the bronchoalveolar lavage fluid, peripheral blood, and skin of patients with systemic sclerosis. J Clin Pathol 2005;58: 178–84.
38. Sakaguchi S. Naturally arising Foxp3-expressing $CD25^+$ $CD4^+$ regulatory T cells in immunological tolerance to self and non-self. Nat Immunol 2005;6:345–52.
39. Nakahara M, Nagayama Y, Ichikawa T, Yu L, Eisenbarth GS, Abiru N. The effect of regulatory T-cell depletion on the spectrum of organ-specific autoimmune diseases in nonobese diabetic mice at different ages. Autoimmunity 2011;44:504–10.
40. Tang Q, Adams JY, Penaranda C, Melli K, Piaggio E, Sgouroudis E, et al. Central role of defective interleukin-2 production in the triggering of islet autoimmune destruction. Immunity 2008;28: 687–97.
41. Hamaguchi Y. Autoantibody profiles in systemic sclerosis: predictive value for clinical evaluation and prognosis. J Dermatol 2010;37:4253.
42. Sticherling M. Systemic sclerosis: dermatological aspects. Part 1. Pathogenesis, epidemiology, clinical findings. J Dtsch Dermatol Ges 2012;10:705–18.
43. Schroeder K, Herrmann M, Winkler TH. The role of somatic hypermutation in the generation of pathogenic antibodies in SLE. Autoimmunity 2013;46:121–7.
44. Zhang J, Jacobi AM, Wang T, Diamond B. Pathogenic autoantibodies in systemic lupus erythematosus are derived from both self-reactive and non-self-reactive B cells. Mol Med 2008;14: 675–81.
45. Caron M, Hudson M, Baron M, Nessim S, Canadian Scleroderma Research Group, Steele R. Longitudinal study of renal function in systemic sclerosis. J Rheumatol 2012;39:1829–34.
46. Iaccarino L, Gatto M, Bettio S, Caso F, Rampudda M, Zen M, et al. Overlap connective tissue disease syndromes. Autoimmun Rev 2013;12:363–73.
47. Distler JH, Gay S, Distler O. Angiogenesis and vasculogenesis in systemic sclerosis [published erratum appears in Rheumatology (Oxford) 2008;47:234–5]. Rheumatology (Oxford) 2006;45 Suppl 3:iii26–7.
48. Rabquer BJ, Koch AE. Angiogenesis and vasculopathy in systemic sclerosis: evolving concepts. Curr Rheumatol Rep 2012;14:56–63.
49. Shahane A. Pulmonary hypertension in rheumatic diseases: epidemiology and pathogenesis. Rheumatol Int 2013;33:1655–67.
50. Del Galdo F, Matucci-Cerinic M. The search for the perfect animal model discloses the importance of biological targets for the treatment of systemic sclerosis. Ann Rheum Dis 2014;73:635–6.

AngII involvement in lung endothelial dysfunction and spontaneous PAH development in PSGL-1 deficient female mice

Rafael González-Tajuelo[1], PhD Student; María de la Fuente-Fernández[†1], Graduate Student; Daniel Morales-Cano[†2], PhD; Bianca Barreira[2], Technician; Javier Silván[1], PhD Student; Carlos Gamallo[1], PhD, MD; Esther Vicente-Rabaneda[3], PhD, MD; Santos Castañeda[3], PhD, MD; Francisco Pérez-Vizcaíno[2], PhD; Ángel Cogolludo[2], PhD; Luis Jesús Jiménez-Borreguero[4], MD and Ana Urzainqui*[1], PhD

Short title: PSGL-1 deficiency leads to PAH

[1]Fundación de Investigación Biomédica (FIB), Instituto de Investigación Sanitaria-Princesa (IIS-Princesa), Hospital de la Princesa, Immunology Department, C/ Diego de León 62, 28006-Madrid, Spain.. [2]Department of Pharmacology, School of Medicine, University Complutense of Madrid, Instituto de Investigación Sanitaria Gregorio Marañón (IiSGM), 28040 Madrid. Ciber Enfermedades Respiratorias (CIBERES), Spain. [3]FIB, IIS-Princesa, Hospital de la Princesa, Rheumatology Department, C/ Diego de León 62, 28006-Madrid, Spain. [4]Centro Nacional de Investigaciones Cardiovasculares (CNIC), Melchor Fernández Almagro, 3, 28029-Madrid, Spain andCardiology Department, Hospital de la Princesa, C/ Diego de León 62, 28006-Madrid, Spain.

*Corresponding author. Mailing address: ana.urzainqui@salud.madrid.org

Telephone Number: +34915202307 Fax Number: +34915202374

[†]Both authors contributed equally; [*]Corresponding author

Total word count: 8.305

Subject codes: ACE/Angiotensin Receptors/Renin Angiotensin System; Pulmonary hypertension; Animal Models of Human Disease; Endothelium/Vascular Type/Nitric Oxide; Inflammation

Abstract

Rationale: Pulmonary arterial hypertension (PAH) is a rare disease whose etiopathogenesis is poorly understood, and existing treatments are neither curative nor sufficient for stopping disease progression. PAH is one of the major complications of connective tissue diseases, and 7-15% of patients with systemic sclerosis (SSc) develop PAH. Mice deficient for the leukocytic receptor P-selectin glycoprotein ligand-1 (*PSGL-1*$^{-/-}$) spontaneously develop a progressive SSc-like autoimmune syndrome.

Results and Methods: *PSGL-1*$^{-/-}$ mice presented vascular remodeling of distal lung blood vessels. Accordingly, Doppler pulse echochardiography demonstrated that aged *PSGL-1*$^{-/-}$ females showed reduced pulmonary acceleration time/ejection time ratio (PAT/ET) and heart remodeling, indicating PAH. Chronic hypoxia exposure killed 40% of *PSGL-1*$^{-/-}$ females during the first week. Isolated pulmonary arterial rings from aged *PSGL-1*$^{-/-}$ females presented increased vasoconstriction response to KCL and reduced vasodilation response to acetylcholine. Importantly, NO production by lung endothelial cells was reduced in aged *PSGL-1*$^{-/-}$ females. Expression of angiotensin II receptor 2 (AT2R) was reduced in lungs of *PSGL-1*$^{-/-}$ females from a young age and, remarkably, ageing increased the levels of angiotensin II (AngII) and the percentages of IFN-γ-producing interstitial macrophages, T and B lymphocytes in PSGL-1$^{-/-}$ females.

Conclusions: Together, our results show that the absence of PSGL-1 leads to endothelial dysfunction and PAH, coinciding with an increase in pulmonary AngII concentration and reduced NO production by endothelial cells. These studies implicate leukocyte-endothelium interactions for the maintenance of vascular homeostasis and protection against PAH in female mice.

Keywords: PSGL-1; pulmonary hypertension; angiotensin II; nitric oxide; immune sytem

Non-standard Abbreviations and Acronyms
PSGL-1: P-Selectin Glycoprotein Ligand 1
PAT: Pulmonary Acceleration Time
ET: Ejection Time

Introduction

Pulmonary arterial hypertension (PAH) is a rare, progressive and severe disease that affects mainly women. PAH is characterized by hypertrophic distal pulmonary vascular remodeling resulting from endothelial dysfunction, deregulated vascular smooth muscle cell proliferation and inflammation, which together promote medial thickening of pulmonary arteries and luminal obliteration [1]. These pathologic events increase pulmonary vascular resistance and pulmonary artery pressure, which lead to increased hemodynamic load on the right ventricle (RV). The RV adapts by a compensatory increase in wall thickness and contractility [2, 3]. PAH develops in 7–12% of patients with systemic sclerosis and is a leading cause of death in this setting [4-6]. Indeed, systemic sclerosis represents the major cause of connective tissue disease (CTD)-associated PAH [4].

Several molecular mechanisms have been implicated in the control of pulmonary pressure and to be deregulated in PAH. Pulmonary artery endothelial cells from patients with idiopathic PAH (iPAH) produce reduced amounts of nitric oxide (NO), a vasodilator that acts primarily through the soluble guanylate cyclase-cyclic guanosine monophosphate (cGMP) pathway [4]. Other important vasoregulatory properties of NO include regulation of smooth muscle cell proliferation and migration, platelet aggregation, and leukocyte adhesion to endothelium [7]. Accordingly, sildenafil or tadalafil, type 5 phosphodiesterase inhibitors, have proven their efficacy in the treatment of PAH [4]. Another molecule implicated in PAH development is angiotensin II (AngII). AngII is the major effector of the renin-angiotensin-aldosterone system (RAAS), and is mostly produced by cleavage of angiotensin I by angiotensin converting enzyme (ACE), which is located predominantly in lung and renal endothelium[8, 9]. The main functions of AngII are the control of blood pressure and the maintenance of vascular tone in peripheral blood vessels [8-10]. Control of vascular tone by AngII is mediated *via* AngII receptors 1 and 2 (AT1R and AT2R), triggering vasoconstriction by binding to AT1R, and vasodilation by binding to AT2R [9]. In addition, AngII can be hydrolyzed by ACE2 to Ang-(1-7), which counteracts the vasoconstrictor effects of AngII [11]. Thus, elevated levels of renin, ACE, AngII and AT1R receptors have been observed in experimental models as well as patients with pulmonary hypertension (PH) [12-14].

PAH progression has also been associated with inflammatory processes such as viral infections [15]. AngII has been described as a proinflammatory molecule by regulating the expression of cytokines such as IL-12 or tumor necrosis factor-α (TNF-α) in monocytes and macrophages, as well as by producing NO through the activation of AT1R [8]. Additionally, AngII promotes the expression of endothelial adhesion molecules such as E-selectin, P-selectin, VCAM-1 and ICAM-1, facilitating leukocyte rolling and extravasation, and consequently driving inflammation [16]. Moreover, in inflammatory conditions, local macrophage chemoattractant protein-1 (MCP-1) augments AngII synthesis [17]. Collectively, these data suggest an important crosstalk between AngII and inflammation.

P-selectin glycoprotein ligand 1 (PSGL-1) is a leukocytic receptor responsible for the initial contacts between white blood cells and endothelium. PSGL-1 interacts with P-, E- and L-selectin, allowing leukocyte tethering and rolling before extravasation to the inflammatory foci [18]. Moreover, PSGL-1 associates with the tyrosine kinase Syk *via* the actin-linking proteins moesin and ezrin in an immunoreceptor tyrosine-based activation motif (ITAM)-dependent manner, inducing serum response element (SRE) transcriptional activity [19]. PSGL-1/P-selectin interaction triggers a tolerogenic program in human monocyte-derived dendritic cells characterized by the upregulation of IL-10, indoleamine 2,3-dioxygenase (IDO) and TGF-β, and by the downregulation of costimulatory molecules such as CD86, MHC-II and CD40, which drive Treg generation [20]. As a consequence, disease exacerbation has been described in *PSGL-1*-deficient (*PSGL-1*$^{-/-}$) mice in different experimental inflammatory models [21-25]. More importantly, *PSGL-1*$^{-/-}$ mice progressively develop an autoimmune syndrome which shares multiple features with human systemic sclerosis (SSc), such as autoimmunity, dermal fibrosis, vascular damage, and involvement of internal organs [21].

Given that *PSGL-1*$^{-/-}$ mice develop an autoimmune syndrome similar to SSc, and that there are not good mouse models for SSc-PAH, we questioned whether, as a part of the scleroderma-like syndrome, these mice develop PAH. Interestingly, there is a validated non-invasive method [26] to assess the systolic pressure in the pulmonary artery and right ventricle, by measuring pulmonary acceleration time (PAT) corrected by the pulmonary ejection time (ET) at the level of pulmonary valve. The reduction in pulmonary acceleration time/ejection time (PAT/ET) is associated in humans [27] and in

mice [26] with high pulmonary artery pressure. The non-invasive feature of this method allows to analyze in-vivo the presence of PAH and, hence, to perform longitudinal studies of functional changes in pulmonary pressure and right ventricle remodeling.
In the present work, we have analyzed the lungs and heart of *PSGL-1*$^{-/-}$ mice and found pulmonary small vessel and heart remodeling and increased pulmonary artery pressure, detected by a reduced ratio PAT/ET, in female *PSGL-1*$^{-/-}$ mice. In addition, pulmonary arteries of aged *PSGL-1*$^{-/-}$ females showed reduced response to the vasodilator acetylcholine. Accordingly, we found decreased levels of AT2R from a young age, and increased AngII levels and reduced endothelial NO production in lungs of aged female *PSGL-1*$^{-/-}$ mice. Remarkably, the percentage of IFN-□□□interstitial□macrophages, which have been associated with endothelial nitric oxide synthase (eNOS) uncoupling [28], was significantly increased in lung of *PSGL-1*$^{-/-}$ female mice.

Methods

Animals

C57BL/6 *PSGL-1*$^{-/-}$ mice were kindly provided by Dr. M. K. Wild and Dr. D. Vestweber (Max Planck Institute for Molecular Biomedicine, Münster, Germany). Wild-type (WT) C57BL/6 mice were obtained from The Jackson Laboratory and were backcrossed with *PSGL-1*$^{-/-}$ mice. Mice were kept in pathogen-free conditions at the Animal Facility of the School of Medicine, Universidad Autónoma de Madrid (UAM; Madrid, Spain) and the Animal Facility of the Centro Nacional de Investigaciones Cardiovasculares (CNIC; Madrid, Spain). Mice were sacrificed by cervical dislocation, and blood and internal organs were extracted for analysis. All experiments and breeding were performed in accordance with national and institutional guidelines for animal care (EU Directive 2010/63/EU for animal experiments). The experimental procedures were approved by the Director General de Medio Ambiente of Madrid (Ref: PROEX 69/14 and PROEX 162/15).

Immunohistochemistry and vessel wall thickness calculation

Immunohistochemistry against murine α-SMA was performed in paraffin-embedded lung sections. Small blood vessel (diameter <50 μm) wall thickness was calculated by measuring the internal and total vessel diameter of anti-α-SMA-stained lungs and calculating the vessel wall area occupied by the vessel wall using ImageJ (NIH). Vessels were clustered according to their diameter and the mean wall thickness area was calculated.

Transthoracic Doppler echocardiography and Fulton Index calculation

All transthoracic echocadiography measurements were obtained with an echocardiography system (VEVO 2100, Visualsonics) and a 18-38 Hz ultrasound probe. Chest hair was removed with hypoallergenic depilatory cream and animals were kept anesthetized by continuous influx of 2% isofluorane with an oxygen flow rate of 1.5 l/min. The B-mode was used for morphometric measurement of right ventricle (RV) wall and the pulsed wave Doppler mode was used for measuring the pulmonary acceleration time (PAT) and the ejection time (ET) of blood flow in the pulmonary artery at the level of the pulmonary valve. The PAT/ET ratio was then calculated and used as an indirect evaluation of systolic pulmonary artery blood pressure. The ratio of RV weight to left ventricule (LV) weight plus septum (S) (RV/LV + S) was used as an index of RV hypertrophy (Fulton Index)[29].

Vascular reactivity

Murine pulmonary arteries were carefully dissected free of surrounding tissue and cut into rings (1.8–2 mm length). Vessel segments were mounted on a wire myograph in Krebs physiological solution. Buffer solutions were continuously bubbled with 21% O_2, 5% CO_2, and 74% N_2 (pO2¼ 17–19 kPa) [30], and stretched to a transmural pressure equivalent to 30 mmHg. Contractility was recorded by an isometric force transducer and a displacement device coupled with a digitalization and data acquisition system (PowerLab). To confirm smooth muscle viability, arteries were first stimulated by raising the K+ concentration of the buffer to 80 mmol/l and then allowed to recover. After washout, arteries were stimulated with serotonin (5-HT, 10^{-8}–10^{-5} mol/l; Sigma-Aldrich) in a concentration-response fashion performed by cumulative addition. Thereafter, concentration-response curves to Ach (10^{-9}–10^{-5} mol/l)

and sodium nitroprusside (SNP, 10^{-11}–10^{-5} mol/l) were performed by cumulative addition to analyze the endothelium-dependent and endothelium-independent vasodilatation, respectively.

Hypoxia experiments
Female *PSGL-1*$^{-/-}$ and WT mice were exposed to chronic hypoxia (mixture of 10% O_2 and 90% N_2) for 24 days in an airtight chamber with inflow and outflow valves. Mice were removed from the chamber to undergo echocardiography at day 10, 18 and 22. Mice were sacrificed at day 24.

ELISA
The left lung was mechanically disrupted in PBS. After four freeze/defreeze cycles to break cell membranes, samples were centrifuged at 5000 *g* for 5 min at 4ºC and supernatants were recovered. AngII and ET-1 concentrations were measured with the following specific ELISA kits: AngII ELISA kit CSB-E04495m (Cusabio) and endothelin-1 ELISA kit #17165 (IBL).

Western blotting
The right lung was frozen, pulverized, and diluted in RIPA buffer (1% Triton X-100, 0.24 M sodium deoxycolate, 0.35 M SDS in 1xTBS) with protease and phosphatase inhibitors. Lung lysates were used for WB assays. Primary antibodies and their corresponding dilutions are listed in Table 1.
Bound antibodies were visualized by chemiluminiscence with the Luminata™ Forte Western HRP Substrate (Merck KGaA) using an HRP-conjugated goat anti rabbit IgG secondary antibody. Band intensity was analyzed with ImageJ and results were normalized to the expression of β-actin or vinculin considered as loading controls.

Flow cytometry
Lungs were weighed, minced into ~1 mm^2 pieces and digested for 1 h with 1 mg/ml collagenase A (Sigma), 2.5 mg/ml dispase II (Roche) and 40 µg/ml DNase (Sigma) in RPMI 1640 medium. Cell aggregates and undigested pieces of tissue were eliminated using a 70-µm cell strainer (BD Falcon). Cells were then washed with 25 ml of PBS, 0.5% BSA, 5 mM EDTA, concentrated in 700 µl, and filtered through a 30-µm cell strainer (BD Pharmingen). After incubating with 1:200 Fc Block (BD Pharmingen) to saturate surface myeloid Fc receptors, cells were stained with the cocktail of surface antibodies (1:100). Then, cells were incubated for 15 min at 4ºC with the antibody cocktail to label surface markers. Subsequently, cells were permeabilized with 2 ml of FACS Lysing Solution (BD Pharmingen) for 15 min, washed, and stained for 30 min at 4 ºC with a cocktail of antibodies directed against intracellular cytokines. Flow cytometric analysis was performed on a FACSCanto II using FACS Diva Software (BD Pharmingen).

Cell gating strategy
T cells and B cells were gated as $CD45.2^+CD3^+$ and $CD45.2^+CD19^+$, respectively. Alveolar macrophages were gated as $CD45.2^+CD11c^+F4/80^+$, interstitial macrophages were gated as $CD45.2^+CD11c^-F4/80^+$, and dendritic cells were gated as $CD45.2^+CD11c^+F4/80^-$. The expression of IL-10, IL-17 and IFNγ was analyzed in these subsets. Lung endothelial cells were identified as $CD45.2^-CD31^+$. E and P-selectin-positive cells were gated into the $CD45.2^-CD31^+$ subpopulation.

Antibodies
CD3e-PE-Cy7 and CD11c-PE-Cy7 (eBioscience); IL-17A-APC-Cy7, CD45.2-BV421, CD45.2-FITC, CD31-BV421 and CD31-APC (BD Pharmingen); CD62E-APC, CD62P-PE, F4/80-FITC and IFNγ-APC (Miltenyi Biotec); IL-10-PerCP/Cy5.5 (BioLegend).

Intracellular NO evaluation
After blocking and surface molecules staining (CD45, CD31, P-selectin and E-selectin), cells were washed and incubated with the NO-sensing fluorescent probe diaminorhodamine-4M acetoxymethyl ester (DAR-4M AM) (5 µM; Sigma) in PBS for 30 min at 37 ºC. Then, cells were fixed and erythrocytes were lysed by a 15-min incubation with Lysing Solution, and samples were analyzed with a FACSCanto II cytometer. Cells that were not incubated with the probe were used as negative control for fluorescence. Two groups of cells could be distinguished according to the fluorescence levels at Em=580 nm.

Statistics

Statistical significance between two groups was calculated using two-tailed Student's *t* test for parametric variables and Mann-Whitney's U test for nonparametric variables. Statistical significance between three groups was calculated by one-way ANOVA with Bonferroni *post hoc* test. Differences were considered statistically significant with $P < 0.05$ (*,#,$) and highly significant at $P < 0.01$ (**,##,$$) and $P < 0.005$ (***,###,$$$). All statistical analyses were performed using SPSS 15.0 program (IBM).

Results

PSGL-1$^{-/-}$ mice exhibit remodeling of pulmonary small vessels

Immunohistochemical staining of lung sections from wild-type (WT) and *PSGL-1*$^{-/-}$ mice with an antibody against α-smooth muscle actin (□SMA) revealed a thicker medial wall of small vessels in *PSGL-1*$^{-/-}$ lung (Figure 1A). Quantification demonstrated a significant increase of the relative wall area in almost all groups of *PSGL-1*$^{-/-}$ vessels independently of age (Figure 1B), becoming twice as thick in *PSGL-1*$^{-/-}$ animals as in WT, especially in aged animals (Figure 1B).

PSGL-1$^{-/-}$ mice present altered echocardiographic parameters consistent with PAH

Given the remodeling observed in the lung small vessels and our previous observation of an elevated rate of death in *PSGL*$^{-/-}$ mice after reaching one year of age [21], we used echocardiography and Doppler to measure parameters that change to adapt RV to the increasing vascular load in high pulmonary pressure, including PAT/ET ratio and RV wall thickness. Follow-up transthoracic Doppler echocardiography performed on WT and *PSGL-1*$^{-/-}$ mice at the age of 14, 18 and 22 months showed an increased pulmonary artery pressure detected by a reduction in PAT/ET in 14-month aged female *PSGL-1*$^{-/-}$ mice as compared with WT mice, which was maintained throughout the longitudinal study (Figure 2A,B). Interestingly, this was not observed in male *PSGL-1*$^{-/-}$ mice (Figure 2A,B). Likewise, we found remodeling of RV consisted in an increased ventricular wall thickness in aged female *PSGL-1*$^{-/-}$ mice that was statistically significant at 14 months. (Figure 2C).

To determine the age at which the elevation in pulmonary artery pressure takes place, periodical echocardiography was performed on WT and *PSGL-1*$^{-/-}$ female littermates between the ages of 1.5 and 18 months. Recurrent tendency to reduced PAT/ET ratio was observed in animals from 3 months of age (Figure 2D). Because a group of three *PSGL-1*$^{-/-}$ females died between 15 and 18 months of age, we differentiated the dead and survivor groups. The group of *PSGL-1*$^{-/-}$ mice that died prematurely showed increased pulmonary artery pressure detected by a reduced PAT/ET ratio as compared not only with WT mice, but also with the surviving group of *PSGL-1*$^{-/-}$ mice (Figure 2D). Surviving *PSGL-1*$^{-/-}$ mice maintained PAT/ET ratio below that observed in WT mice along their life. At 18 months, animals were sacrificed and the Fulton index was calculated for each mouse. Surviving female *PSGL-1*$^{-/-}$ mice presented a higher Fulton index than their female WT littermates (Figure 2E).

Decreased endothelial NO-dependent relaxing response in pulmonary arteries from PSGL-1$^{-/-}$ female mice

We next assessed vascular reactivity in pulmonary and mesenteric arterial rings using wire myography. When compared with littermates WT females, pulmonary arteries (PA) isolated from female *PSGL-1*$^{-/-}$ mice showed increased vasoconstriction in response to 80 mM KCl (Figure 3A), whereas the contractile response to serotonin (5-HT) was similar (Figure 3B). The vasodilating response to acetylcholine (Ach) was impaired in *PSGL-1*$^{-/-}$ aterial rings (Figure 3C); however, the addition of an external NO donor (sodium nitroprusside) was sufficient to fully relax both WT and *PSGL-1*$^{-/-}$ arterial rings (Figure 3D). Conversely, vascular reactivity was not different between mesenteric arterial rings of *PSGL-1*$^{-/-}$ and WT littermates (Figure 3E,F), suggesting that the endothelial dysfunction is not systemic.

Reduced pulmonary endothelial NO production in PSGL-1$^{-/-}$ mice

The percentage of NO-producing lung endothelial cells (ECs) was reduced in aged *PSGL-1*$^{-/-}$ mice (Figure 3G), although this was significant only among the highest NO-producing EC subset (Figure

3H). Additionally, the mean fluorescence intensity (MFI) for the NO-sensing probe diaminorhodamine-4M acetoxymethyl ester (DAR-4M AM) was lower in lung EC of *PSGL-1*$^{-/-}$ than of WT mice (Figure 3I). These changes were not observed in 3-month-old mice.

Unaltered eNOS expression in the lung of PSGL$^{-/-}$ mice

Given the reduced NO production by *PSGL-1*$^{-/-}$ lung endothelial cells, eNOS protein expression was measured in lung lysates and no differences were found between WT and *PSGL-1*$^{-/-}$ females (Figure 3J).

Impaired adaptation of PSGL-1$^{-/-}$ females to chronic hypoxia

Exposure to chronic hypoxia (10% O_2) killed 40% (2 out of 5 animals) of *PSLG-1*$^{-/-}$ mice during the first week, and surviving animals showed decreased TPV/ET ratio as compared with WT littermates (Figure 4A). The Fulton index at day 24 was similar between WT and *PSGL-1*$^{-/-}$ mice (Figure 4B). *PSGL-1*$^{-/-}$ lung arteries showed a trend toward a greater vasoconstriction response to 5-HT than those of WT animals, but differences did not reach statistical significance (Figure 4C). The relaxing response to Ach was lower in PA from WT mice exposed to hypoxia (Figure 4D) than from WT mice in normoxia (Figure 3C). Thus, after hypoxic exposure, the relaxation induced by Ach was similar between WT and *PSGL-1*$^{-/-}$ arteries (Figure 4D). Likewise, the relaxation in the presence of an external NO donor was similar in WT and *PSGL-1*$^{-/-}$ lung arteries (Figure 4E).

Reduced endothelin-1 concentration in the lung of aged PSGL-1$^{-/-}$ mice

As endothelin (ET-1) is a key mediator involved in PH, we measured its level in lung tissue of young *PSGL-1*$^{-/-}$ and WT female mice and found no differences; however, it was reduced in aged male and female *PSGL-1*$^{-/-}$ mice (Figure 5A). No significant differences were found for endothelin-1 receptor A (ENDRA) and B (ENDRB) protein expression between WT and *PSGL-1*$^{-/-}$ females (Figure 5B).

Aged PSGL-1$^{-/-}$ female mice present increased pulmonary levels of AngII and reduced expression of AT2R

No differences were found in the pulmonary concentration of AngII between young WT and *PSGL-1*$^{-/-}$ females; however, AngII was significantly higher in aged *PSGL-1*$^{-/-}$ female mice (78.02±28.09 pg/g lung tissue) than in aged WT mice (48.70±5.13 pg/g lung tissue) (Figure 6A, left and middle panels). By contrast, AngII levels in aged males were similar between the two genotypes (Figure 6A, right panel).

Although not statistically significant, the expression of ACE was lower both in young and aged *PSGL-1*$^{-/-}$ females than in WT (Figure 6B). Levels of ACE2 level were similar between WT and *PSGL-1*$^{-/-}$ females. Regarding AngII receptors, the expression of AT2R was lower in young (WT: 0.227±0.088 vs KO: 0.089±0.024) and aged *PSGL-1*$^{-/-}$ females than in WT (WT: 0.337±0.094 vs KO: 0.189±0.072) (Figure 6B), whereas no differences were found for the expression of AT1R (Figure 6B).

Gamma-interferon (IFN-γ) producing T cells, B cells and macrophages are overrepresented in the lung of aged PSGL-1$^{-/-}$ female mice

Analysis of the resident lung immune system in WT and *PSGL-1*$^{-/-}$ females revealed that the percentages of T and B cells producing IFN-γ were already higher (Figure 7A,B) in young *PSGL-1*$^{-/-}$ females than in WT, becoming statistically significant in aged mice. IL-10^{+} T cells were reduced in *PSGL-1*$^{-/-}$ lungs, and IL-17^{+} T and B cell subpopulations were similar between WT and *PSGL-1*$^{-/-}$ females (Figure 7A-B). Moreover, the percentage of IFN-γ^{+} cells in the alveolar macrophage subset was higher in young *PSGL-1*$^{-/-}$ females than in WT (Figure 7C) and a higher percentage of IFN-γ^{+} interstitial macrophages was found in aged *PSGL-1*$^{-/-}$ females as compared with WT mice (Figure 7D).

Discussion

PAH is a particularly severe, life-threatening complication of some CTDs that leads to RV remodeling, right heart failure and premature death[15]. Although great effort has been invested in searching for an efficient treatment for PAH, no curative therapy is available. Our work shows that female mice deficient for PSGL-1 present reduced expression of pulmonary AT2R and thickened small vessel walls. With aging, pulmonary levels of AngII increase in *PSGL-1*$^{-/-}$ females coinciding with increased thickening of pulmonary small vessel walls, greater contractility and reduced capability of relaxation of lung arteries, and decreased endothelial NO production, driving RV dysfunction and death.

The increase in relative wall vessel area in lung vasculature has been described as a histological marker of PAH in both animal models and patients with PAH [1, 4, 15], and is considered as one of the first events occurring in the development of PAH [2, 14]. We did not observe plexiform lesions or intimal fibrosis in the lung of *PSGL-1*$^{-/-}$ mice, although these lesions do not appear in all the rodent models of PAH [31]. In general terms, the models that reproduce the plexiform arteropathy are "second hit" models such as monocrotaline (MCT) + pneumonectomy in young rats (under 200 g of weight) and Sugen 5416 + hypoxia in rats and mice; or knock-in genetic models such as IL-6- and S100A4-overexpressing transgenic mice [31].

The vascular remodeling observed in *PSGL-1*$^{-/-}$ mice might cause an increase in the lung vascular resistance to blood flow, the main consequence of which would be the elevation of the pressure in the pulmonary artery. Transthoracic Doppler echocardiography is a non-invasive diagnostic tool for patients with suspected PAH, giving information not only on diagnosis but also providing further information on the causes or consequences of the PAH [15, 32]. This method has been validated for estimating pulmonary artery pressure (PAP) in patients with PAH and in rat and mouse models of PAH [26, 27, 33], and is becoming increasingly more relevant in the study of murine models of heart diseases [34]. Using this echocardiography modality, and in accordance with the pulmonary vessel remodeling, we found a reduced PAT/ET ratio in the pulmonary artery of *PSGL-1*$^{-/-}$ female mice. Our results from a longitudinal study show a consistently increased pulmonary artery pressure detected by a reduced TPV/ET ratio in *PSGL-1*$^{-/-}$ female mice from 3 months of age consistent with the vessel wall thickening, suggesting that *PSGL-1*$^{-/-}$ mice are susceptible to PAH at young age.

Chronic hypoxia killed 40% of *PSGL-1*$^{-/-}$ females during the first days of treatment, suggesting that some *PSGL-1*$^{-/-}$ mice are unable to adapt to reduced O_2 pressure. WT and surviving *PSGL-1*$^{-/-}$ females showed an increased pulmonary artery pressure during the first week of hypoxia and both groups were able to partially compensate pulmonary artery pressure (increase PAT/ET ratio) during the next two weeks of exposure, although the recovery was slower for *PSGL-1*$^{-/-}$ mice. However, WT and *PSGL-1*$^{-/-}$ littermates showed a similar Fulton index and loss of NO-dependent relaxation, indicating that some hypoxia changes are not additive to PSGL-1 absence after the 3-week exposure to low oxygen pressure. These data suggest that the endothelial dysfunction promoted by hypoxia in WT mice is already present in PSGL-1$^{-/-}$ females. Importantly, and according with this hypothesis, we found that lung of aged *PSGL-1*$^{-/-}$ females, in addition to having a lower expression of AT2R, showed increased AngII concentration and reduced NO production by ECs, which might explain the higher contractility and reduced relaxation capability of lung arteries at this age, ultimately leading to elevated flow resistance and hence to increased pulmonary pressure and reduced TPV/ET.

In this context, pentraxin-3 (PTX3) is a soluble ligand of P-selectin that interferes with P-sel/PSGL-1 interaction [35, 36]. The administration of PTX3 to wild-type mice induced endothelial dysfunction and increased blood pressure [36]. Interestingly, PTX3 circulating levels were elevated in patients with hypertension [36] and SSc [37]. These data suggest that, after binding to PSGL-1, signals transduced by P-selectin on endothelial cells may by implicated in the maintenance of the correct endothelial function and integrity.

Molecular systems implicated in the control of the vascular tone, such as ET-1, AngII and NO, have been described to be altered in several animal models and in patients with PAH [4, 9, 15]. Thus, hypoxic and MCT-treated rats showed increased AngII and AT1R levels [13, 38, 39], and patients with iPAH showed higher levels of pulmonary AngII due to increased activity of ACE, as well as increased

expression and signaling of AT1R, resulting in augmented vascular smooth muscle cell (VSMC) proliferation [40]. Inhibitors of the RAAS have been proven to have an effect in reducing PAP and other PAH signs in some animal models and also in pilot studies with small patient cohorts, underscoring the role of RAAS in the pathology of PAH. For example, treatment with losartan (AT1R antagonist) or captopril (inhibitor of ACE) was able to reduce mean PAP, RV hypertrophy and lung vascular remodeling in rats exposed to hypobaric hypoxia for 14 days [40, 41]. Furthermore, treatment with captopril showed a clear effect in reducing PAP in some studies, whereas in others captopril was unable to lower PAP [9].

The increased levels of pulmonary AngII found in aged *PSGL-1*$^{-/-}$ female mice might be explained by either an enhanced activity of ACE, which has been previously reported for patients with PAH and animal models [40, 42], or an overexpression/overactivity of chymase. Mast cell chymase, expressed mainly in kidney and heart tissue, is an enzyme that cleaves both Ang(1-12) and angiotensinogen into AngII [43-45]. It can be released by mast cell degranulation, and might account for the elevated AngII levels not only in inflammatory conditions such as atherosclerosis but also in heart failure [17]. Interestingly, the chymase-dependent increase of cardiac AngII is related to aging [44] and aged *PSGL-1*$^{-/-}$ mice are massively infiltrated by immune cells, as previously reported [21].

NO is a critical regulator of vascular homeostasis, not only by modulating vascular tone, but also by controlling VSMC proliferation and migration as well as leukocyte adhesion to endothelium [15, 46]. We found reduced NO production by *PSGL-1*$^{-/-}$ lung endothelial cells, but similar expression levels of eNOS. However, differences in eNOS activity due to changes in the post-translational modifications could account for the reduced NO levels of *PSGL-1*$^{-/-}$ lung endothelial cells [47]. Also, it has been reported that an increase in AngII could lead to eNOS uncoupling, which results in reduced NO production [28]. In addition, several reports have highlighted the relevant role of inflammation and the immune system in endothelial dysfunction [28, 31, 48]. In this context, vascular dysfunction in aortic endothelial cells can be mediated by inflammatory monocytes and NK cells producing IFN-γ and IL-12 in an AngII-dependent manner [28, 48]. A similar mechanism could be operating in the pulmonary vasculature of female *PSGL-1*$^{-/-}$ mice, in which aging increases IFN-γ production in macrophages, B cells and T cells, and AngII pulmonary levels that can account for the endothelial dysfunction and eNOS uncoupling with the ensuing reduction in the endothelial NO.

Inflammation has emerged as a pivotal contributor to the development of PAH [49-51]. Perivascular infiltration of mononuclear immune cells has been reported in almost all animal models, especially in rodents subjected to chronic hypoxia or MCT administration, and in IL-6 knock-in transgenic mice [31]. Additionally, the upregulation of chemokines (CCL-2, CCL-5, RANTES, fractalkine) and proinflammatory cytokines (IL-6, IL-1, IFN-γ) has been described in patients with severe PAH [4, 52-56]. In the case of CTD-associated PAH, it has been proposed that autoantibodies (anti-U1-RNP and anti-dsDNA) forming immune complexes could trigger the upregulation of endothelial ligands for leukocytes, such as ICAM-1 or E-selectin, initiating or contributing to lung vasculopathology [57]. Interestingly, *PSGL-1*$^{-/-}$ mice showed increased expression of P-selectin and E-selectin in lung endothelial cells. The activation of the lung endothelium has been previously described for PAH patients. Plasma levels of soluble (s)P-selectin, sE-selectin, sICAM-1 and sVCAM-1 were reported to be higher in patients with PAH than in healthy controls [51, 54, 58]. In another study, treatment with prostacyclin reduced the levels of sP-selectin in a cohort of mainly iPAH patients[59]. Similar results have been reported in MCT-induced PAH in rats, which present increased expression of pulmonary ICAM-1, VCAM-1 and E-selectin [49]. Moreover, it has been demonstrated by immunohistochemistry that infusion of AngII was able to induce the expression of P-selectin, E-selectin, ICAM-1 and VCAM-1 in mesenteric arterioles and venules in rats [16].

In the present study, we highlight the importance of leukocyte-endothelium interactions for the maintenance of vascular homeostasis and protection against PAH. Deficieny for leukocytic PSGL-1, which interacts with P-selectin and E-selectin on the surface of activated endothelium, induces AngII-dependent endothelial dysfunction characterized by reduced vasodilation response due to impaired NO production. This impairment in endothelial function leads to vascular remodeling, PAH and, ultimately, to premature death in mice. Our work contributes to the identification of new pathways and

possible pharmaceutical targets for the treatment of PAH, which is crucial to improve the survival and the long-term prognosis of patients with this disease.

Author Contributions

AU conceived and supervised the study. RG-T and AU designed and interpreted the experiments and analyzed data. RG-T performed most of the experiments and wrote the manuscript. JS and MF-F performed ELISA and western blotting experiments. LJ J-B performed, analyzed and interpreted echocardiography experiments. AC, FP-V, DM-C and BB performed and analyzed the myography and cardiac morphometry experiments. EV-R SC, CG and LJ J-B gave clinical advice. CG analyzed and interpreted histological samples. SC provided reagents. All the authors contributed to discuss the data and revised the manuscript.

Acknowledgments

We thank the UAM and CNIC animal facilities for animal breeding and care. We are indebted to Ana Vanesa Alonso and Lorena Flores of the Vascular Imaging Unit at CNIC for the echocardiography performance. We also thank the Cytometry Unit and Statistical and Methodological Support Unit of the Hospital de la Princesa for technical support. We thank Dr. Kenneth McCreath for manuscript editing and Juan M. Serrador for generously supplying the anti-eNOS antibody.

Sources of Funding

This work was supported by Spanish Ministry of Health and ISCIII (cofinanced by Fondos FEDER) (FIS-PI14-01698, FIS-PI12-01578, Proyecto Coordinado de Excelencia PIE13-00041) and the Spanish Ministry of Economy and Competitiveness (predoctoral FPI grant to D.M-C.; research grants SAF2011-28150 to F.P.V. and SAF 2014-55399 and SAF2016-77222-R to F.P.V. and A.C.). Rafael González-Tajuelo was supported by the Proyecto Coordinado de Excelencia PIE13/00041.

Disclosures

The authors have declared that non conflict of interest exists

REFERENCES

1. Farber H, Loscalzo J. Pulmonary Arterial Hypertension. *N Engl J Med.* 2004;351:1655-1665.

2. Leopold JA, Maron BA. Molecular Mechanisms of Pulmonary Vascular Remodeling in Pulmonary Arterial Hypertension. *Int J Mol Sci.* 2016;17(761).

3. Vonk Noordegraaf A, Westerhof B, Westerhof N. The Relationship Between the Right Ventricle and its Load in Pulmonary Hypertension. *J Am Coll Cardiol.* 2017;69(2):236-243.

4. Montani D, Günther S, Dorfmüller P, Perros F, Girerd B, Garcia G, Jaïs X, Savale L, Artaud-Macari E, Price LC, Humbert M, Simonneau G, Sitbon O. Pulmonary arterial hypertension. *Orphanet Journal of Rare Diseases.* 2013;8(97).

5. Derrett-Smith EC, Dooley A, Gilbane AJ, Trinder SL, Khan K, Baliga R, Holmes AM, Hobbs AJ, Abraham D, Denton CP. Endothelial Injury in a Transforming Growth Factor β–Dependent Mouse Model of Scleroderma Induces Pulmonary Arterial Hypertension. *Arthritis Rheumatol.* 2013;65(11):2928–2939.

6. Rhee RL, Gabler NB, Praestgaard A, Merkel PA, Kawut SM. Adverse Events in Connective Tissue Disease–Associated Pulmonary Arterial Hypertension. *Arthritis Rheumatol.* 2015;67(9):2457–2465.

7. Zuckerbraun BS, George P, Gladwin MT. Nitrite in pulmonary arterial hypertension: therapeutic avenues in the setting of dysregulated arginine/nitric oxide synthase signalling. *Cardiovascular Research.* 2011;89:542–552.

8. Gaddam RR, Chambers S, Bhatia M. ACE and ACE2 in Inflammation: A Tale of Two Enzymes. *Inflammation & Allergy - Drug Targets.* 2014;13:224-234.

9. Maron BA, Leopold JA. The role of the renin-angiotensin-aldosterone system in the pathobiology of pulmonary arterial hypertension *Pulm Circ.* 2014;4(2):200-210.

10. Liu S-S, Wang H-Y, Tang J-M, Zhou X-M. Hypoxia-Induced Collagen Synthesis of Human Lung Fibroblasts by Activating the Angiotensin System. *Int J Mol Sci.* 2013;14:24029-24045.

11. Santos RA, Ferreira AJ, Simoes E. Recent advances in the angiotensin-converting enzyme 2-angiotensin(1-7)-Mas axis. *Exp Physiol.* 2008;93(5):519-527.

12. Bruce E, Shenoy V, Rathinasabapathy A, Espejo A, Horowitz A, Oswalt A, Francis J, Nair A, Unger T, Raizada MK, Steckelings UM, Sumners C, Katovich MJ. Selective activation of angiotensin AT2 receptors attenuates progression of pulmonary hypertension and inhibits cardiopulmonary fibrosis. *British Journal of Pharmacology* 2015;172:2219–2231.

13. Yuan Y-M, Luo L, Guo Z, Yang M, Ye R-S, Luo C. Activation of renin–angiotensin–aldosterone system (RAAS) in the lung of smoking-induced pulmonary arterial hypertension (PAH) rats. *Journal of the Renin-Angiotensin-Aldosterone System.* 2015;16(2):249-253.

14. Maron BA, Loscalzo J. Pulmonary Hypertension: Pathophysiology and Signaling Pathways. In: Marc Humbert, Evgenov OV, Stasch J-P, eds. *Pharmacotherapy of Pulmonary Hypertension*. Heidelberg: Springer; 2013.

15. Rabinovitch M. Molecular pathogenesis of pulmonary arterial hypertension. *J Clin Invest.* 2012;122(12):4306-4313.

16. Álvarez Á, Cerdá-Nicolás M, Nabah YNA, Mata M, Issekutz AC, Panés J, Lobb RR, Sanz M-J. Direct evidence of leukocyte adhesion in arterioles by angiotensin II. *Blood.* 2004;104:402-407.

17. Company C, Piqueras L, Nabah YNA, Escudero P, Blanes JI, Jose PJ, Morcillo EJ, Sanz M-J. Contributions of ACE and mast cell chymase to endogenous angiotensin II generation and leucocyte recruitment in vivo. *Cardiovascular Research.* 2011;92:48-56.

18. Zarbock A, Ley K, McEver RP, Hidalgo A. Leukocyte ligands for endothelial selectins: specialized glycoconjugates that mediate rolling and signaling under flow. *Blood.* 2011;118:6743-6751.

19. Urzainqui A, Serrador JM, Viedma F, Yáñez-Mó M, Rodríguez A, Corbí AL, Alonso-Lebrero JL, Luque A, Deckert M, Vázquez J, Sánchez-Madrid F. ITAM-Based Interaction of ERM Proteins with Syk Mediates Signaling by the Leukocyte Adhesion Receptor PSGL-1. *Immunity.* 2002;17:401–412.

20. Urzainqui A, Hoyo GMd, Lamana A, Fuente Hdl, Barreiro O, Olazabal I, Martin P, Wild M, Vestweber D, González-Amaro R, Sánchez-Madrid F. Functional role of P-selectin glycoprotein ligand 1/P-selectin interaction in the generation of tolerogenic dendritic cells. *J Immunol.* 2007;179(11):7457-7465.

21. Pérez-Frías A, González-Tajuelo R, Núñez-Andrade N, Tejedor R, García-Blanco M, Vicente-Rabaneda E, Castañeda S, Gamallo C, Silván J, Esteban-Villafruela A, Cubero-Rueda L, García-García C, Muñoz-Calleja C, García-Diez A, Urzainqui A. Development of an autoimmune syndrome affecting the skin and internal organs in P-selectin glycoprotein ligand 1 leukocyte receptor-deficient mice. *Arthritis Rheumatol.* 2014;66(11):3178-3189.

22. Nuñez-Andrade N, Lamana A, Sancho D, Gisbert J, Gonzalez-Amaro R, Sanchez-Madrid F, Urzainqui A. P-selectin glycoprotein ligand-1 modulates immune inflammatory responses in the enteric lamina propria. *J Pathol.* 2011;224(2):212-221.

23. He X, Schoeb TR, Panoskaltsis-Mortari A, Zinn KR, Kesterson RA, Zhang J, Samuel S, Hicks MJ, Hickey MJ, Bullard DC. Deficiency of P-Selectin or P-Selectin Glycoprotein Ligand-1 Leads to Accelerated Development of Glomerulonephritis and Increased Expression of CC Chemokine Ligand 2 in Lupus-Prone Mice. *J Immunol.* 2006;177:8748-8756.

24. Rivera-Nieves J, Burcin T, Olson T, Morris M, McDuffie M, Cominelli F, Ley K. Critical role of endothelial P-selectin glycoprotein ligand 1 in chronic murine ileitis. *J Exp Med.* 2006;203(4):907-917.

25. Angiari S, Rossi B, Piccio L, Zinselmeyer BH, Budui S, Zenaro E, Bianca VD, Bach SD, Scarpini E, Bolomini-Vittori M, Piacentino G, Dusi S, Laudanna C, Cross AH, Miller MJ,

Constantin G. Regulatory T Cells Suppress the Late Phase of the Immune Response in Lymph Nodes through P-Selectin Glycoprotein Ligand-1. *J Immunol.* 2013;191:5489–5500.

26. Thibault H, Kurtz B, Raher M, Shaik R, Waxman A, Derumeaux G, Halpern E, Bloch K, Scherrer-Crosbie M. Noninvasive assessment of murine pulmonary arterial pressure: validation and application to models of pulmonary hypertension. *Circ Cardiovasc Imaging.* 2010 3(2):157-163.

27. Urboniene D, Haber I, Fang Y, Thenappan T, Archer S. Validation of high-resolution echocardiography and magnetic resonance imaging vs. high-fidelity catheterization in experimental pulmonary hypertension. *Am J Physiol Lung Cell Mol Physiol.* 2010;299:401-412.

28. Kossmann S, Hu H, Steven S, Schönfelder T, Fraccarollo D, Mikhed Y, Brähler M, Knorr M, Brandt M, Karbach SH, Becker C, Oelze M, Bauersachs J, Widder J, Münzel T, Daiber A, Wenzel P. Inflammatory Monocytes Determine Endothelial Nitric-oxide Synthase Uncoupling and Nitro-oxidative Stress Induced by Angiotensin II. *J Biol Chem.* 2014;289(40):27540–27550.

29. Morales-Cano D, Menendez C, Moreno E, Moral-Sanz J, Barreira B, Galindo P, Pandolfi R, Jimenez R, Moreno L, Cogolludo A, Duarte J, Perez-Vizcaino F. The Flavonoid Quercetin Reverses Pulmonary Hypertension in Rats. *PLoS ONE.* 2014;9(12).

30. Cogolludo A, Frazziano G, Briones A, Cobeño L, Moreno L, Lodi F, Salaices M, Tamargo J, Perez-Vizcaino F. The dietary flavonoid quercetin activates BKCa currents in coronary arteries via production of H2O2. Role in vasodilatation. *Cardiovasc Res.* 2007 73(2):424-431.

31. Stenmark K, Meyrick B, Galie N, Mooi WJ, McMurtry IF. Animal models of pulmonary arterial hypertension: the hope for etiological discovery and pharmacological cure. *Am J Physiol Lung Cell Mol Physiol.* 2009;297:L1013-L1032.

32. Bleeker GB, Steendijk P, Holman ER, Yu C-M, Breithardt OA, Kaandorp TAM, Schalij MJ, Wall EEvd, Nihoyannopoulos P, Bax JJ. Assessing right ventricular function: the role of echocardiography and complementary technologies. *Heart.* 2006;92:i19-i26.

33. Brittain E, Penner NL, West J, Hemnes A. Echocardiographic Assessment of the Right Heart in Mice. *J Vis Exp.* 2013;81:e50912.

34. Chen G, Li Y, Tian J, Zhang L, Jean-Charles P, Gobara N, Nan C, Jin J, Huang XP. Application of Echocardiography on TransgenicMice with Cardiomyopathies. *Biochemistry Research International.* 2012.

35. Deban L, Russo R, Sironi M, Moalli F, Scanziani M, Zambelli V, Cuccovillo I, Bastone A, Gobbi M, Valentino S, Doni A, Garlanda C, Danese S, Salvatori G, Sassano M, Evangelista V, Rossi B, Zenaro E, Constantin G, Laudanna C, Bottazzi B, Mantovani A. Regulation of leukocyte recruitment by the long pentraxin PTX3. *Nat Immunol.* 2010;11(4):328-334.

36. Carrizzo A, Lenzi P, Procaccini C, Damato A, Biagioni F, Ambrosio M, Amodio G, Remondelli P, Giudice CD, Izzo R, Malovini A, Formisano L, Gigantino V, Madonna M, Puca AA, Trimarco B, Matarese G, Fornai F, Vecchione C. Pentraxin 3 Induces Vascular Endothelial Dysfunction Through a P-selectin/Matrix Metalloproteinase-1 Pathway. *Circulation.* 2015;131:1495-1505.

37. Ílgen U, Yayla M, Düzgün N. Low serum fibroblast growth factor 2 levels not accompanied by increased serum pentraxin 3 levels in patients with systemic sclerosis. *Clin Rheumatol.* 2017;36(2):367-372.

38. Becker MO, Kill A, Kutsche M, Guenther J, Rose A, Tabeling C, Witzenrath M, Kühl AA, Heidecke H, Ghofrani HA, Tiede H, Schermuly RT, Nickel N, Hoeper MM, Lukitsch I, Gollasch M, Kuebler WM, Bock S, Burmester GR, Dragun D, Riemekasten G. Vascular receptor autoantibodies in pulmonary arterial hypertension associated with systemic sclerosis. *Am J Respir Crit Care Med.* 2014;190(7):808-817.

39. Li G, Liu Y, Zhu Y, Liu A, Xu Y, Li X, Li Z, Su J, Sun L. ACE2 Activation Confers Endothelial Protection and Attenuates Neointimal Lesions in Prevention of Severe Pulmonary Arterial Hypertension in Rats. *Lung.* 2013;191:327-336.

40. Man FSd, Tu L, Handoko ML, Rain S, Ruiter G, François C, Schalij I, Dorfmüller P, Simonneau G, Fadel E, Perros F, Boonstra A, Postmus PE, Velden Jvd, Vonk-Noordegraaf A, Humbert M, Eddahibi S, Guignabert C. Dysregulated Renin–Angiotensin–Aldosterone System Contributes to Pulmonary Arterial Hypertension. *Am J Respir Crit Care Med.* 2012;186(8):780–789.

41. Morrell N, Morris K, Stenmark K. Role of angiotensin-converting enzyme and angiotensin II in development of hypoxic pulmonary hypertension. *Am J Physiol* 1995;269(4):1186-1894.
42. Shenoy V, Qi Y, Katovich MJ, Raizada MK. ACE2, a Promising Therapeutic Target for Pulmonary Hypertension. *Curr Opin Pharmacol.* 2011;11(2):150–155.
43. Ahmad S, Varagic J, VonCannon JL, Groban L, Collawn JF, Dell'Italia LJ, Ferrario CM. Primacy of cardiac chymase over angiotensin converting enzyme as an angiotensin-(1-12) metabolizing enzyme. *Biochem Biophys Res Commun.* 2016;478(2):559–564.
44. Froogh G, Pinto JT, Le Y, Kandhi S, Aleligne Y, Huang A, Sun D. Chymase-dependent production of angiotensin II: an old enzyme in old hearts. *Am J Physiol Heart Circ Physiol.* 2016.
45. Jessup JA, Trask AJ, Chappell MC, Nagata S, Kato J, Kitamura K, Ferrario CM. Localization of the novel angiotensin peptide, angiotensin-(1-12), in heart and kidney of hypertensive and normotensive rats *Am J Physiol Heart Circ Physiol.* 2008;294(6):H2614–H2618.
46. Martinelli R, Gegg M, Longbottom R, Adamson P, Turowski P, Greenwood J. ICAM-1–mediated Endothelial Nitric Oxide Synthase Activation via Calcium and AMP-activated Protein Kinase Is Required for Transendothelial Lymphocyte Migration *Mol Biol Cell.* 2009 20(3):995–1005.
47. Siragusa M, Fleming I. The eNOS signalosome and its link to endothelial dysfunction. *Eur J Physiol.* 2016;468:1125–1137.
48. Kossmann S, Schwenk M, Hausding M, Karbach SH, Schmidgen MI, Brandt M, Knorr M, Hu H, Kröller-Schön S, Schönfelder T, Grabbe S, Oelze M, Daiber A, Münzel T, Becker C, Wenzel P. Angiotensin II–Induced Vascular Dysfunction Depends on Interferon-γ–Driven Immune Cell Recruitment and Mutual Activation of Monocytes and NK-Cells. *Arterioscler Thromb Vasc Biol.* 2013;33:1313-1319.
49. Zhao H, Xue Y, Guoa Y, Sun Y, Liu D, Wang X. Inhibition of endocan attenuates monocrotaline-induced connective tissue disease related pulmonary arterial hypertension. *International Immunopharmacology*. 2017;42: 115–121.
50. Steiner MK, Syrkina OL, Kolliputi N, Mark EJ, Hales CA, Waxman AB. Interleukin-6 Overexpression Induces Pulmonary Hypertension. *Circ Res.* 2009;104:236-244.
51. Dorfmüller P, Perros F, Balabanian K, Humbert M. Inflammation in pulmonary arterial hypertension. *Eur Respir J.* 2003;22:358–363.
52. Savai R, Pullamsetti SS, Kolbe J, Bieniek E, Voswinckel R, Fink L, Scheed A, Ritter C, Dahal BK, Vater A, Klussmann S, Ghofrani HA, Weissmann N, Klepetko W, Banat GA, Seeger W, Grimminger F, Schermuly RT. Immune and Inflammatory Cell Involvement in the Pathology of Idiopathic Pulmonary Arterial Hypertension. *Am J Respir Crit Care Med.* 2012;186(9):897-908.
53. Humbert M, Monti G, Brenot F, Sitbon O, Portier A, Grangeot-Keros L, Duroux P, Galanaud P, Simonneau G, Emilie D. Increased interleukin-1 and interleukin-6 serum concentrations in severe primary pulmonary hypertension. *Am J Respir Crit Care Med.* 1995;151:1628–1631.
54. Balabanian K, Foussat A, Dorfmüller P, Durand-Gasselin I, Capel F, Bouchet-Delbos L, Portier A, Marfaing-Koka A, Krzysiek R, Rimaniol A, Simonneau G, Emilie D, Humbert M. CX(3)C chemokine fractalkine in pulmonary arterial hypertension. *Am J Respir Crit Care Med.* 2002;165:1419–1425.
55. Dorfmüller P, Zarka V, Durand-Gasselin I, Monti G, Balabanian K, Garcia G, Capron F, Coulomb-Lherminé A, Marfaing-Koka A, Simonneau G, Emilie D, Humbert M. Chemokine RANTES in severe pulmonary arterial hypertension. *Am J Respir Crit Care Med.* 2002;165:534–539.
56. Sanchez O, Marcos E, Perros F, Fadel E, Tu L, Humbert M, Dartevelle P, Simonneau G, Adnot S, Eddahibi S. Role of endothelium-derived cc chemokine ligand 2 in idiopathic pulmonary arterial hypertension. *Am J Respir Crit Care Med.* 2007;176:1041–1047.
57. Okawa-Takatsuji M, Aotsuka S, Fujinami M, Uwatoko S, Kinoshita M, Sumiya M. Up-regulation of intercellular adhesion molecule-1 (ICAM-1), endothelial leucocyte adhesion molecule-1 (ELAM-1) and class II MHC molecules on pulmonary artery endothelial cells by antibodies against U1-ribonucleoprotein. *Clin Exp Immunol.* 1999;116(1):174-180.
58. Iannone F, Riccardi MT, Guiducci S, Bizzoca R, Cinelli M, Matucci-Cerinic M, Lapadula G. Bosentan regulates the expression of adhesion molecules on circulating T cells and serum

soluble adhesion molecules in systemic sclerosis-associated pulmonary arterial hypertension. *Ann Rheum Dis.* 2008;67:1121-1126.

59. Sakamaki F, Kyotani S, Nagaya N, Sato N, Oya H, Satoh T, Nakanishi N. Increased plasma P-selectin and decreased thrombomodulin in pulmonary arterial hypertension were improved by continuous prostacyclin therapy. *Circulation.* 2000;102(22):2720–2725.

TABLES

Table 1

Antibody	Origin	Dilution	Reference	Manufacturer
Anti-ACE	Rabbit	1/1000	LS-C291661/61036	LifeSpan BioSciences
Anti-ACE2	Rabbit	1/1000	NBP1-76614	Novus Biologicals
Anti-AT1R	Rabbit	1/1000	NBP1-77078	Novus Biologicals
Anti-AT2R	Rabbit	1/1000	NBP1-77368	Novus Biologicals
Anti-ET_A	Rabbit	1/1000	NBP1-87467	Novus Biologicals
Anti-ET_B	Rabbit	1/1000	NBP2-16334	Novus Biologicals
Anti-β-actin	Rabbit	1/5000	V4505-100UL	Sigma Aldrich
Anti-Vinculin	Rabbit	1/2000	A5316-100UL	Sigma Aldrich
Anti-eNOS	Mouse	1/1000	610297	BD Pharmingen

Table 1. Antibodies used for immunoblotting

FIGURES

Fig.1

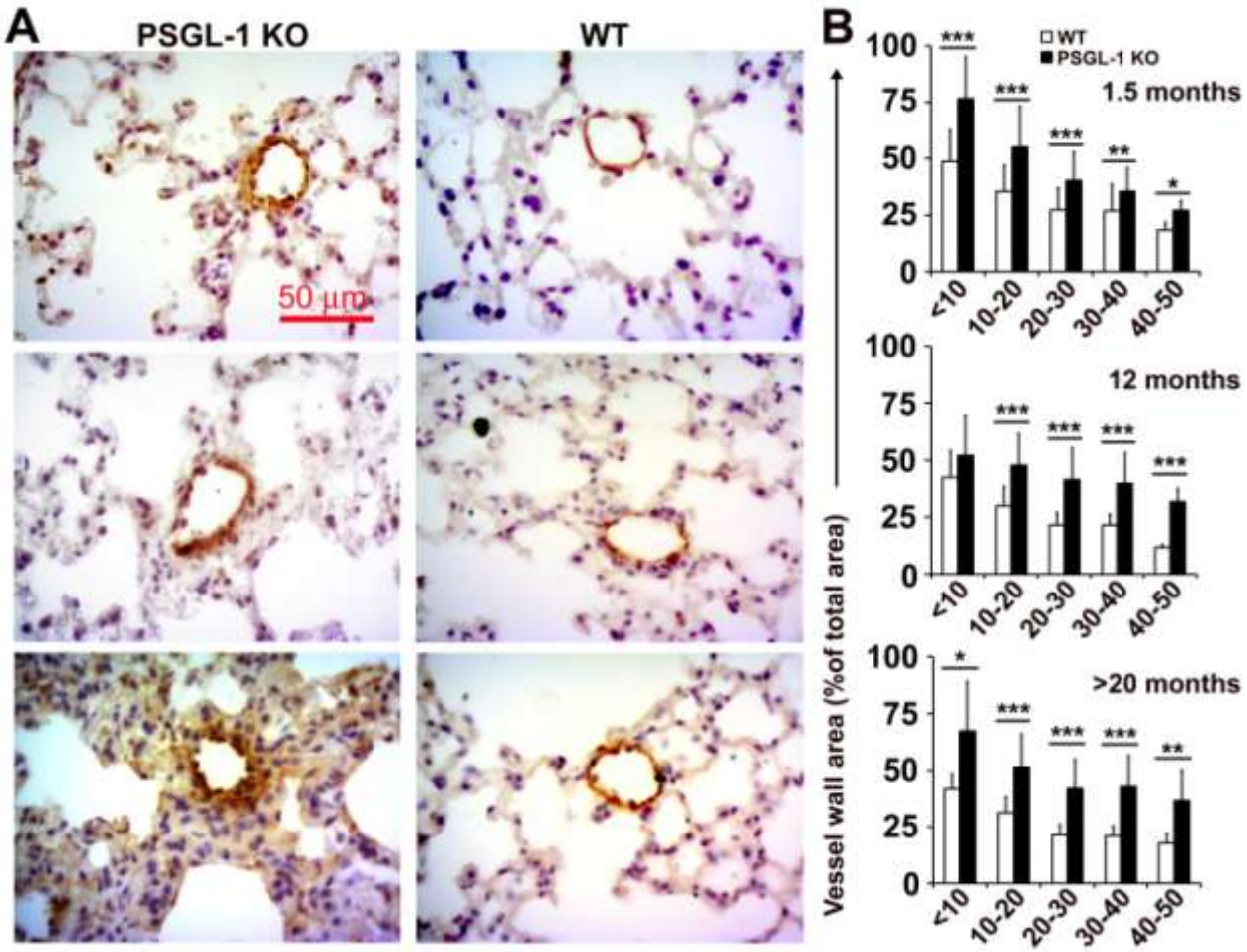

Figure 1. Vascular remodeling in pulmonary small vessels of *PSGL-1*$^{-/-}$ mice. (A) Representative microphotographs of anti-αSMA-immunostained lung sections of 1.5, 12 and >20-month-old mice (*n* = 5–6 per group). Scale bar = 50 □m. **(B)** Percentage of vessel wall area in <50 µm-diameter pulmonary blood vessels at 1.5, 12 and >20 months of age (>150 vessels analyzed for each group of age). Data are expressed as the mean ± SD. **P* < 0.05, ***P* < 0.01, ****P* < 0.005, by 2-tailed Student's t test.

Fig.2

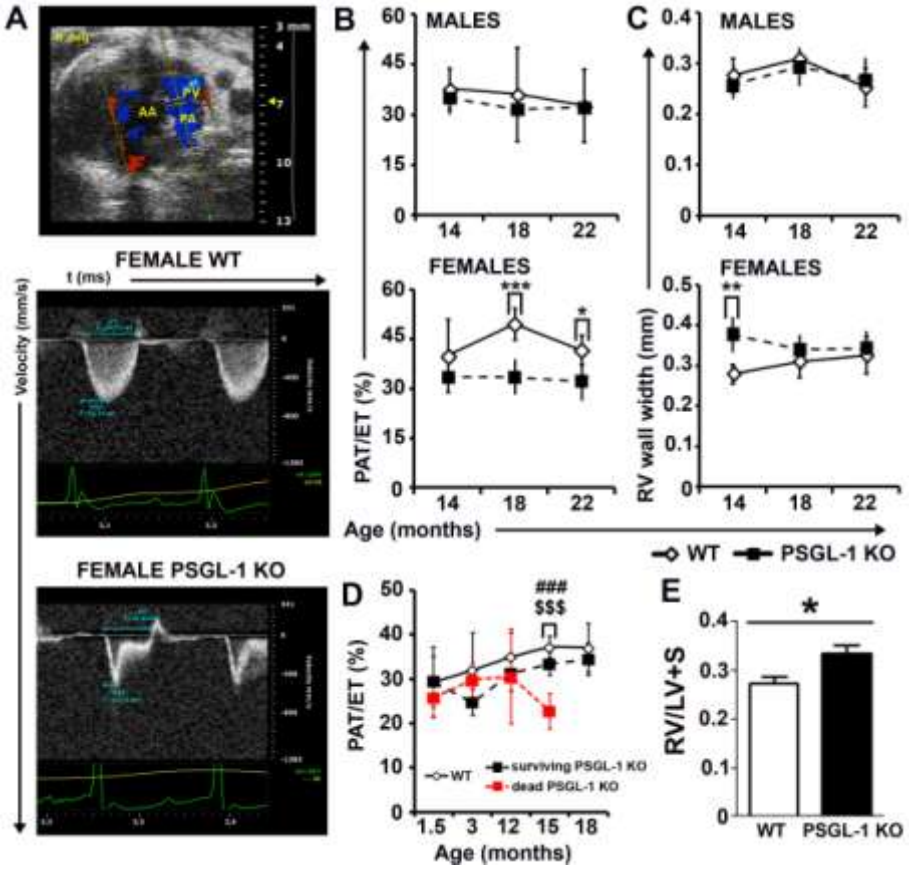

Figure 2. RV echocardiographic parameters of PAH in *PSGL-1*$^{-/-}$ mice. (A) Upper panel: B-Mode showing the echocardiographic plane used for Doppler pulmonary flow acquisition. PV=pulmonary valve; PA=pulmonary artery; AA=ascending aorta. Lower panels: representative Doppler pulmonary artery flow of female WT and *PSGL-1*$^{-/-}$ mice. **(B** and **C)** Longitudinal study of PAT/ET **(B)** and RV wall thickness **(C)** in male and female WT and *PSGL-1*$^{-/-}$ mice at 14, 18 and 22 months of age (n = 5 mice per group). **(D** and **E)** Longitudinal study of PAT/ET **(D)** and body weight **(E)** between 1.5 and 18 months of age in WT mice (n = 4), surviving *PSGL-1*$^{-/-}$ mice (n = 6) and *PSGL-1*$^{-/-}$ mice dying prematurely (n = 3). **(F)** Fulton index (RV/LV+S) measured in WT and surviving *PSGL-1*$^{-/-}$ mice. Data are expressed as the mean ± SD. * WT vs surviving *PSGL-1*$^{-/-}$; # WT vs dead *PSGL-1*$^{-/-}$; $ surviving *PSGL-1*$^{-/-}$ vs dead *PSGL-1*$^{-/-}$ mice, by one-way ANOVA with Bonferroni *post hoc* test.

Fig.3

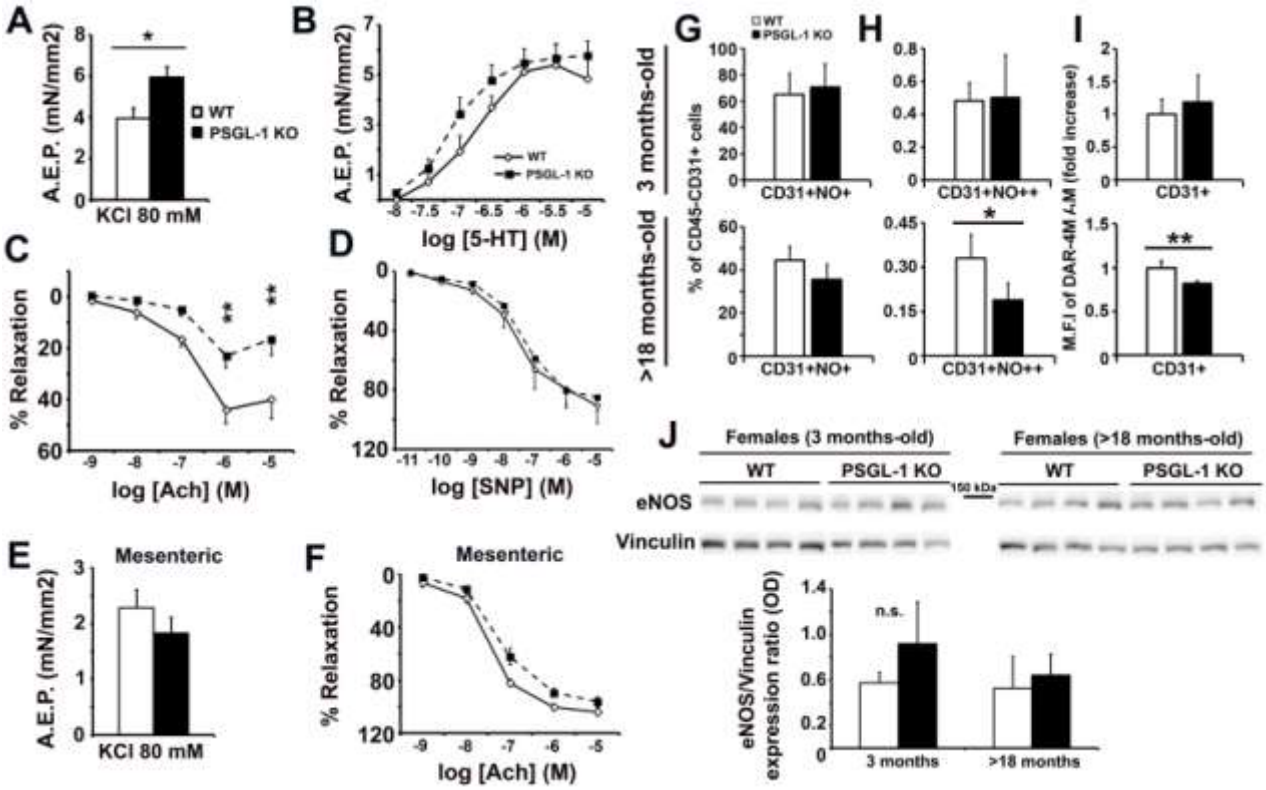

Figure 3. Vascular response to vasoconstrictor and vasodilator agents and quantification of NO production by lung endothelial cells. (A and **B)** Contractile response to KCl **(A)** and serotonin **(B)** in pulmonary arterial rings obtained from 18-month-old female WT and *PSGL-1*$^{-/-}$ mice. A.E.P: Active Effective Pressure. **(C** and **D)** Vasodilating response to acetylcholine **(C)** and sodium nitroprusside **(D)** in pulmonary arterial rings obtained from 18-month-old female WT and *PSGL-1*$^{-/-}$ mice. **(E** and **F)** Vascular response of mesenteric arterial rings to KCl **(E)** and acetylcholine **(F)** obtained from 18-month-old female WT and *PSGL-1*$^{-/-}$ mice. **(G** and **H)** Percentage of lung endothelial cells producing moderate **(G)** or high **(H)** amounts of NO measured in 3 and >18-month-old female WT and *PSGL-1*$^{-/-}$ *mice*. **(I)** Fold change of medium fluorescence intensity (M.F.I.) for the NO-sensing probe DAR-4M AM measured in lung endothelial cells of 3 and >18-month-old female WT and *PSGL-1*$^{-/-}$ mice. **(J)** Western blot showing eNOS expression in the lungs of female WT (n = 4) and *PSGL-1*$^{-/-}$ (n = 4) (upper panels) mice and densitometry quantification (lower panel). Vinculin was used as loading control. Data are expressed as the mean ± SD. **(A-I)** **P* < 0.05, ***P* < 0.01 by 2-tailed Student's t test. **(J)** Non significant (n.s.) differences were found by Mann-Whitney's U test.

Fig.4

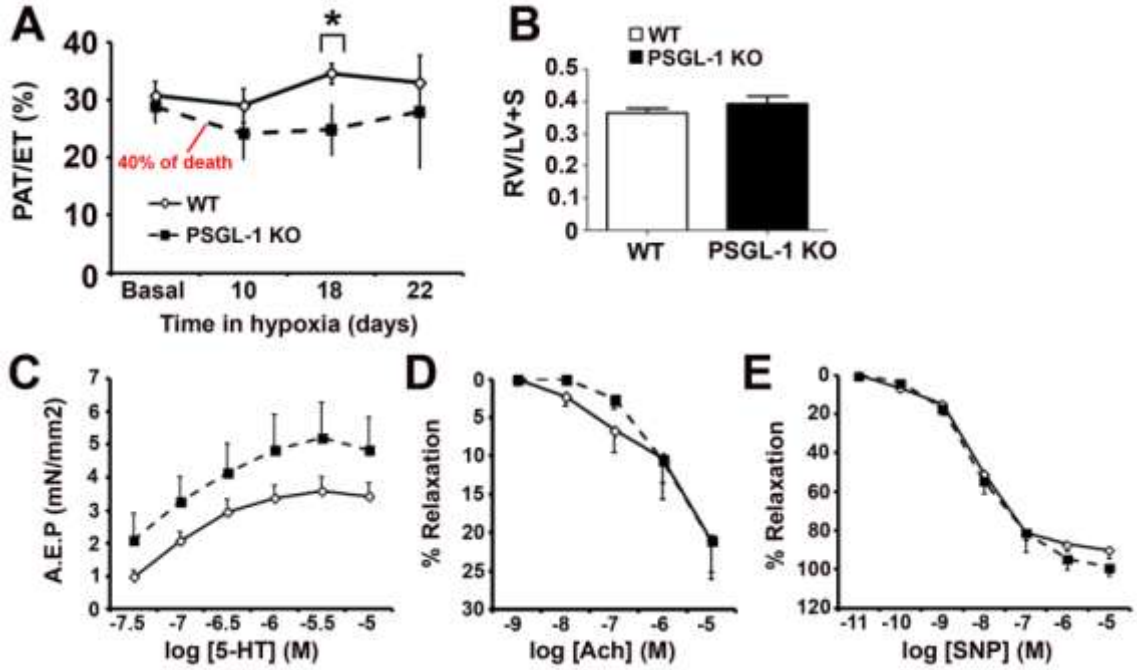

Figure 4. Effects of 24-day exposure to 10% O_2 on WT and *PSGL-1*$^{-/-}$ mice. (A) PAT/ET measures from basal to day 22 of hypoxia in female WT (n = 4) and surviving *PSGL-1*$^{-/-}$ (n = 5) mice. Shown in red is the percentage of dead *PSGL-1*$^{-/-}$ mice before day 10. **(B)** Fulton index calculated at day 24 for WT (n = 4) and surviving *PSGL-1*$^{-/-}$ (n = 5) mice exposed to hypoxia. **(C)** Contractile response to serotonin of pulmonary arterial rings obtained from female WT (n = 4) and surviving *PSGL-1*$^{-/-}$ (n = 5) mice exposed to hypoxia. **(D** and **E)** Vasodilating response to acetylcholine **(D)** and sodium nitroprusside **(E)** of pulmonary arterial rings obtained from female WT (n = 4) and surviving *PSGL-1*$^{-/-}$ (n = 5) mice exposed to hypoxia. Data are expressed as the mean ± SD. *P < 0.05 by 2-tailed Student's t test.

Fig.5

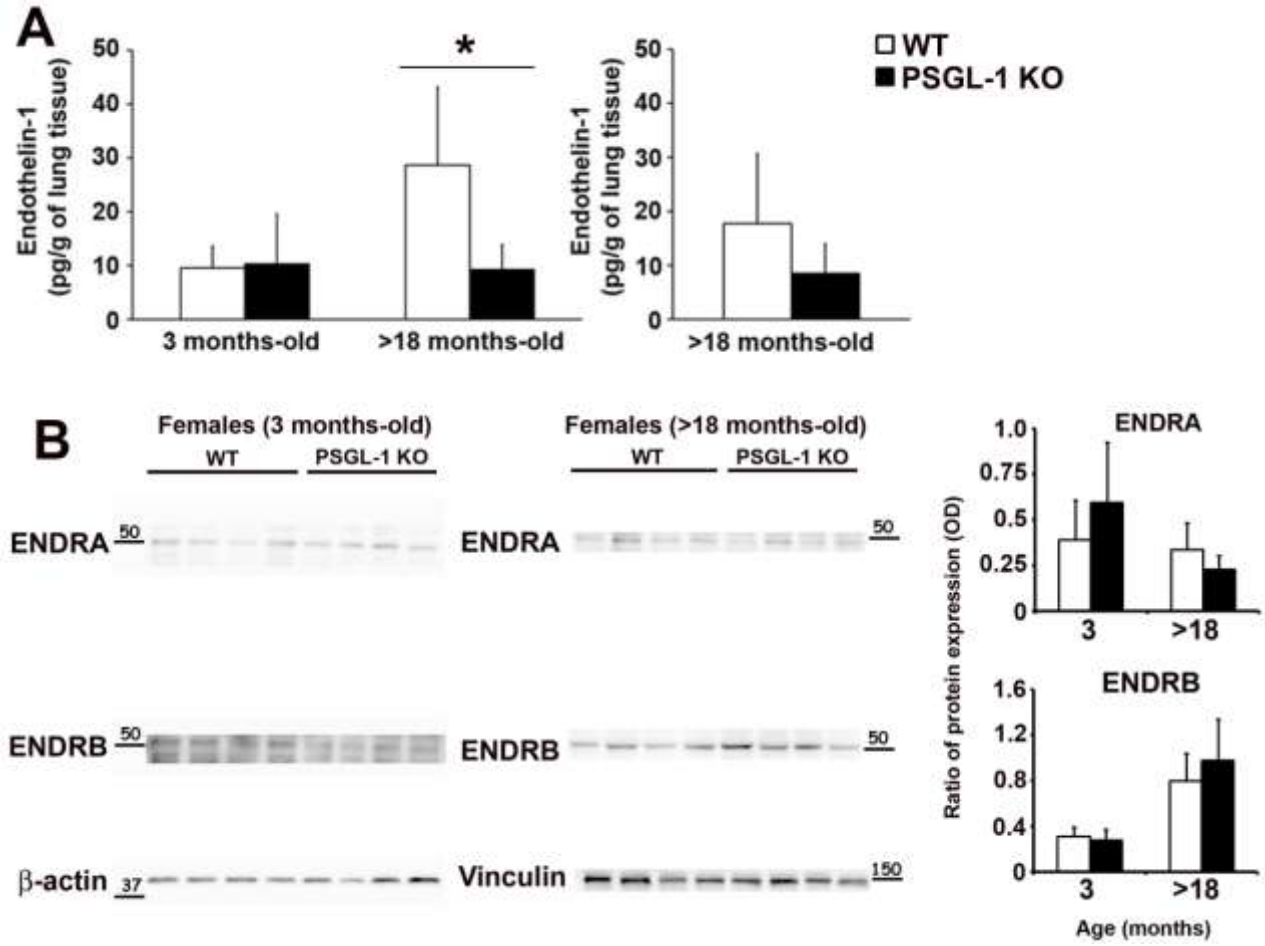

Figure 5. Endothelin-1, ENDRA and ENDRB expression in lungs of WT and PSGL-1$^{-/-}$ mice. (A) ET-1 concentration in lung lysates of WT (n = 4) and *PSGL-1*$^{-/-}$ (n = 4) mice. (B) Western blot showing ENDRA and ENDRB (left panels) expression in the lungs of female WT (n = 4) and *PSGL-1*$^{-/-}$ (n = 4) mice and densitometry quantification (right panels). β-actin and vinculin were used as loading controls. Data are expressed as the mean ± SD. **P* < 0.05 by Mann-Whitney's U test.

Fig.6

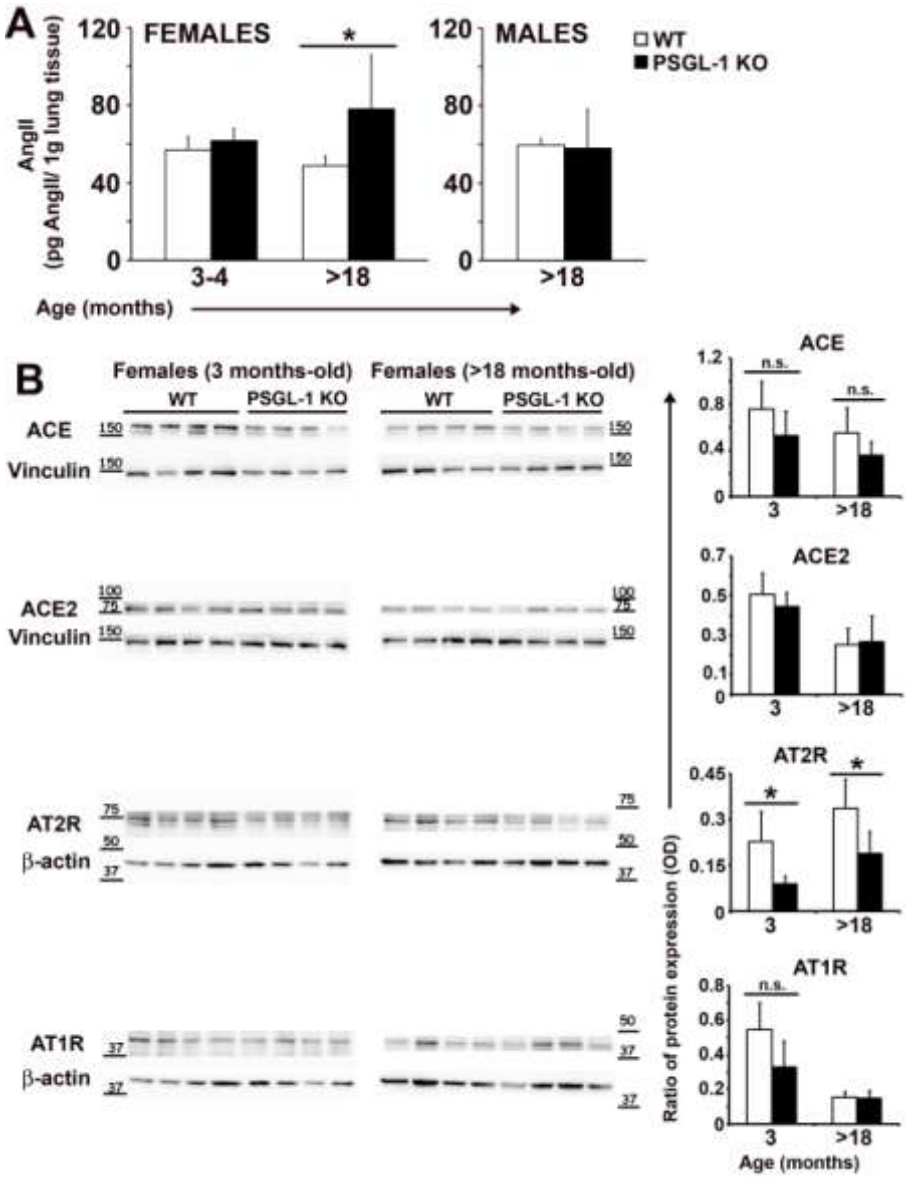

Figure 6. Angiotensin II pathway analysis in the lung of WT and *PSGL-1*$^{-/-}$ mice. (A) AngII concentration in lung lysates of WT (n = 4) and *PSGL-1*$^{-/-}$ (n = 4) mice. **(B)** Immunoblots showing ACE, ACE2, AT2R and AT1R (left panels) expression in the lungs of female WT (n = 4) and *PSGL-1*$^{-/-}$ (n = 5) mice and densitometric quantification (right panels). β-actin and vinculin were used as loading controls. Data are expressed as the mean ± SD. *P < 0.05 by Mann-Whitney's U test. n.s. not significant.

Fig.7

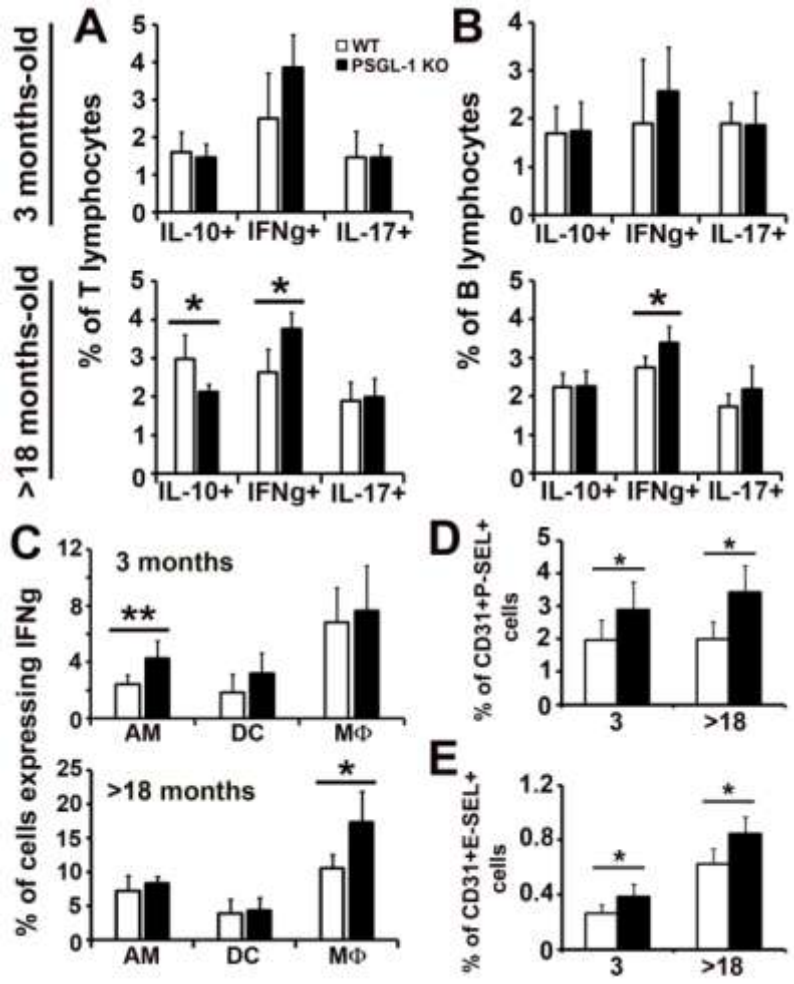

Figure 7. Immune system analysis and expression of endothelial P-selectin and E-selectin in lung of WT and *PSGL-1*$^{-/-}$ mice. (A) Percentage of T lymphocytes producing IL-10, IFN-γ, IL-17 in 3 and >18-month-old WT and *PSGL-1*$^{-/-}$ mice. **(B)** Percentage of B lymphocytes producing IL-10, IFN-γ, IL-17 in 3 and >18-month-old WT and *PSGL-1*$^{-/-}$ mice. **(C)** Percentage of macrophages and dendritic cells producing IFN-γ in 3 and >18-month-old WT and *PSGL-1*$^{-/-}$ mice. AM: alveolar macrophages; DC: dendritic cells; MΦ: interstitial macrophages. **(D** and **E)** Percentage of endothelial cells expressing P-selectin **(D**) or E-selectin **(E)**. **P* < 0.05, ***P* < 0.01 by 2-tailed Student's t test.